Title
Framework to Define Performance Requirements for Structural Component Models and Application to Reinforced Concrete Wall Shear Strength

Author
Rojas, Matias

Publication Date
2022

Peer reviewed|Thesis/dissertation

UNIVERSITY OF CALIFORNIA

Los Angeles

Framework to Define Performance Requirements for Structural Component Models

And

Application to Reinforced Concrete Wall Shear Strength

A dissertation submitted in partial satisfaction of the

requirements for the degree Doctor of Philosophy

in Civil Engineering

by

Matías Andrés Rojas León

2022

ABSTRACT OF THE DISSERTATION

Framework to Define Performance Requirements for Structural Component Models

And

Application to Reinforced Concrete Wall Shear Strength

by

Matías Andrés Rojas León

Doctor of Philosophy in Civil Engineering

University of California, Los Angeles, 2022

Professor John Wright Wallace, Chair

A large number of models to predict shear strength of structural walls have been proposed in the literature to replace models adopted in codes and standards. Evaluation of the predictive performance of new models relative to existing models is often difficult because the models were developed using different databases and a model may have substantially different performance (high, versus low variance) when evaluated against a different database. In addition, more complex models are expected to have less variance than relatively simple models and target performance metrics for models of different complexity

do not exist. To address these issues, a study was conducted applying statistical and machine learning approaches to establish target model performance for different model complexities. The methodology is demonstrated by addressing the problem of assessing wall shear strength using a comprehensive database of 333 walls reported to have failed in shear.

Wall shear strength equations reported in the literature and used in building codes are assessed using a comprehensive database of reinforced concrete wall tests reported to have failed in shear. Based on this assessment, it is concluded that mean values varied significantly, and coefficient of variations were relatively large (> 0.30) and exceeded the target error for a code-oriented equation defined in the companion paper. Therefore, a methodology employing statistical and machine learning methods was used to develop a new equation with form similar to that currently used in ACI 318-19. The proposed equation is applicable to walls with rectangular, barbell, and flanged cross-sections and includes additional parameters not considered in ACI 318-19, such as axial stress and quantity of boundary longitudinal reinforcement. Parameter limits, e.g., on wall shear and axial stresses, and an assessment of the relative contributions to shear strength also are addressed. Finally, a reliability analysis is performed to study the relationship between probability of failure and strength reduction factor applicable to the proposed equation.

The dissertation of Matías Andrés Rojas León is approved.

Jingy Li

Scott Joseph Brandenberg

Henry J. Burton

John Wright Wallace, Committee Chair

University of California, Los Angeles

2022

To my mémé, mom and dad.

TABLE OF CONTENTS

LIST OF FIGURES

LIST OF TABLES

ACKNOWLEDGEMENTS

I acknowledge the support from the National Agency for Research and Development (ANID) Scholarship Program/DOCTORADO BECAS CHILE/2019-72200499.

Any opinions, findings, and conclusions expressed in this material are those of the author and do not necessarily reflect those of the sponsors.

I thank all the people I work with and shared time with during these four years. Particularly, thanks to Saman Abdullah and Kristijan Kolozvari; both of you are always willing to help, which contributed to the teamwork spirit in the projects we worked on together.

I express my gratitude to all Professors of my Committee, not only about the technical staff (I was a student of all of you during my time at UCLA), but also for your good disposition and mood when it was about more administrative matters. I know how much we would like to not have to deal with those matters sometimes!

Special thanks to my advisor, Professor John Wallace. I truly appreciate the opportunity of working together, the support and trust you placed in me, at the same time of keeping a critical eye on the tasks we were working on. All of it put me in a position of learning at the same time of actually contributing to important and impactful topics of Structural Engineering. It has been always fascinating to me the process of identifying a need, thinking on how to address it, understanding limitations/implications of doing or not doing something, go back to thinking, an eventually finding a solution. In this period, you were an eye opener in terms of linking needs, what can be done about it, and potential practical implications. It is definitely motivating!

VITA

2008 - 2012 B.S., Structural Engineering

University of Chile, Chile

2011 - 2015 Teaching Assistant

Department of Civil Engineering & Department of Mathematics

University of Chile, Chile

2014 Junior Structural Engineer

Ruben Boroschek & Associates

Santiago, Chile

2013 - 2015 P.E., Structural Engineering

University of Chile, Chile

2014 - 2015 M.S., Structural Engineering

University of Chile, Chile

2015 - 2018 Structural Engineer

Moffatt & Nichol

Santiago, Chile

2018 - 2022 Graduate Student Researcher & Teaching Assistant

Department of Civil and Environmental Engineering

University of California, Los Angeles

Chapter 1. Introduction

In civil and structural engineering, design checks are typically accomplished by comparing demands (e.g., moment, M_u; shear V_u; displacement, δ_u) with capacities (e.g., M_n; shear V_n; displacement, δ_c). These equations that estimate capacities have been developed based on models capturing the mechanics (e.g., free body diagrams) and calibrated using relatively little data available at the moment. Unlike 20 to 30 years ago, more recently, comprehensive databases are being assembled to enable the development of more complex capacity models using more sophisticated statistical approaches, and also including Machine Learning (ML). Evaluation of the predictive performance of different models is often difficult because of one or more of the following reasons:

- They were developed using different databases and a model may have substantially different performance (bias, variance) when evaluated against a different database.
- More complex models are expected to have less variance than relatively simple models and however, approaches to judge the relative merits of models with different complexities have not been proposed.
- Optimal model performance is often not studied, so it is unknown whether a model with better performance is possible. In other words, even having one model that performs better than a second one with similar complexity level and calibrated using the same database, does not exclude the possibility than another better model could be obtained. Therefore, for a given model complexity, how should the model

performance be assessed to judge if the model error has been minimized and what are the relative benefits of the more complex model.

To address these issues, a study was conducted applying statistical and ML approaches to establish target model performance for different model complexities. The framework is particularly useful when addressing a mechanics-based problem with a small database.

The methodology is demonstrated by addressing the problem of assessing wall shear strength, and the target errors are expressed in terms of the mean value and coefficient of variation of the true-to-predicted ratio. This application was picked because:

- The wall shear strength equation in ACI 318-19 has remained essentially unchanged for the last 50 years despite a large number of models being published in the literature.
- Even though most of the published equations are similar in complexity, they show a significant variance when assessed against a database of wall tests that is not the same as that used to develop and calibrate the model (Gulec and Whittaker, 2011; Sánchez-Alejandre and Alcocer, 2010; Carrillo and Alcocer, 2013; Kassem, 2015).

This can be ascribed to the issues before mentioned. First, it is typically more difficult to obtain a better fit when a wider range of variables exist (e.g., one database includes only walls with rectangular cross sections whereas the other database includes walls with both rectangular, barbell, and flanged cross sections) and, if this is the case, the number of tests is likely to have an impact too. Second, in most of the studies reported in the literature, wall aspect ratio (h_w/l_w) was typically used as a means to determine which tests were included in the database (e.g., $h_w/l_w < 1.0$ or 1.5); however, studies have shown (Abdullah and

Wallace, 2021) that wall aspect ratio is not the best indicator of wall failure mode. Therefore, most of the databases used to develop the models reported in the literature included some walls that actually experienced flexural failures. Finally, in most cases, the databases were typically not large enough to split into training and testing sets and did not assess issues associated with underfitting versus overfitting (Höge et al., 2018) to examine the possibility that a model of equivalent complexity might have better predictive performance.

Over the last five decades, a significant number of wall tests have been reported in the literature and have recently been complied in a comprehensive database with more than 1100 wall experiments (Abdullah and Wallace, 2020). The database was filtered to identify wall tests with reported shear failure modes (flexure-shear, diagonal tension, or diagonal compression), resulting in 412 tests, and then a detailed review was conducted to identify reasons why would be inappropriate to include some tests (i.e., outliers identification, key step of the methodology). The availability of this database of shear-controlled walls enabled the application of the proposed ML-statistics based framework to establish a relationship between model complexity and model performance requirements, which includes a target error interval expressed in terms of the mean and COV of the true-to-predicted ratio (V_{true}/V_{pred}). This error indicator was selected because is well known and widely used in this field, and therefore, researchers have a good understanding of what is means (e.g., how much is small versus large).

Chapter 2. Review of Existing Wall Shear Strength Models

2.1 Models Calibrated Using Statistical Inferences and its Drawbacks

This section provides a detailed review and summary of existing models for predicting shear strength of RC walls that are available in building codes and standards worldwide (**Table 2.1**) and reported in the literature (**Table 2.2**). **Table 2.1** reveals that all existing models compute wall nominal shear strength (V_n) using a $V_n = V_c + V_s$ format, where V_c and V_s are the concrete and reinforcement contributions to nominal shear strength, respectively. However, the parameters considered that influence the concrete and reinforcement contributions sometimes differ. For example, the NZS 3101 (2006) and ASCE/SEI 43 (2005) models consider the influence of axial load on V_c (ACI 318-19 does not), the EC8 (2005) and ASCE/SEI 43 (2005) models include the impact of the vertical web reinforcement, and the detailed model of NZS 3101 (2006) use $M_u/(V_u l_w)$ instead of h_w/l_w, which is used by the remaining models shown in **Table 2.1**.

***Table 2.1**: Existing wall shear strength models in building codes and standards*

Model	Comments
ACI 318-19, Section 18.10 $V_n = A_{cv}(\alpha_c \lambda \sqrt{f_c'} + \rho_{wh} f_{ywh}) \leq 0.83 A_{cv} \sqrt{f_c'}$ $\alpha_c = \begin{cases} 0.25 & \text{for } h_w/l_w \leq 1.5 \\ 0.17 & \text{for } h_w/l_w \geq 2.0 \\ 0.25 - 0.17\left(\frac{h_w}{l_w} - 1.5\right) & \text{for } 1.5 < h_w/l_w < 2.0 \end{cases}$ λ = 1.0 for normalweight concrete. For lightweight concrete, it ranges from 0.75 to 0.85 depending on the composition of the aggregates.	Wall shear strength is determined using Equation 18.10.4.1. The upper limit of $0.83 A_{cv} \sqrt{f_c'}$ (for an individual wall) is intended to prevent diagonal compression failure and has been in the ACI 318 Code since 1971. For walls with $h_w/l_w \leq 2.0$ it is required that ρ_v is no less than ρ_h.
EC8-2004 $V_n = v_n t_w d$ $v_n = v_c + v_s$	Concrete contribution is ignored for walls subjected to low axial stresses ($1.5P_u/(A_t f_c') < 0.1$). Wall shear strength depends on vertical and horizontal

Model	Comments
$v_n = \begin{cases} 0 & \text{if } \frac{1.5P_u}{A_t f_c'} < 0.1 \\ 0.15\sqrt{f_c'} & \text{if } \frac{1.5P_u}{A_t f_c'} \geq 0.1 \end{cases}$ $v_s = \rho_h f_{yh}\left(\frac{M_u}{V_u l_w} - 0.3\right) + \rho_v f_{yv}\left(1.3 - \frac{M_u}{V_u l_w}\right)$	web reinforcement, and the ratio of applied moment to shear.
NZS 3101-2006 $V_n = V_c + V_s$ $V_s = \frac{A_v f_{ywh} d}{s}$ $\frac{V_c}{A_{cv}} = \begin{cases} min\begin{cases} 0.17\sqrt{f_c'} \\ 0.17\left(\sqrt{f_c'} + \frac{P_u}{A_g}\right) \end{cases} & \text{Simplified Method} \\ min\begin{cases} 0.27\sqrt{f_c'} + \frac{P_u}{4A_g} \\ 0.05\sqrt{f_c'} + \frac{l_w\left(0.1\sqrt{f_c'} + 0.2\frac{P_u}{A_g}\right)}{\frac{M_u}{V_u} - \frac{l_w}{2}} \end{cases} & \text{Detailed Method} \end{cases}$	The simplified method may only be used when the vertical reinforcement ratio along the entire wall exceeds 0.003, and the spacing of reinforcement does not exceed 300 mm (12 in) in any direction. The detailed equation does not apply if $\left(\frac{M_u}{V_u} - \frac{l_w}{2}\right) \leq 0$.
AIJ-1999 $V_n = V_c + V_s$ $V_c = \frac{tan(\theta)(1-\beta)t_w l_w \nu f_c'}{2} \geq 0$ $V_s = \rho_{wh} f_{ywh} t_w l_w cot(\xi)$ $tan(\theta) = \sqrt{\left(\frac{h_w}{l_w}\right)^2 + 1} - \frac{h_w}{l_w}$ $\nu = 0.7 - \frac{f_c'}{2000}$ $\beta = \frac{(1+cot^2(\xi))\rho_{wh} f_{ywh}}{\nu f_c'}$ $cot(\xi) = 1$ (for truss mechanisms)	In this model, besides the truss analogy, shear is assumed to be resisted through an arch mechanism. The contribution of the arch mechanism decreases with the amount of the web horizontal steel.
ASCE/SEI 43-05 $V_n = v_n t_w d_w \leq 1.66 A_{cv}\sqrt{f_c'}$ $v_n = min\begin{cases} 0.70\sqrt{f_c'} - 0.28\sqrt{f_c'}\left(\frac{h_w}{l_w} - 0.5\right) + \frac{P_u}{4 l_w t_w} + \rho_{se} f_{y1} \\ 20\sqrt{f_c'} \end{cases}$ $d_w = 0.61 l_w$ $\rho_{se} = A\rho_v + B\rho_h$ $A = \begin{cases} 1 & \text{for } \frac{h_w}{l_w} \leq 0.5 \\ 1.5 - \frac{h_w}{l_w} & \text{for } 0.5 < \frac{h_w}{l_w} \leq 1.5 \\ 0 & \text{for } \frac{h_w}{l_w} > 1.5 \end{cases}$ $B = \begin{cases} 1 & \text{for } \frac{h_w}{l_w} \leq 0.5 \\ \frac{h_w}{l_w} - 0.5 & \text{for } 0.5 < \frac{h_w}{l_w} \leq 1.5 \\ 0 & \text{for } \frac{h_w}{l_w} > 1.5 \end{cases}$	ASCE/SEI 43-05 adopted the work done by Barda et al. (1977), with modifications to extend its applicability. This equation is meant to predict the peak shear strength of walls with barbells or flanges, common in nuclear power plants, and is applicable to walls with $\frac{h_w}{l_w} \leq 2.0$ and vertical and horizontal web reinforcement ratios ≤ 1%. If the reinforcement ratios exceed 1%, the combined reinforcement ratio ρ_{se} is limited to 1%.

Table 2.2 presents wall shear strength equations reported in the literature, along with a description of the databases used in calibration/validation of the models. In these studies, wall shear strength relations were generally developed by identifying relevant parameters based on literature review, investigating the mechanics of problem, and using statistical analysis of data sets. Subsequently, a calibration process was employed to fit the coefficients of the proposed model to the data. Therefore, these equations are typically valid and perform well only when the model is used to estimate wall shear strength (e.g., shear stress, or shear force) for a wall with parameters within the ranges of the parameters used to calibrate the model. Because different databases were used to develop existing models, and these databases used different criteria to determine which wall tests to include in the database, as well as different test parameters, different ranges of test parameters and different numbers of tests, a model developed with a given database can be biased when it is evaluated with a different database.

***Table 2.2**: Existing wall shear strength models reported in the literature*

Model	Database	Comments
Barda et al. (1977) $V_n = v_n t_w d$ $v_n = 0.66\sqrt{f_c'} - 0.21\sqrt{f_c'}\frac{h_w}{l_w} + \frac{P_u}{4 l_w t_w} + \rho_v f_{yv}$	• 8 flanged walls • $\frac{h_w}{l_w} \in [0.25\ ,\ 1.00]$ • $\rho_{be} \in [1.8\%\ ,\ 6.4\%]$ 1.8% - 6.4% • ρ_{wh} and $\rho_{wv} \in [0\%\ ,\ 0.5\%]$	Meant to predict the peak shear strength of walls in low-rise buildings.
Wood (1990) $V_n = \frac{A_{vf} f_y}{4}$ $0.5 A_{cv}\sqrt{f_c'} \le V_n \le 0.83 A_{cv}\sqrt{f_c'}$ $A_{vf} f_y = 2 A_{be} f_{ybe} + A_{wv} f_{ywv}$	• 143 squat walls reported to have failed in shear • ~105 barbell, ~20 flanged walls, and ~18 rectangular cross-sections.	The model does not consider the concrete and steel contributions as two different terms. Instead, it uses the concrete contribution to define a lower and upper limit only.

Model	Database	Comments
	• $\frac{M_u}{V_u l_w} \leq 2.0$, with $0.5 \leq \frac{M_u}{V_u l_w} \leq 1.0$ for more than 75% of the test specimens. • $0.7 \leq \frac{P_u}{A_g f_c'} \leq 0.18$ for 18 specimens, and $\frac{P_u}{A_g f_c'} = 0$ for the rest.	
Sánchez-Alejandre and Alcocer (2010) $V_n = \left(\gamma\eta_v + 0.04\frac{P_u}{A_g}\right)\sqrt{f_c'} + \eta_h\rho_h f_{yh}$ $\gamma = min\begin{cases}0.42 - 0.08\frac{M_u}{V_u l_w} & \text{Option 1}\\ 0.42 - 0.08(\%R_{max}) & \text{Option 2}\end{cases}$ $\eta_v = 0.75 + 0.05\rho_v f_{yv}$ $\eta_h = 1 - 0.16\rho_h f_{yh} \geq 0.20$ R_{max} = drift angle	• 80 rectangular walls with diagonal tension failure mode • Most of the walls have $\frac{M_u}{V_u l_w} \leq 1.0$ • Low web reinforcement ratios and axial loads. • Drift angles < 1%.	The model depends on the amount of web reinforcement (hor. and ver.) that has reached plastic strains at a given drift angle (R_{max}), and although the γ factor that depends on R_{max}, it can also be expressed in terms of $M_u/(V_u l_w)$.
Gulec and Whittaker (2011) For rectangular walls: $V_n = V_{rec} \leq 0.83\sqrt{f_c'}A_{cv}$ For barbell/flanged walls with $\frac{A_t}{A_{cv}} \geq 1.25$: $V_n = V_{be} \leq 1.25\sqrt{f_c'}A_g$ For barbell/flanged walls with $\frac{A_t}{A_{cv}} < 1.25$: $V_n = min(V_{rec}, V_{be}) \leq 10\sqrt{f_c'}A_{cv}$ $V_{rec} = \frac{0.83\sqrt{f_c'}A_{cv} + 0.25F_{vw} + 0.20F_{vbe} + 0.40P_u}{\sqrt{\frac{h_w}{l_w}}}$ $V_{be} = \frac{0.04f_c'A_{\text{eff}} + 0.40F_{vw} + 0.15F_{vbe} + 0.35P_u}{\sqrt{\frac{h_w}{l_w}}}$ F_{vw}: force attributed to vertical web reinforcement F_{vbe}: force attributed to both BEs reinforcement	• Cantilever walls • One database of 74 rectangular walls • Second database of 153 walls (79 barbell walls, and 74 flanged walls) • $\frac{h_w}{l_w} \in [0.25\ ,\ 2.00]$ • $f_c' \in [13.7\text{ MPa}\ ,\ 51.0\text{ MPa}]$ • $\frac{P_u}{A_t f_c'} \in [0\ ,\ 0.14]$ • $\rho_{wh}f_{ywh} \in [0\ ,\ 5.8\text{ MPa}]$ • $\rho_{wv}f_{ywv} \in [0\ ,\ 12.8\text{ MPa}]$ • $\rho_{be}f_{ybe} \in [0\ ,\ 14.1\text{ MPa}]$	The model is based on a free-body diagram of a low aspect ratio wall with an inclined (shear) crack. The boundary element reinforcement (ρ_{be*}) is calculated as $2A_{s,be}/A_t$, where $A_{s,be}$ is the area of vertical reinforcement in each BE.
Carrillo and Alcocer (2013) $V_n = (\alpha_1\sqrt{f_c'} + \eta_h\rho_h f_{yh})A_{cv} \leq \alpha_2\sqrt{f_c'}A_{cv}$	• 39 walls from quasi-static and shake-table tests.	Meant to be used for walls in typical low-rise housing

Model	Database	Comments
$\eta_h = \begin{cases} 0.8 & for\ deformed\ bars \\ 0.7 & for\ welded-wire\ mesh \end{cases}$ $\alpha_1 = 0.21 - 0.02\left(\frac{M_u}{V_u l_w}\right)$ $\alpha_2 = 0.40$	• $\frac{h_w}{l_w} \approx 0.5, 1.0, 2.0$ • Normalweight, lightweight, and self-consolidating concrete. • ρ_{wh} and $\rho_{wv} \in [0\% , 0.28\%]$ • $\rho_{be} \in [0.22\% , 1.50\%]$	in Latin America (low concrete strength and wall thickness of ~4 in.)
Kassem (2015) $V_n = v_n t_w d_w$ For rectangular walls: $v_n = 0.44 f_c' \left[\psi k_s sin(2\alpha) + 0.10\omega_h \frac{h_w}{d_w} + 0.30\omega_v cot(\alpha)\right]$ For flanged walls: $v_n = 0.67 f_c' \left[\psi k_s sin(2\alpha) + 0.16\omega_h \frac{h_w}{d_w} + 1.74\omega_v cot(\alpha)\right]$ $\psi = 0.95 - \frac{f_c'}{250}$ $k_s = \frac{a_s}{d_w}$ $\alpha = tan^{-1}\left(\frac{h_w}{d_w}\right)$ $d_w = d - \frac{a_s}{3}$ $\omega_h = \frac{\rho_h f_{yh}}{f_c'}$ $\omega_v = \frac{\rho_v f_{yv}}{f_c'}$ a_s: horizontal length of the compression zone at the wall base	• 287 cantilever rectangular walls • $\frac{h_w}{l_w} \in [0.25 , 1.00]$ • $\frac{P_u}{A_g f_c'} \in [0, 0.23]$ • $\rho_{wh} \in [0\% , 1.61\%]$ • $\rho_{wv} \in [0\% , 2.87\%]$ • 358 cantilever flanged walls • $\frac{h_w}{l_w} \in [0.21 , 1.60]$ 0.21 – 1.60 • $\frac{P_u}{A_g f_c'} \in [0 , 0.34]$ • $\rho_{wh} \in [0\% , 2.89\%]$ • $\rho_{wv} \in [0\% , 2.89\%]$	It is a mathematical equation based on the strut-and-tie model. Since flanged walls are more susceptible to diagonal compression failure than rectangular walls, two separate databases of rectangular and flanged walls were used to calibrate the equations.
Looi and Su (2017) $V_n = v_n A_g f_c'$ $\frac{v_n}{f_c'} = 0.034 + A\left(\frac{P_u}{A_g f_c'}\right)^{1.3} + B\rho_v \frac{f_{yv}}{f_c'} + C\rho_h \frac{f_{yh}}{f_c'} + D\rho_{be} \frac{f_{ybe}}{f_{cc}'}$ $\frac{v_n}{f_c'} \leq 0.24$ $A = 0.283 - 0.084 \frac{M_u}{V_u d}$ $B = 0.4 - 0.15 \frac{M_u}{V_u d}$ $C = 0.5 - 0.2 \frac{M_u}{V_u d}$ $D = -0.08 + 0.06 \frac{M_u}{V_u d}$ f_{cc}': confined concrete strength	• ~ 150 rectangular walls with shear and flexure-shear failure modes • $f_c' \in [15.7$ MPa , 70.3 MPa] • $\frac{P_u}{A_g f_c'} \in [0 , 0.40]$ • $\frac{M_u}{V_u l_w} \in [0.4 , 2.6]$ • $\rho_{wh} \in [0.11\% , 1.72\%]$ • $\rho_{wv} \in [0.13\% , 2.84\%]$ • $\rho_{be} \in [0\% , 13.46\%]$	The proposed model is entirely based on a multi-parameter regression, with relevant parameters based on review of literature. The coefficients in the equation do not have units; therefore, they are the same no matter the set of units being used as long as they are consistent.
Note: 1 MPa = 145 psi		

Table 2.3 presents the comparison of wall shear strength models reported in four different studies (Sánchez-Alejandre and Alcocer, 2010; Carrillo and Alcocer, 2013; Kassem, 2015; Looi and Su, 2017) in terms of their mean and COV. The information in the table reveals that the performance of a given model can be very different when assessed against a database different from the one used to develop the model. It is also noted that the size of databases influences the reported means and COVs even if the ranges of relevant parameters are comparable. This is because small databases might not capture the inherent parameter variability (which, for instance, might come from considering walls with different cross sections), and thus, having a smaller model error is not necessarily an indicator of a good predictive model (Tanaka, 1987).

***Table 2.3**: Wall shear strength model comparison reported in different studies: V_{true}/V_{pred}*

Model	Sánchez-Alejandre & Alcocer (2010)		Carillo & Alcocer (2013)		Kassem (2015)		Looi & Su (2017)	
	Mean	COV	Mean	COV	Mean	COV	Mean	COV
ACI 318-19, Ch. 18 [a]	1.43	0.26	0.82	0.24	1.65	0.37	1.01	0.37
ACI 318-11, Ch. 11	-[b]	-	0.90	0.21	-	-	-	-
ACI 318-14, Ch. 11	-	-	-	-	-	-	0.96	0.37
AIJ 1999	1.00	0.27	-	-	-	-	-	-
CSA (2014) A23.3-14	-	-	-	-	-	-	1.35	0.44
EC8 (2004)	-	-	-	-	2.54	0.71	-	-
Barda et al., 1977	-	-	-	-	1.39	0.47	-	-
Wood, 1990	0.99	0.24	-	-	0.78	0.32	-	-
Hwang & Lee, 2002	1.06	0.22	-	-	1.26	0.56	-	-
Sánchez & Alcocer, 2010	1.00	0.13	0.79	0.12	1.91	0.29	0.84	0.35
Gulec & Whittaker, 2011	-	-	1.06	0.09	1.34	0.24	0.89	0.31

Model	Sánchez-Alejandre & Alcocer (2010)		Carillo & Alcocer (2013)		Kassem (2015)		Looi & Su (2017)	
	Mean	COV	Mean	COV	Mean	COV	Mean	COV
Carrillo & Alcocer, 2013	-	-	1.00	0.08	-	-	-	-
Kassem, 2015	-	-	-	-	1.00	0.21	-	-
Looi & Su, 2017	-	-	-	-	-	-	1.04	0.27

(a) Sánchez and Alcocer (2010) uses ACI 318-09 Ch. 21. Carrillo and Alcocer (2013) and Kassem (2015) use ACI 318-11 Ch. 21. Looi and Su (2017) use ACI 318-14, Ch. 18. These equations are the same as that in ACI 318-19 Ch.18.
(b) "-" indicates the model was not included in the comparison.

2.2 ML Models and its Drawbacks

Models presented in **Table 2.1**, **Table 2.2**, and **Table 2.3** were mainly calibrated using statistical inference, which characterizes the relationship between the data (all of it) and the outcome variable, i.e., the models are not predicting values for unknown data (Bzdok et al., 2018). Statistical models can still be used to make predictions, but predictive power is not their strength. In addition, as databases become large, it often becomes unfeasible to completely interpret the data using statistical models. In such cases, application of ML is valuable (Dey, 2016). Although ML models can provide very accurate predictions, the models tend to be complex and difficult to use, and they also may be difficult to interpret (Bzdok et al., 2018).

***Table 2.4**: Predictive RC wall shear strength models obtained with ML*

Chen et al. (2018)	Moradi-Ardebili (2019)	Keshtegar et al. (2021)
ANN-PSO[(a)] with 1 hidden later and 13 neurons • 6 input variables h_w/l_w, P_u, f_c', A_{cv}, $\rho_h f_y$, $\rho_v f_y$	**ANN**[(b)] with 13 input parameters, 1 hidden layer, and 10 neurons • 13 input variables P_u, h_w, l_w, t_w, b_f, t_f, ρ_{wh}, ρ_{wv}, f_y, f_c', vertical column reinf. ratio, horizontal column reinf. ratio.	**SVR-RSM**[(c)] • 15 input variables: f_c', ρ_{wh}, ρ_{vw}, f_{ywh}, f_{ywv}, b_f, t_f, t_w, h_w, h_w/l_w, P_u, A_{tot}, effective length of wall,

Chen et al. (2018)	Moradi-Ardebili (2019)	Keshtegar et al. (2021)
		longitudinal reinf. ratio of flanges, yield strength of bars in flanges
• Output variable V_{true}	• Output variables – V_{true} – Lateral in-plane stiffness – Drift ratio	• Output variable: V_{true}
• Database – 139 tests – 80% for training test and 20% for testing set – Rectangular walls – $\frac{h_w}{l_w} \in [0.25, 2.0]$ – $\frac{P_u}{A_g f_c'} \in [0.0, 0.35]$ – $\rho_h \in [0.0, 1.96\%]$ – $\rho_v \in [0.0, 2.93\%]$	• Database – 329 tests – 85% for training and 15% testing set – $\rho_{wh} \in [0.0, 6.69\%]$ – $\rho_{wv} \in [0.0, 14.33\%]$ – Horizontal column reinforcement ratio between 0.0 – 6.69% – Vertical column reinforcement ratio between 0.0 – 14.33% – $V_{true} \in [15.42\ kN, 3231\ kN]$	• Database – 208 tests – 70% for training test and 30% for testing set – $\frac{h_w}{l_w} \in [0.21, 2.4]$ – $\rho_{wh} \in [0.0, 2.44\%]$ – $\rho_{wv} \in [0.0, 2.90\%]$ – $V_{true} \in [70\ kN, 2483\ kN]$
• Error indicator used in the training – Root mean square error (RMSE) – Coefficient of determination (R^2)	• Error indicator used in the training – Mean square error (MSE)	• Error indicator used in the training – Root mean square error (RMSE)

[a] Artificial Neural Network implemented with Particle Swarm Optimization (Chen et al., 2018)
[b] Artificial Neural Network
[c] Support Vector Regression coupled with Response Surface Model (Keshtegar et al., 2021)

Table 2.4 shows three ML models developed to predict wall shear strength. The databases used for the ML studies in **Table 2.4** are typically larger than the databases used for the studies listed in **Table 2.2**. ML models as the ones shown in **Table 2.4** show the potential and significant predictive power of ML algorithms when compared to simpler models (**Table 2.1**, **Table 2.2**); however, these ML studies can suffer several drawbacks, as described next. Due to test lab limitations, most wall tests reported in the literature have been conducted at modest scale, typically in the range of 1/5 to 1/2. Several of the input variables used in

models of **Table 2.4** are not expressed in a form that allow them to extrapolate the results of reduced-scale tests with full-scale walls. For example, the models used the geometry of the wall directly (e.g., h_w, l_w, t_w, b_f, t_f) instead of using aspect ratios, or forces (e.g., P_u, $\rho_h f_y$, $\rho_v f_y$) instead of using associated stresses based on the mechanics of the problem, or, more importantly, used shear strength (V_{true}) as the output variable instead of some mechanic-based definition of shear stress (v_n). It is essential to use dimensionless (e.g., aspect ratios) or mechanic-based normalized (e.g., stress) model parameters, otherwise, the model is not valid when applied to full-scale walls, since the parameters of the full-scale walls are not within the ranges that were used to calibrate the model. Note that the normalization referred here is based on the physics of the problem and is not the normalization or scaling concepts used in statistics, which are still important to do before training a model. Another limitation identified in models listed in **Table 2.4** is associated with the combination of the selected predicted variable and the error indicator used in the optimization process; which for these studies, results in minimizing the direct difference between the observed and the predicted shear strength values (i.e., not an error percentage). It is important to use a mechanics-based, normalized predicted variable (e.g., stress) when using error indicators such as the mean squared error (MSE), root mean squared error (RMSE), or the mean absolute error (MAE), otherwise, inconsistent error results are obtained. For example, the same error value for two cases (wall specimens) could represent a predicted shear strength with 10% error with respect to the experimental shear strength for one case, whereas it could represent a 100% error for a wall with a smaller shear strength. The coefficient of determination ($R^2 \in [0,1]$), which is another type of error indicator, compares a given model with the null model, i.e., the model that predicts the mean value of the data set used in the training process for any input;

therefore, it does not necessarily measure the goodness of fit. For instance, predictions for a model with a steep regression surface would tend to have a larger R^2 values but could be less precise than the prediction based on a model with a less steep regression surface with a smaller R2 (Barrett, 1974). The use of an error indicator that uses the true-to-predicted difference with respect to the true value might be helpful in these studies, but the issue of related results of reduced scale test specimens in the database to full-scale walls noted previously remains.

For ML models, it is common to use two data sets, a training set and a testing set. The training set is used to train (calibrate) the model and the testing set is used to verify that the trained model will perform very similarly when predicting unseen data (testing set). This means the error obtained when predicting values of the testing set must be similar to the error obtained when predicting the values of the training set. Although this comparison should be carefully addressed and ideally verified in terms of the error used in the optimization process and also in terms of other meaningful error indicators to demonstrate model robustness, often this added step is not properly considered. To help with this and avoid not noticing the problems the model might have, model performance should be reported including an error indicator that is well-known, such as mean and COV of the true-to-predicted ratio, assessed with several relevant parameters. Also, if a ML model is compared with other models (e.g., **Table 2.1**, **Table 2.2**), the comparison should also include results for other (properly trained) ML models to judge the performance of the proposed ML model. ML models are more complex than models developed based on a (simple) equation; therefore, better performance is expected.

Chapter 3. Framework to Define Performance Requirements

To address the limitations highlighted in the previous section, a systematic methodology is proposed to establish a relationship between the desired model complexity and its performance. In this study, this methodology is applied to the prediction of RC wall shear strength (V_{true}/V_{pred}), and the obtained target errors are expressed in terms of mean and coefficient of variance (COV) of the true-to-predicted ratio. It is relevant to highlight that the methodology could be applied to other problems (e.g., column shear strength, beam flexural strength, reinforcement development length, etc.). As detailed below, in addition to adopting the generic steps of ML, i.e., collection and preparation of data, feature selection, selection of ML algorithm, selection of model and hyper-parameters, model training, and model performance evaluation (Alzubi et al., 2018), this framework requires specific sub-steps such as defining relevant (starting) features based on the mechanics of the problem and addressing the issue of using reduced-scale tests to predict capacities of full-scale specimens, developing an iterative sensitivity analysis when a ML model is trained, and training Elastic Net Models (ENMs) using engineered features defined from the starting features.

3.1 Step 1: Collection and Preparation of Data

Data from a comprehensive database of RC wall tests, called UCLA-RC Walls Database (Abdullah, 2019; Abdullah and Wallace, 2020), was utilized in this study. The database contains detailed and parameterized information for over 1100 RC wall tests assembled from more than 250 test programs published in the literature, and it includes detailed and

parameterized information about the test specimen, tests setup, loading protocols, test results (e.g., backbone relations, failure modes), and analytically computed data (e.g., c, M_n, M_y, ϕ_n, ϕ_y, V_n). The reported failure modes are classified in the database as:

- Flexure failure modes, including bar buckling and concrete crushing, bar fracture, or global or local lateral instability.
- Shear failure modes, including diagonal tension, diagonal compression (web crushing), or shear sliding at the base.
- Flexure-shear failure modes, including yielding in flexure prior to failing in one of the shear failure modes.
- Lap-splice failure mode.

The authors of the database did their best to validate that the reported failure mode was consistent with the observed wall response and damage before reporting this information in the database. The availability of the detailed and parameterized information in the database enabled this study to assess the role of various parameters on wall shear strength.

A dataset of walls with reported flexure-shear, diagonal tension, or diagonal compression failure modes was obtained from the UCLA-RC Walls Database. Tests with incomplete information or test results were excluded. The reduced dataset included a total of 412 wall tests. The dataset was further refined and 79 wall tests were removed because of the next reasons:

- They either had artificial cracks for corrosion studies (6 tests, Zheng et al., 2015).

- The reported lateral load readings do not match the values in the respective figures (9 tests, Li and Li, 2002).
- The walls had non-symmetric cross-section shapes such as T-shape, L-shape, half barbell, and wing walls (20 tests).
- The specimens had a tested f'_c less than the limit of 20.7 MPa (3.0 ksi) given in ACI 318-19 Section 18.2.5 for special seismic systems (37 tests).
- The longitudinal reinforcement yielding stress f_y exceeded 100 ksi while f'_c was less than 5 ksi (7 tests).

Asymmetric walls were excluded because the number of walls with these cross-sectional shapes was low (20 walls) in comparison with the number of rectangular, barbell or flanged walls. This means it is possible to overlook the inherit differences of the different groups of asymmetrical walls if incorporating these little data into a much larger database of symmetric walls, because all of them are probably following the same general trends. In other words, the error of a model performance already calibrated with a large database of symmetric walls will likely not see a drastic increase when including little data of asymmetrical walls. Furthermore, when a shear strength model is proposed, it is expected it can be generalized to be applicable to asymmetrical walls as well, i.e., the unsymmetrical walls data can be part of the testing set. Based on the above filters, a final data set of 333 symmetric wall tests was obtained.

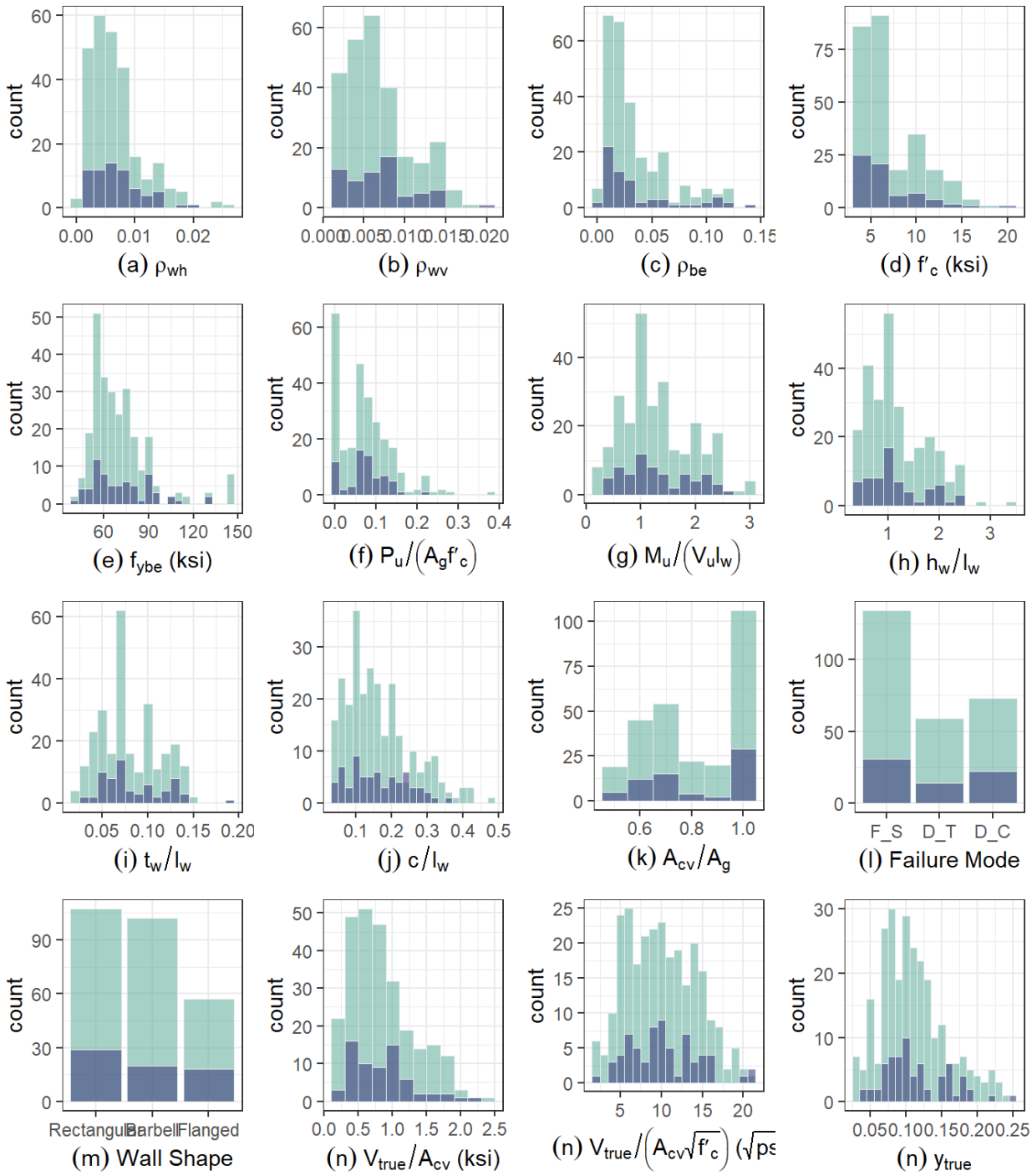

***Figure 3.1**: Histogram of relevant variables*

After a comprehensive and clean database was created for the study, a testing set to verify the performance of the models was created by randomly selecting 20% of the database of

333 wall tests, which resulted in 67 wall tests. The testing set is kept totally unknown for the models and is used only after the training process of the models is completed. **Figure 3.1** compares histograms for various database parameters of the entire dataset and the testing set, where f_c' is the specified compressive strength of concrete, ρ_{be} is the boundary region longitudinal reinforcement ratio, f_{ybe} is the specified yield strength of the boundary region longitudinal reinforcement, ρ_{wh} and f_{ywh} are the ratio and specified yield strength of the horizontal web reinforcement, respectively, ρ_{wv} and f_{ywv} are the ratio and specified yield strength of the vertical web reinforcement, respectively, P_u, M_u, and V_u are the factored (or test) axial load, moment, and shear, respectively, l_w is the wall length in the direction of the applied shear force, h_w is the total wall height, A_{be} is the cross-sectional area bounding the longitudinal reinforcement at a wall boundary, A_{cv} is the cross-sectional area bounded by the wall length and the web thickness (t_w), A_g is the cross-sectional gross area, c is the neutral axis depth, and y_{true} is the normalized shear stress (introduced later).

3.2 Step 2: Defining the ML Models and Features

This step involves first identifying the potentially relevant parameters based on literature review, which are then used to define the ML models. Considering a free body diagram of a wall with a diagonal crack that helps to identify all relevant parameters (**Figure 3.2**), it is possible to obtain the rough relationships shown in Eq. (3.1) through Eq. (3.6) between the main variables and shear strength.

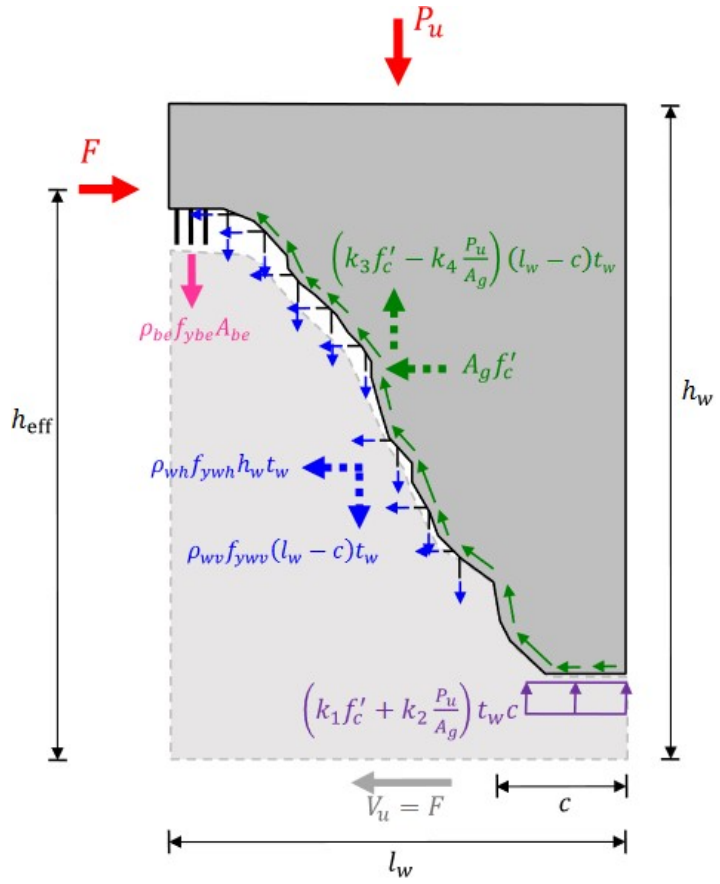

***Figure 3.2**: Free body diagram of RC shear wall with a diagonal crack*

$$V_u \overset{\propto}{\sim} A_g f_c' \tag{3.1}$$

$$V_u \overset{\propto}{\sim} \rho_{wh} f_{ywh} h_w t_w \tag{3.2}$$

$$V_u h_{\text{eff}} \overset{\propto}{\sim} \rho_{wv} f_{ywv} (l_w - c)^2 t_w \tag{3.3}$$

$$V_u h_{\text{eff}} \overset{\propto}{\sim} \rho_{be} f_{ybe} A_{be} l_w \tag{3.4}$$

$$V_u h_{\text{eff}} \overset{\propto}{\sim} \left(f_c' + \frac{P_u}{A_g}\right) t_w c^2 \tag{3.5}$$

$$V_u h_{\text{eff}} \overset{\propto}{\sim} \left(f_c' - \frac{P_u}{A_g}\right) t_w (l_w - c)^2 \tag{3.6}$$

Non-dimensional parameters are used because it makes the coefficients defined from the training process to be weights of each parameter, without physical or mechanical interpretation. In accordance with the literature review, the following 10 variables are selected and are named as the "starting features".

$$x_1 = \rho_{wh} \frac{f_{ywh}}{f_c'} \tag{3.7}$$

$$x_2 = \rho_{wv} \frac{f_{ywv}}{f_c'} \tag{3.8}$$

$$x_3 = \rho_{wbe} \frac{f_{ybe}}{f_c'} \tag{3.9}$$

$$x_4 = 1 + \frac{P_u}{A_g f_c'} \tag{3.10}$$

$$x_5 = \frac{c}{l_w} \tag{3.11}$$

$$x_6 = \frac{M_u}{V_u l_w} \tag{3.12}$$

$$x_7 = \frac{t_w}{l_w} \tag{3.13}$$

$$x_8 = \frac{t_w}{h_w} \tag{3.14}$$

$$x_9 = \frac{h_w}{l_w} \tag{3.15}$$

$$x_{10} = \frac{A_{be}}{A_g} \tag{3.16}$$

The predicted variable is the normalized shear strength defined as:

$$y = \frac{V_{true}}{A_g f_c'} \tag{3.17}$$

These starting features and the predicted variable can actually be identified by making the left side in Eq. (3.1) through Eq. (3.6) to be the normalize shear strength $V_u/(A_g f_c')$ and by applying reasonable approximations in some cases (e.g., considering c as a fraction of l_w, neglecting constants because the model calibration will handle that), as shown below.

$$\frac{V_u}{A_g f_c'} \underset{\sim}{\propto} 1 \tag{3.17}$$

$$\frac{V_u}{A_g f_c'} \underset{\sim}{\propto} \frac{\rho_{wh} f_{ywh}}{f_c'} \frac{h_w}{l_w} \tag{3.18}$$

$$\frac{V_u}{A_g f_c'} \underset{\sim}{\propto} \frac{\rho_{wv} f_{ywv}}{f_c'} \frac{l_w}{h_{\text{eff}}} \tag{3.19}$$

$$\frac{V_u}{A_g f_c'} \underset{\sim}{\propto} \frac{\rho_{be} f_{ybe}}{f_c'} \frac{c}{l_w} \frac{l_w}{h_{\text{eff}}} \tag{3.20}$$

$$\frac{V_u}{A_g f_c'} \underset{\sim}{\propto} \left(1 + \frac{P_u}{A_g f_c'}\right) \frac{c}{l_w} \frac{l_w}{h_{\text{eff}}} \tag{3.21}$$

$$\frac{V_u}{A_g f_c'} \underset{\sim}{\propto} \left(1 - \frac{P_u}{A_g f_c'}\right) \frac{A_{be}}{A_{cv}} \frac{l_w}{h_{\text{eff}}} \tag{3.22}$$

Between $\left(1 + P_u/(A_g f'_c)\right)$ and $\left(1 - P_u/(A_g f'_c)\right)$, only one is considered because they are related to the practically the same parameters in Eq. (3.5) and Eq. (3.6), and also in Eq. (3.21) and Eq. (3.22) (again, c can be considered as a fraction of l_w), and because the presence of a constant (i.e., "intercept" or equivalent) in the calibration process would suggest dropping one of them for being linearly dependent of the other.

The height of the wall used to define the effective flange width according to ACI 318-19 Section 18.10.5.2 was estimated as $h_w \approx h_{\text{eff}}/0.7$, where h_{eff} (effective height) corresponds

to the shear span, defined as M_u/V_u. Abdullah and Wallace (2021) show that there is no significant increase in the shear strength of walls with small barbell column at the boundary regions, and is well established that flanged walls have a larger shear strength (Gulec and Whittaker, 2011; Kassem, 2015; Kim and Park, 2020). Because $A_g = A_{cv}$ for rectangular walls, $A_g \approx A_{cv}$ for barbell walls with barbell column at the boundary regions, and $A_g > A_{cv}$ for flanged walls, the cross-sectional area A_g is used instead of A_{cv} when associated with f_c'.

Four different feature matrices are defined:

- The first feature matrix, $\mathbf{X}$, contains the 10 starting features defined in Eq. (4.7) through (4.16) and, therefore, is a matrix with 10 columns.
- The next feature matrix, $\widetilde{\mathbf{X}}$, contains 140 features because the following 14 functions were applied to the 10 starting features: identity function, $(.)^{-1}$, $(.)^{2}$, $(.)^{-2}$, $(.)^{1/2}$, $(.)^{-1/2}$, $(.)^{3}$, $(.)^{-3}$, $(.)^{1/3}$, $(.)^{-1/3}$, exp(.), exp(-.), ln(.), and $-\ln(1+.)$.
- Feature matrix $\mathbf{X}_{\text{poly}}$ has 285 features that are obtained by combining the 10 starting features into all possible multiplications a cubic polynom has.
- Feature matrix $\widetilde{\mathbf{X}}_{\text{poly}}$ has 679 features that are obtained by combining the 14 more significant features of the $\widetilde{\mathbf{X}}$ matrix into all possible multiplications a cubic polynom has.

Cubic polynoms were used because Eq. (3.17) through Eq. (3.22) can be formed by multiplying up to 3 starting features on the right side. Also, to reduce skewness or highlighting trends, other variations of the output variable y (see Eq. (3.17)) are defined as

$\sqrt[3]{y}$ and $\ln(y)$. The 14 more significant features of $\widetilde{\mathbf{X}}$ are obtained after performing the sensitivity analysis (explained later) for ENM2 (introduced later in **Table 3.1**).

The starting features $x_1, \ldots, x_{10}$ (Eqs. (4.7) to (4.16)) will be the input parameters of one or more complex ML models, which will be predicting the normalized shear stress y (Eq. (4.17)). The selected complex ML models for this study are the Artificial Neural Network (ANN) and Random Forest (RF) Regression because they are applicable for this study (the predicted parameter is a continuous variable), and because they are well known models that are not complicated to implement in programming languages (e.g., Matlab, R, Python, which have various built-in functions to simplify their implementation). The starting and engineered features are used to create a suite of Elastic Net Models (ENMs). In this case, a total of 10 ENMs are defined (see **Table 3.1**).

***Table 3.1**: Elastic Net Models definition*

Model	Short Reference	Long Reference[(a)]
ENM1	$y \sim \boldsymbol{X}$	$y_j \sim N(\mu_j, \sigma)$, $\mu_j = \boldsymbol{x_j'}\beta$, $\forall j \epsilon \{1,2, \ldots n\}$
ENM2	$y \sim \widetilde{\boldsymbol{X}}$	$y_j \sim N(\mu_j, \sigma)$, $\mu_j = \widetilde{\boldsymbol{x}}_{\boldsymbol{j}}'\beta$, $\forall j \epsilon \{1,2, \ldots n\}$
ENM3	$\sqrt[3]{y} \sim \widetilde{\boldsymbol{X}}$	$\sqrt[3]{y_j} \sim N(\mu_j, \sigma)$, $\mu_j = \widetilde{\boldsymbol{x}}_{\boldsymbol{j}}'\beta$, $\forall j \epsilon \{1,2, \ldots n\}$
ENM4	$\ln(y) \sim \widetilde{\boldsymbol{X}}$	$\ln(y_j) \sim N(\mu_j, \sigma)$, $\mu_j = \widetilde{\boldsymbol{x}}_{\boldsymbol{j}}'\beta$, $\forall j \epsilon \{1,2, \ldots n\}$
ENM5	$y \sim \boldsymbol{X_{poly}}$	$y_j \sim N(\mu_j, \sigma)$, $\mu_j = \boldsymbol{x'_{poly_j}}\beta$, $\forall j \epsilon \{1,2, \ldots n\}$
ENM6	$\sqrt[3]{y} \sim \boldsymbol{X_{poly}}$	$\sqrt[3]{y_j} \sim N(\mu_j, \sigma)$, $\mu_j = \boldsymbol{x'_{poly_j}}\beta$, $\forall j \epsilon \{1,2, \ldots n\}$
ENM7	$\ln(y) \sim \boldsymbol{X_{poly}}$	$\ln(y_j) \sim N(\mu_j, \sigma)$, $\mu_j = \boldsymbol{x'_{poly_j}}\beta$, $\forall j \epsilon \{1,2, \ldots n\}$
ENM8	$y \sim \widetilde{\boldsymbol{X}}_{\boldsymbol{poly}}$	$y_j \sim N(\mu_j, \sigma)$, $\mu_j = \widetilde{\boldsymbol{x}}'_{\boldsymbol{poly_j}}\beta$, $\forall j \epsilon \{1,2, \ldots n\}$
ENM9	$\sqrt[3]{y} \sim \widetilde{\boldsymbol{X}}_{\boldsymbol{poly}}$	$\sqrt[3]{y_j} \sim N(\mu_j, \sigma)$, $\mu_j = \widetilde{\boldsymbol{x}}'_{\boldsymbol{poly_j}}\beta$, $\forall j \epsilon \{1,2, \ldots n\}$
ENM10	$\ln(y) \sim \widetilde{\boldsymbol{X}}_{\boldsymbol{poly}}$	$\ln(y_j) \sim N(\mu_j, \sigma)$, $\mu_j = \widetilde{\boldsymbol{x}}'_{\boldsymbol{poly_j}}\beta$, $\forall j \epsilon \{1,2, \ldots n\}$

[(a)] $\boldsymbol{n}$ is te number of features the model uses

ENMs (Zou and Hastie, 2005) are a simple and more interpretable ML model type because they are a penalized linear modeling approach with a mixture of Ridge Regression (Hoerl and Kennard, 1970) and Least Absolute Shrinkage and Selection Operator (LASSO) regression (Tibshirani, 1996). Ridge regression reduces the impact of collinearity on the features, whereas LASSO reduces the dimension of the problem by shrinking some of the coefficients to zero (less significant parameters). ENMs have two hyper-parameters: (a) $\lambda > 0$ is the complexity parameter that controls the weight of the penalization factors; (b) $\alpha \in [0,1]$ is the compromise between Ridge ($\alpha = 0$) and LASSO ($\alpha = 1$). Small λ values can result in an overfitted model (too complex), whereas high λ values can result in an underfitted model (too simple).

3.3 Step 3: Sensitivity Analysis and Selection of Hyper-Parameters

For the 12 ML models defined in the previous step (1 ANN, 1 RF Regression, and 10 ENMs), a sensitivity analysis on their main hyper-parameters is performed to assess the underfitting-overfitting trade-off. The implemented sensitivity analysis (algorithm shown in **Figure 3.3**) consists of using an iterative k-fold Cross-Validation (CV) method with $N_{iter} = 100$ iterations and $k = 4$ folds. K-fold CV is useful for data scientists when dealing with small databases (a few thousands of data samples). Iterations are included because in Structural Engineering the database are typically even smaller (just a few tens or hundreds). **Figure 3.3** shows that each iteration requires randomly dividing the training set into k folds and performing a k-fold CV analysis for all possible hyper-parameter configurations. Once the sensitivity analysis is completed, $k \times N_{iter} = 4 \times 100 = 400$ RMSE values are computed for

each configuration of hyper-parameters. Then, for each of these configurations, the mean and standard deviation of the computed RMSE are obtained. Based on the lower mean error and lower standard deviation, the optimal hyper-parameters are selected.

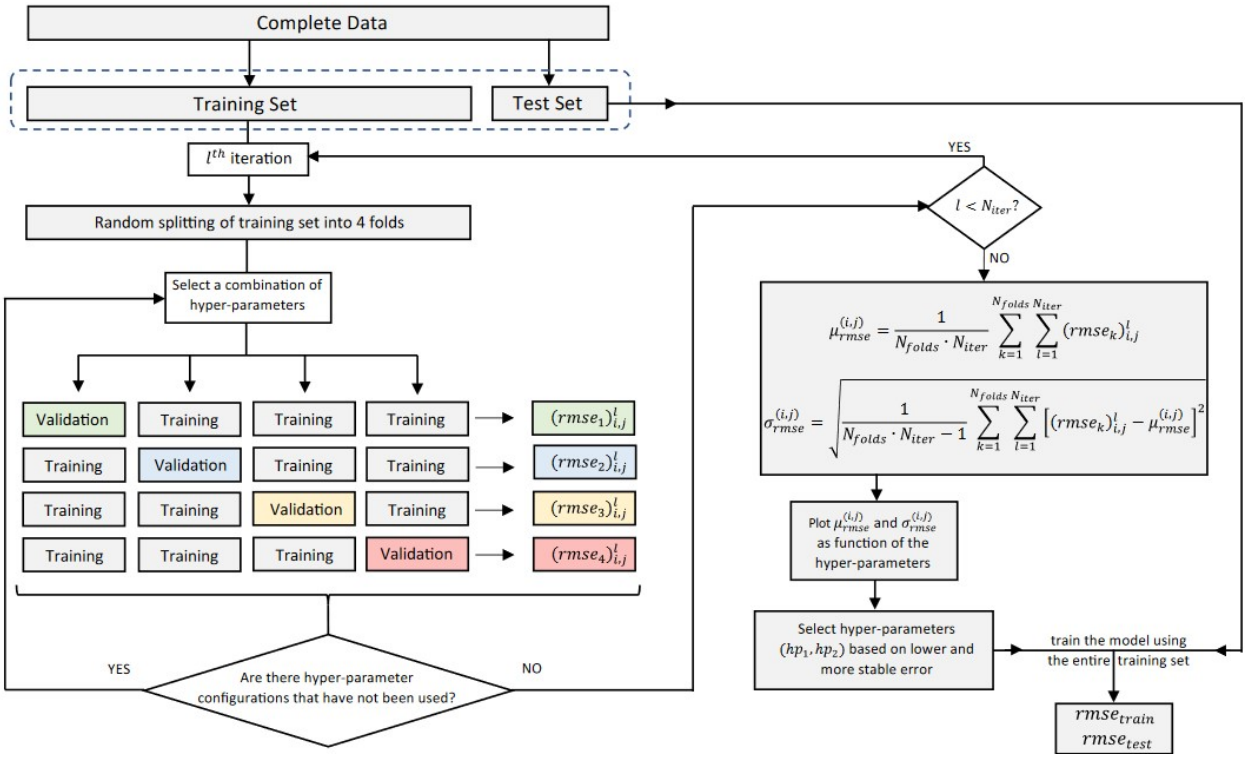

***Figure 3.3**: Sensitivity analysis algorithm to select the optimum set of hyper-parameter values*

3.3.1 ANN

The main hyper-parameters for an ANN model are the number of hidden layers and neurons per layer. General rules regarding these hyper-parameters depend on the size of the database or on the number of input features. Suggested rules can be found in the literature (Chen et al. 2018; Moradi and Hariri-Ardebili, 2019), which are covered by the ranges selected for the sensitivity analysis:

- The number of hidden layers was varied from 1 to 6

- The number of neurons per hidden layer was varied from 1 to 30. For all ANN trained in the sensitivity analysis, all hidden layers were implemented with the same number of neurons.

The results of the sensitivity analysis are shown in **Figure 3.4**. The best ANN configuration for each number of hidden layers considered is indicated with a blue dashed line. From these, the optimum ANN is the one with 4 hidden layers and 30 neurons in each layer because it has the minimum mean error (MIN RMSE) and the lowest standard deviation (SD). All previous configurations (same 4 hidden layers, but fewer neurons) show a large range of similar and stable results in terms of both mean error and SD.

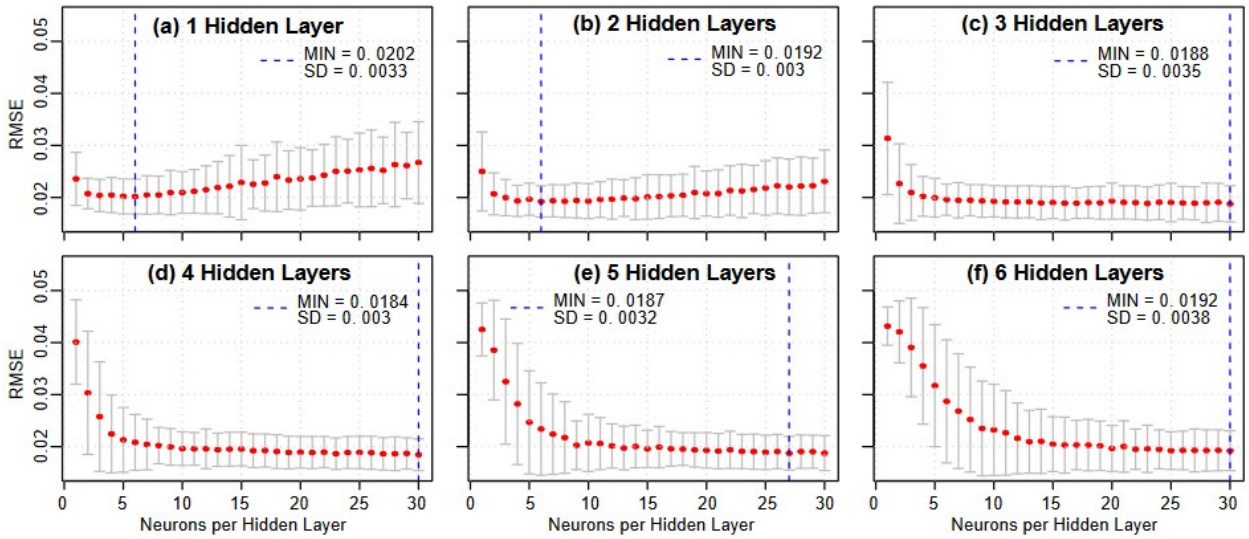

***Figure 3.4**: Sensitivity analysis to define the optimum ANN configuration*

3.3.2 RF Regression

A large number of decision trees (1000 trees) is selected to ensure that a stable error level is reached. For this study, the error became stable at around 300 trees. There are two other hyper-parameters that could have an impact on the performance of the model (Zhang and Ma, 2012): (1) the number of variables (selected among all the features) in each cell ($mtry$),

and (2) the pre-specified threshold of maximum observation per cell ($nodesize$). For classification problems, $mtry$ is lower than p and is commonly taken as $\sqrt{p}$, where p is the number of input variables. For regressions, $mtry$ is commonly taken as one-third of the number of samples in the dataset. Although there are suggested values for $mtry$, RFs are not too sensitive to $mtry$ (Zhang and Ma, 2012). In the sensitivity analysis, values of $mtry$ from both rules are used, i.e., $mtry$ values smaller than p and values around one-third of the training and complete sets. As for the $nodesize$ parameter, it is thought that having large trees (associated with small $nodesize$ values) always produces better results (Breiman, 2001). However, a recent study (Segal and Xiao, 2011) shows that there could be cases where large trees overfit the model. Although this is probably not the case because of the database size, the sensitivity analysis covered a broad range of $nodesize$ values to verify the behavior.

Figure 3.5 shows that the RF results are only slightly sensitive to $mtry$, and that having large trees (small $nodesize$) results in low errors (RMSE). The stability of the results for $mtry$ values of 50, 90, and 130 is reached at smaller $nodesize$ values. **Figure 3.5** also shows that the optimal RF model is obtained for the case with $mtry = 50$ and $nodesize = 1$ (minimum mean and SD).

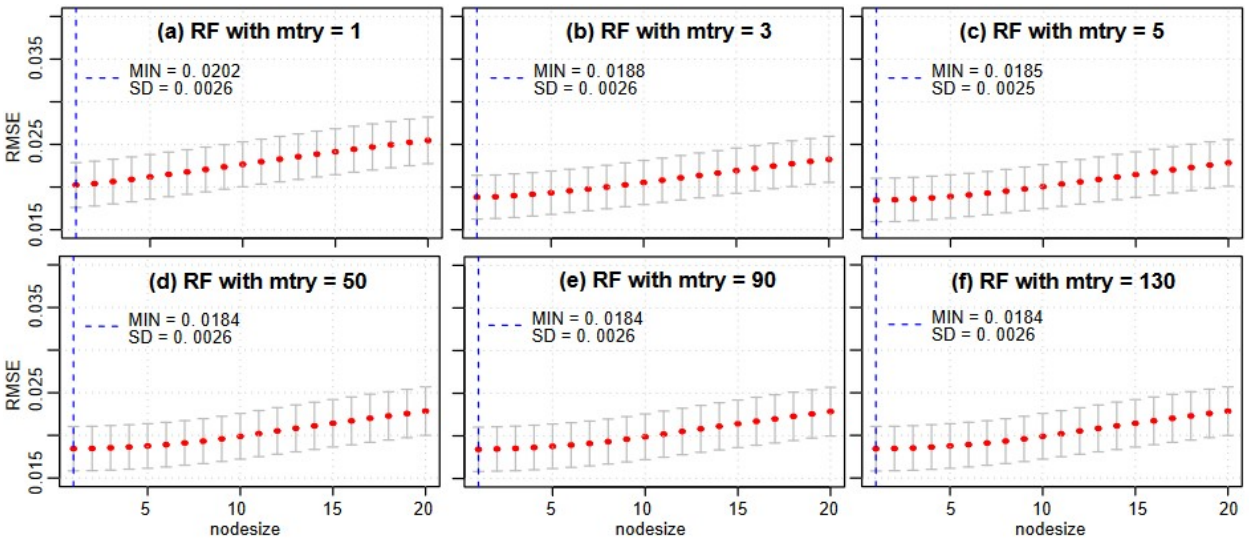

***Figure 3.5**: Sensitivity analysis to define the optimum RF Regression configuration*

3.3.3 ENMs

The same sensitivity analysis approach was implemented for each of the 10 ENMs defined in **Table 3.1**. The $\log(\lambda)$ values ranged from -12 to -2, while the α values were 1.0, 0.8, 0.6, 0.4, 0.2, and 0.0. As an example, **Figure 3.6** presents the sensitivity analysis results for ENM6.

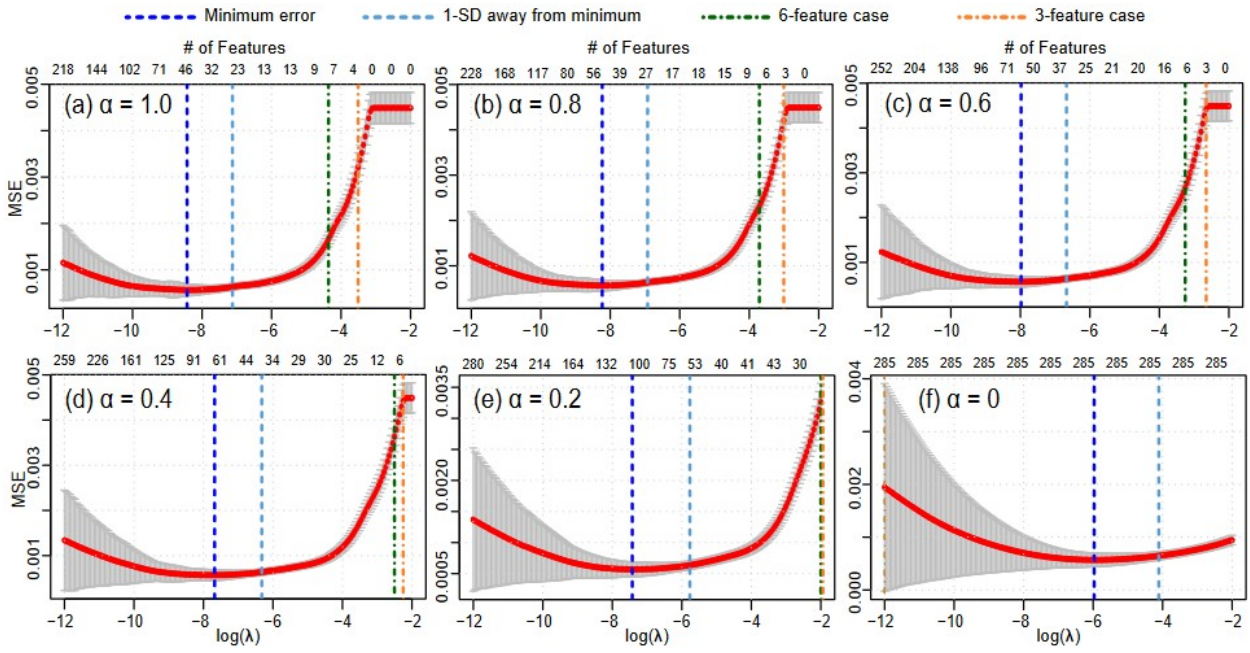

***Figure 3.6**: Sensitivity analysis for ENM6 model: $\sqrt[3]{y_j} \sim N(\mu_j, \sigma)$, $\mu_j = \boldsymbol{x}'_{poly_j}\beta$*

For the ENMs, in addition to the optimum set of hyper-parameters, hyper-parameter sets associated with different underfitting levels are defined. In this study, the three underfitting levels selected include:

- One in which error corresponds to the error that is one standard deviation away from the error of the optimum model ("1-SD away" version).
- An underfitted model that uses six features only ("6-feature" version).
- An underfitted model that uses three features only ("3-feature" version).

The reason for selecting these underfitting levels is because a model with a complexity-level applicable for a code-oriented shear strength equation is of particular interest in this study.

Figure 3.7 presents the mean errors obtained from the sensitivity analysis of all 10 ENM models and demonstrates that regardless of the value of α considered (compromise between Ridge and LASSO), there is a λ value where practically the same optimum error is reached.

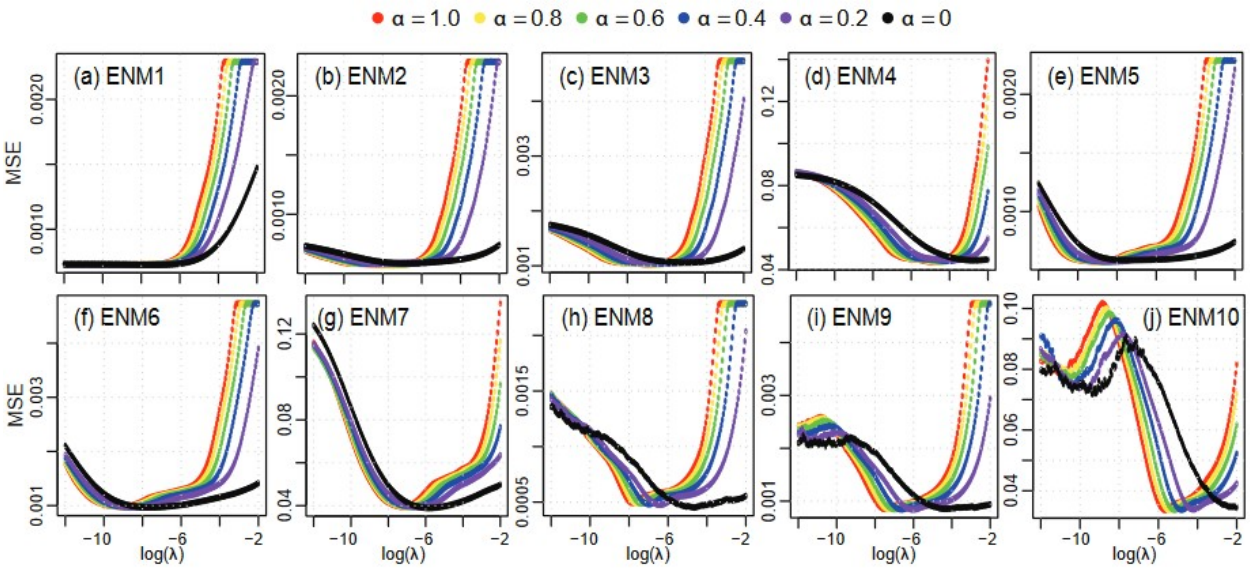

***Figure 3.7**: Mean of MSE obtained from the sensitivity analysis of all ENM models*

Figure 3.8 shows that the number of coefficients shrinks faster for higher α values (as expected). More importantly, it indicates that it is difficult for the models to exclude features to reach the defined underfitted levels of interest (models with only between 3 and 6 features) for lower α values. Because of these reasons, for each ENM in this study, the selected optimum hyper-parameter configuration is $\alpha = 1$ and its associated corresponding λ optimum value, i.e., all selected ENMs are LASSO models.

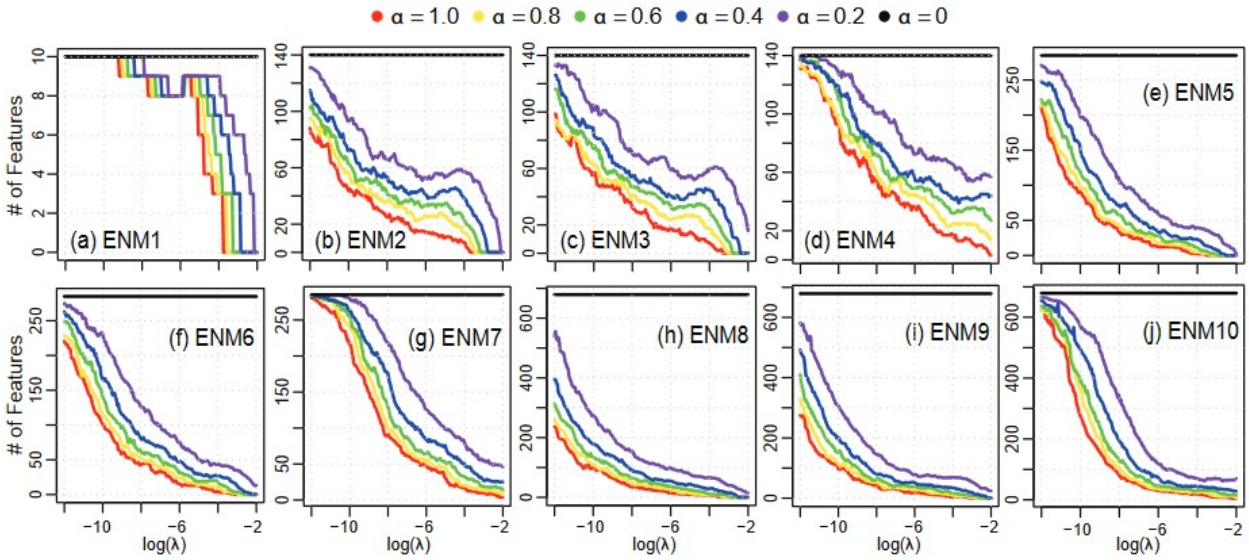

***Figure 3.8**: Mean non-zero coefficients obtained from the sensitivity analysis of all ENM models*

Therefore, from each ENM, one optimum version is selected along with three underfitted versions. As an example, the blue, green, and orange vertical dashed lines in **Figure 3.6(a)** indicate the λ values associated with the selected underfitting levels for the LASSO model #6, in addition to the optimum version indicated with a black dashed vertical line. The λ value associated with each underfitted level for all ten LASSO models is selected in the same manner.

3.4 Step 4: Training, Verification, and Selection of Best Performing Models

All the models are trained with the selected sets of hyper-parameters using the training set. This results in 42 trained ML models:

- Optimum ANN (1 model)
- Optimum RF Regression (1 model)
- Optimum version of each LASSO (10 models)
- The 1-SD away version of each LASSO (10 models)
- The 6-feature version of each LASSO (10 models)
- The 3-feature version of each LASSO (10 models)

The best performing model of each of these groups are selected. The acceptability criterion adopted in this study defines a model as acceptable when the errors of the training and testing sets are both within a defined margin away from the converging error, which is $\pm 20\%$ for the optimum models and $\pm 10\%$ for the underfitted models. The converging error is taken as the average of the training and testing errors. Optimum models have a larger margin because they are right on the balanced point between the underfitted and overfitted models, and thus they have the potential to "keep learning" (i.e., re-adjust their coefficients a bit) if new data are provided for training. On the other hand, by definition, underfitted models are not capable of capturing enough details of the process they are representing, and they follow more rough trends identified from the data, which is the reason for the stricter margin around the converging error. More details on this and the definition of the acceptability criterion are given in Section 3.4.3.

3.4.1 Optimum ANN and RF Regression

The complex ML models, ANN and RF, are trained using the configurations based on the selected optimum hyper-parameters. Although the training process was based on the RMSE between y_{true} and y_{pred}, see **Figure 3.9(a)** and **Figure 3.10(a)**, similar model performance (i.e., training and testing errors within $\pm 20\%$ of the converging error) is obtained when predicting values from the training and testing sets in terms of the mean and COV of V_{true}/V_{pred}, as shown in **Figure 3.9(b)** and **Figure 3.9(c)** for the optimum ANN and in **Figure 3.10(b)** and **Figure 3.10(c)** for the optimum RF. **Figure 3.9(c)** and **Figure 3.10(c)** also show that the predictions for the training and testing sets have the same distribution shapes.

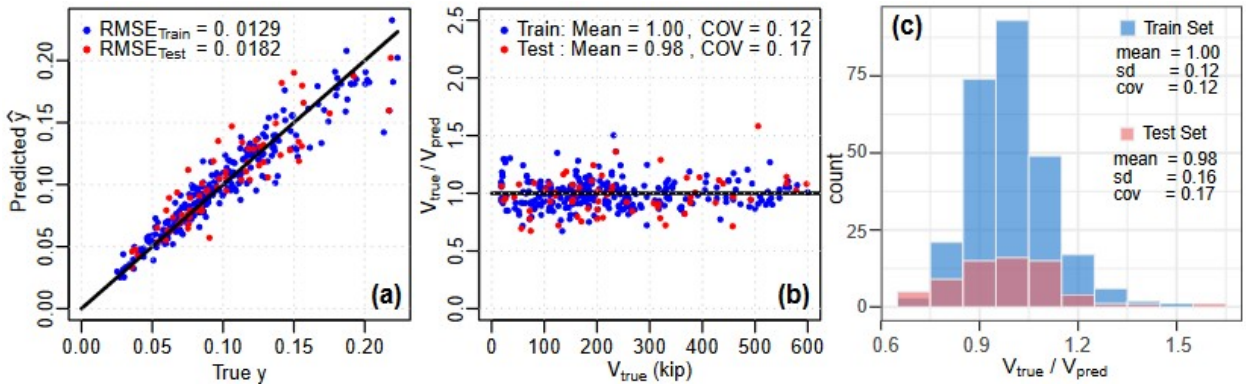

***Figure 3.9**: Performance of selected ANN on the training and testing sets in terms of: (a) normalized shear stress; (b) V_{true}/V_{pred} vs V_{true}; (c) distributions of V_{true}/V_{pred}. (Note: 1 kip = 4.448 kN)*

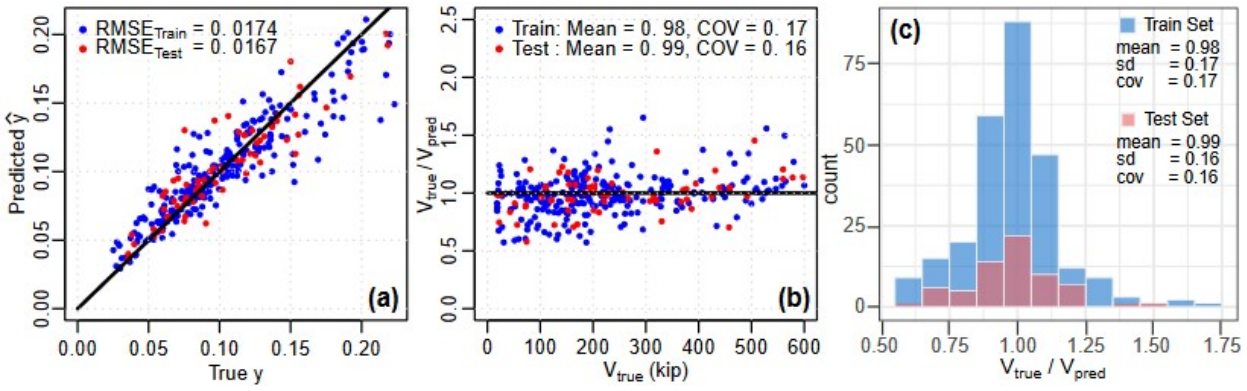

***Figure 3.10**: Performance of selected RF Regression on the training and testing sets in terms of: (a) normalized shear stress; (b) V_{true}/V_{pred} vs V_{true}; (c) distributions of V_{true}/V_{pred}. (Note: 1 kip = 4.448 kN)*

3.4.2 Optimum and Underfitted LASSO Models

All 40 LASSO models selected (4 from each ENM defined in **Table 3.1**) are trained using only the features associated with each selected hyper-parameter configuration. This means that the 40 models are linear regressions with different engineered features. **Table 3.2** through **Table 3.5** show the error of the 40 models (sorted from smaller to larger converging error) when predicting values from both the training and testing sets and include a column that to show the acceptability of the model based on the criterion defined earlier. The error is expressed in terms RMSE between y_{true} and y_{pred}. As can be seen from these tables, there are some model versions that do not meet the acceptability criterion. For each complexity level (i.e., LASSO version), the model meeting the acceptability criterion (among those associated with the same complexity level) and with the smaller converging error was selected. A total of 4 ENMs are selected, which are highlighted in yellow in **Table 3.2**, **Table 3.3**, **Table 3.4**, and **Table 3.5**): the best optimal LASSO model, the best 1-SD away LASSO model, the best 6-feature LASSO model, and the best 3-feature version. The same result is presented graphically in **Figure 3.11**. Note that the optimum LASSO model #9 and #10 have large errors, which is attributable to the implemented automated selecting of hyper-

parameters, which for this case are just a little past the underfitted-overfitted sweet point; this is part the reason for which including the 1-sd away (especially for those LASSO models that are more complex).

***Table 3.2**: Optimum LASSO models*

Model	RMSE (train)	RMSE (test)	RMSE (conv)	Passes?
6	**0.0117**	**0.0137**	**0.0127**	**Yes**
5	0.0114	0.0167	0.0140	Yes
7	0.0112	0.0177	0.0145	No
3	0.0131	0.0181	0.0156	Yes
8	0.0120	0.0207	0.0163	No
4	0.0148	0.0186	0.0167	Yes
2	0.0134	0.0202	0.0168	No
1	0.0197	0.0216	0.0207	Yes
9	0.0122	0.0631	0.0377	No
10	0.0122	0.3469	0.1795	No

***Table 3.3**: 1-sd away LASSO models*

Model	RMSE (train)	RMSE (test)	RMSE (conv)	Passes?
9	**0.0137**	**0.0147**	**0.0142**	**Yes**
6	0.0140	0.0175	0.0158	No
10	0.0139	0.0185	0.0162	No
3	0.0137	0.0189	0.0163	No
5	0.0146	0.0181	0.0164	No
4	0.0144	0.0183	0.0164	No
2	0.0138	0.0199	0.0169	No
7	0.0140	0.0213	0.0176	No
8	0.0145	0.0244	0.0195	No
1	0.0203	0.0219	0.0211	Yes

***Table 3.4**: 6-feature LASSO models*

Model	RMSE (train)	RMSE (test)	RMSE (conv)	Passes?
3	0.0153	0.0194	0.0174	No
9	0.0152	0.0201	0.0176	No
4	**0.0164**	**0.0190**	**0.0177**	**Yes**
8	0.0147	0.0209	0.0178	No
10	0.0164	0.0198	0.0181	Yes
6	0.0203	0.0212	0.0207	Yes
1	0.0203	0.0219	0.0211	Yes
5	0.0200	0.0222	0.0211	Yes
7	0.0220	0.0233	0.0226	Yes
2	0.0213	0.0240	0.0226	Yes

***Table 3.5**: 3-feature LASSO models*

Model	RMSE (train)	RMSE (test)	RMSE (conv)	Passes?
10	**0.0192**	**0.0218**	**0.0205**	**Yes**
8	0.0184	0.0256	0.0220	No
4	0.0218	0.0237	0.0227	Yes
9	0.0208	0.0291	0.0250	No
2	0.0245	0.0292	0.0268	Yes
3	0.0249	0.0288	0.0268	Yes
1	0.0273	0.0289	0.0281	Yes
5	0.0264	0.0310	0.0287	Yes
6	0.0279	0.0320	0.0300	Yes
7	0.0276	0.0360	0.0318	No

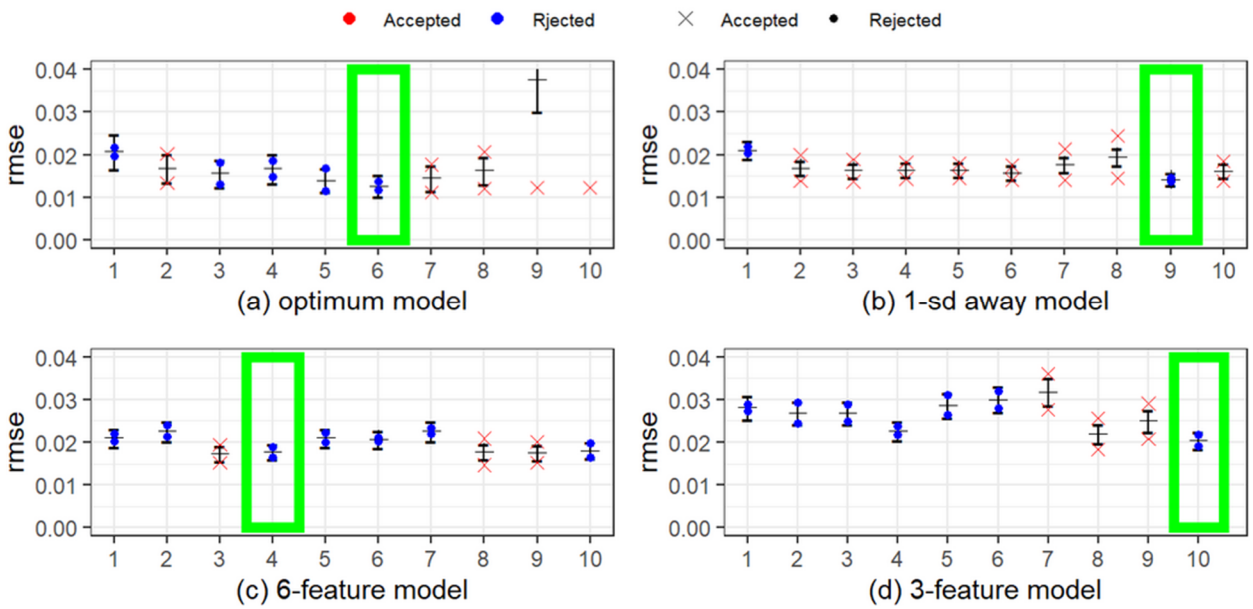

***Figure 3.11**: Error of each LASSO model version – accepted vs rejected models*

Figure 3.12 shows the similar behavior of these four trained LASSO models when predicting values from both the training and testing sets. In this figure, the error is expressed in terms RMSE between y_{true} and y_{pred}, and in terms of mean and COV of the V_{true}/V_{pred} ratio and its distribution. It can be seen that the errors go up and the distributions of the y_{true}/y_{pred} become wider as the complexity level of the models is relaxed, but they maintain the shape of a normal distribution. Nonetheless, the errors obtained for the 6-feature and 3-feature linear regressions are still very low when compared against the results of previous proposed equations (see **Table 2.3**). In this comparison, it is important to consider the size of the database, the ranges its parameters cover, and that for the database used in this study, all wall tests were reported to have failed in shear.

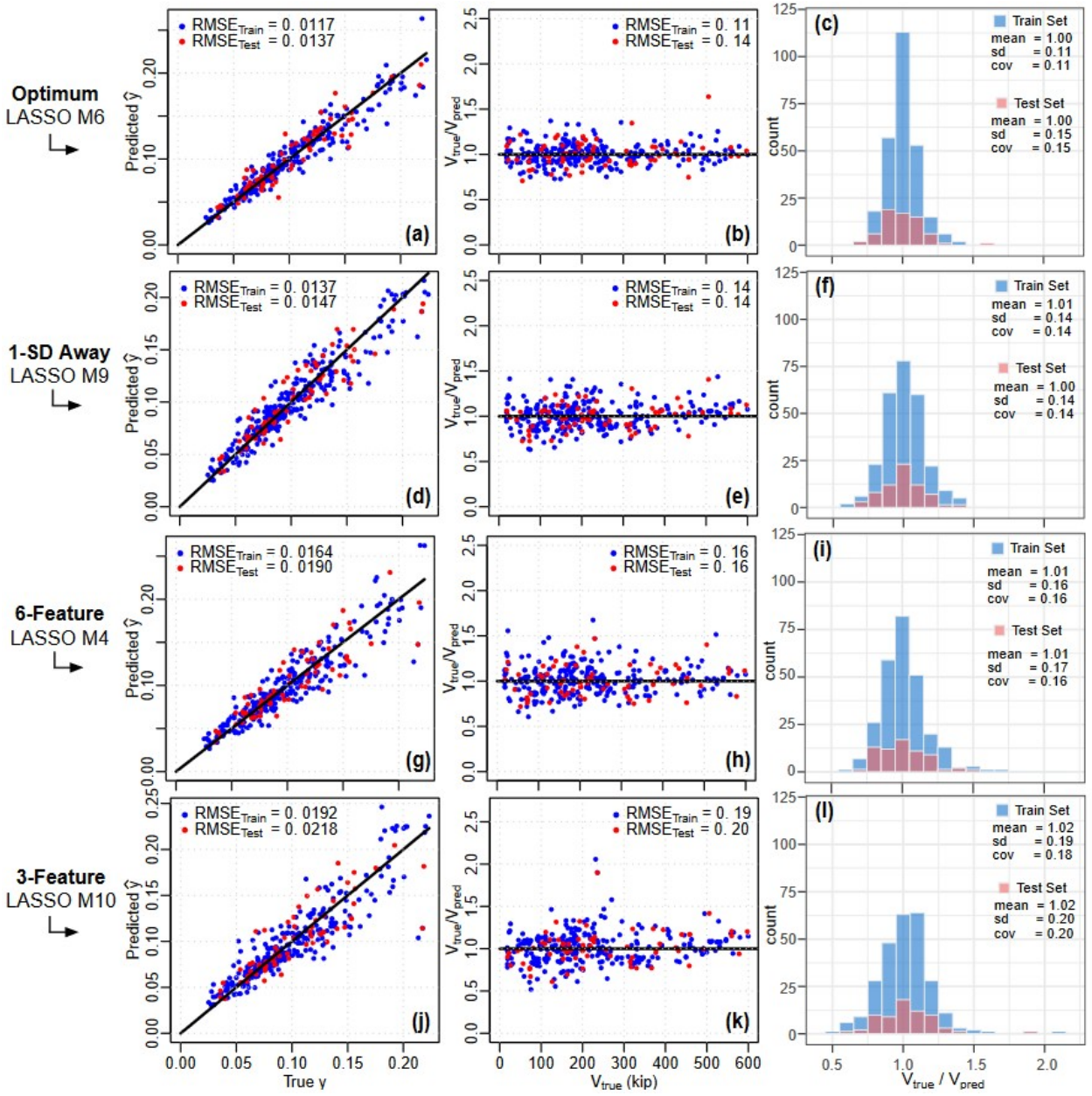

***Figure 3.12**: Performance LASSO models on the training and testing sets in terms of: (a, d, g, j) normalized shear stress; (b, e, h, k) V_{true}/V_{pred} vs V_{true}; (c, f, i, l) distributions of V_{true}/V_{pred}. (Note: 1 kip = 4.448 kN)*

Another way to verify the performance of the models is to plot the learning curves of the 6 selected models computed using the training and testing sets (**Figure 3.13**). Learning curves also provide a tool to understand how the models would behave if new data are available. The learning curves, similar to what was done for the sensitivity analysis, are obtained using

iterations; the training and testing errors associated with each size of the training dataset are obtained as the average of 50 RMSE values coming from models trained using 50 different subgroups of the same size randomly extracted from the training set. Except for the RF regression, all the learning curves shown in **Figure 3.13** have a gap between the training and testing curves and reach a plateau when approaching the use of 100% of the training set. Because of this, the error obtained when including future data in the training set to retrain these same models (i.e., keeping the same hyper-parameters and relevant features already identified) should fall between the training and testing errors but closer to the training error. On the other hand, the training and testing learning curves for the RF regression are very close to each other due to selecting a very large number of trees, but it can still be seen that the slope of the learning curves are becoming less steep (reaching a plateau) when the training size becomes larger. This means that, when providing additional data for training the same RF regression model (i.e., same hyper-parameters and input features), the converging error would get closer to that plateau, resulting in a slightly lower error.

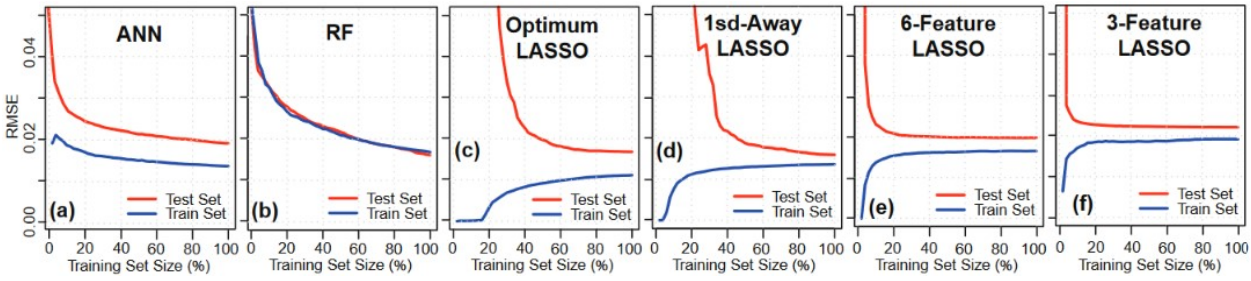

***Figure 3.13**: Performance LASSO models on the training and testing sets in terms of: (a, d, g, j) normalized shear stress; (b, e, h, k) V_{true}/V_{pred} vs V_{true}; (c, f, i, l) distributions of V_{true}/V_{pred}. (Note: 1 kip = 4.448 kN)*

3.4.3 Definition of the Acceptable Bandwidth Around the Converging Error

Part of the understanding of how well a model is working and if it is meeting the expectations, comes from analyzing the converging error. The proposed framework results in having optimum models which training and testing errors have a small difference between them. However, judgment is required to define *"how small"* is acceptable. The experience of the authors comes from reviewing and understanding how existing models work and the error they have (see Section 3). After reviewing several studies addressing both simple models (see **Table 2.1**, **Table 2.2**, and **Table 2.3**) and complex ML models (see **Table 2.4**), and analyzing several relevant existing models against the comprehensive database collected for this study (see **Figure 4.2**), it is known that there are equations than can get a true-to-predicted mean ratio very close to 1.0 with a COV as low as 0.30. Therefore, when training a much more complex model, it is desired and expected to obtain a converging error that is much lower than the ones obtained by the best existing equations, and of course it is also expected that both training and testing error are smaller than the errors obtained by the best existing equations.

The errors of the several existing models when predicting the values of the common comprehensive database also give a sense of how much could be an acceptable low range around the converging error. However, it was already introduced another ML tool that provides valuable information regarding this: the "learning curves". The learning curve tells how fast the model learns; if the model sees a very small portion of the training set, it will not learn enough to make good predictions of the testing set, but when the model has seen almost the entire training set, it is expected to be already producing good predictions of the testing set. A learning curve has a particular shape if the model is underfitted, overfitted, or

optimum (balanced), as conceptually shown in **Figure 3.14** for regression models. It is relevant to add that reaching a plateau for both training and testing error learning curves before reaching the 100% of the training set is important, otherwise, the model is still capable of learning.

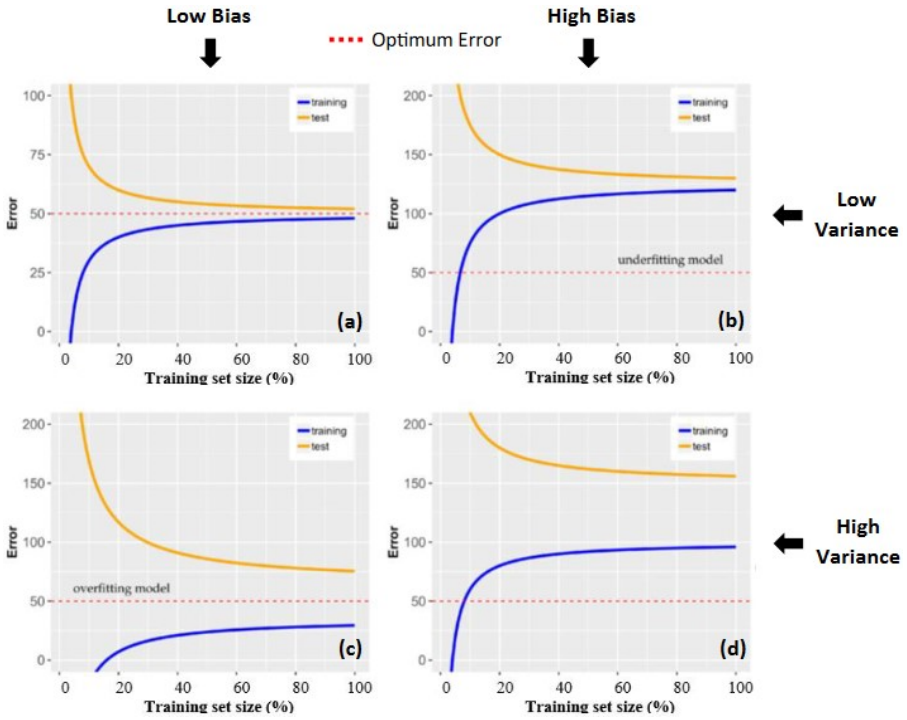

***Figure 3.14**: Typical learning curve shapes for Regression Models* (Emmert-Streib and Dehmer, 2019)

In addition to the understanding of how existing models behave, it is crucial that the framework requires training not only one, but a group of models to its optimum version along with underfitted versions of them as well. In this study, 12 optimum ML model versions were selected and trained (1 ANN, 1 RF Regression, and 10 LASSO models). Also, three underfitted versions for each LASSO model was defined, which means there are three groups of 10 underfitted LASSO model versions. The group of optimum models reached training errors (in terms of COV) between 0.11 and 0.13 for almost all of them (except for two of the

simplest LASSO models) and reached testing errors between 0.15 and 0.20 for almost all of them (except for two of the more complex LASSO models). The acceptable bandwidth around the converging error was gradually increased from 0% of the converging error, and the results were analyzed as it is shown in **Table 3.6**.

***Table 3.6**: Results of using different acceptable bandwidths around the converging error for the training and testing errors*

Acceptable Bandwidth	Results and Comments
0% of the converging error	No model was accepted
5% of the converging error	Only one model was accepted, and it had a converging error of COV=0.20. This band error was discarded because the converging error was too high to be set as the target optimum error. This decision was made based on the values obtained for the training errors, and also based on the same analysis being done in parallel with the underfitted models.
10% of the converging error	Only one (same) model was accepted. Discarded for the same reasons as before.
15% of the converging error	Two models were accepted. The converging errors were COV=0.20 and COV=0.16. Discarded for the same reasons as before.
20% of the converging error	Six models were accepted. The smallest converging error was COV=0.13.

Because of the results shown in **Table 3.6** and the results of the same analysis but developed on the underfitted model versions, the acceptable bandwidth is set as 20% of the converging error. This results in all the following:

- The optimum ANN passes the 20% of the converging error criterion.
- The optimum ANN has a converging error of COV = 0.14, which is aligned with the smallest converging error of the group of six models passing the 20% criterion in **Table 3.6**.

- It leaves room to set a stricter acceptable bandwidth for the underfitted models, which is defined as 10% of the converging error.
- Setting a 10% of the converging error as criterion for the underfitted models makes it easier but still strict for them the comply with it. 70% of the simpler underfitted models (3- and 6-feature LASSO models) pass the criterion, while only 20% of the more complex but still underfitted models pass it (1-sd away LASSO models). Refer to **Table 3.3**, **Table 3.4**, and **Table 3.5** to see this.

An underfitted model must be assigned with a stricter acceptable bandwidth because it is "easier to learn" for them. This means, underfitted models have a larger converging error, but they can reach it faster than the optimum models reach their converging error. For instance, **Figure 3.13(c)** shows the learning curve for the selected optimum LASSO models (in terms of the error indicator used for the training, RMSE), and it can be seen that a plateau is obtained at around 80% of the training dataset. **Figure 3.13(e)** and **Figure 3.13(f)** show the learning curve of the selected 6-feature and 3-feature LASSO models, respectively, and they reach their plateaus at about 30% and 20% of the training dataset, respectively.

3.5 Step 5: Setting Target Errors for Different Model Complexity Levels

The 6 selected models can be retrained by adding the testing data to the training set and keeping the same selected hyper-parameters and input features. Because these models have a good performance that has been verified and the testing data have a distribution similar to the testing data (see **Figure 3.1**), the retraining process will only refine them (Amazon Web Services, 2019). The results are presented side by side in **Figure 3.15**, sorted from higher

model complexity level (left) to lower model complexity level (right): optimum ANN, optimum RF, optimum LASSO M6, 1-sd away LASSO M9, 6-feature LASSO M4, 3-feature LASSO M10. As expected, performances very similar to those obtained before the retraining process and aligned with the observations derived from the learning curves are obtained. This good behavior is verified with different error indicators, in terms of the RMSE between y_{true} and y_{pred} (error used in the training process, 1st row of plots of **Figure 3.15**, RMSE between 1.0 and V_{true}/V_{pred} (2nd row of plots of **Figure 3.15**), and mean and COV of V_{true}/V_{pred} (3rd row of plots of **Figure 3.15**).

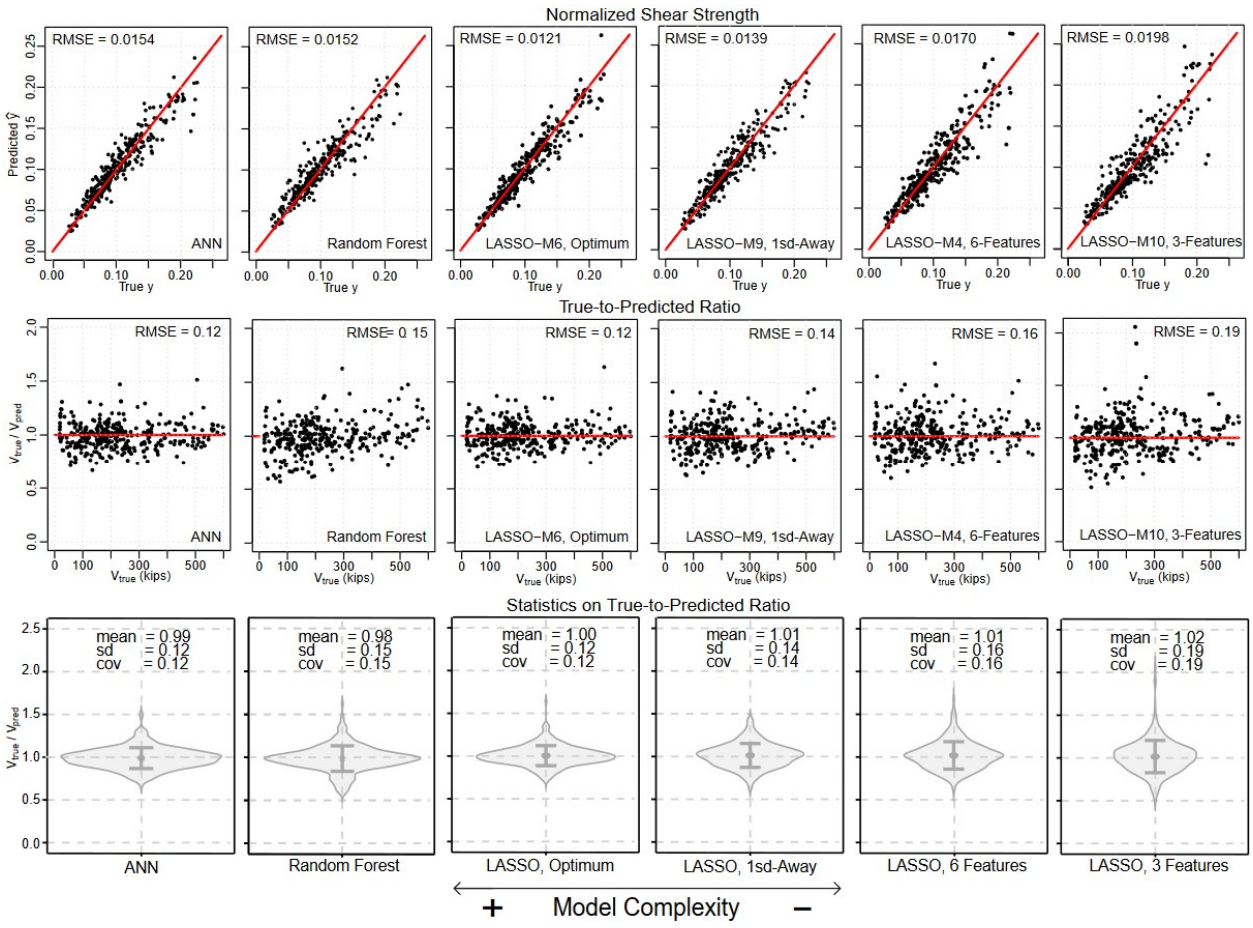

***Figure 3.15**: Retrained ML models*

Figure 3.15 shows that the ANN performs better (smaller error) than RF, but there is still room for the RF to improve when additional data are added to the database. The optimum LASSO model performs practically the same as the optimum ANN, or even slightly better if the RMSE between y_{true} and y_{pred} is considered. This is a relevant finding for two main reasons:

- The complexity level of a LASSO model is much less than that of an ANN model because the penalization factors included in the error definition used in the training process to define which features are kept, are removed and the models are treated as linear regressions using those selected features only, which in the case of the optimum LASSO model in this study, are 45 features engineered from the 10 starting features.
- The underfitted LASSO models can be understood as a soft relaxation away from the optimum when looking for target model performances (errors) that fulfill user requirements for less complex models. The 1-SD away LASSO model is a linear regression of 14 features engineered from 7 of the 10 starting features (x_1, x_2, x_3, x_6, x_8, x_9 and x_{10}), the 6-feature LASSO model is a linear regression of 6 features engineered from 6 of the 10 starting features (x_1, x_2, x_3, x_4, x_6 and x_8), and the 3-feature LASSO model is a linear regression that uses 3 features engineered from 5 of the 10 starting features (x_1, x_2, x_3, x_6 and x_{10}).

An equation with 3 to 6 terms defined from 5 to 6 parameters is representative of the complexity level of equations adopted in building codes and standards, as it can be seen from **Table 2.1**. The wall shear strength equation in Section 18.10 of ACI 318-19 (see **Table 2.1**)

is shorter, but it does not consider some parameters that are important based on the literature review, such as the effect of the boundary element (longitudinal reinforcement and/or flanges) and axial load ratio. Therefore, for the comprehensive database presented in this study or for a similar database (similar ranges and distributions for at least the same parameters included in this database, as is the case of the testing set with respect to the entire database accordingly with **Figure 3.15**), models with the different levels of complexity noted should comply with the requirements stipulated in **Table 3.7**.

***Table 3.7**: Target Performances*

Acceptable Bandwidth	**Complex ML Models**	**Simple Models**
Number of parameters	$-$	$\sim 3-6$
V_{true}/V_{pred} mean ratio	$0.99-1.01$	$0.98-1.02$
COV of V_{true}/V_{pred} ratio	≤ 0.12	$0.16-0.19$
Training Vs testing Error margin	$\pm 20\%$ of the converging error	$\pm 10\%$ of the converging error

Note that the verification of the last requirement in **Table 3.7** should be verified at least in terms of the error indicator used in the training process. Ideally, additional error indicator should be included in the performance verification to confirm model robustness.

Chapter 4. Insights Related to the RC Wall Shear Strength Problem

4.1 Comments on Relevant Parameters

Among the starting features defined from Eq. (4.7) to Eq. (4.16), the ones used in the 6- and/or the 3-feature LASSO models defining the performance requirement for a code-oriented equation are:

$$
\begin{aligned}
x_1 &= \rho_{wh}\frac{f_{ywh}}{f_c'} \\
x_2 &= \rho_{wv}\frac{f_{ywv}}{f_c'} \\
x_3 &= \rho_{wbe}\frac{f_{ybe}}{f_c'} \\
x_4 &= 1+\frac{P_u}{A_g f_c'} \\
x_6 &= \frac{M_u}{V_u l_w} \\
x_8 &= \frac{t_w}{l_w} \\
x_{10} &= \frac{A_{be}}{A_g}
\end{aligned}
$$

The only ones that are not listed here are $x_5 = c/l_w$, $x_7 = t_w/l_w$ and $x_9 = h_w/l_w$. The absence of $x_5 = c/l_w$ can be attributable to the presence of $x_{10} = A_{be}/A_{cv}$ and $x_3 = \rho_{wbe} f_{ybe}/f'_c$, because these two features can be used to represent the forces of compression or tension that are developed at the wall edges. The absence of $x_7 = t_w/l_w$ can be attributable to the presence of $x_8 = t_w/h_w$, which already accounts for the wall thickness and can be used together with $x_6 = M_u/(V_u l_w)$ to reproduce values that have high correlation with $x_7 = t_w/l_w$. On the other hand, the absence of $x_9 = h_w/l_w$ among the previous parameters is striking, but there is a good reason for it. Some of the models

reported in **Table 2.1** or **Table 2.2** use wall aspect ratio (h_w/l_w) as a parameter to estimate wall shear strength (ACI 318-19 is one of those), whereas some other models use moment-to-shear span ratio ($M_u/(V_u l_w)$). In many of the tests reported in the literature (82% of the tests in the database used), these values are the same because the test involves a cantilever wall, fixed at the base, with a single point load applied near the top of the wall, i.e., $M_u = V_u h_w$ (see **Figure 4.1**).

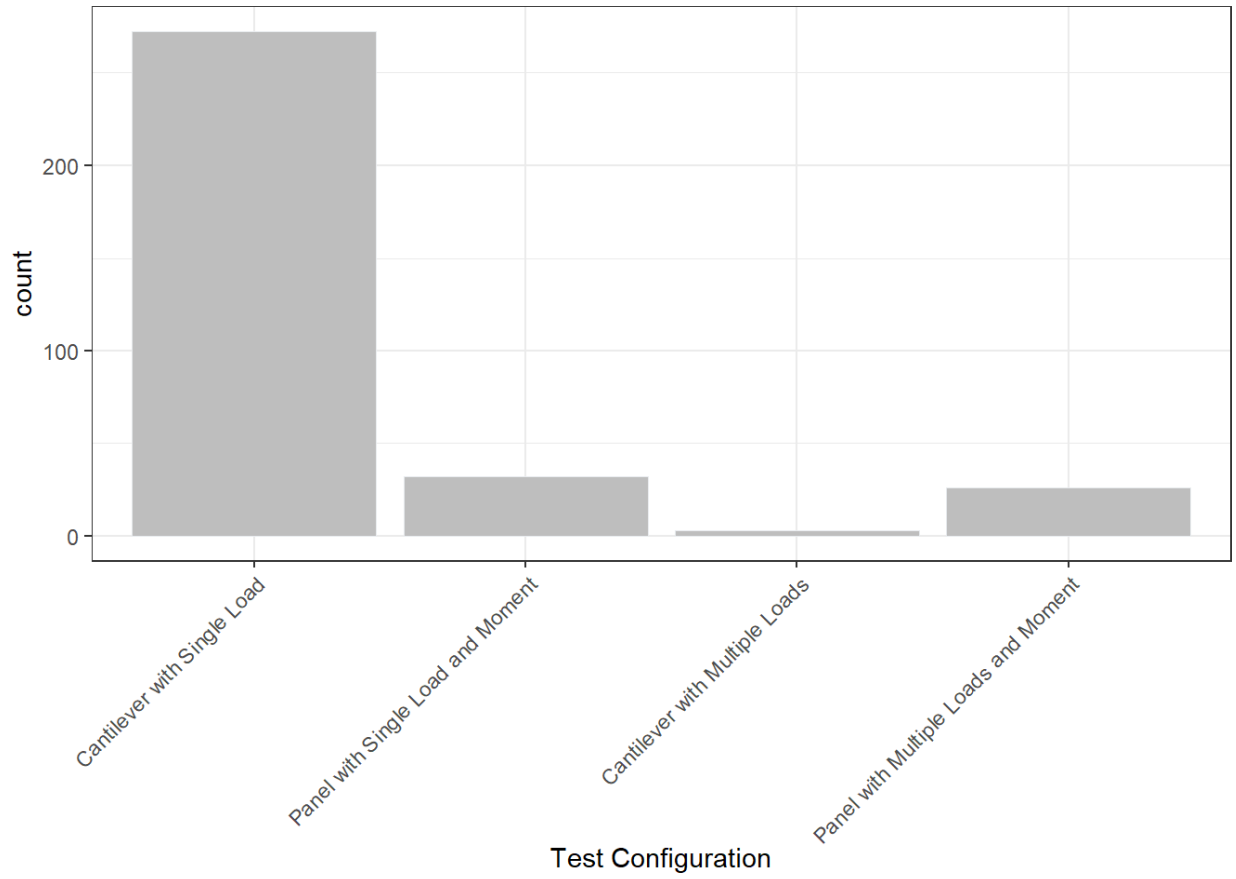

***Figure 4.1**: Histogram of test configuration*

For some tests reported in the literature, these values are not the same (e.g., for a partial height wall with an applied lateral load and moment at the top of the wall) and it is necessary to define an effective wall height $h_{w,eff}$ and wall aspect ratio ($h_{w,eff}/l_w$) for these tests.

Figure 4.1 shows that, for the database used, there are 32 specimens with a moment applied to the top of a partial height wall, 3 cantilever walls with 2 or more lateral loads, and 26 specimens tested with double curvature configuration. For tests with multiple applied lateral loads (e.g., see Cardenas and Magura, 1972) and/or a moment applied at the top of the wall test (e.g., see Segura and Wallace, 2018), the effective wall aspect ratio $h_{w,eff}/l_w$ was defined as $M_u/(V_u l_w)$ at the wall critical section (wall-foundation interface). If this approach is used, then identical results are produced from the test database using either h_w/l_w or $M_u/(V_u l_w)$. Thus, to define $x_9 = h_w/l_w$, the constructed wall height was used because that is how the aspect ratio has been defined in other studies. However, for the reasons given above, it was expected that $x_6 = M_u/(V_u l_w)$ would be a better parameter.

4.2 Comments on Existing Models Performances

The performance of the existing models in codes and standards was evaluated using the common, comprehensive database gathered for this study (see **Figure 4.2**). **Figure 4.2** shows that mean values varied from 0.70 to 1.97, and the COV values vary from 0.30 to 0.47 and that none of the existing models performed particularly well. The AIJ (1999) model had the least variation (but with mean value of 0.7). The Barda et al. (1977) model and the Sánchez-Alejandre and Alcocer (2010) model had mean values very close to 1.0, but COV values greater than 0.30. The ASCE 43-05 model (which is based on Barda et al., 1977) resulted in a mean value of 1.22 and COV of 0.30. None of these models meets the requirements for the simplified model complexity level stated in **Table 3.7**.

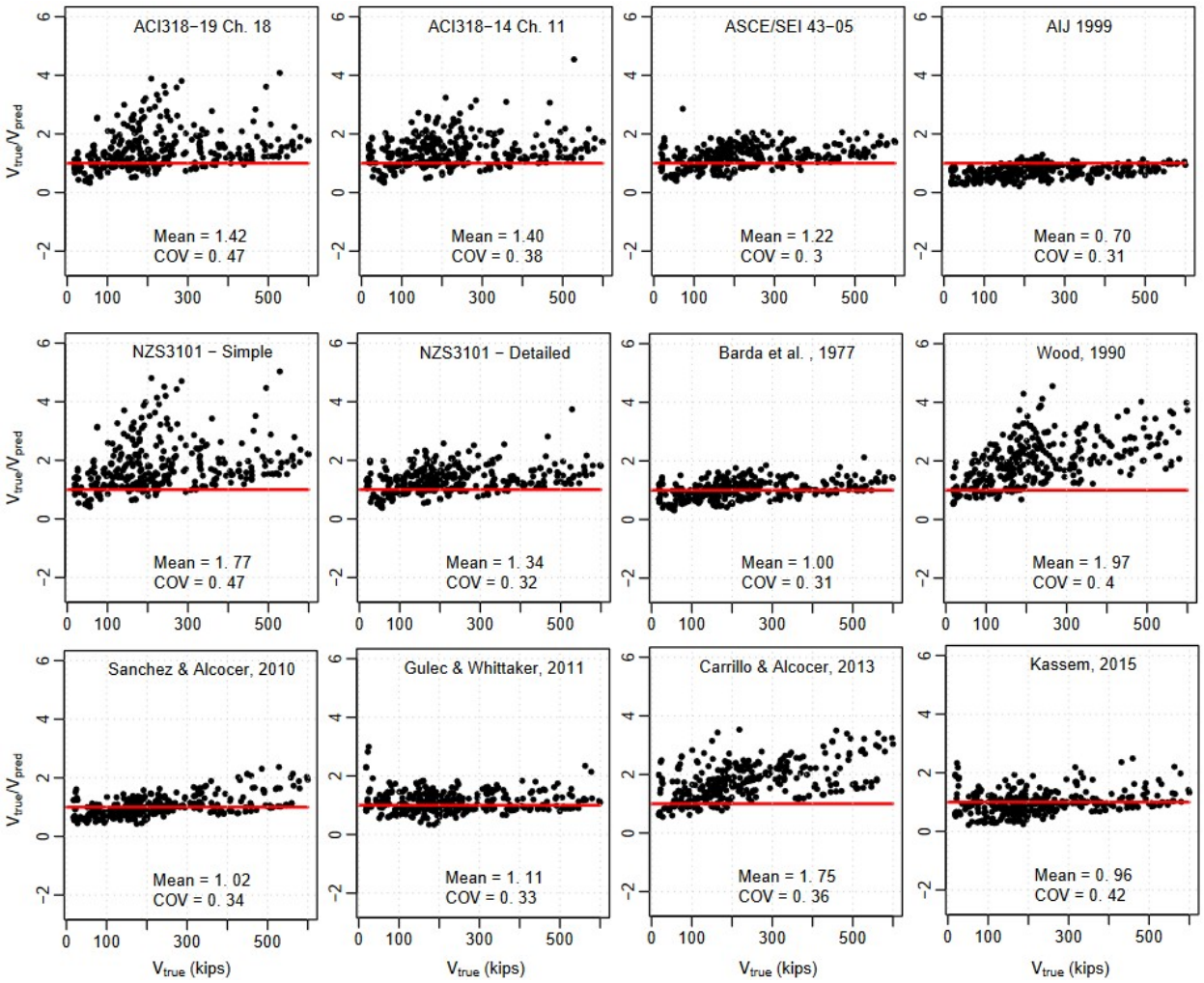

***Figure 4.2**: Performance comparison of existing models using the single, comprehensive database gather for this study*

Additionally, **Table 2.2** shows that Kassem (2015) and Looi and Su (2017) calibrated their models using a database similar in size to the one used in this study. **Table 2.3** shows that, although close (COV of 0.21 and 0.27 of the true-to-predicted ratio, with a mean value close to 1.0), not even these models reached the target performance defined for simple models, even though all data was used in the calibration process and no assessment of unseen data was developed.

As for the ML models analyzed in the literature review; no one meets the complex model level target performance either because the error is not small enough or because the difference between the training and testing error is too large. The proposed approach provides a framework to better train ML models, particularly when the problem being addressed is based on basic mechanical principles. The application of the framework made all ML model types studied here to provide very similar results at their respective optimum complexity level.

Achieving the same good performance of complex ML model with a simple LASSO model emphasizes that the size of databases used for many civil engineer problems may still be too small to benefit from the use of complex ML model types (such as ANN and RF regressions) because a linear regression with the right features can still perform as good, or even slightly better, as the complex ML models. This is aligned with the rule of thumb that says ML models should be train on at least an order of magnitude more samples than input model parameters (Morgan and Bourlard, 1989; Google ML Education n.d.; Gonfalonieri, 2019). The optimum LASSO model presented in this study uses 45 features, which are engineered from the 10 starting features presented in Eqs. (4.7) to (4.16), which can be easily implemented in an excel spreadsheet. This would not be the case for the ANN or RF regression models.

Chapter 5. Methodology to Define a Code-Oriented Equation

A new equation to predict wall shear strength is desired because the current equation in ACI 318-19 Section 18.10 nor the existing models (see **Figure 4.2**) meet the target model performance required for a code-oriented model complexity level (see 4.7) when predicting values of a common, comprehensive database of walls reported to have failed in shear as the one gathered for this study.

As mentioned before, the databases used by Kassem (2015) and Looi and Su (2017) are comparable in size with the database used in this study. The model comparisons reported by these authors in their respective studies (presented in the last columns of **Table 2.3**) show that only their own proposed models are close to the target performance for a simple model. However:

- The databases used in their studies use the assumption that walls with $h_w/l_w \leq 2.0$ fail in shear, which although reasonable, might not always be true and thus it can cause the proposed model to be biased.
- Both studies used the entire databases to calibrate their models and as a consequence it is uncertain if the model will present high bias or variance (see **Figure 3.14**) when faced against new data.
- The proposed models are still complex mainly because of their format.

In this chapter, an approach combining ML and statistical methods is implemented to shrink an equation (starting equation) with a code-oriented format ($V_n = V_c + V_s$) up to the point where the corresponding target performance is achieved. The same database with the same

training and testing sets used in the previous chapters is used here. It is relevant to mention that once a code appropriate equation was developed using the database of 333 walls with symmetrical cross sections (rectangular, barbell, H-shaped), additional studies are conducted to determine modifications need to apply the equation to walls with unsymmetrical cross sections (L- and T-shaped), since these wall shapes are commonly used.

5.1 Step 1: Collection and Preparation of Data

The same database of 333 symmetrical walls reported to have failed in shear used before is used here as well. This database has already been rigorously reviewed to filter out tests that do not meet predefined criteria or where inconsistent results were reported (see 4.1). In addition to the same training set of 266 samples and testing set of 67 samples, a second testing set of unsymmetrical walls is included for this part of the study.

The second testing set of unsymmetrical walls consists of 13 samples out of the 20 unsymmetrical walls identified with T-shaped and L-shaped, or walls with a column (half barbell shaped or column with wing walls) in the original (larger) dataset (see 4.1). This approach was used because 13 tests was insufficient compared to 333, i.e., the inherit differences associated with these tests would be overlooked by the training process if included as part of the training and testing datasets. Since use of wing walls is not common in the U.S., the Japanese Code (AIJ 1999) includes detailed recommendations on determination of wing wall shear strength), the 7 wing wall samples among the 2-unsymmetrical walls were excluded. The dataset of 13 tests is derived from 11 tests, because

2 of the tests reported were failed in both directions of loading (specimen HW2 tested by Kabeyasawa et al, 1996, and specimen SWBT-L40 tested by Baek et al., 2020).

5.2 Step 2: Identification of Relevant Parameters and Starting Equation

The first step involves identifying the relevant parameters based on a literature review, and then normalizing these parameters (e.g., using shear stress versus shear strength, since most tests were done on reduced scale test specimens). In this case, the parameters considered in the starting model are the relevant features used in the simplest ML models (6- and 3-feature LASSO models) indicated in Section 5.1:

$$\rho_{wh}\frac{f_{ywh}}{f_c'} \quad , \quad \rho_{wv}\frac{f_{ywv}}{f_c'} \quad , \quad \rho_{wbe}\frac{f_{ybe}}{f_c'} \quad , \quad 1+\frac{P_u}{A_g f_c'} \quad , \quad \frac{M_u}{V_u l_w} \quad , \quad \frac{t_w}{h_w} \quad , \quad \frac{A_{be}}{A_g}$$

The selected parameters include material-related parameters (V_i) and other parameters ($\gamma_{j,i}$):

- Material-related parameters (V_i): concrete strength and correlated cross-sectional area (A_g'; f_c'), quantity and yield stress of longitudinal reinforcement at the wall boundary (ρ_{be}; f_{ybe}), quantity and yield stress of horizontal web reinforcement (ρ_{wh}; f_{ywh}), and quantity and yield stress of vertical web reinforcement (ρ_{wv}; f_{ywv})
- Other parameters ($\gamma_{j,i}$): axial load ratio $P_u/(A_g' f_g')$, shear-span ratio $M_u/(V_u l_w)$ (or aspect ratio h_w/l_w).

Where all these variables have been already introduced, except for A_g'. The gross-section A_g' is the wall web area (A_{cv}) plus the area of the effective overhanging flange width (if present)

at the edge (or boundary) of the wall subjected to compressive stresses due to overturning moment. It is also introduced now A_{sb}, which is the area of concentrated longitudinal tension reinforcement at a wall boundary within $0.20l_w$ from the wall edge, as well as the area of longitudinal reinforcement located within an effective tension flange width, if it exists. If wall web longitudinal reinforcement is uniformly distributed, then A_{sb} includes the area of longitudinal reinforcement within $0.20l_w$ from the wall edge, as well as longitudinal reinforcement within the effective flange.

It is noted that initially, gross cross-sectional area (A_g), which represents the wall web area and the area of the effective overhanging tension and compression flange width for an H-shaped wall cross sections, or the entire area of barbell-shaped cross sections, was used in this methodology (just like in the previous chapters, because it was convenient, and due to symmetry, did not influence the results). However, evaluation of the second dataset (of unsymmetric wall cross sections) indicated that this approach was difficult to interpret for unsymmetrical walls (additional comments on why this term is used are presented in Step 4).

These parameters are rearranged into an equation that follows the "$V_c + V_s$" (concrete contribution plus steel contribution) format. The "Other Parameters" ($\gamma_{j,i}$) are normalized and unitless and are weights that multiply each of the "Material Parameters" (V_i) terms, which have units of force (e.g., kN, kips, etc.). **Figure 5.1** shows the general form of the equation that is used to form the starting equation that is then reduced (shrinking process). The starting equation is normalized to avoid the many potential issues that could arise during the training process (see Section 3.2. It is noted that this normalization process is

based on the physics of the problem, i.e., different than the normalization or scaling concepts used in statistics, which are still required prior to training a model. The predicted variable is almost the same as the one when applying the framework to set target model performances:

$$y_{true} = \frac{V_u}{A'_g f'_c} \tag{7.1}$$

The only what changes in the definition of y_{true} respect to that of Eq. (4.17) is that in Eq. (7.1) A'_g is used instead of A_g.

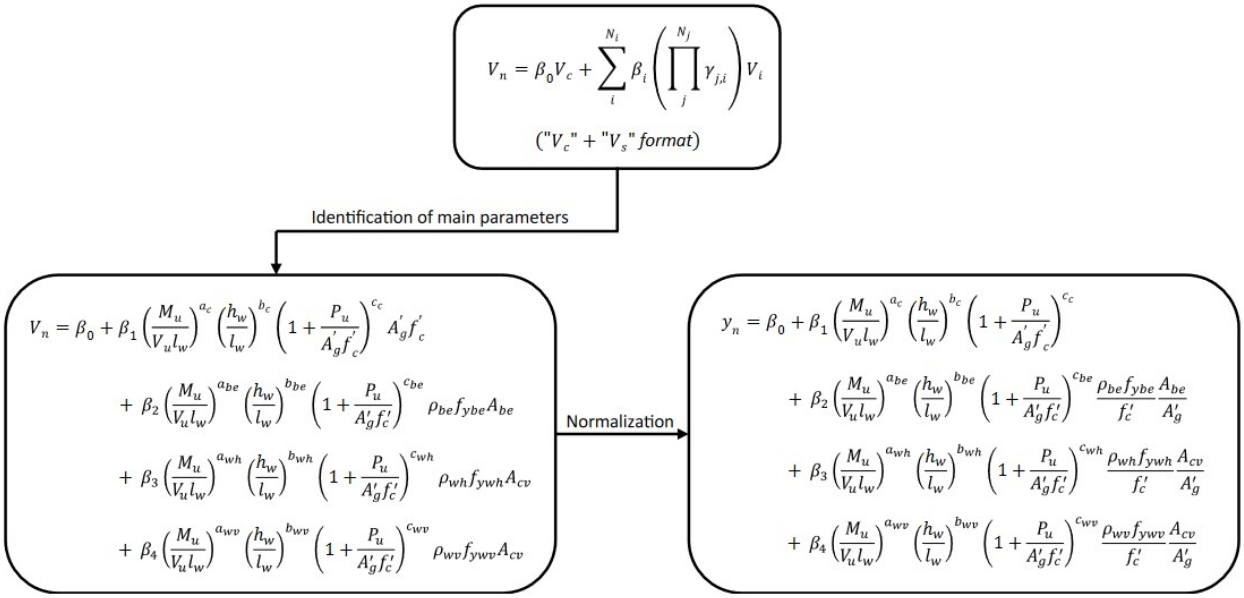

Figure 5.1*: Definition of the starting equation*

For the reasons mentioned in Section 5.1, it is necessary to define an effective wall height $h_{w,eff}$ for wall tests with multiple lateral loads applied over the wall test specimen height or for walls with a moment applied at the top of the wall. As said in Section 5.1, a common approach is to use $h_{w,eff} = M_u/V_u$; therefore, for most of the tests in the database, with a single point load applied near the top of a fixed-based, cantilever wall (see **Figure 5.1**),

$h_{w,eff} = h_w$. With this definition, the same predictive equation would be achieved using either $h_{w,eff}/l_w$ or $M_u/(V_u l_w)$. In this study, $M_u/(V_u l_w)$ is used. However, for a real building, use of h_w/l_w versus $M_u/(V_u l_w)$ would produce different results. This issue is addressed later in Section 8.3.

5.3 Step 3: Training Process, Equation Simplification and Performance Verification

5.3.1 Training Process and Equation Simplification

The unknown coefficients to be studied and fitted are the a_i, b_i and β_i coefficients of the normalized equation shown in **Figure 5.1**. The database was split into the same training (80%) and testing (20%) sets used before (Section 4). The iterative k-Fold Cross Validation method implemented before is used here as well (see **Figure 3.3**). In this case, in addition to keeping track of the model error, p-values are also recorded. The algorithm shown in **Figure 5.2** is implemented to shrink (simplify) the starting equation until the model error meets the target error (see **Table 3.7**).

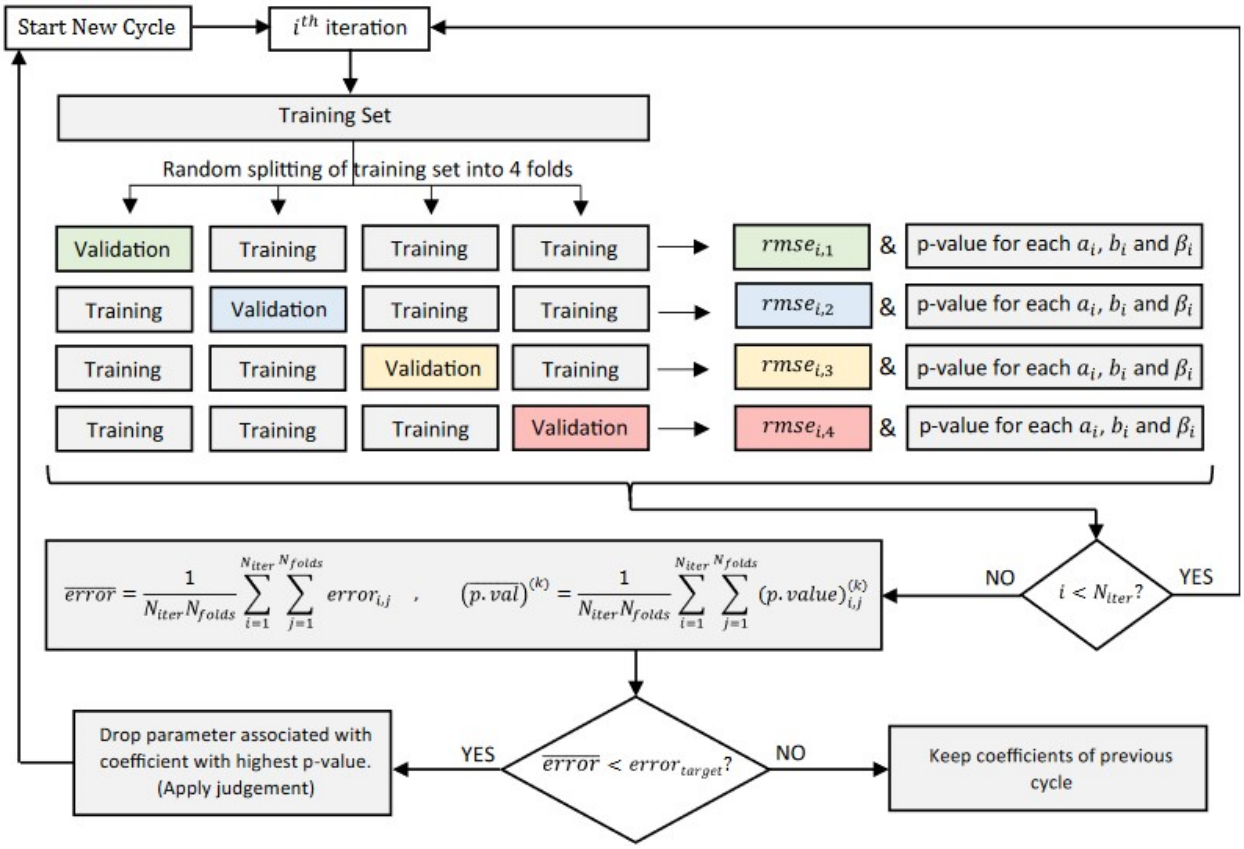

***Figure 5.2**: Algorithm implementing 4-Fold CV to shrink the starting equation*

The methodology involves splitting the training dataset randomly into k folds, $k-1$ of the folds are used as sub-training datasets to train a nonlinear regression model and the remaining fold is used as a validation dataset. All this is done k times within each iteration. The training process produces p-values for each a_i, b_i and β_i coefficients, whereas model error is computed from model predictions using the validation dataset. Although root mean square error (RMSE) is used in the optimization process, the mean and COV of the true-to-predicted ratio (V_{true}/V_{pred}) are also computed. Once the iterative process is done, $N_{iter} \times k = 200$ errors and $N_iter \times k = 200$ p-values for each a_i, b_i and β_i coefficients are obtained (in this case, $k = 4$ and $N_{iter} = 50$ were used). The average error and the average p-value for each coefficient are calculated. The p-values indicate the statistical significance

for each model variable, the higher the p-value, the less significant the variable (Murtaugh, 2014). If the average error is lower than the target error, then the variable associated to the largest average p-value is dropped. Judgement is applied so that the shrinking process is gradual, e.g., if the p-values of β_4 and b_{wv} are the first and second highest (respectively), the parameter associated with b_{wv} is the one that is dropped because it results in a more gradual shrinking of the equation.

The starting equation (with all the parameters) had an average RMSE of 0.0150, and a mean and COV of the true-to-predicted ratio of 1.00 and 0.147, respectively. The resulting equation at the end of the shrinking process, see Eq. (7.2), has an average RMSE of 0.0164 and a mean and COV of the true-to-predicted ratio of 1.00 and 0.154, respectively. Because the nonlinear regressions resulted in very similar values for a_{be} and a_{wh} (after the axial load ratio parameter associated with coefficients b_{be} and b_{wh} were both dropped), these values were set equal to each other ($a_s = a_{be} = a_{wh}$).

$$y_n = \beta_0 + \beta_1 \left(\frac{M_u}{V_u l_w}\right)^{a_c} \left(1 + \frac{P_u}{A'_g f'_c}\right)^{b_c} + \left(\frac{M_u}{V_u l_w}\right)^{a_s} \left[\beta_2 \frac{\rho_{be} f_{ybe}}{f'_c} \frac{A_{be}}{A'_g} + \beta_3 \frac{\rho_{wh} f_{ywh}}{f'_c} \frac{A_{cv}}{A'_g}\right] \quad (7.2)$$

Results of the nonlinear regressions also produce results for fitted values for the a_c, b_c, a_s and β coefficients of Eq. (7.2). However, these fitted values (e.g., $a_c = -0.387$, $b_c = 2.900$ and $a_s = -0.391$) are not commonly used (or typical) of a code equation. Therefore, the algorithm shown in **Figure 5.3** was implemented to simplify the equation.

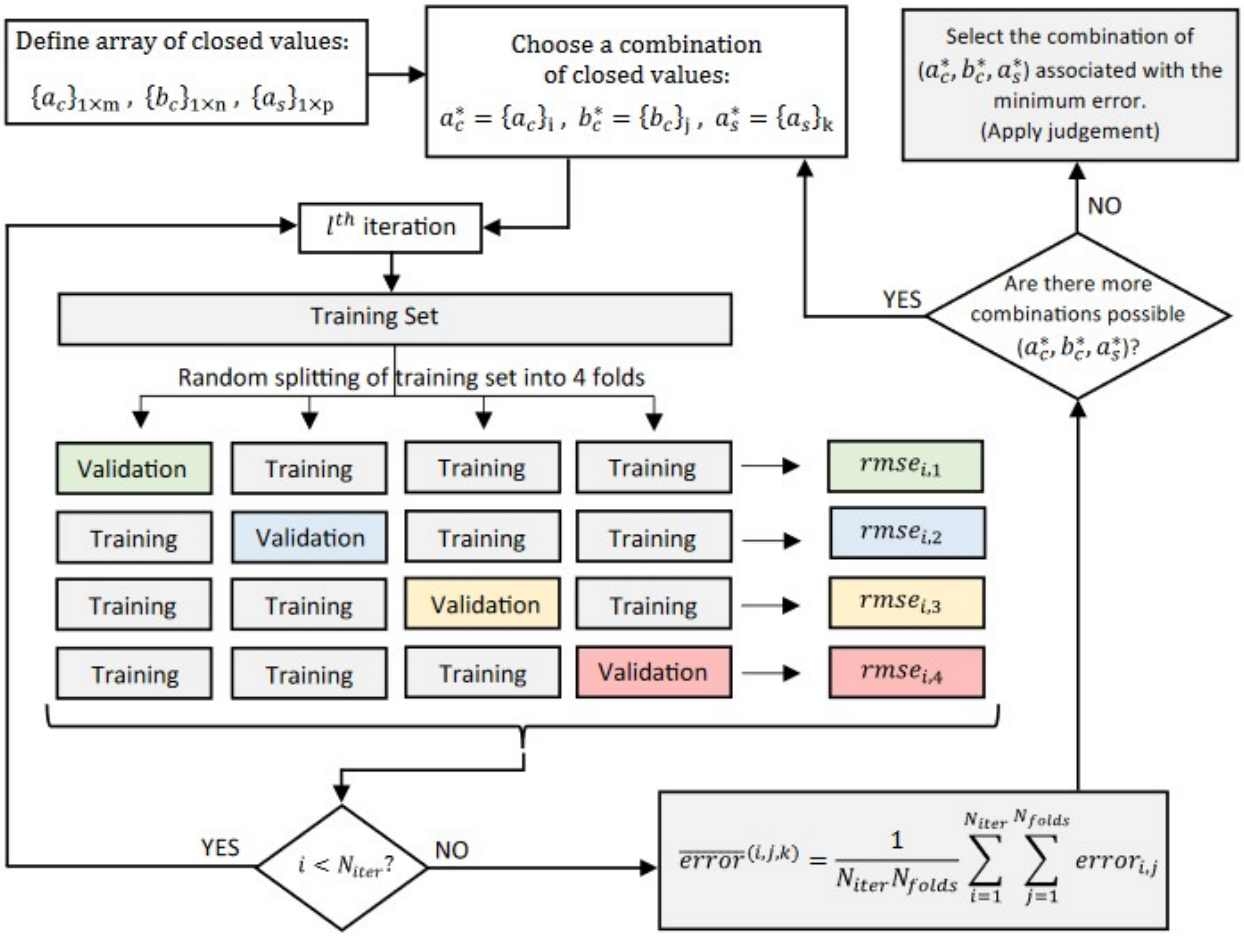

***Figure 5.3**: Algorithm to find the optimum round up values for a_c, b_c and a_s coefficients*

This process involved selecting a range of values around the fitted values, e.g., $\{a_c\} = (0, -1/5, -1/4, -1/3, -2/5, -1/2)$, $\{b_c\} = (1.5, 2.0, 2.5, 3.0, 3.5)$, and $\{a_s\} = (0, -1/5, -1/4, -1/3, -2/5, -1/2)$, and calibrating β_i coefficients using linear regression for each combination. The algorithm for this process shown in **Figure 5.3** was implemented using $k = 4$ folds and $N_{iter} = 50$ iterations. Note that since the coefficients a_c^*, b_c^* and a_s^* are assumed before the training process, only the β_i coefficients are calibrated. The combination of (a_c^*, b_c^*, a_s^*) values associated with the minimum average error are selected for use in the final equation. Some judgement can be applied in this process, i.e., the error associated for various combinations of a_c, b_c and a_s values might be similar (and meet the target error);

therefore, the most "convenient" values can be selected. Finally, values for β_0, β_1, β_2 and β_3 are selected based on the average values obtained from the $N_{iter} \times k = 200$ linear regressions associated with the selected (a_c^*, b_c^*, a_s^*) values. The obtained equation is shown in Eq. (7.3).

$$V_n = \alpha_c A_g' f_c' + \alpha_s \left(\rho_{sb} f_{ysb} + \rho_{wh} f_{ywh}\right) A_{cv} \tag{7.3}$$

Where ρ_{sb} is the longitudinal reinforcement at the tensioned edge ratio defined as A_{sb}/A_{cv}, and the α_c and α_s coefficients are:

$$\alpha_c = \frac{1}{100}\left(9\frac{\left(1+\frac{P_u}{A_g' f_c'}\right)^3}{\left(\frac{M_u}{V_u l_w}\right)^{1/3}} - 6\right) \tag{7.4}$$

$$\alpha_s = \frac{2}{5\left(\frac{M_u}{V_u l_w}\right)^{1/3}} \tag{7.5}$$

5.3.2 Performance Verification - Symmetrical Walls

The performance of Eq. (7.3) is first assessed with the testing set defined from the database of 333 symmetrical walls reported to have failed in shear. **Figure 5.4** shows that similar values of RMSE, mean, and COV are obtained for both the training and testing sets and error indicators meet the requirements for a code-oriented model given in **Table 3.7**. Thus, the performance of the equation is verified when predicting values of an unknown dataset of symmetrical walls (rectangular, barbell, and H-shaped walls).

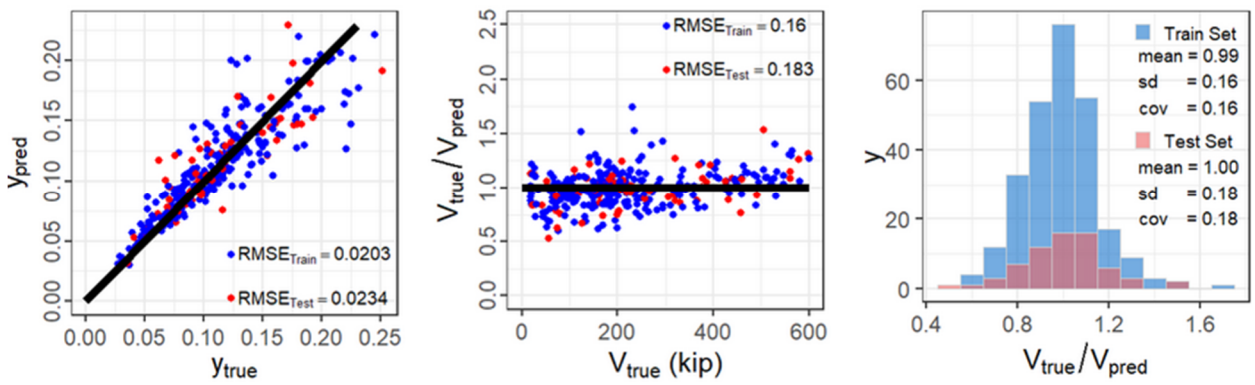

***Figure 5.4**: Obtained equation performance and verification: Symmetrical Walls*

5.3.3 Performance Verification - Asymmetrical Walls

As noted previously, the entire methodology was first applied using A_g and a model similar to that shown in Eqs. (7.3), (7.4), and (7.5), was obtained. However, use of A_g could not easily be applied to walls with unsymmetrical cross-sectional shapes, because the longitudinal reinforcement at the wall boundaries and the area of concrete in compression are different depending on the loading direction.

Prior studies have shown that beams (Shear, Committee on Masonry, and Structural Division, 1973) and walls (Kim and Park, 2020) with flanges in compression have larger shear strengths than beams and walls with rectangular cross sections and the same area longitudinal tension reinforcement, and that walls with flanges have higher shear strength (Gulec and Whittaker, 2011; Kassem, 2015). Since the equation developed in the first run of the methodology already accounted for the boundary longitudinal reinforcement in tension explicitly (including any reinforcement within the effective tension flange width), A_{sb}, it was decided to use the variable A'_g (instead of A_g) because this still captures the difference of the size of the area in compression of walls with a flange in compression respect to rectangular walls. It is highlighted again that Eq. (7.3) was developed using the dataset of 333 walls,

which included walls with both tension and compression flanges (H-shaped sections) and barbell-shaped sections, using variable A'_g. It is noted that the performance of the equation obtain in the first run of the methodology and Eq. (7.3) were essentially the same. **Figure 5.5** demonstrates how A'_g and A_{sb} are defined for an unsymmetrical wall (a T-shaped wall in this case) based on the direction of loading and, therefore, different wall shear strengths are obtained for each direction of loading.

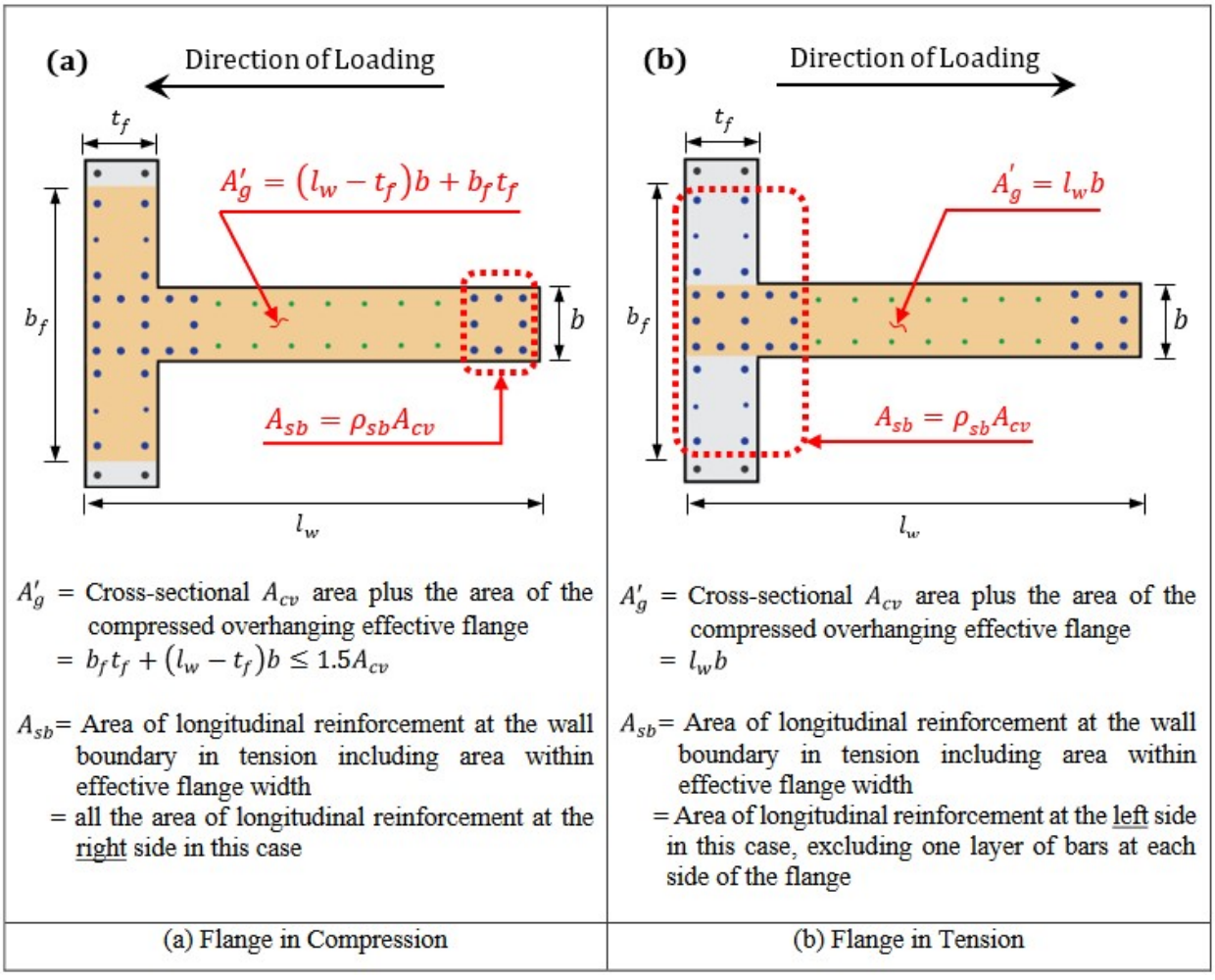

***Figure 5.5**: Example of concrete cross-sectional area and tensioned longitudinal steel reinforcement*

Results presented for the dataset of unsymmetric walls are provided in **Figure 5.6** and demonstrate that the performance of the proposed approach is similar to that for the dataset of 333 symmetric walls. It is noted that the dataset of unsymmetrical walls is limited and that this approach should be reassessed if additional data become available.

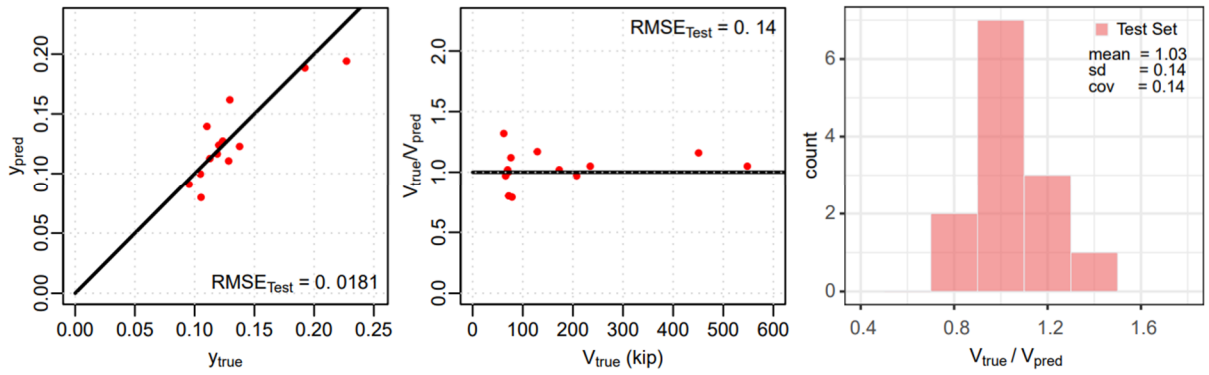

***Figure 5.6**: Obtained equation performance and verification: Unsymmetrical Walls*

5.4 Step 4: Performance of the Obtained Equation over the Complete Dataset

Figure 5.7 shows the learning curves of the model using the training and testing sets in terms of the error computed as RMSE between y_{true} and y_{pred}, and as COV between the ratio V_{true}/V_{pred} and 1.0. The learning curves have the signature of an underfitted model (rapid convergence and a long plateau of the training and testing error), but with the converging error meeting the target error range and with the training and testing errors within the $\pm$10% bandwidth around the converging error (see **Table 3.7**). This means the predictive performance of the model is stable and will be essentially the same even if new data (that follow a similar distribution) are added to the training dataset (Amazon Web Services, 2019). **Figure 5.8** presents the performance of Eq. (7.3) against the total database of 333 symmetric

walls that were reported to fail in shear. No retraining was done, i.e., the same equation obtained was applied to the combined training and testing dataset to compute RMSE, mean, and COV.

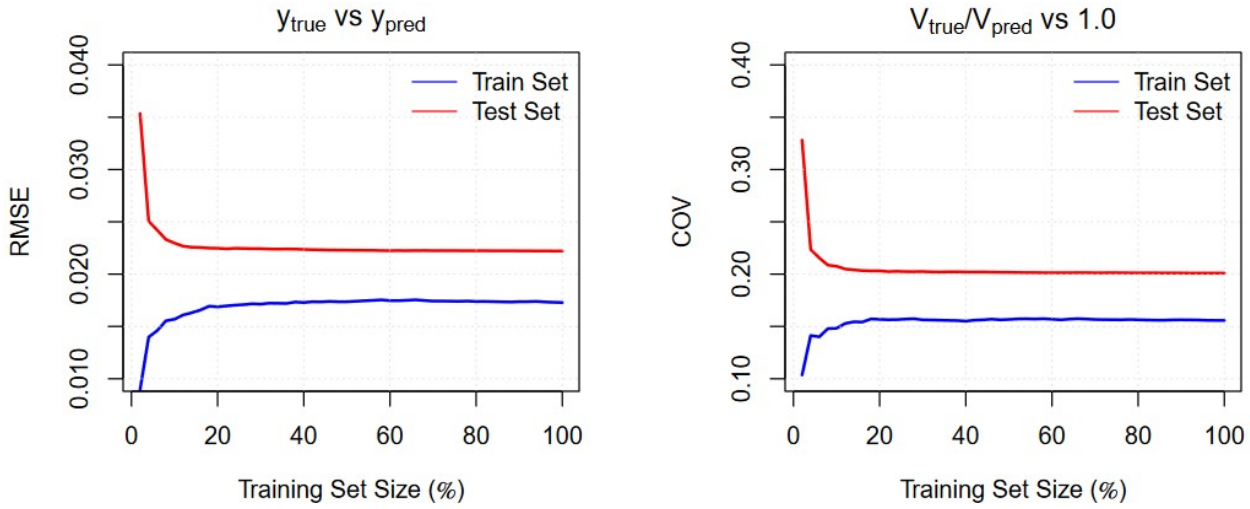

***Figure 5.7**: Learning curves in terms of: (a) RMSE of y_{true} vs y_{pred}; (b) COV of V_{true}/V_{pred} vs* 1.0

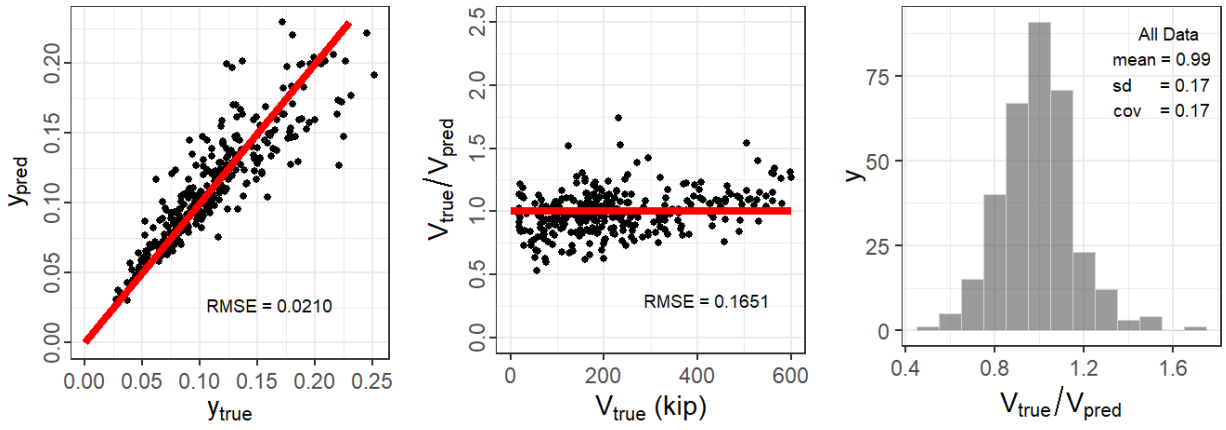

***Figure 5.8**: Obtained equation performance and verification: complete dataset of symmetrical walls*

Chapter 6. Definition of the Proposed Equation

The parameters involved in the equation obtained after applying the methodology described in the previous section (see Eq. (7.3)) must be analyzed prior giving a formal definition of the proposed equation, particularly those parameters that are new respect to the current equation in the ACI 318-19 Section 18.10.

6.1 Dataset Parameter Range Limitations

Histograms for axial load ratio $P_u/(A'_g f'_c)$, A'_g/A_{cv}, and $M_u/(V_u l_w)$ are presented in **Figure 6.1(a)**, **Figure 6.1(b)**, and **Figure 6.1(c)**, respectively. Based on the histograms for $P_u/(A'_g f'_c)$ and A'_g/A_{cv}, limits of $0 \leq P_u/(A'_g f'_c) \leq 0.20$ and $A'_g/A_{cv} \leq 1.5$ are proposed for Eq. (7.3) because of the lack (limited) data outside these ranges. Given that shear strength tends to increase with increases in these ratios, the proposed limits should produce conservative predictions for ratios outside of these limits, except for the case of wall tension. However, the ACI 318-19 equation for wall shear strength also does not address wall tension. The histogram for $M_u/(V_u l_w)$ reveals that there are relatively few tests for $2.5 \leq M_u/(V_u l_w) \leq 3.0$ and no data for $M_u/(V_u l_w) > 3.0$; however, instead of limiting values for $M_u/(V_u l_w)$, a limit of $\alpha_s \geq 0.30$ is proposed (because $\alpha_s = 0.30$ for $M_u/(V_u l_w) = 2.5$, and would barely decrease to $\alpha_s = 0.28$ for a value of $M_u/(V_u l_w) = 3.0$).

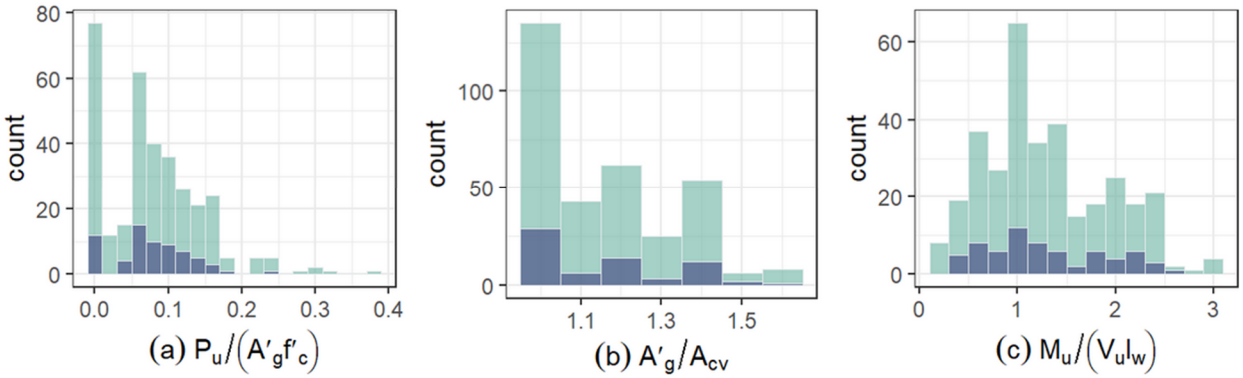

***Figure 6.1**: Histograms of parameters involved in the proposed equation*

6.2 Lower limit for α_c

Figure 6.2 shows that the α_c coefficient obtained in this study do not follow a lognormal distribution, but a truncated normal distribution (Burkardt, 2014), because it can be seen the distribution has an abrupt ending in its left side. This truncation is understandable due to the mechanics of the problem actually; the coefficient α_c is directly related with the concrete contribution, and therefore it is natural to have a lower limit for it.

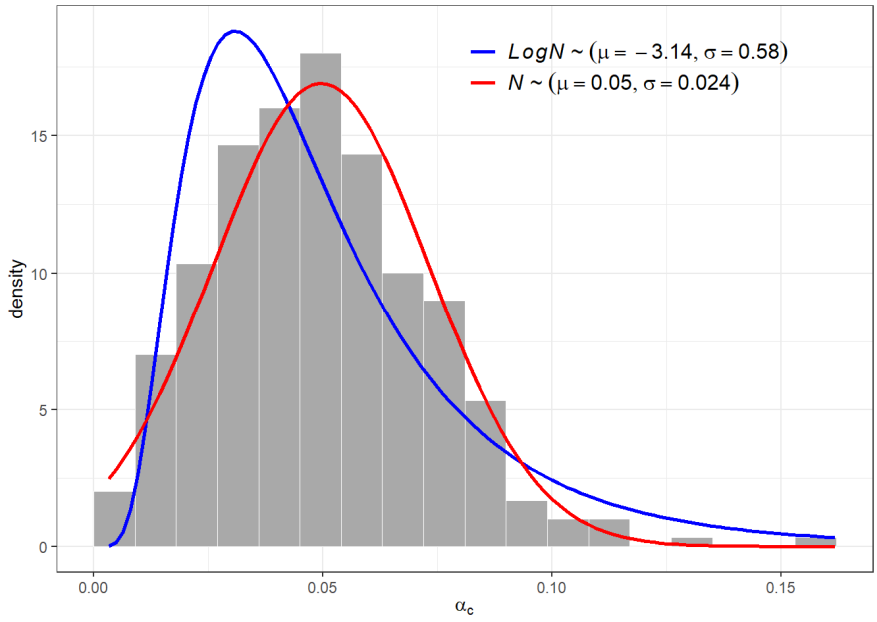

***Figure 6.2**: Histograms of parameters involved in the proposed equation*

Table 6.1 shows the 5% of the data with lowest α_c values. These coefficients have an average α_c value of 0.009, no axial load applied and shear-span ratios $\geq$ 2.0. Because of these values, and having in consideration that nice round numbers are always preferred for an expression meant for a code or standard, the minimum value for α_c is set to 0.010.

***Table 6.1**: 5% of the data with lower α_c values*

Num.	$M_u/(V_u l_w)$	$P_u/(A'_g f'_c)$	α_c
1	2.87	0	0.003
2	2.39	0	0.007
3	2.39	0	0.007
4	2.39	0	0.007
5	2.39	0	0.007
6	2.39	0	0.007
7	2.13	0	0.010
8	2.13	0	0.010
9	2.13	0	0.010
10	2.13	0	0.010
11	2.13	0	0.010
12	2.00	0	0.011
13	2.00	0	0.011
14	2.00	0	0.011
15	2.00	0	0.011
16	2.00	0	0.011
17	2.00	0	0.011
Mean	**2.20**	**0**	**0.009**

In addition to the information given in **Table 6.1**, the defined minimum value for α_c can be understood by using the upper limit for the shear-span ratio imposed by the lower limit $\alpha_s \geq$ 0.30, i.e., $M_u/(V_u l_w) \leq 2.5$, and a small axial load ratio that could represent the wall self-weight:

$$\frac{P_u}{A_g' f_c'} = 0.02 \;\&\; \frac{M_u}{V_u l_w} = 2.5 \qquad \rightarrow \qquad \alpha_c = \frac{1}{100}\left(9\frac{(1+0.02)^3}{\sqrt[3]{2.5}} - 6\right) = 0.010$$

6.3 Comments on the Use of $M_u/(V_u l_w)$

Current engineering practice is to use total wall height above the critical section (e.g., see ACI 318-19 Chapter 2, h_w or $h_{w,cs}$) to determine the value of h_w/l_w to use in ACI 318-19 Equation 18.10.4.1 (to determine α_c). In general, the aspect ratio h_w/l_w will be significantly larger than the value of the shear-span ratio $M_u/(V_u l_w)$ since this latter term uses the height of the resultant lateral force.

Ratios of shear-span ratio and aspect ratio are compared in **Figure 6.3** for a single cantilever wall representing the lateral-force-resisting system for buildings with 1 to 15 stories using the ASCE 7-16 ELF (Section 12.8) with $T_u = C_u T_a$. The results presented in **Figure 6.3** indicate that using h_w/l_w versus $M_u/(V_u l_w)$ produces a conservative estimate of wall shear strength.

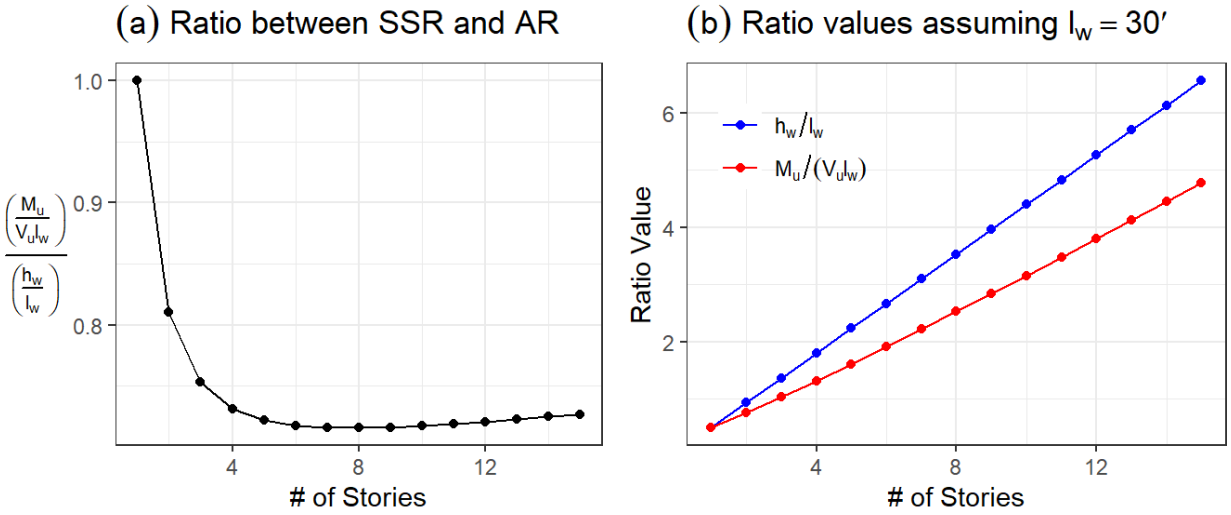

***Figure 6.3**: Comparison of shear-span ratio to aspect ratio*

As well, in ACI 318-19, the ASCE 7 wall shear demand V_u is amplified, i.e., $V_e = \Omega_v \omega_v V_u$ to account for overstrength and higher mode contributions, where $\Omega_v = M_{pr}/M_u$ for walls with $h_w/l_w > 1.5$ and $\Omega_v = 1.0$ for $h_w/l_w \leq 1.5$. Therefore, to account for overstrength and higher modes, a more realistic value of moment-to-shear demand would be:

$$\frac{M_{pr}}{V_e l_w} = \frac{\Omega_v M_u}{\Omega_v \omega_v V_u l_w} = \frac{M_u}{\omega_v V_u l_w}$$

Since $\omega_v \geq 1.0$, again, use of overall wall height ($h_{w,cs}/l_w$) to estimate wall shear strength will produce even more conservative results as shown in **Figure 6.4** for wall aspect ratios of 1.0, 2.0, 3.0, 4.0 and 5.0. Given these observations, the proposed shear strength equation is based on using $M_u/(\omega_v V_u l_w)$ versus h_w/l_w. An alternative approach would be to propose modifications to h_w/l_w to address these issues.

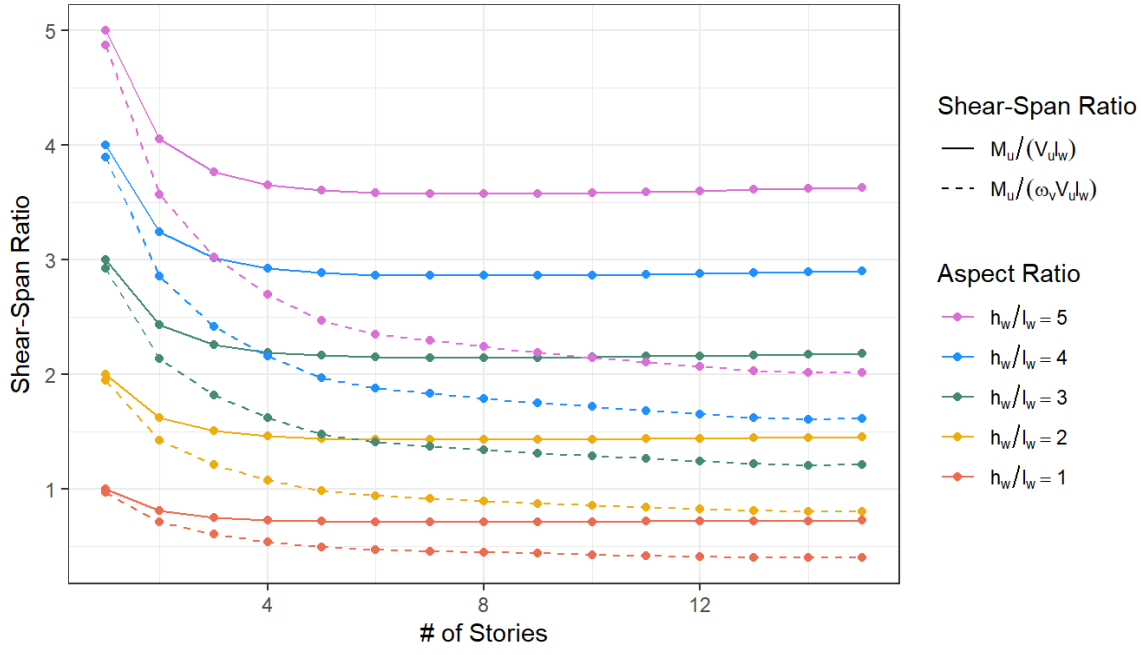

***Figure 6.4**: Impact of overstrength and dynamic amplification factors in the shear-span ratio to aspect ratio relationship*

6.4 Proposed Equation

$$V_n = \alpha_c A'_g f'_c + \alpha_s \left(\rho_{sb} f_{ysb} + \rho_{wh} f_{ywh}\right) A_{cv} \tag{8.1}$$

Where the α_c and α_s coefficients are:

$$\alpha_c = \frac{1}{100}\left(9\frac{\left(1 + \frac{P_u}{A'_g f'_c}\right)^3}{\left(\frac{M_u}{\omega_v V_u l_w}\right)^{1/3}} - 6 \right) \geq 0.010 \tag{8.2}$$

$$\alpha_s = \frac{2}{5\left(\frac{M_u}{\omega_v V_u l_w}\right)^{1/3}} \geq 0.30 \tag{8.3}$$

and:

- A'_g is the wall web area A_{cv} plus the area of the overhanging effective flange width (if present) at the edge (or boundary) of the wall subjected to compression stresses due to overturning moment. A'_g shall not taken greater than $1.5A_{cv}$.
- ρ_{sb} is the boundary region longitudinal reinforcement ratio defined as A_{sb}/A_{cv}
- A_{sb} is the area of nonprestressed longitudinal tension reinforcement at a wall boundary, including area within an effective tension flange width. If the wall has uniformly distributed longitudinal reinforcement, or concentrated longitudinal steel distributed in a region larger than $0.20l_w$ from the wall edge, then A_{sb} is taken as the longitudinal reinforcement area within $0.20l_w$ from the wall edge and all effective flange (if it is the case).
- $P_u\left(A'_g f'_c\right)$ shall not be taken larger than 0.20.
- f_{ysb} is the specified yield strength of the boundary region longitudinal reinforcement

- ρ_{wh} and f_{ywh} are the web horizontal reinforcement ratio and specified yield strength, respectively.
- ρ_{wv} and f_{ywv} are the web vertical reinforcement ratio and specified yield strength, respectively.
- P_u is the factored axial load
- M_u is the factored moment
- V_u is the factored shear

Finally, **Figure 6.5** confirms the proper predictive performance of the proposed model defined as shown in Eqs. (8.1), (8.2) and (8.3) when assessing it with the training and testing sets. **Figure 6.6** does the same, but using the complete dataset of walls with symmetrical cross-section.

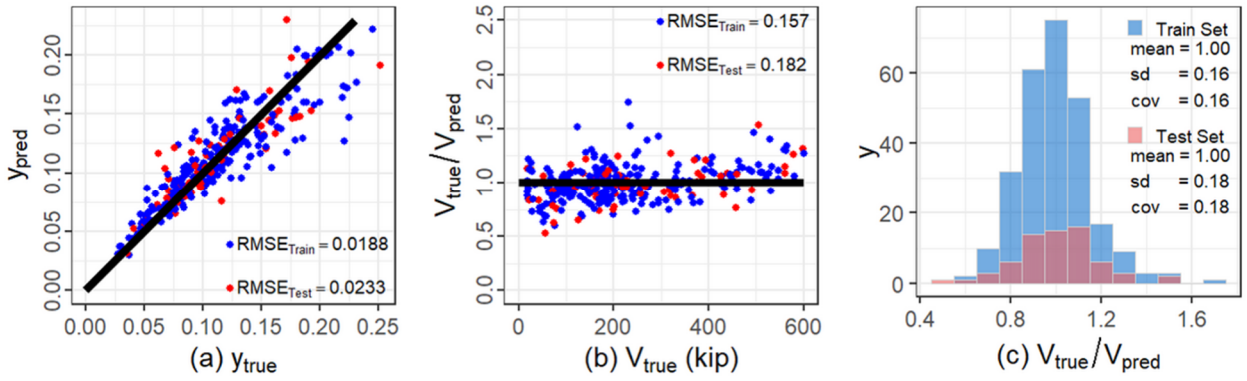

***Figure 6.5**: Proposed equation performance and verification: Symmetrical Walls*

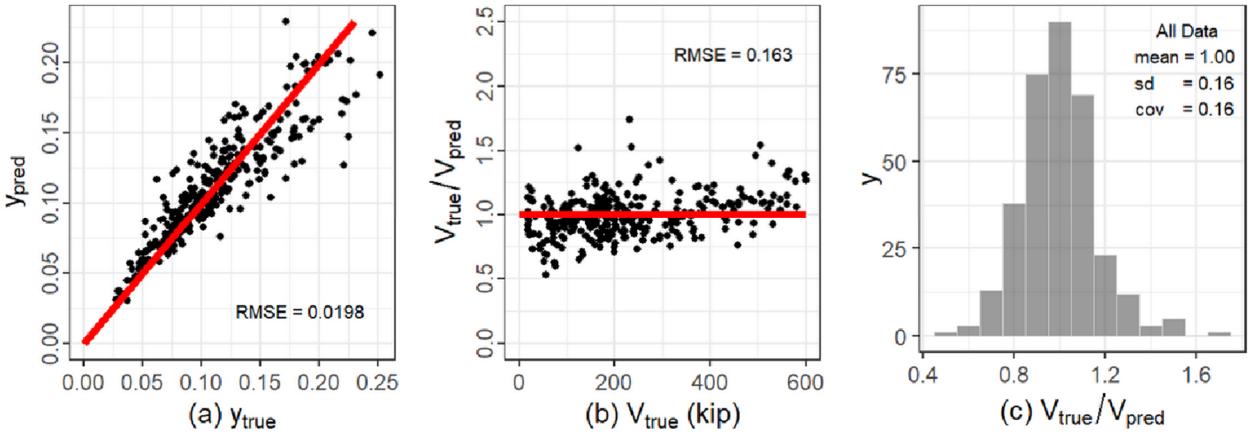

***Figure 6.6**: Proposed equation performance and verification: complete dataset of symmetrical walls*

Chapter 7. Simplified Version of the Proposed Equation

To provide an alternative, simplified, approach, as is commonly done in ACI 318, values for α_c and α_s are obtained based on dividing the database into sub-groups which, as shown in **Figure 7.1**, are defined by setting specific ranges for the axial load ratio and shear-span ratio. An iterative process was required to obtain these limits so they allow each sub-group to contain a reasonable amount of samples at the same time that the limits itself are "round up" values.

It is relevant to mention that, in a first instance, the α_c and α_s coefficients are estimated from the average values obtained with the regression coefficients (Eq. (7.2)). However, these values were manipulated according with what the α_c and α_s equations (Eq. (8.2) and Eq. (8.3)) suggest for each range combination of $M_u/(V_u l_w)$ and $P_u/\left(A'_g f'_c\right)$. The reasons to do this are because nice round up numbers are preferred and also because it helps to provide a better understanding of the range of values that can be obtained for those sub-groups with less samples (specially *Group 1D*).

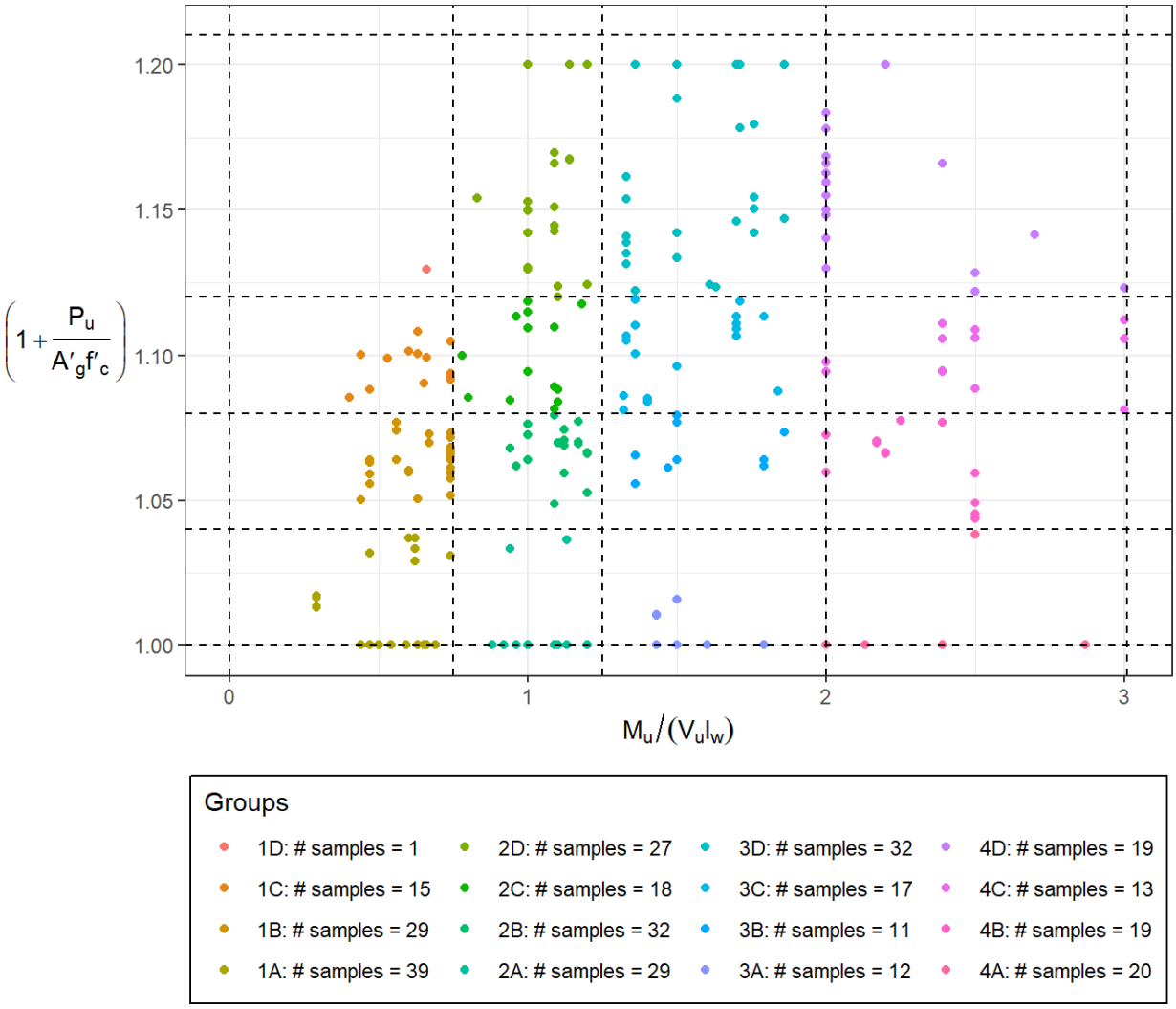

***Figure 7.1**: Definition of sub-groups*

Therefore, the simplified version of the proposed model consists in using the same proposed equation to predict wall shear strength (Eq. (8.1), shown again below), but the values of α_c and α_s can be obtain directly from **Table 7.1** instead of using the equations for it. An example of a potential benefit of using the simple model version is that α_c and α_s will remain constant if the axial load ratio and shear-span ratio values remain within the same range.

$$V_n = \alpha_c A'_g f'_c + \alpha_s(\rho_{sb} f_{ysb} + \rho_{wh} f_{ywh})$$

***Table 7.1**: Simplified method – Values for α_c and α_s coefficients*

$\frac{M_u}{\omega_v V_u l_w}$	α_c				α_s
	$0 \le \frac{P_u}{A'_g f'_c} < 0.04$	$0.04 \le \frac{P_u}{A'_g f'_c} < 0.08$	$0.08 \le \frac{P_u}{A'_g f'_c} < 0.12$	$\frac{P_u}{A'_g f'_c} \ge 0.12$	
[0, 0.75)	0.070	0.090	0.095	0.100	0.45
[0.75, 1.25)	0.025	0.045	0.075	0.080	0.40
[1.25, 2.00)	0.015	0.035	0.040	0.045	0.35
≥2.0	0.010	0.015	0.020	0.040	0.30

The performance of this simplified model is shown in **Figure 7.2** for the training and testing datasets and in **Figure 7.3** for the entire dataset. The mean values for all three datasets still meet the target values identified in **Table 3.7**. The COV value is still low and substantially lower than the value of 0.47 determined for the entire dataset for the ACI 318-19 Equation (18.10.4.1) and other models evaluated (**Figure 4.2**). It is noted that it would be a relatively simple process to develop an even more simplified model (with higher error) that could be used to simplify design for cases where wall shear demands are not expected to control.

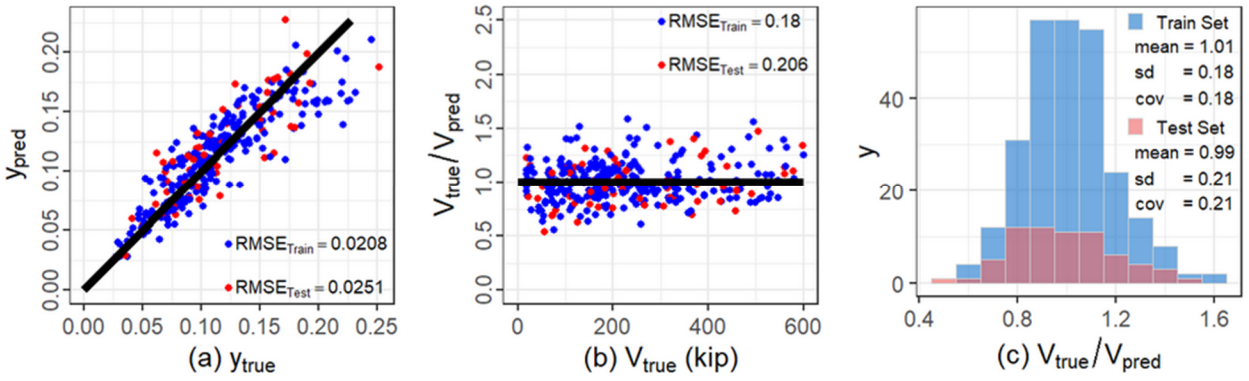

***Figure 7.2**: Performance and verification of the simplified model version*

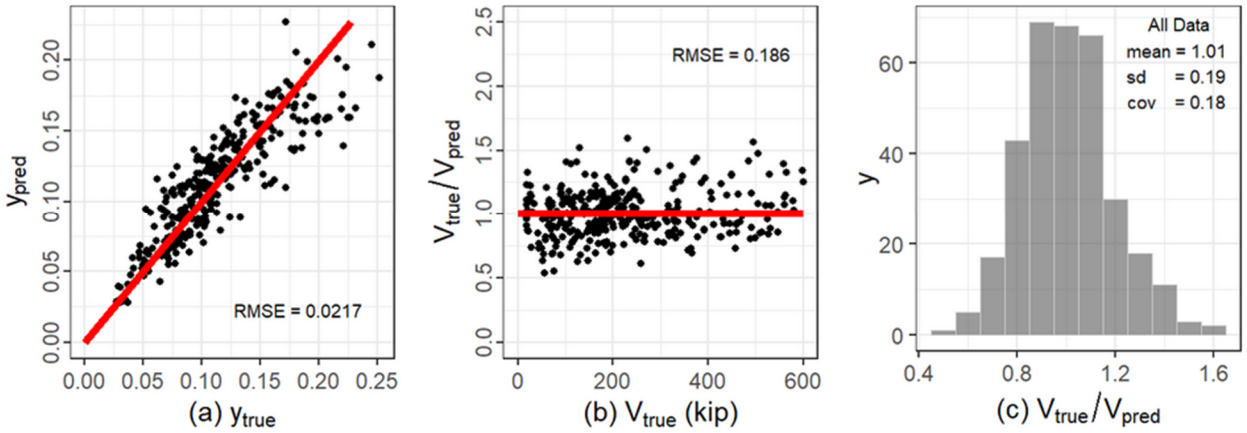

***Figure 7.3**: Performance of the proposed model over the complete dataset of symmetric walls*

Chapter 8. New Shear Stress Upper Limit

To avoid diagonal compression failures (Barda et al., 1977), ACI 318-19 includes an upper limit on wall shear stress (strength) of $10\sqrt{f_c'}A_{cv}$ for an individual wall segment and $8\sqrt{f_c'}A_{cv}$ for wall segments sharing a common lateral force. The $10\sqrt{f_c'}A_{cv}$ limit was reevaluated using the entire dataset, which included walls failing due to flexure-shear (F-S), diagonal tension (D-T), and diagonal compression (D-C). Results are presented in **Figure 8.1**, which also make the difference between rectangular walls and walls with flanges (in this study, walls with H-shaped and barbell cross-sections). The results presented in **Figure 8.1** demonstrate that the current shear strength upper limit is too conservative when applied to the entire dataset; however, the limit does provide a reasonable upper limit on wall shear strength for walls with rectangular cross sections with D-C failures (blue dots symbols).

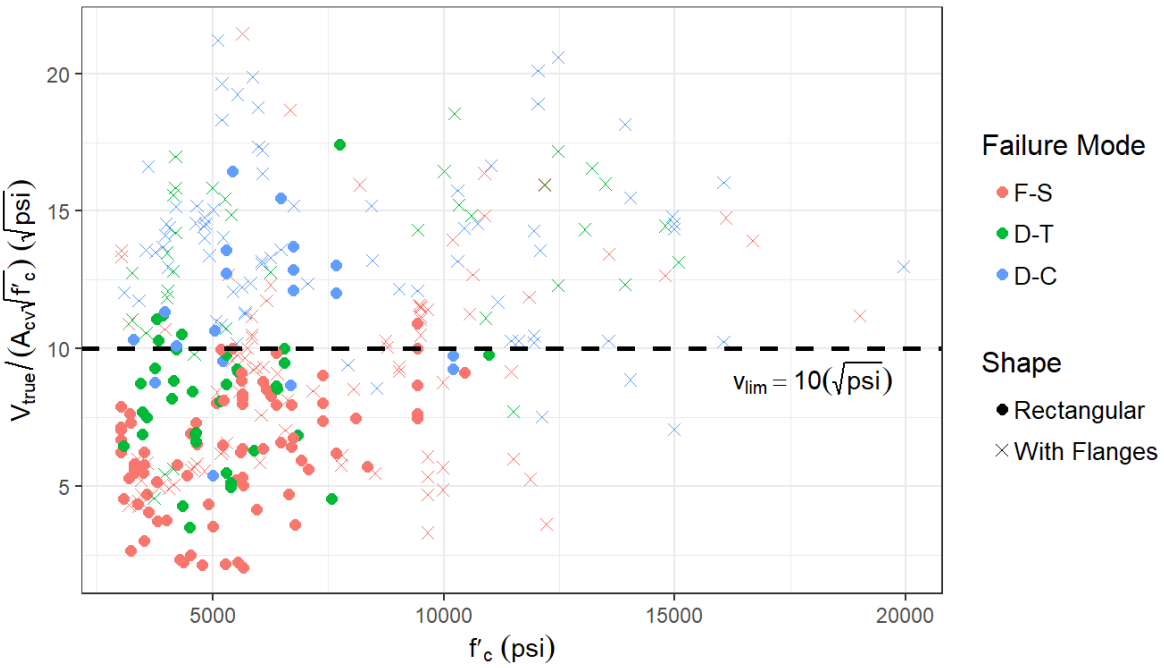

***Figure 8.1**: ACI 318-19 wall shear stress limit*

To further investigate this issue, histograms are plotted for the ratio of shear stress at failure to the current ACI 318-19 limit of $10\sqrt{f_c'}$ in **Figure 8.2**. Most of the rectangular walls failing in flexure-shear (F-S) (**Figure 8.2 (a)**) or in diagonal-tension (D-T) (**Figure 8.2(b)**) are below the current ACI 318-19 limit (indicated by a vertical dashed line), whereas about half of the rectangular walls failing in diagonal-compression (D-C) are above the limit (**Figure 8.2(c)**). However, the current limit does not do a good job at separating flanged walls that fail in diagonal-compression from flanged walls that do not fail in diagonal-compression, as several walls that failed in flexure-shear and diagonal-tension exceed the current limit.

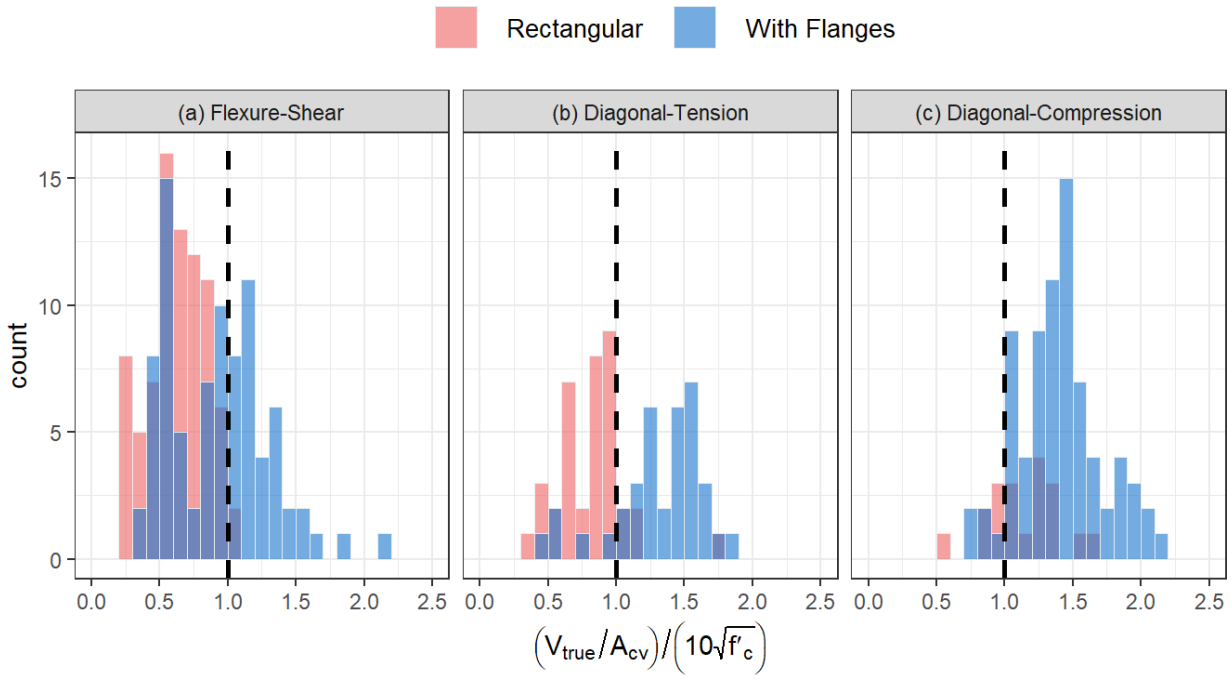

***Figure 8.2**: Current limit on ACI 318-19 vs wall shapes and shear failure types*

Therefore, a study was conducted to assess the potential to propose a new upper limit by using a logistic regression model designed to differentiate between walls that failed in F-S and D-T from walls that failed in D-C.

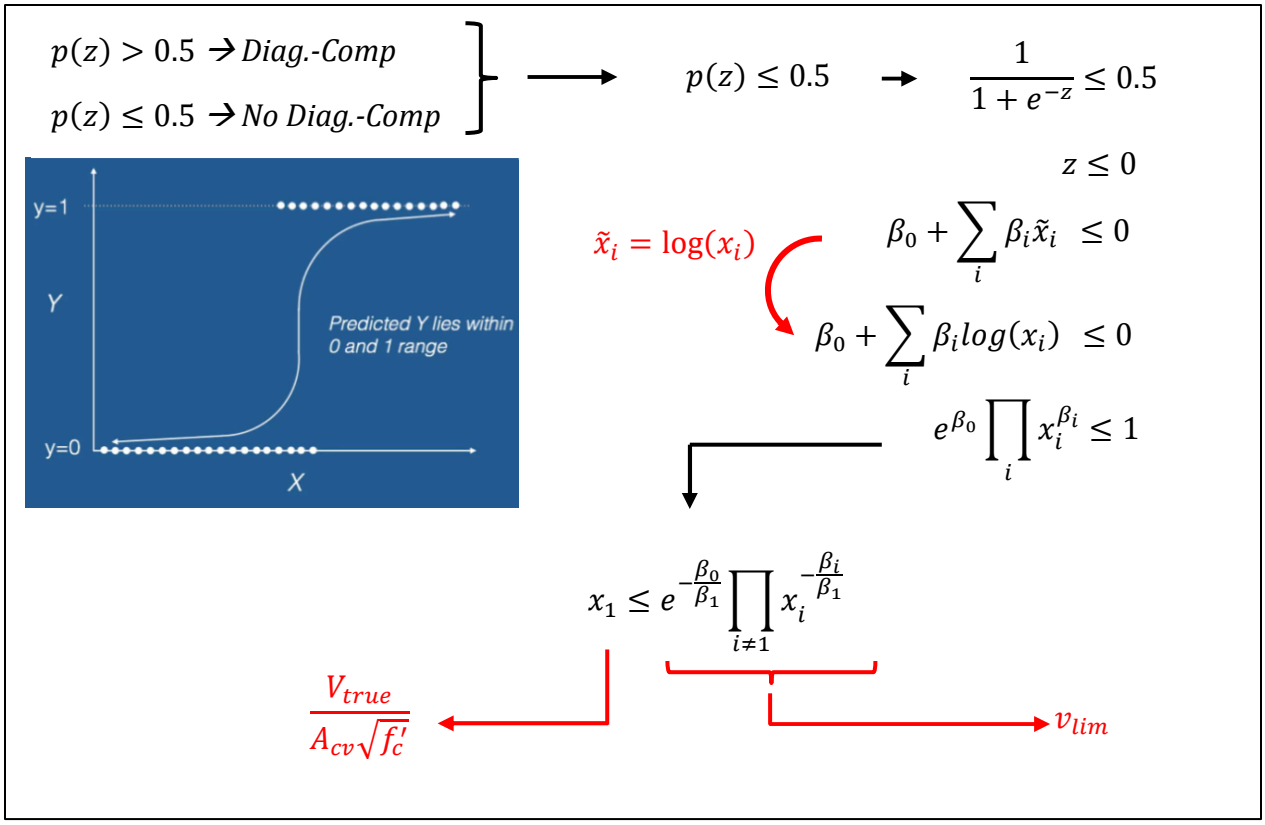

***Figure 8.3**: Manipulation of logistic regression to accommodate the desired problem*

The variables $\tilde{x}_i$ used to define the polynom $z = \beta_0 + \sum_i \beta_i \tilde{x}_i$ that defines the logistic function $p(z)$ are set up as the logarithm of variables (i.e.,$\tilde{x}_i = ln(x_i)$) that engineers would expect to find in an equation defining the shear stress limit. By doing so, the condition $p(z) \leq 0.5$ on the logistic function can be translated into $x_1 \leq e^{-\beta_0/\beta_1} \Pi_{i \neq 1} x_i^{-\beta_i/\beta_1}$ (see **Figure 8.3**). Therefore, by defining x_1 as the shear stress (any version of it according to the needs of the problem) and the rest of the x_i as relevant variables (such as shear-span ratio, axial load ratio, ratio of flange area over A_g or A_{cv}, etc.), it is possible to obtain an upper limit for the shear stress based on a multiplication of factors that results in walls below the limit to more likely to fail in either F-S or D-T than in D-C. Several models were studied, and although better

results could be obtained using a complex model (see **Figure 8.4** as an example), results obtained from a simple model more appropriate for implementation in a code or standard is used to develop a proposal.

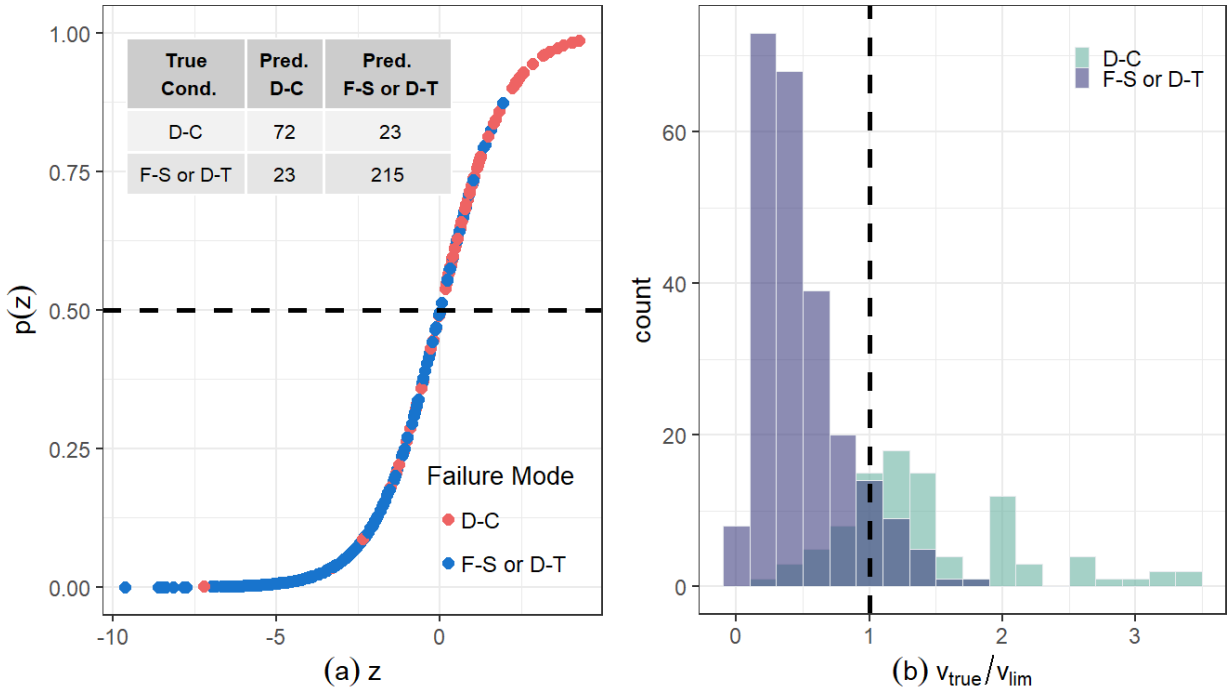

***Figure 8.4**: Example of a more complex logistic regression results*

To make the proposed new shear stress upper limit similar to the currently used in ACI 318-19, just one single parameter associated with wall cross-sectional shape was included in the simple logistic regression (see **Figure 8.5**) along with the shear stress, which was expressed in the same way that is currently defined in ACI 318-19, i.e., $V_n/\left(A_{cv}\sqrt{f_c'}\right)$. Also, since the objective is to include a modification in the current shear stress limit so it behaves similarly on both rectangular cross-sectional shaped walls and walls with flanges.

The coefficients of the logistic regression of **Figure 8.5** are rounded so the shear stress upper limit has a nicer expression. This results in the condition that wall shear stress $v_n = V_n/A_{cv}$ shall satisfy the following equation:

$$v_n = \frac{V_n}{A_{cv}} \leq \alpha_{shape} 10\sqrt{f_c'} \tag{11.1}$$

Where α_{shape} is 1.0 for walls with a rectangular cross section. Otherwise, for wall cross-sections with flanges, α_{shape} is compted using Eq. (11.2):

$$\alpha_{shape} = 0.7\left(1 + \frac{b_f t_f}{A_{cv}}\right)^2 \tag{11.2}$$

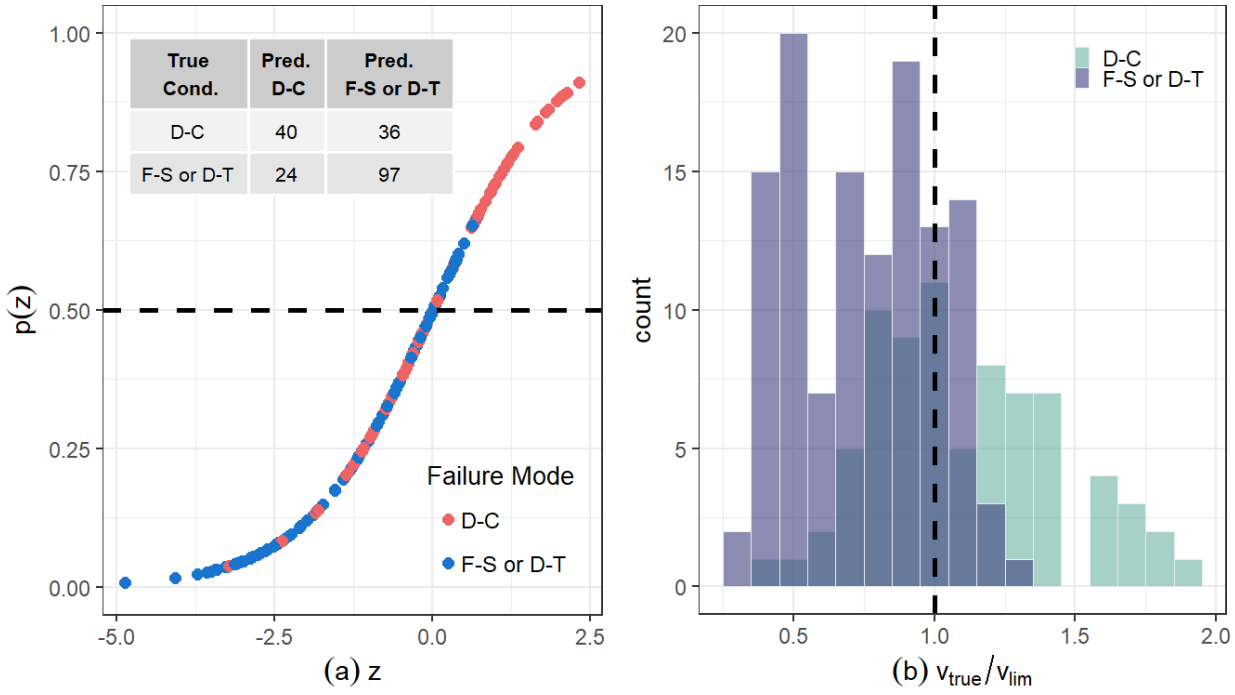

***Figure 8.5**: Simple logistic regression used to propose a new shear stress upper limit*

Using Eq. (11.2), α_{shape} need not be taken less than 1.0 and shall not exceed 1.5 and $b_f t_f$ is the total area of the overhanging effective flange width (on both sides of the web, if flanges

exist on both sides) for the compression flange. If the flange length is different on each end (boundary) of a wall, then the wall shear strength may be evaluated for each direction of loading independently or the wall shear strength may be conservatively based on the smaller flange width.

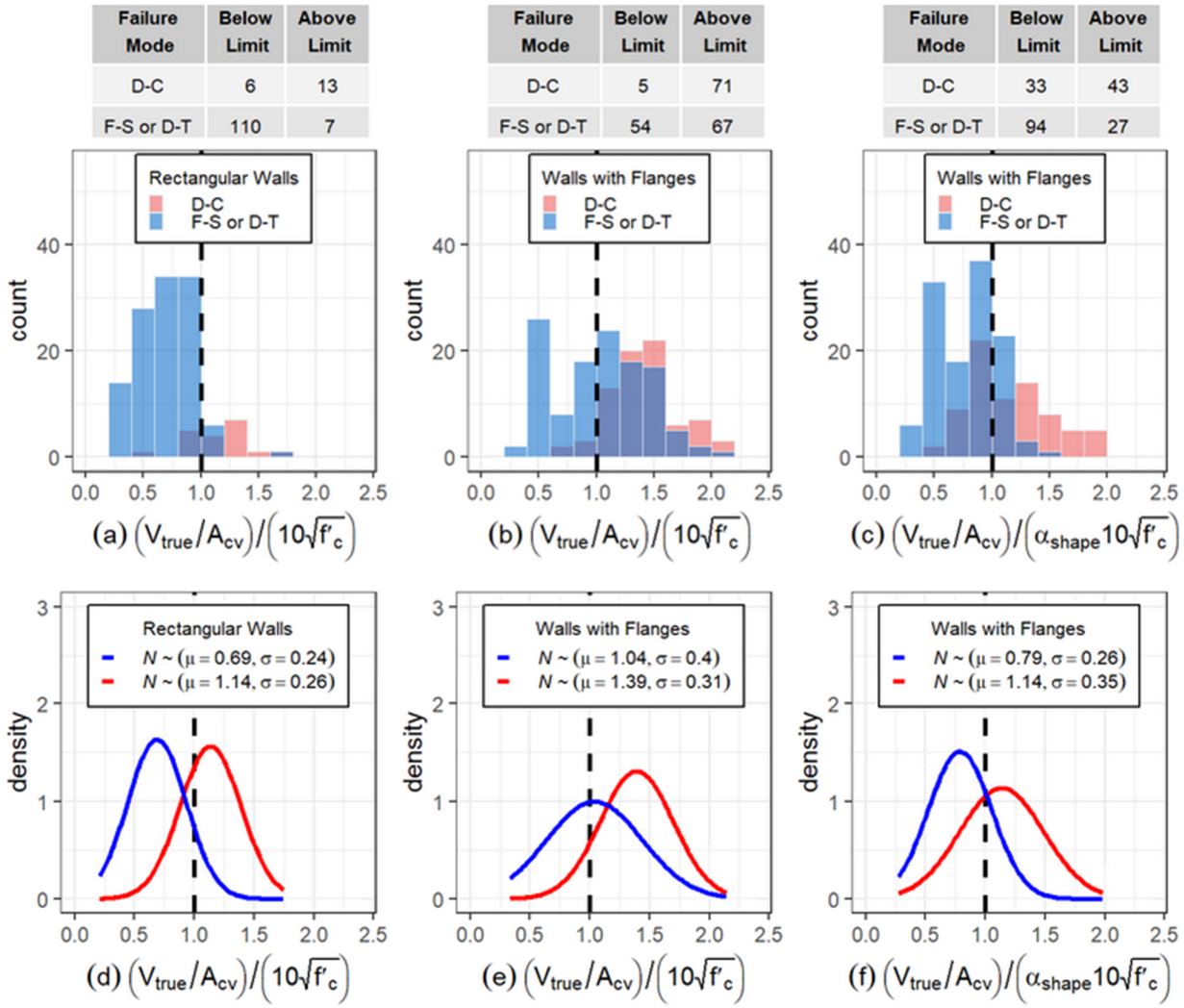

***Figure 8.6**: Comparison of current ACI 318-19 upper shear stress limit with proposed limit in function of wall shapes and shear failure types*

The distribution obtained with the proposed upper limit (**Figure 8.6(c)**) is similar to that for the current limit for walls with rectangular cross sections (**Figure 8.6(a)**), i.e., most of the walls failing in flexure-shear or diagonal-tension are below the limit and those failing in diagonal-compression are roughly half below and half above the limit. The latter is not as clear in **Figure 8.6(a)**, because there are not many rectangular walls failing in D-C, but **Figure 8.6(d)** shows that the fitted normal distribution have means of $\mu = 0.69$ and $\mu = 1.14$ for rectangular walls failing in F-S or D-T and for rectangular walls failing in D-C, respectively. **Figure 8.6(e)** shows the fitted normal distributions for walls with flanges with the current ACI 318-19 limit applied, and **Figure 8.6(f)** shows the fitted normal distributions for walls with flanges with the proposed limit applied. Distributions obtained with the proposed upper limit (**Figure 8.6(f)**) are much more similar to the distributions obtained for the rectangular walls with the current ACI 318-19 limit applied (**Figure 8.6(d)**).

Finally, for walls sharing a common lateral force, the limiting stress would be taken as $0.8\alpha_{shape}$, similarly to what ACI 318-19 currently does.

Chapter 9. Comparison Study between Proposed Equation and ACI 318-19 Equation

In this chapter, a detailed assessment of the performances of the proposed equation and the ACI 318-19 equation is developed. First, it is noted that ACI 318-19 Eq. 18.10.4.1 assumes that wall shear strength is directly proportional to the quantity of web horizontal reinforcement provided. This assumption applied to the proposed equation (Eq. (8.1)) would mean to force the term α_s to be equal to 1.0. In the first sub-section, this assumption is evaluated with the data, and it is found that it is not correct; it over-predicts what the data shows. In addition, the ACI318-19 concrete contribution term is evaluated, and it is found that under-predicts what the data shows (second sub-section of the chapter). Finally, in the last sub-section, a global interpretation of the proposed equation is presented, and it is compared along with the ACI 318-19 equation against key parameters, such as axial load ratio and wall cross-section shape.

9.1 Relative Contribution of Web Horizontal Reinforcement to Shear Strength

Figure 9.1(a) shows the histogram for ratios of $\rho_{wh}f_{ywh}A_{cv}/V_{true}$, while **Figure 9.1(b)** shows the histogram of $\rho_{wh}f_{ywh}A_{cv}/V_{(ACI318-19)}$. First, it is noted that the range of values for **Figure 9.1(a)** is broad, with a mean of 0.61, median of 0.52, standard deviation of 0.35, and 7.8% of the values greater than 1.0. Second, the two histograms do not line up; the data concentration in histogram of **Figure 9.1(b)** is slightly moved to the right respect to

histogram of **Figure 9.1(a)**. This suggests that the ACI 318-19 approach over-predicts the contribution of web horizontal reinforcement to wall shear strength.

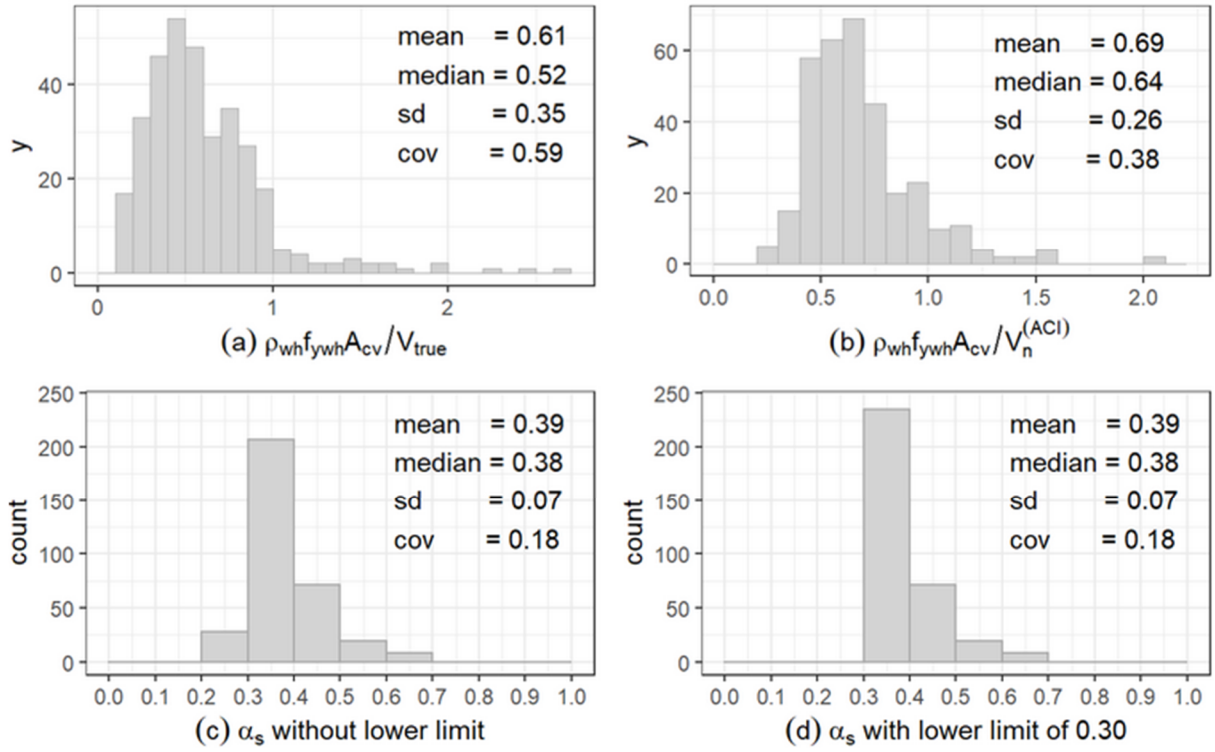

***Figure 9.1**: Upper horizontal reinforcement contribution relative to: (a) $\boldsymbol{V_{true}}$ and (b) $\boldsymbol{V_n}$ accordingly with ACI 318-19, and $\boldsymbol{\alpha_s}$: (c) without lower limit and (d) with lower limit*

In the proposed equation, α_s multiplies $\rho_{wh}f_{ywh}A_{cv}$ and thus represents an effectiveness factor. **Figure 9.1(c)** and **Figure 9.1(d)** present the histogram of α_s with and without the lower limit applied, respectively. These plots show that the mean value of the effectiveness of horizontal web steel in the proposed equation is much smaller than 1.0; it is 0.39 for both with and without application of the lower limit. In both cases the range of these values is fairly small (COV of 0.18 with or without the lower limit applied).

To further evaluate the contribution of web horizontal reinforcement, pairs of companion test were looked for within the database where the only variable that was allow to

significantly change between each companion couple was the web horizontal reinforcement strength $\rho_{wh}f_{ywh}A_{cv}$ (note that including A_{cv} has no effect since the cross-section was a variable that was kept as constant between the companion couples). From the total of 55278 different pairs that can be formed out of the 333 samples in the database, 67 pairs of companion tests were found. The difference in $\rho_{wh}f_{ywh}A_{cv}$ values was at least 3%, with an average difference of 72%, whereas all other parameters did not very by more than 10%. Therefore, since the only change between wall specimen (Test 1) and its companion wall specimen (Test 2) is primarily related to $\rho_{wh}f_{ywh}$, the variation in shear strength estimated by the current equation in ACI 318-19 and by the proposed equation are shown below (see Eq.(10.1) and Eq.(10.2)).

$$\begin{aligned}\Delta V_n^{(ACI)} &= \Delta\left(\alpha_c\sqrt{f_c'}A_{cv} + \rho_{wh}f_{ywh}A_{cv}\right)\\ &= \overbrace{\Delta\left(\alpha_c\sqrt{f_c'}A_{cv}\right)}^{0} + \Delta\left(\rho_{wh}f_{ywh}A_{cv}\right)\\ &= \Delta\left(\rho_{wh}f_{ywh}A_{cv}\right)\end{aligned} \tag{10.1}$$

$$\begin{aligned}\Delta V_n^{(PropEq)} &= \Delta\left(\alpha_c A_g' f_c' + \alpha_s\left(\rho_{sb}f_{ysb} + \rho_{wh}f_{ywh}\right)A_{cv}\right)\\ &= \overbrace{\Delta\left(\alpha_c A_g' f_c'\right)}^{0} + \overbrace{\Delta\left(\alpha_s\rho_{sb}f_{ysb}A_{cv}\right)}^{0} + \Delta\left(\alpha_s\rho_{wh}f_{ywh}A_{cv}\right)\\ &= \Delta\left(\alpha_s\rho_{wh}f_{ywh}A_{cv}\right)\\ &= \alpha_s A_{cv}\Delta\left(\rho_{wh}f_{ywh}\right)\end{aligned} \tag{10.2}$$

In both cases, the change in shear strength is function only of the web horizontal steel term. **Figure 9.2** shows the predicted shear strength by ACI 318-19 equation, versus the actual (true, measured) change in shear strength. Both axes are normalized by the measured shear strength of companion Test 1 (V_{true}). This normalization is helpful because it converts the

difference as a percentage of the "initial value", which makes the differences coming from all companion couples comparable.

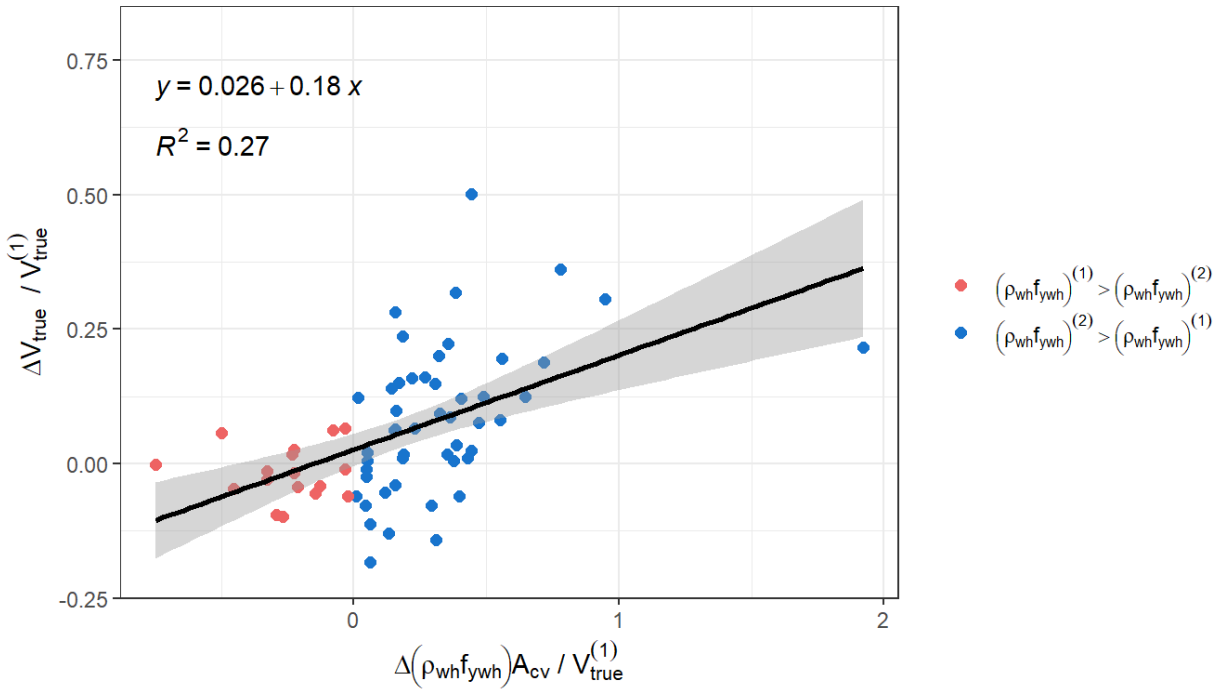

***Figure 9.2**: Change in shear strength of web horizontal steel companion tests*

From **Figure 9.2** it can be seen that there are cases where the companion Test 2 has a larger steel contribution term than companion Test 1, i.e., $(\rho_{wh}f_{ywh})^{(2)} > (\rho_{wh}f_{ywh})^{(1)}$. There are cases where the opposite happens as well. This condition is random, it just depend on what test was decided to be called "first" in the companion couple. Acknowledging this, it was decided to reverse the order of the companion couples with $(\rho_{wh}f_{ywh})^{(1)} > (\rho_{wh}f_{ywh})^{(2)}$. The reason to do this is because it allows to highlight the trends by reducing the range covered by the samples, which is helpful in this case given that there are only 67 data points in the plot and that they have a large variance. **Figure 9.3(a)** shows the same plot that in **Figure 9.2** but with the changes just mentioned. **Figure 9.3(b)** it is the same plot, but the

predicted shear strength variation is obtained with the proposed equation (see Eq. (10.2)). One pair of companion tests (Zhang et al., 2007) was too deviated from the trends, and it was found that both companion tests had a flexure-shear failure type, but the shear failure of both happened in sliding. Since the failure in both specimens happens due to a different mechanism, it was removed. Results from this point ae obtained with the remaining 66 companion pairs.

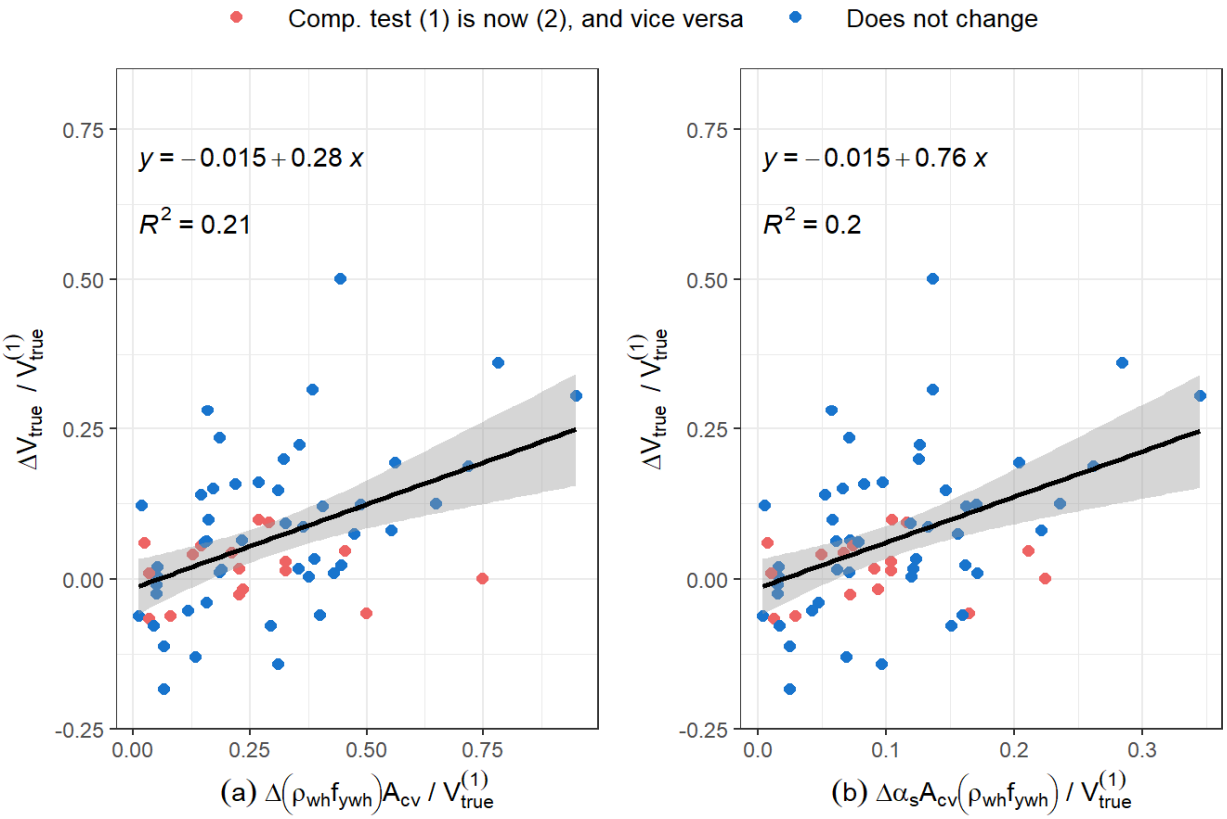

***Figure 9.3**: Change in shear strength of web horizontal steel companion tests with initial and final conditions inverted such as $\Delta\rho_{wh}f_{ywh} > 0$*

At first sight, **Figure 9.3(a)** and **Figure 9.3(b)** look very similar. However, the difference happens in the values of the x-axis. **Figure 9.4** highlights the difference (the figure is the same, but it keeps the axis limits constant).

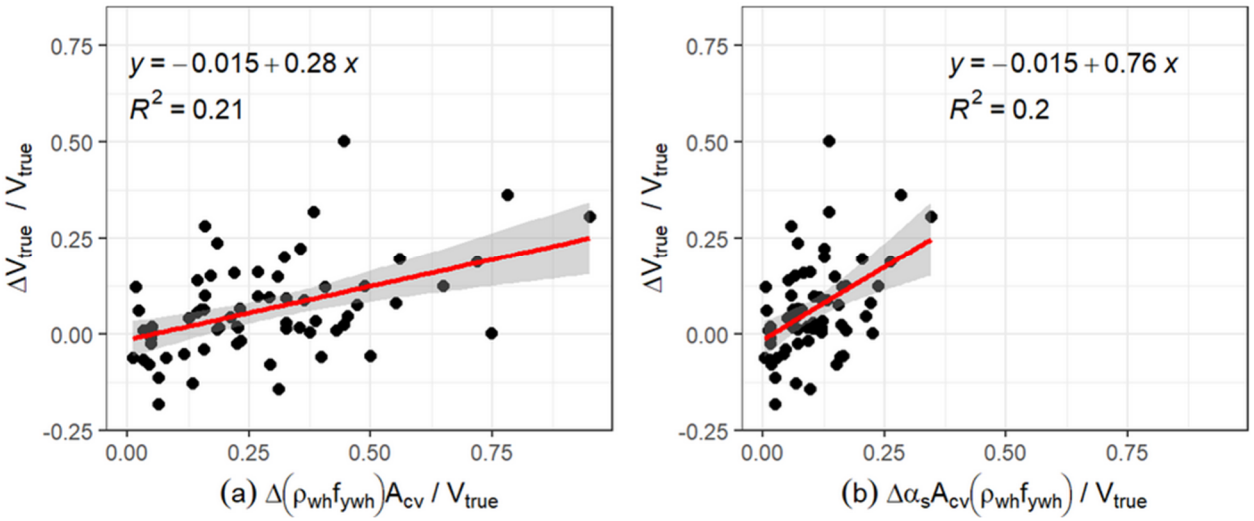

***Figure 9.4**: Change in shear strength of companion group 1 tests predicted with: (a) V_s in ACI 318-19, and (b) V_s in Proposed Equation*

The slope of the linear regressions in **Figure 9.4** can be interpreted as the efficiency multiplier weighting the web horizontal reinforcement contribution term. **Figure 9.4 (a)** indicate that assuming 100% of efficiency on the web horizontal reinforcement overestimates the actual contribution coming from this term significantly because the slope of the regression is just 0.28. On the other hand, **Figure 9.4(b)** shows that when incorporating the α_s coefficient of the proposed equation (Eq. (8.1)), the slope of the regression goes up to 0.76. Even though 0.76 is much closer to 1.0, it is not as close to it. However, there are only 332 pairs of companion tests in these plots (one companion couple was removed as an outlier), and considerable dispersion is observed as well.

Additionally, the slopes obtained in the plots shown in **Figure 9.5** and **Figure 9.6** are close to the values of the proposed α_s (see **Figure 9.1**), or slightly smaller. However, considerable dispersion is observed for walls failing in F-S and D-T. Additional data are needed to enable further interpretation of these trends.

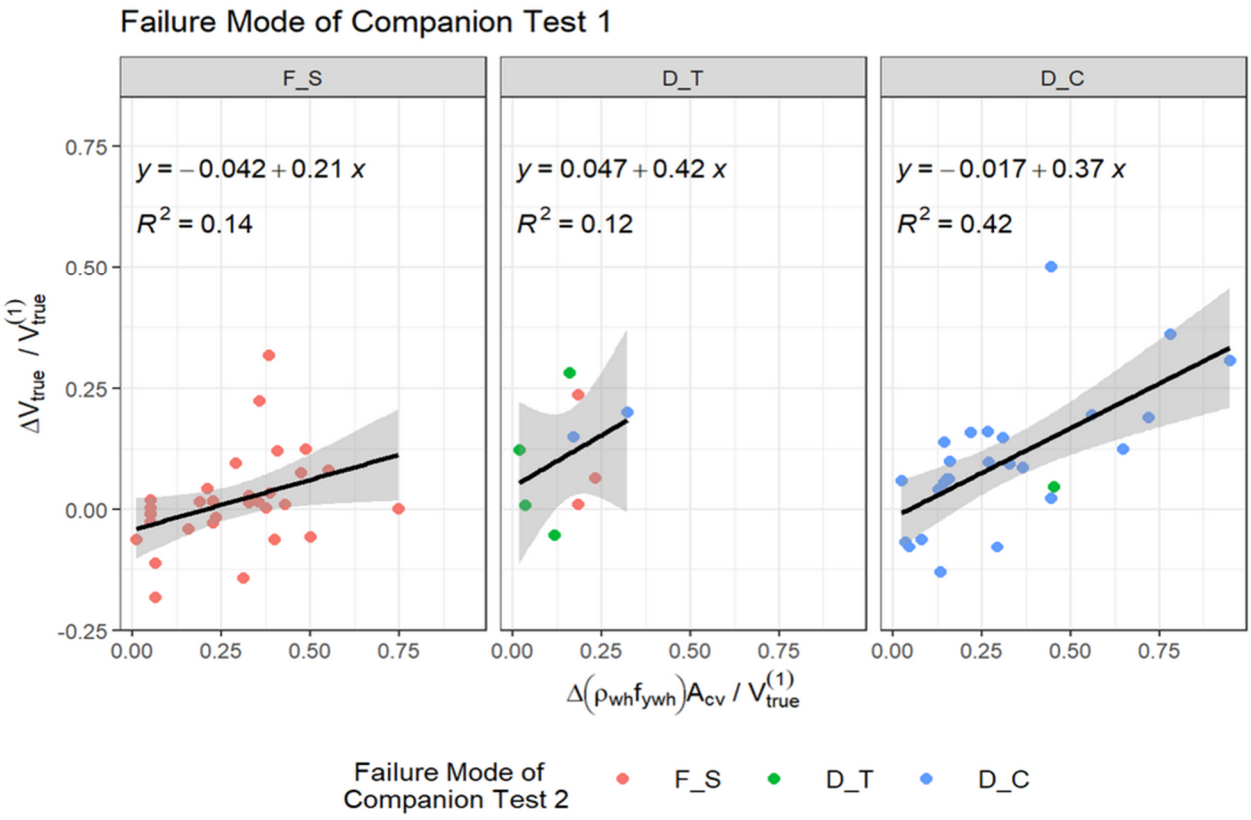

Figure 9.5*: Change in shear strength of web horizontal steel companion tests: Groups by failure mode of test (1), colors by failure mode of test (1) as well*

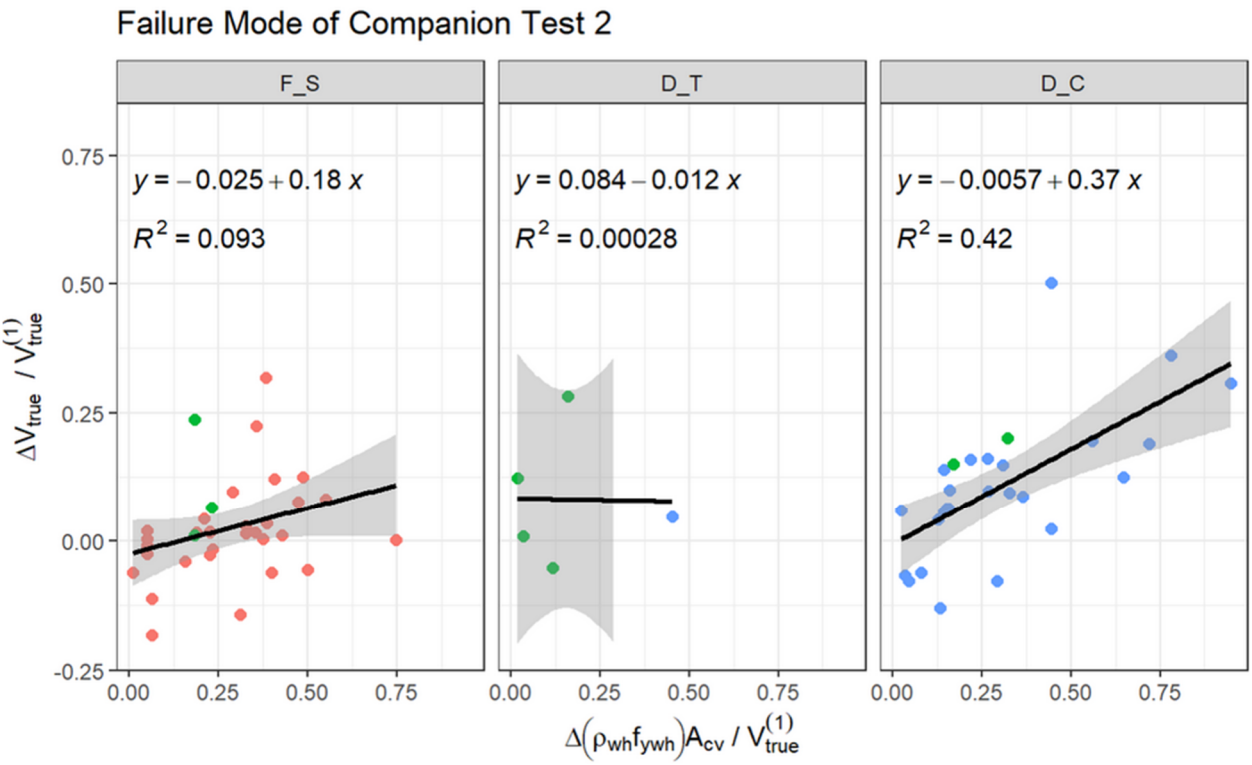

***Figure 9.6**: Change in shear strength of web horizontal steel companion tests: Groups by failure mode of test (2), colors by failure mode of test (1)*

9.2 Relative Contribution of Concrete to Shear Strength

A second analysis of companion tests is carried out. In this case, from the total of 55278 different pairs that can be formed out of the 333 samples in the database, 675 pairs of companion tests having the same shape, same horizontal web steel term (difference in $\rho_{wh}f_{ywh}A_{cv}$ values is zero for 238 pairs and is less than 3% for the rest), and no restriction on any other parameters were identified.

According to the current ACI 318-19 equation, the change in the total shear strength comes from the change in the concrete term only:

$$\begin{aligned}\Delta V_n^{(ACI)} &= \Delta\left(\alpha_c\sqrt{f_c'}A_{cv} + \rho_{wh}f_{ywh}A_{cv}\right)\\ &= \Delta\left(\alpha_c\sqrt{f_c'}A_{cv}\right) + \overbrace{\Delta\left(\rho_{wh}f_{ywh}A_{cv}\right)}^{0}\\ &= A_{cv}\Delta\left(\alpha_c\sqrt{f_c'}\right)\end{aligned} \tag{10.3}$$

On the other hand, the change in the total shear strength for these companion tests depends on two of the three terms of the proposed equation:

$$\begin{aligned}\Delta V_n^{(PropEq)} &= \Delta\left(\alpha_c A_g' f_c' + \alpha_s\left(\rho_{sb}f_{ysb} + \rho_{wh}f_{ywh}\right)A_{cv}\right)\\ &= \Delta\left(\alpha_c A_g' f_c'\right) + \Delta\left(\alpha_s\rho_{sb}f_{ysb}A_{cv}\right) + \overbrace{\Delta\left(\alpha_s\rho_{wh}f_{ywh}A_{cv}\right)}^{0}\\ &= \Delta\left(\alpha_c A_g' f_c'\right) + A_{cv}\Delta\left(\alpha_s\rho_{sb}f_{ysb}\right)\end{aligned} \tag{10.4}$$

Figure 9.7(a) shows that the ACI318-19 equation underpredicts the change in shear strength by 56.4 of the true value (because the slope of the linear regression is 2.29). **Figure 9.7(b)** shows that the proposed equation predicts the true shear strength change much more accurately, because the linear regression slope is 1.04. Note that in this case there is a

significant larger number of companion couples, which reduces the impact in the trends coming from the order in which the test within each companion couple were named.

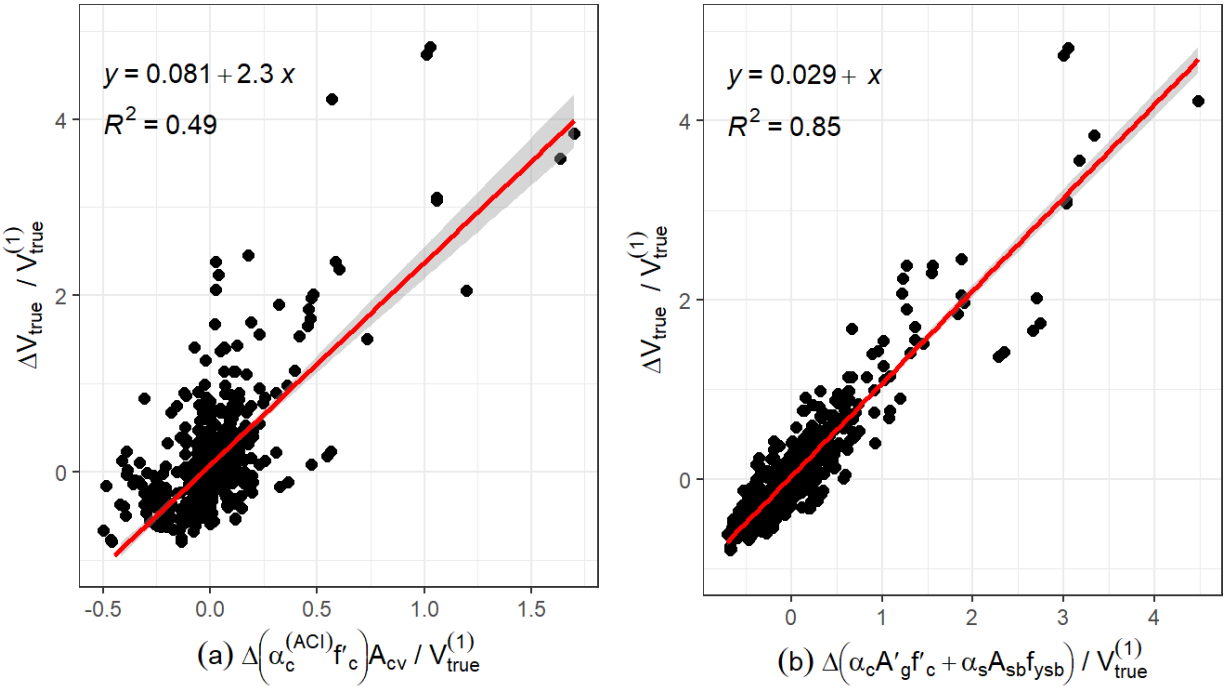

***Figure 9.7**: Prediction of the shear strength*

Figure 9.8(a), **Figure 9.8(b)**, and **Figure 9.8(c)** shows the change in wall shear strength for the companion tests with constant web horizontal reinforcement using the ACI318-19 equation for walls with rectangular cross section, barbell cross section, and cross sections with flanges, respectively. **Figure 9.8(d)**, **Figure 9.8(e)**, and **Figure 9.8(f)** plot the same but using the proposed equation. The results indicate that the proposed equation does a significantly better job at predicting the change in wall shear strength for all three wall cross-section shapes. Also, the performance of the proposed equation is very similar for the three wall cross-sectional shapes.

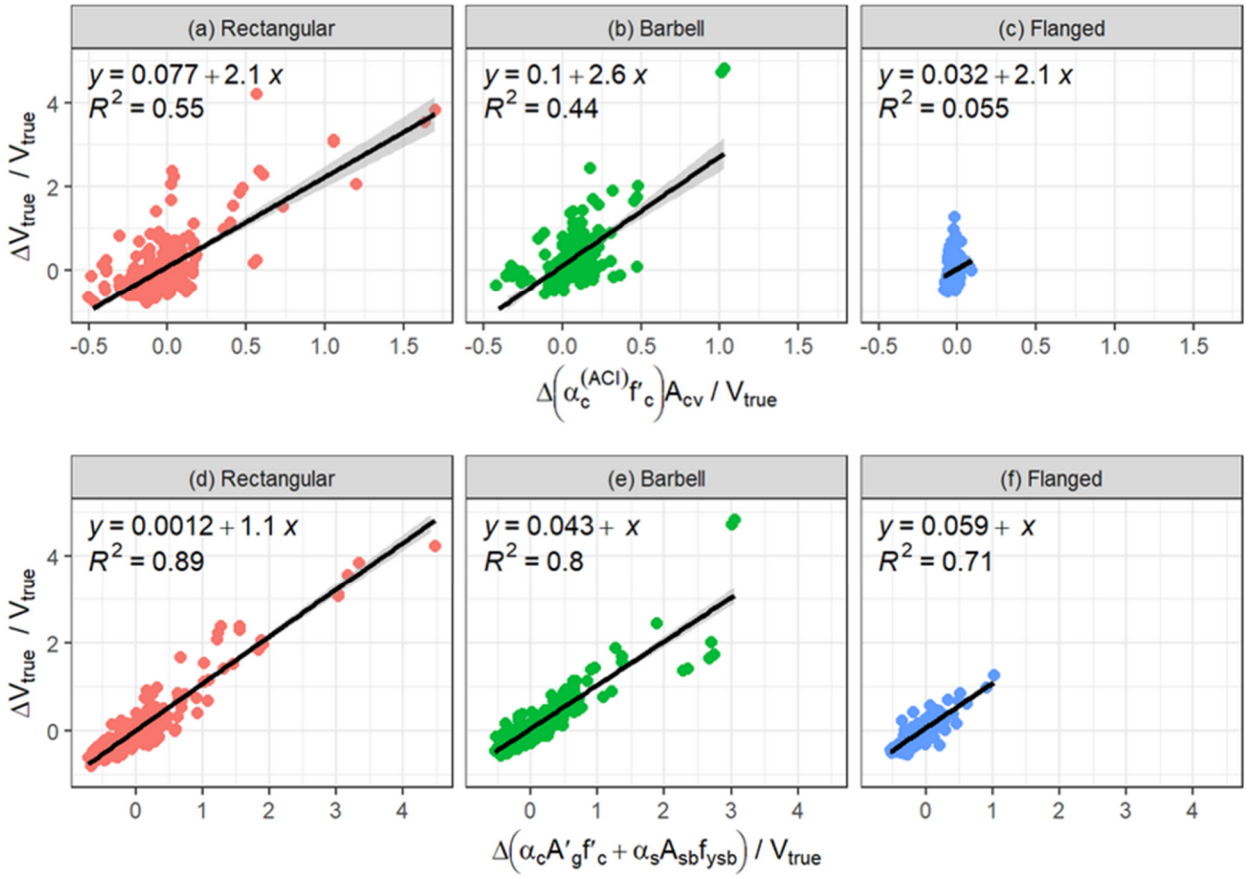

***Figure 9.8**: Shear strength change prediction by wall cross-sectional shape using ACI 318-19 equation*

The concrete contribution from the ACI318-19 equation and the proposed equation also are compared to enable better understanding of the proposed equation. To accomplish this, the α_c coefficient in ACI 318-19 Equation 18.10.4.1, which has units of $\sqrt{psi}$ is normalized by pre- and post-multiplying the ACI 318-19 concrete contribution by $\sqrt{f_c'}$, i.e.:

$$V_c = \alpha_c \lambda A_{cv} \sqrt{f_c'}$$

$$= \left(\frac{\alpha_c}{\sqrt{f_c'}}\right) \lambda A_{cv} \sqrt{f_c'} \sqrt{f_c'}$$

$$= \left(\frac{\alpha_c}{\sqrt{f_c'}}\right) \lambda A_{cv} f_c'$$

Therefore, the normalized ACI 318-19 normalized α_c coefficient is defined as:

$$\alpha_{c,norm}^{(ACI)} = \frac{\alpha_c^{(ACI)}}{\sqrt{f_c'}}$$

And, from the database, the mean value of $1/\sqrt{f_c'}$ is 0.013 $\sqrt{psi}$.

Figure 9.9(a) shows the proposed α_c values using the shear-span ratio and axial load ratio from the database to show the range of applicability. **Figure 9.9(b)** shows the analytical values for the proposed α_c (obtained with Eq. (8.2)) and $\alpha_{c,norm}^{(ACI)}$. To generate this plot, the shear-span ratio was taken equal to the aspect ratio, i.e., $h_w/l_w = M_u/(V_u l_w)$, which is a reasonable assumption for wall specimens tested in the laboratory (see Section 5.1). However, as noted in Section 6.3 (particularly, **Figure 6.3** and **Figure 6.4**), h_w/l_w is likely to be considerably greater than $M_u/(V_u l_w)$. The normalized $\alpha_{c,norm}^{(ACI)}$ corresponds to values associated to axial load ratios $P_u/(A_g' f_c')$ between 5% and 10% for $M_u/(V_u l_w) \geq 1.0$, and tends to significantly underestimate the concrete contribution for higher axial loads and for $M_u/(V_u l_w) < 1.0$.

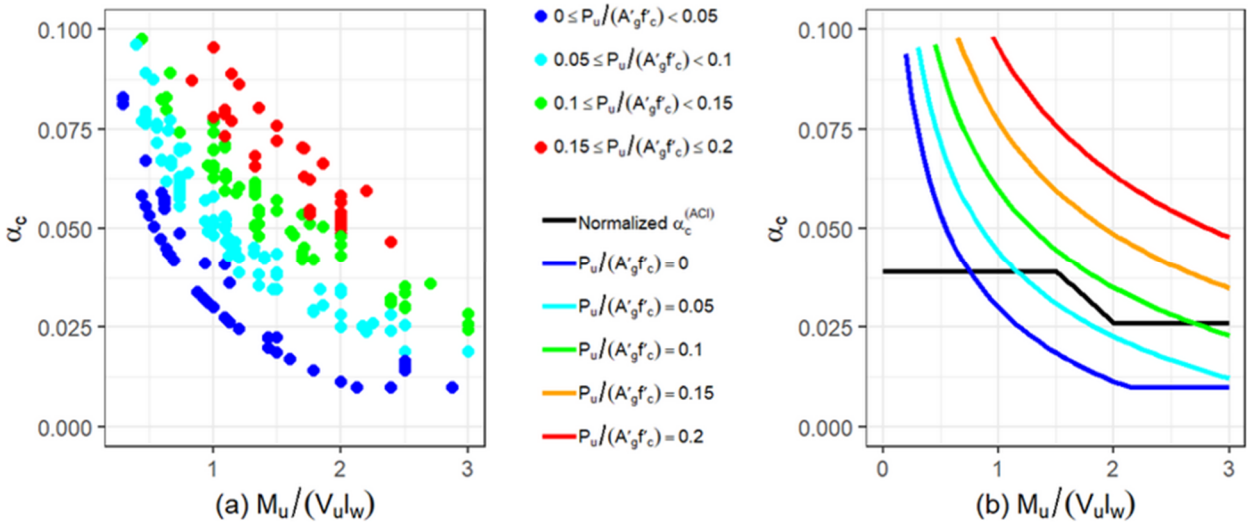

***Figure 9.9**: Understanding of proposed α_c*

It is important to note that, in this comparison (and in Eq. (8.1)), the influence of the boundary longitudinal reinforcement on wall shear strength was included as a "reinforcement contribution", i.e., $V_s = \alpha_s(\rho_{sb} f_{ysb} + \rho_{wh} f_{ywh}) A_{cv}$. The boundary longitudinal reinforcement term ($\alpha_s \rho_{sb} f_{ysb} A_{cv}$) also could be considered as a "concrete contribution", as one physical interpretation as to how this increases wall shear strength is that increases wall neutral axis depth, which results in larger concrete contribution (e.g., as is done in ACI 318-19 Table 22.5.5.1 for one-way shear strength). However, analysis of the data also suggested that the increase in wall shear strength might also be due, in part, to the possibility of increased reinforcement contribution (e.g., dowel action). Therefore, although the proposed model is presented as shown in Eq. (8.1), an alternative form where the boundary longitudinal reinforcement term is treated as a concrete contribution could also be derived.

9.3 Further Interpretation and Comparison Against ACI 318-19 Equation

The proposed equation is explicitly accounting for effect of the axial load and for the longitudinal reinforcement at the edge of the wall in tension, which are not considered in the ACI 318-19 equation. Also, it uses the shear-span ratio instead of aspect ratio. From the mechanics of the problem, all these parameters were known to influence wall shear strength (or column shear strength).

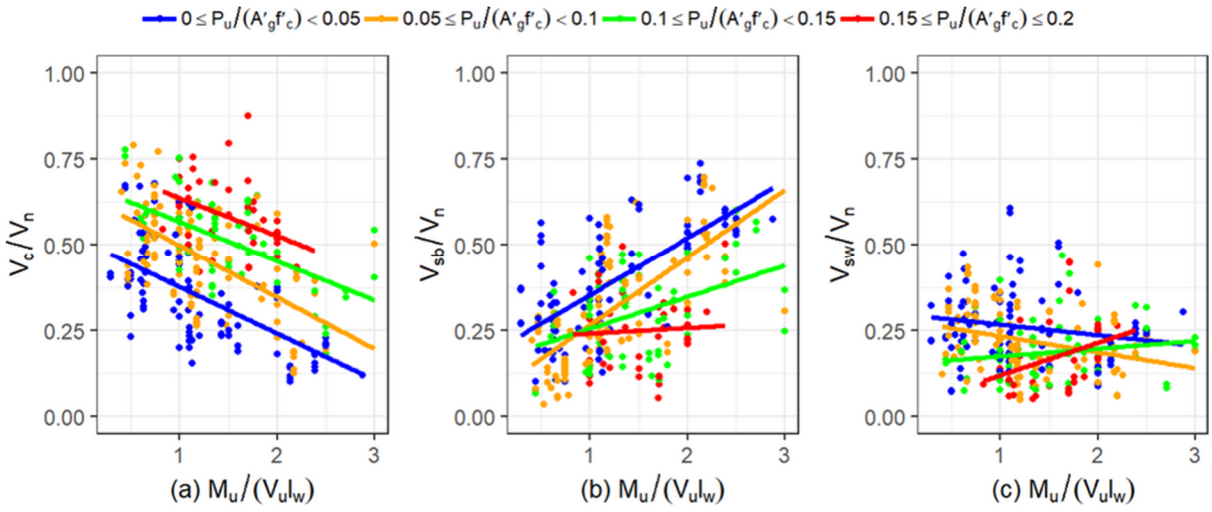

***Figure 9.10**: Relative shear strength contribution from each term of the proposed equation*

Figure 9.10 shows the relative contributions coming from each term of the proposed equation when estimating the shear strength of the walls in the database. **Figure 9.10(a)** indicates that the contribution coming from $V_c = \alpha_c A'_g f'_c$ increases with increasing axial load ratio and with lower shear span ratios, as expected. In **Figure 9.10(b)**, at zero or low axial stress, wall shear strength increases substantially with increases in boundary longitudinal reinforcement $\left(V_{sb} = \alpha_s \rho_{sb} f_{ysb} A_{cv}\right)$, likely because neutral axis depth and dowel action increase, and as shear span increases, likely because overturning moment increases requiring greater quantities of boundary longitudinal reinforcement. **Figure 9.10(c)** shows

that the relative contribution of the third term of the equation (directly related to web horizontal reinforcement contribution, $V_{sw} = \alpha_s \rho_{wh} f_{ywh} A_{cv}$) is, on average 22%, and is not very sensitive to changes in both shear-span ratio and axial load ratio.

Figure 9.11 and **Figure 9.12** show the ACI 318-19 equation is biased and that the proposed equation provides a similar performance against different variables (e.g., axial load ratio, shear-span ratio, shear stress). The ACI 318-19 approach is generally conservative, except for walls low axial load ratios (**Figure 9.11(a)**) or rectangular walls with low normalized shear stress (**Figure 9.12(a)**) (which are likely to be correlated), it produces significantly different mean values for walls with higher axial loads (**Figure 9.11(a)**) or with different cross-section shapes (**Figure 9.12(a)**), and its limiting shear stress has the biggest impact on walls with axial load ratios greater than 0.05 (**Figure 9.11(b)**) and it affects walls with different cross-section shapes similarly (**Figure 9.12(b)**). The proposed approach provides a fairly uniform mean and COV values prior to application of a limiting shear stress (**Figure 9.11(c)** and **Figure 9.12(c)**), except for a modest increase in the dispersion at very low normalized shear strength (**Figure 9.11(a)**), which mainly corresponds to walls with axial load ratios lesser than 0.5. This increase in dispersion is, however, smaller than the one ACI 318-19 equation has in the same range of normalized shear stress. Applying a limiting shear stress for the proposed approach primarily influences barbell-shaped and H-shaped walls (**Figure 9.12(d)**) and walls with axial stress ratios either small (less than 0.05) or high (greater than 0.12) (**Figure 9.11(d)**). These wall configurations are likely to be correlated; a barbell or H-shaped wall with a large axial load might be obtaining a high shear strength contribution coming from $V_c = \alpha_c A'_g f'_c$ (**Figure 9.10(a)**), while a barbell or H-shaped wall

with very low axial load might be getting a large shear strength contribution from $V_{sb} = \alpha_s \rho_{sb} f_{ysb} A_{cv}$ (**Figure 9.10(b)**).

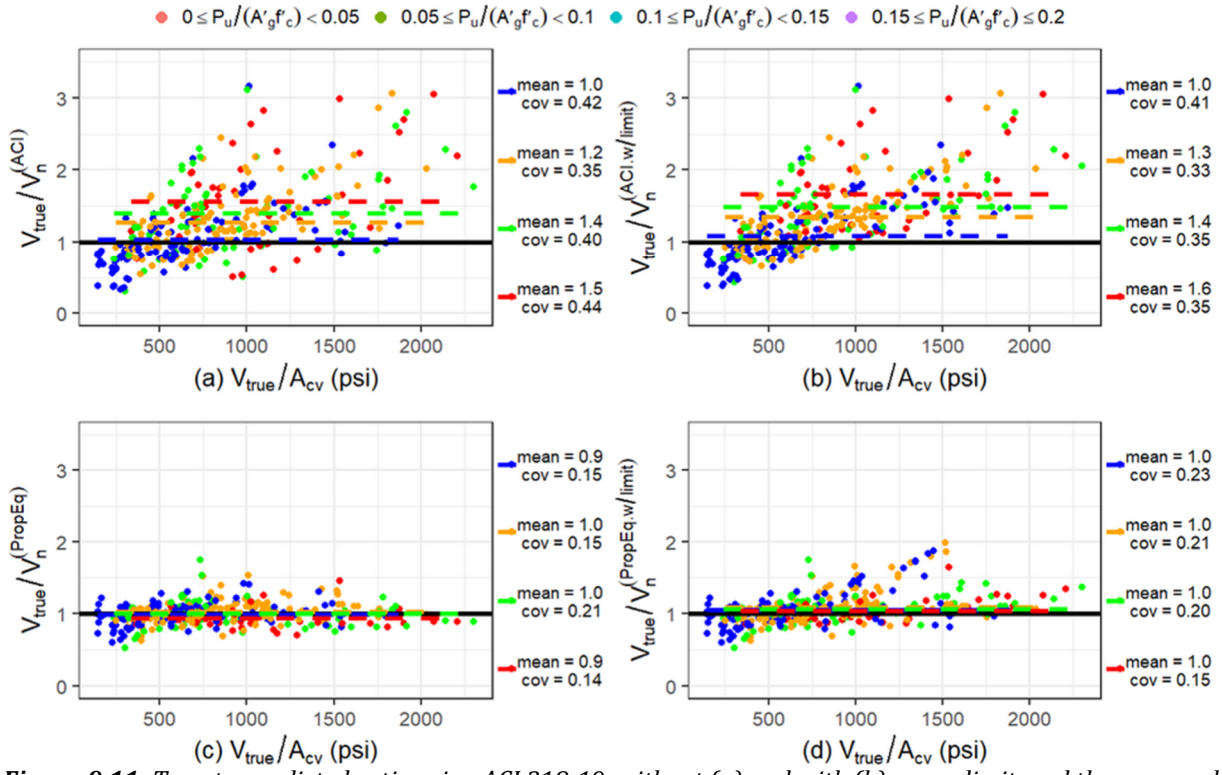

***Figure 9.11**: True-to-predicted ratio using ACI 318-19, without (a) and with (b) upper limit, and the proposed equation without (c) and with (d) upper limit, versus shear stress.*

Figure 9.13(a) confirms that ACI 318-19 equation is generally more conservative than the proposed equation for walls with axial load ratios larger than 5%, or for walls with barbell or H-shaped cross-sections (**Figure 9.13(c)**). On the other hand, the shear strength for rectangular walls with low axial load ratio might be underestimated by the ACI 318-19 equation. This is a cause of concern because short rectangular walls with low axial load ratio are the ones most likely to be subjected to a shear failure. Applying the upper limit on the equations accentuates the over-conservatism of the ACI 318-19 equation respect to the proposed equation for walls with axial load ratios larger than 10% (**Figure 9.13(b)**) and for walls with rectangular cross sections (**Figure 9.13(d)**).

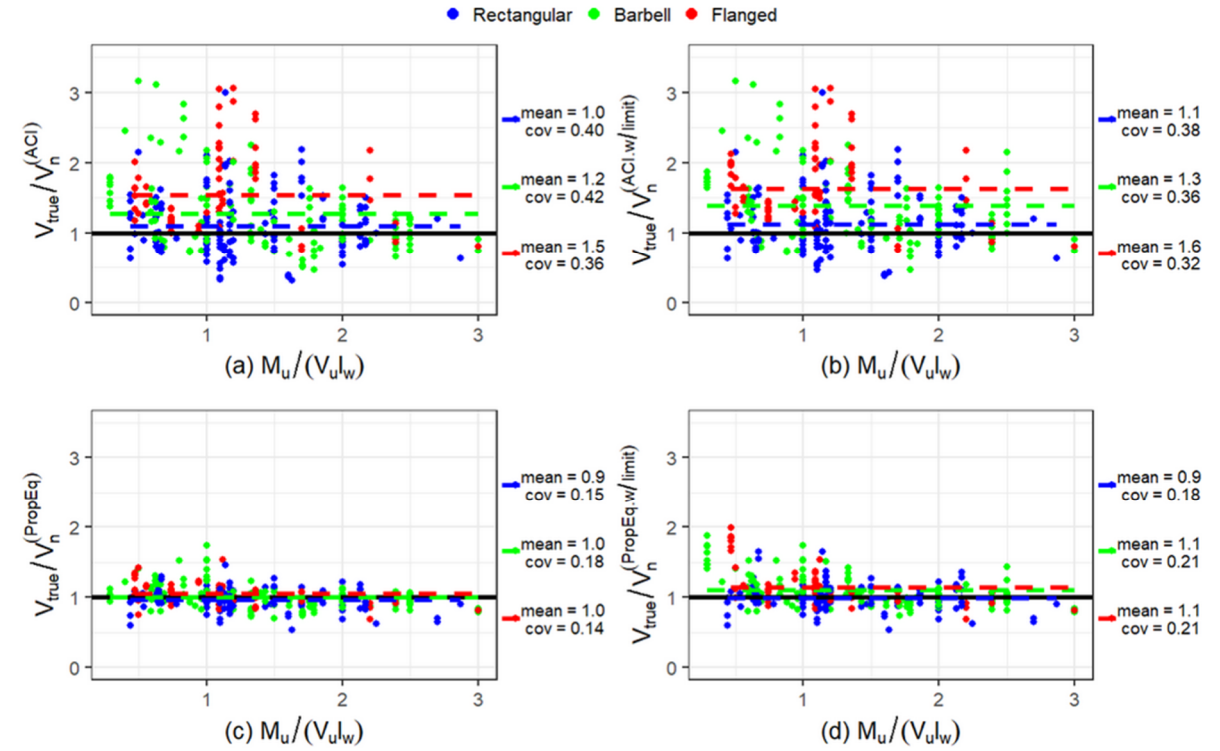

***Figure 9.12**: True- to-predicted ratio using ACI 318-19, without (a) and with (b) upper limit, and the proposed equation without (c) and with (d) upper limit, versus shear span ratio.*

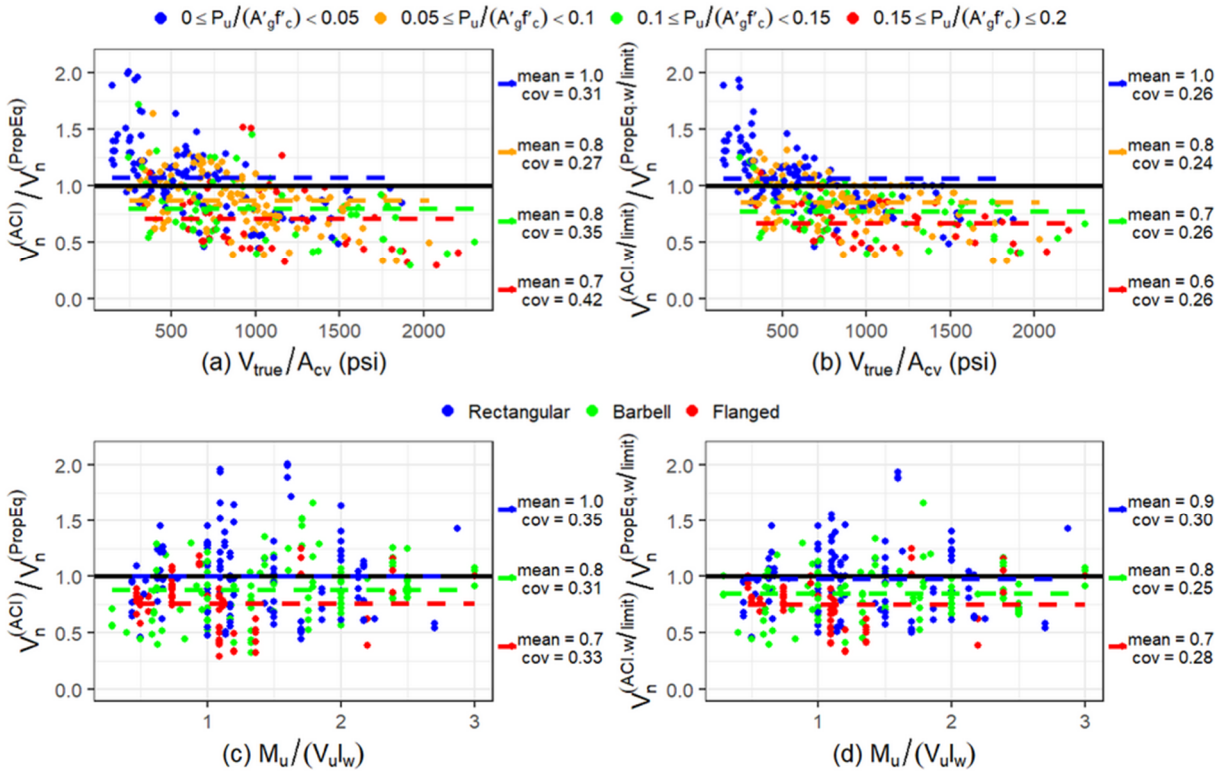

***Figure 9.13**: Ratio of shear strength predicted by ACI 318-19 versus shear strength predicted with the proposed equation.*

Chapter 10. Strength Reduction Factor for Design Purposes

10.1 Introduction

A Monte Carlo Simulation will be run to assess the reliability associated with the strength reduction factor currently used in ACI 318-19, $\phi = 0.75$, for Maximum Considered Earthquake (MCE) GMs. The archetypes are designed with the ACI 318-19 equation, but their shear capacity will also be estimated with the proposed equation. Since it has been shown the performance of the proposed equation to be better than the ACI 318-19 equation, addressing the reliability of these ACI 318-19 compliant archetypes with the proposed equation will provide a better estimation of the probability of failure of these archetypes. Also, a relationship between the resultant strength reduction factor associated with the shear strength estimated by the proposed equation (ϕ_{eq}) and the obtained probability of failure is studied.

Before running the Monte Carlo Simulation, it is necessary to define proper distributions for the variables with uncertainty, which are those associated with material properties (f_c' and f_y) and the demands (axial load, moment, and shear). The variables related to the geometry of the wall are considered as constants. The distributions representing the demands vary for the different archetypes; therefore, these distributions will be selected after analyzing the demands of each archetype.

For each archetype, an OpenSees model was created considering expected material properties and expected axial load (coming from the load combination D+0.25L). A methodology, explained later, was implemented to modify the expected material properties

and allow the model to reproduce strength loss at its predicted roof drift capacity. From this model with expected material properties modified, two more models are defined where the only difference is the axial load applied; for one is (0.9-0.2S_{DS})D, and for the other is (1.2+0.2S_{DS})D+0.5L.

10.2 Design of Archetypes

Table 10.1 presents the main characteristics of the archetypes. All archetypes are Reinforced Concrete (RC) Wall Buildings designed in accordance with the Modal Response Spectrum Analysis (MRSA) of ASCE 7-16 (including accidental torsion). The calculations made to determine the demands and do the design are shown in Appendix A, Appendix B, and Appendix C for the 4-, 8-, and 12-story archetype, respectively. Effective wall flexural stiffness was set at $0.5E_cI_g$ and shear stiffness at $0.4E_cA_g$ over the entire wall height for the code level analysis.

The commentary of ACI 318-19 Section 18.10.6 states that the wall P-M strength over the wall height should be specified so that the critical section (plastic hinge) occurs at the intended location. In this study, this was accomplished by amplifying the ASCE 7-16 moment demand M_u over the wall height by the overstrength factor at the base $\Omega_v = M_{pr,base}/M_{u,base}$, where $M_{pr,base}$ and $M_{u,base}$ are the maximum probable moment at the base using $f_s = 1.25f_y = 75\ ksi$ and the moment demand at the wall base obtained from the MRSA. The result of this process is illustrated in Fig. 10.1. In Fig. 10.1, the amplified moment demand is less than the moment capacity (ϕM_n), at all locations over the wall height except at the

critical section (hinge region). **Table 10.1** summarizes the main design characteristics of the archetypes.

***Table 10.1**: Main design characteristics of the ACI 318-19 compliant RC wall archetypes*

Parameter	4-Story Archetype	8-Story Archetype	12-Story Archetype
MCE spectral acc. at short periods, S_s	2.08g	2.08g	2.08g
MCE spectral acc. at 1-s period, S_1	0.64g	0.64g	0.64g
Wall shape	Rect.	Rect.	Rect.
# of stories	4	8	12
Fundamental period, T_1 (s)	0.24	0.80	1.75
# of walls in each direction	4	4	4
Seismic weight associated with one wall, **W** (kips)	3,420	7,535	11,441
Wall thickness, t_w (in)	24	30	30
Wall length, l_w (ft)	30	30	30
Horizontal web reinforcement ratio, ρ_{wh} (%) *	0.52	0.44	0.52
Longitudinal boundary reinforcement ratio, ρ_{sb} (%) *	0.53	0.33	0.33
Nominal concrete compressive strength, f'_c (ksi) *	5	5	5
Nominal yield stress of hor. web reinforcement, f_{ywh} (ksi)	60	60	60
Nominal yield stress of long. bound. reinforcement, f_{ysb} (ksi)	60	60	60
Axial load in wall due to (0.9-0.2S_{DS})D, $P_{u,\min}$ (kips) *	684	1,584	2,426
Axial load in wall due to D+0.25L, $P_{u,avg}$ (kips) *	1,157	2,674	4,098
Axial load in wall due to (1.2+0.2S_{DS})D+0.5L, $P_{u,\max}$ (kips) *	1,741	4,018	6,159
Moment demand of wall, M_u (kip-ft) *	73,815	82,299	87,139
Shear demand of wall, V_u (kips) *	1,800	1,190	1,158
Expected shear demand of wall, V_e (kips) *	2,984	3,110	3,474
Nominal shear strength of wall, $V_n^{(ACI)}$ (kips)	4,145	4,347	4,875
Nominal shear strength of wall, $V_n^{(PropEq)}$ (kips) **	3,306	3,855	4,663
Nominal shear strength of wall, $\phi V_n^{(ACI)}$ (kips)	3,108	3,260	3,657
DCR using Proposed Eq., $V_e/V_n^{(PropEq)}$	0.90	0.81	0.75

*These parameters are for the critical section, which is at the base for every archetype.

**$V_n^{(PropEq)}$ is obtained using the demands coming from the load combination (1.2D+0.2S_{DS})D+0.5L+E.

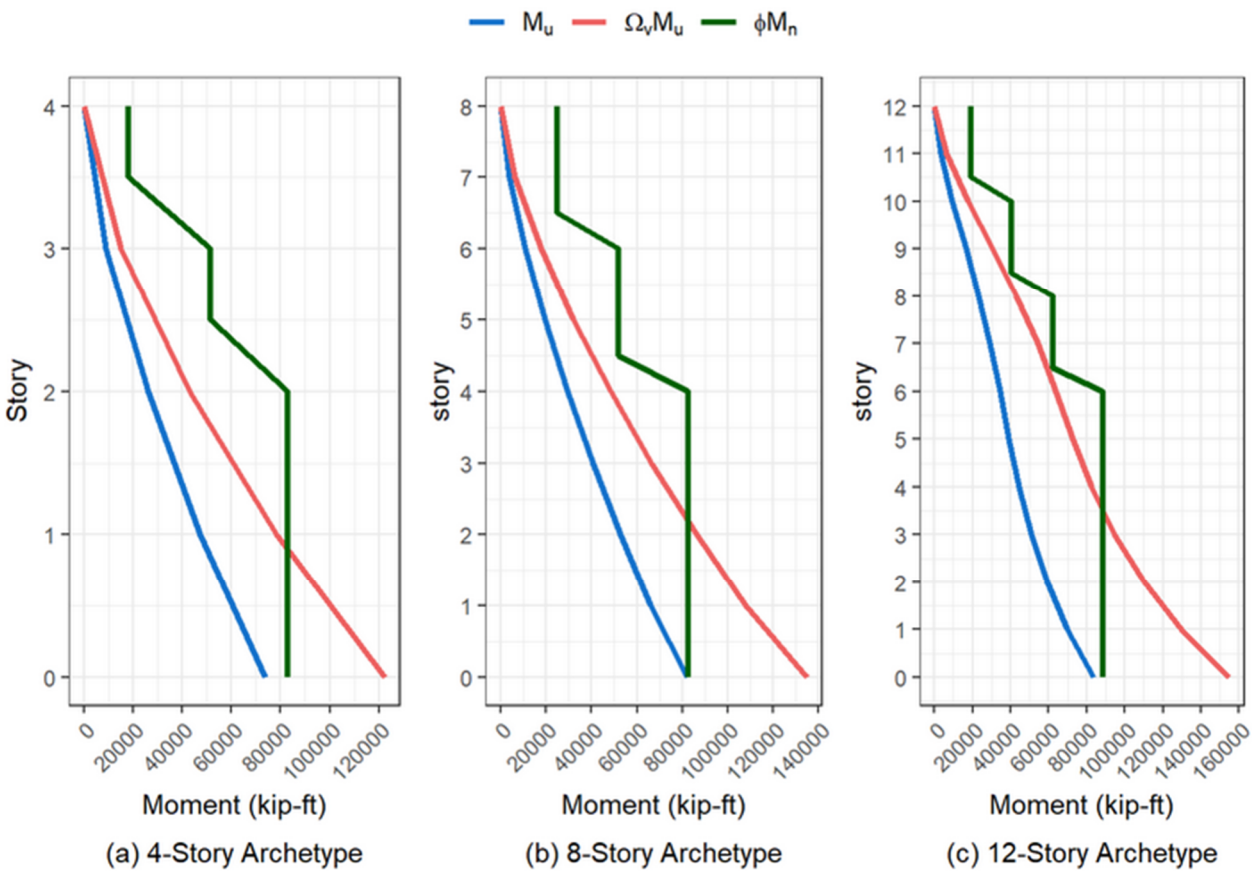

***Figure 10.1**: Moment profile of the archetypes*

10.3 OpenSees Modeling

The objective is to study what the strength reduction factor should be when using the proposed equation in a process of designing a code compliant wall. Because these walls are designed to fail in flexure before than in shear, it is appropriate to produce archetype models that account for strength loss at the predicted roof drift capacity. To do this, models with expected material properties, expected axial load and no strength loss are first produced.

10.3.1 Models with Expected Material Properties, Expected Axial Load, and No Strength Loss

Due to symmetry of the building layout and the lateral system, and to simplify the modeling process, a 2D model consisting of one wall was used to determine the responses of each archetype in each direction. For each archetype model:

- The wall was modeled using the Multi-Vertical-Line-Element (MVLE) model in OpenSees (Kolozvari et al. 2015). Four fiber elements were used for the first and second stories and subsequent levels were modeled with two elements.
- The model considered expected material properties ($f_{ye} = 70\ ksi$; $f'_{ce} = 1.3f'_c = 6.5\ ksi$) and the unconfined and confined concrete uniaxial stress versus strain relationships were estimated using the Saatcioglu and Razvi (1992) model, which allows for consideration of the different levels of confinement for the two principal direction (e.g., x, y) for the boundary elements.
- Parameters were selected for the Concrete02 model in OpenSeeS to fit the stress versus strain relationships obtained with the Saatcioglu and Razvi (1992) model.
- Reinforcement stress versus strain was modeled using the SteelMPF model in OpenSeeS based on the following parameters: $f_{ye} = 70\ ksi$, $E_s = 29000\ ksi$, and 1% post yielding slope.
- One load combination for gravity load was considered; D + 0.25L.

10.3.2 Models with Modified Expected Material Properties to Produce Strength Loss

The algorithm shown in **Figure 10.2** is proposed and implemented to develop models that recreate strength loss at their respective predicted roof drift capacity. Obtaining the

expected material properties as described in the previous section correspond to the 1st step of the algorithm. Once the model was created, a monotonic pushover analysis was conducted (2nd step of **Figure 10.2**) to determine appropriate parameters for modeling strength loss (no strength loss was considered in the initial pushover analysis). The roof drift capacity at significant strength loss (≥20% from peak load) was estimated using the Drift Capacity model proposed by Abdullah and Wallace (2019). To reproduce significant strength loss at the predicted roof drift capacity for each archetype, the neutral axis depth and strain profile at the predicted roof drift capacity using the wall model with expected axial load applied (D+0.25L) are needed (see 3rd step in **Figure 10.2**). The strain at which strength degradation initiates in compression for both confined concrete and longitudinal boundary reinforcement is assumed to be the same (ε_b), i.e., crushing of confined concrete and buckling of longitudinal boundary reinforcement are coupled. If this approach is not adopted, compressive concrete loads are transferred to boundary longitudinal reinforcement, and only moderate strength loss can be achieved. In addition, for this study, the outer steel layer of the boundary element (BE) under tension is assumed to reach its rupture strain when concrete reaches its residual strength in the BE under compression. An upper strain limit, ε_{rupt}, was also set for tension rupture of longitudinal reinforcement. The strain ε_{rupt} must be larger than the maximum tensile strain registered at roof drift capacity with the monotonic pushover analysis in order to not produce strength loss before than desired. Step 4 of **Figure 10.2** details how these values are used to modify the material properties of the BE in the plastic hinge region to achieve strength loss. Step 5 of **Figure 10.2** is to verify that the strength loss objectives are achieved for both monotonic and reversed-cyclic pushover analyses.

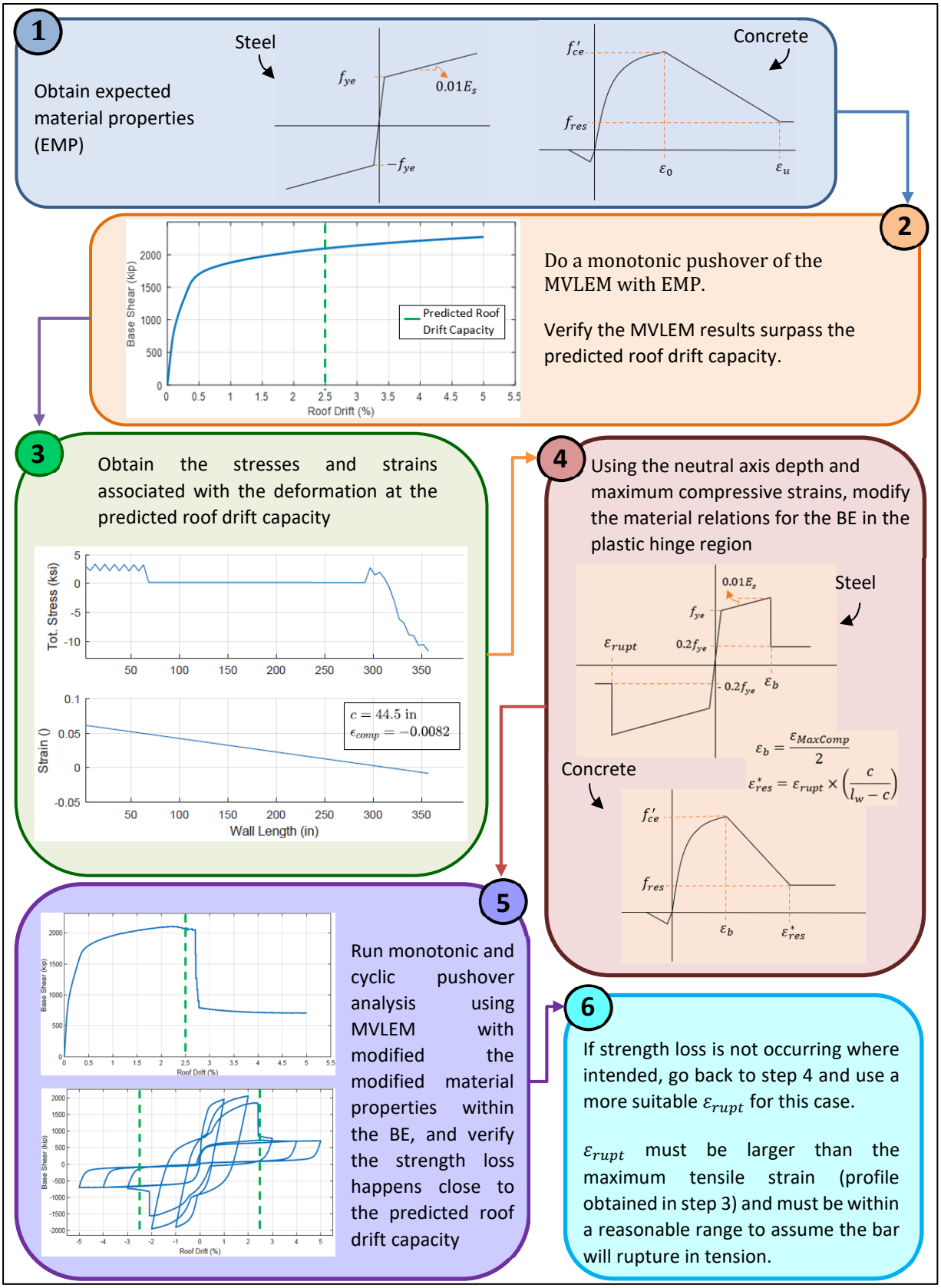

***Figure 10.2**: Algorithm to obtain MVLEM with strength loss at predicted roof drift capacity*

In step 4 of the algorithm, strain values ε_b and ε^*_{res} (the latter is the modified strain at which the residual concrete capacity is reached) are selected from the monotonic pushover analysis of the Multi-Vertical-Line-Element-Model (MVLEM) with expected gravity load applied and without modified material stress versus strain relations. The strain values are determined from the strain profile at the wall critical section (wall-foundation interface) when the roof drift capacity is reached as noted below:

- ε_b selected as the strain at half of the neutral axis depth (i.e., half of the strain of the outer compressed fiber). Once this value is reached in the compression BE of the MVLEM, significant strength loss will occur because half of the compressed boundary longitudinal reinforcement is assumed to buckle and half of the confined concrete in the compressed BE initiates strength loss by starting on the descending branch of the stress-strain relation. The expected material properties are modified to achieve this objective (of strength loss).
- The modified residual concrete strength is obtained from Eq. (10.1), where ε_{rup} is the strain at which the bars in tension rupture ($\varepsilon_{rupt} = 0.14$, 0.12, and 0.10 was used for the 4-story, 8-story, and 12-story archetypes, respectively) and c is the neutral axis depth at roof drift capacity. Eq. (10.1) produces strength loss because the properties of the boundary longitudinal reinforcement in tension are modified to achieve strength loss exactly when the neutral axis associated to the roof drift capacity is reached (if we were only modifying the material relationships in tension).

$$\varepsilon^*_{res} = \varepsilon_{rup} \times \frac{c}{l_w - c} \tag{10.1}$$

It is noted that the material properties also are modified in compression, which also influence wall responses earlier because the strain levels associated for compression are lower than the strain levels associated with strength loss in tension ($\varepsilon_b < \varepsilon^*_{res}$). Once the roof drift capacity is reached, the wall neutral axis depth becomes larger due to degradation in concrete stress capacity, and Eq. (10.1) produces rebar rupture in the BE in tension when the outer fibers in the compressed BE have failed (reached residual strength) as desired to achieve significant strength loss for both directions of loading.

Changing the strains at peak and residual stresses in the Concrete02 material in the OpenSeeS model is sufficient to implement the necessary modification to the concrete stress versus strain relations. However, to implement the necessary modifications for the steel behavior it was necessary to define a Parallel material at the BE, a bilinear SteelMPF material with weight factor of 80% (with a strain hardening ratio equal to 0.0125) to have complete strength loss in tension and compression at the desired strain values (using MinMax option in OpenSees), and another with weight factor of 20% and elastic-perfectly plastic SteelMPF material to be able to reproduce appropriate residual capacity.

10.4 Selection of Ground Motions at MCE_R Level

For each archetype, a suite of ground motions (GMs) is selected to appropriately represent the spectral shape at the risk-targeted maximum considered earthquake (MCE_R) performance level at a site located in Downtown Los Angeles, California (latitude 34.059, longitude -118.238). This location (same considered for the design) has site spectral

acceleration values of $S_s = 2.08g$ and $S_1 = 0.64g$. The Uniform Hazard Response Spectrum for this site is shown in **Figure 10.3**.

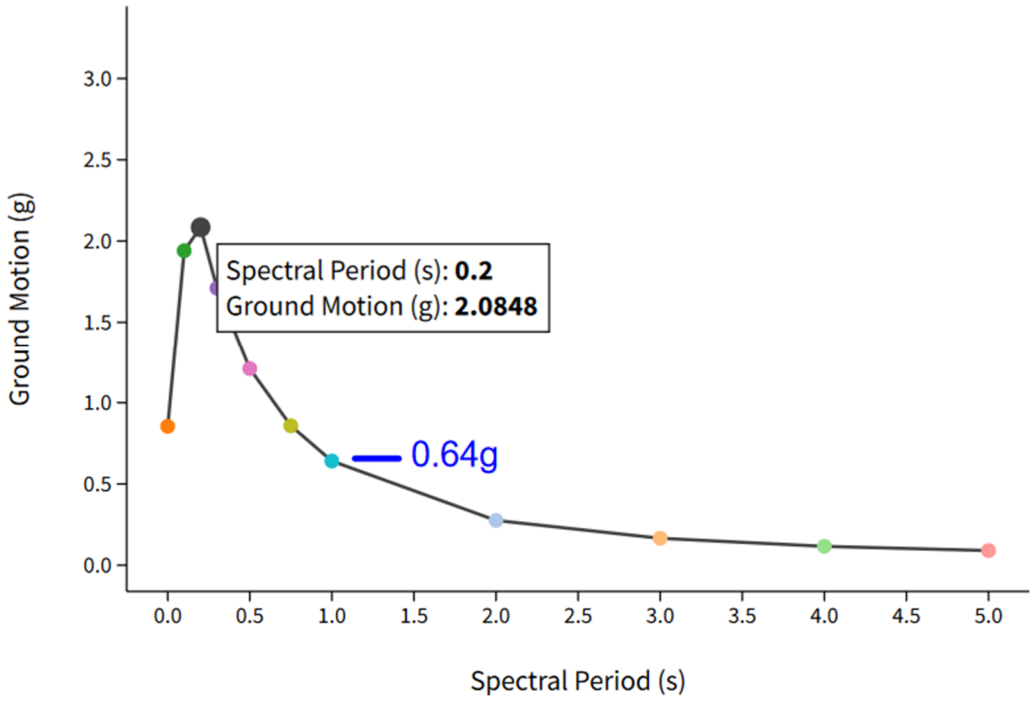

***Figure 10.3**: Uniform Hazard Response Spectrum for Site (USGS Unified Hazard Tool)*

The spectral acceleration associated with the fundamental period of each archetype (shown in **Table 10.2**) was extracted from the Uniform Hazard Response Spectrum (**Figure 10.3**) and then used to generate a Conditional Mean Spectrum (CMS) (Baker, 2011). The period used to match the spectrum is the fundamental period obtained from the Eigen Analysis performed on the OpenSees archetype model with expected gravity load applied (D+0.25L). **Figure 10.4** illustrates how the spectra for each set of performance GM dataset matches the same S_a value at T_1 for each archetype. **Table 10.2** also includes the number of records comprising each of the suits of MCE_R level GMs. The list specifying the GMs and their scale

factor are provided in Appendix A.6, Appendix B.6, and Appendix C.6 for the 4-, 8-, and 12-story archetype, respectively.

***Table 10.2**: Period and spectral acceleration used to generate the CMS*

Archetype	Fundamental Period, T_1 (s) *	Spectral Acceleration, S_a	# of GMs Selected
4-Story Archetype	0.18	2.05g	42
8-Story Archetype	0.52	1.18g	43
12-Story Archetype	1.20	0.57g	46
*The fundamental period is extracted from the OpenSees model with expected material properties that is then subjected to the suite of GMs.			

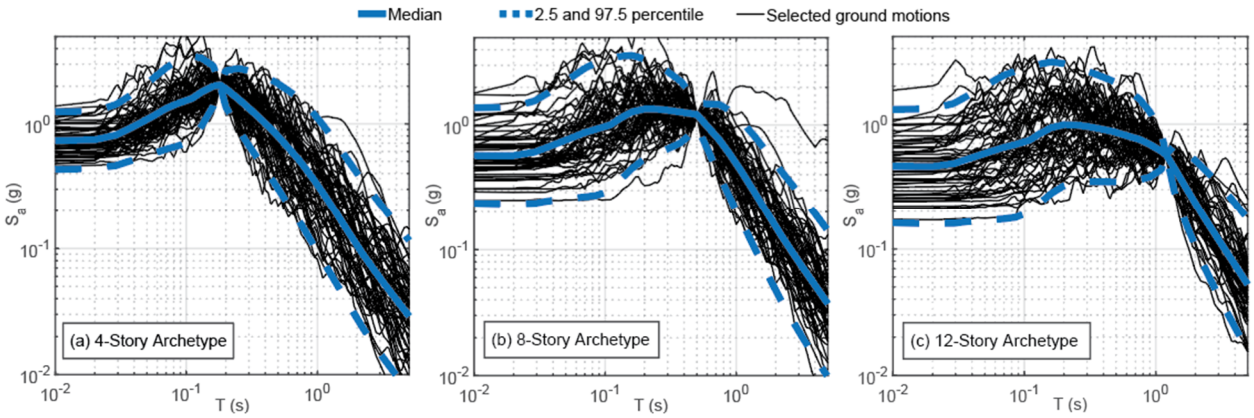

***Figure 10.4**. Response spectra of selected GMs for each archetype*

Once the suite of GMs is selected, dynamic analyses are run with it for each archetype using the three load combinations previously mentioned: $(0.9\text{-}0.2S_{DS})D$, D+0.25L, and $(1.2+0.2S_{DS})D+0.5L$. The hysteretic results are obtained in terms of moment versus curvature at the base because the plots are cleaner compared to base shear vs drift, and because the predicted roof drift capacity can be translated into total plastic hinge rotation as

described by Abdullah and Wallace (2019). **Table 10.3** shows the plastic hinge rotation at strength loss.

***Table 10.3**: Predicted total hinge rotation capacity*

Archetype	Total Hinge Rotation Capacity, θ (rad)
4-Story Archetype	0.031
8-Story Archetype	0.030
12-Story Archetype	0.033

Figure 10.5 shows the moment versus curvature associated with the GM that causes the largest hysteretic cycle (i.e., maximum total rotation in the plastic hinge region) for each archetype. The results in **Figure 10.5** are from the model with gravity load coming from the load combination (1.2+0.2S_{DS})D+0.5L. The rotations are below the total rotation capacity for the 4- and 12-story archetypes. For the 8-story archetype, there is only one GM that make the building to surpass its deformation capacity, and from **Figure 10.5** it can be seen that the strength loss actually starts to happen at around 0.03 rad, as indicated in **Table 10.3**. The results of the dynamic analyses for all GMs can be found in Appendix A.7.2.3, Appendix B.7.2.3, and Appendix C.7.2.3 for the 4-, 8-, and 12-story archetype, respectively.

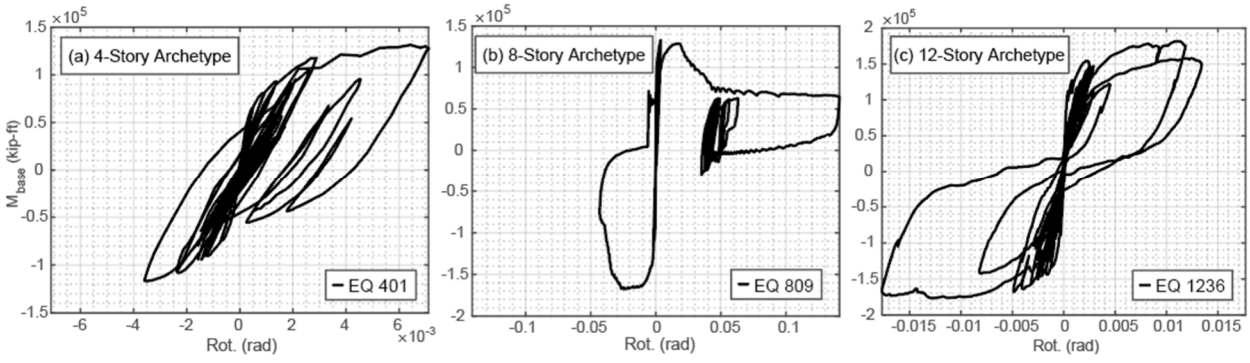

***Figure 10.5**: Moment versus curvature of the GM that causes the largest hysteresis cycle – LC: (1.2+0.2S_{DS})D+0.5L*

10.5 Probability Distributions for Actual-to-Nominal Material Properties Ratio

The database used for this study also includes nominal material properties. However, this information is not always reported. Therefore, there are 254 tests that reported the nominal f_c', 247 tests that reported the nominal f_{ybs} of the longitudinal boundary reinforcement, and 249 tests that reported the nominal f_{ywh} of the horizontal web reinforcement. **Figure 10.6** shows the density histograms of the expected-to-nominal material properties, along with the fitted normal and log-normal distributions. The log-normal distribution is chosen as the one that better represents the data for the three cases.

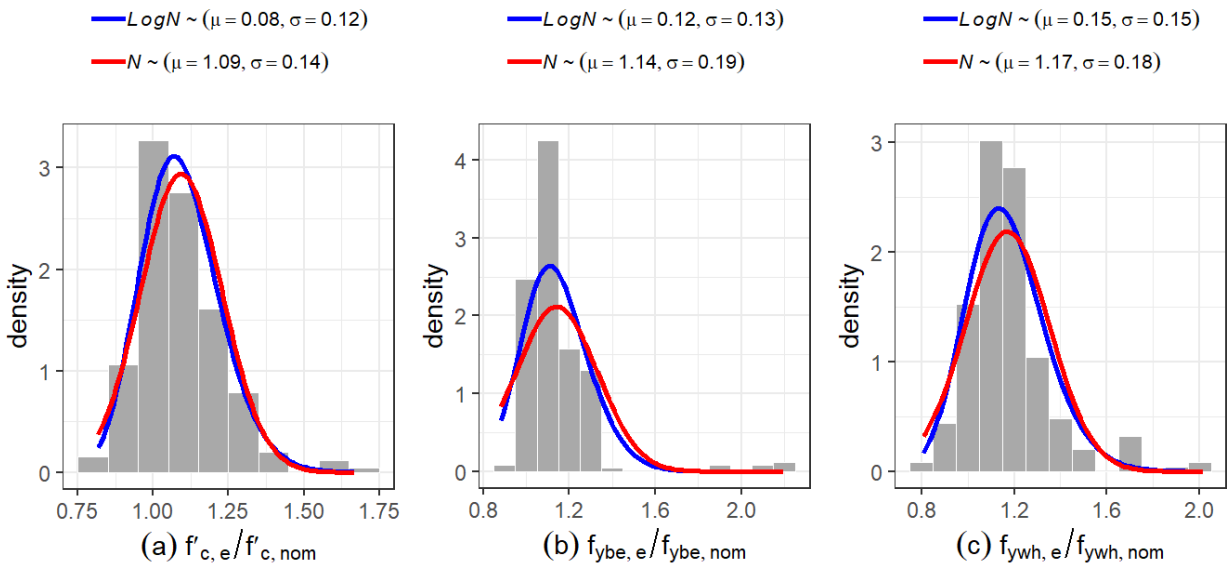

***Figure 10.6**: Density histograms and fitted distributions of the expected-to-nominal material properties*

Therefore, the selected distributions to represent the actual-to-nominal material properties are the ones indicated in **Table 10.4**.

***Table 10.4**: Selected distributions to represent the actual-to-nominal material properties*

Variable	Distribution Type	Parameter 1	Parameter 2
$f'_{c,e}/f'_{c,nom}$	Log-Normal	$\mu_{log} = 0.08$	$\sigma_{log} = 0.12$
$f_{ysb,e}/f_{ysb,nom}$	Log-Normal	$\mu_{log} = 0.12$	$\sigma_{log} = 0.13$
$f_{ywh,e}/f_{ywh,nom}$	Log-Normal	$\mu_{log} = 0.15$	$\sigma_{log} = 0.15$

10.6 Reliability Analysis for the 4-Story Archetype

Before running a Monte Carlo simulation, it is necessary to estimate the probability distributions for actual-to-nominal demand ratios. These distributions vary for the different archetypes and therefore the are obtained by assessing the dynamic analyses run for each of them. Because this is the first archetype, the reasoning and description of the steps will be provided within this section.

10.6.1 Probability Distribution for Actual-to-Nominal Demands Ratio

The density histograms of the actual-to-nominal shear ratios obtained with the OpenSees model for the three load combinations studied are shown in **Figure 10.7** and **Figure 10.8**. **Figure 10.7** shows the ratio of the actual shear demand ($V_{e,e}$) over the nominal amplified shear demand obtained according to the ACI 318-19 prescriptions ($V_{e,nom}$). **Figure 10.8** shows the ratio of the actual shear demand ($V_{e,e}$) over the nominal shear demand obtained by MRSA ($V_{u,nom}$).

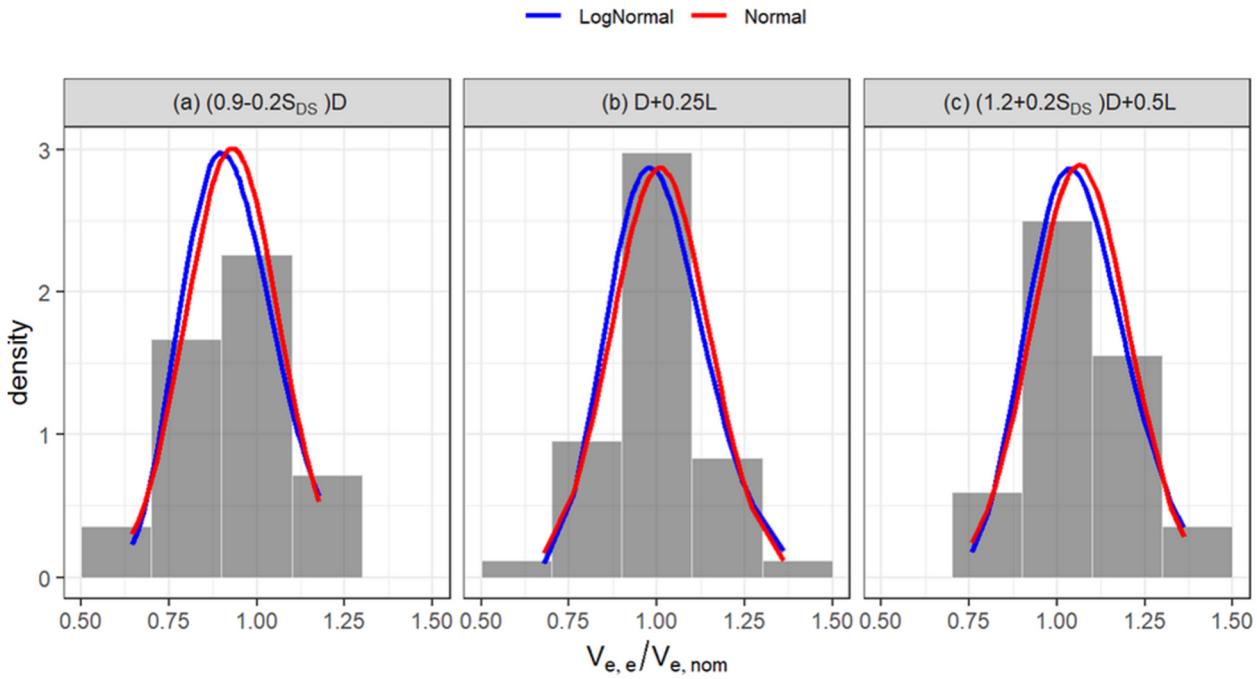

***Figure 10.7**: Density histograms and fitted distributions of the actual-to-demand shear ratios, where the nominal value is the amplified shear demand V_e obtained using ACI 318-10 provisions – 4-Story Archetype*

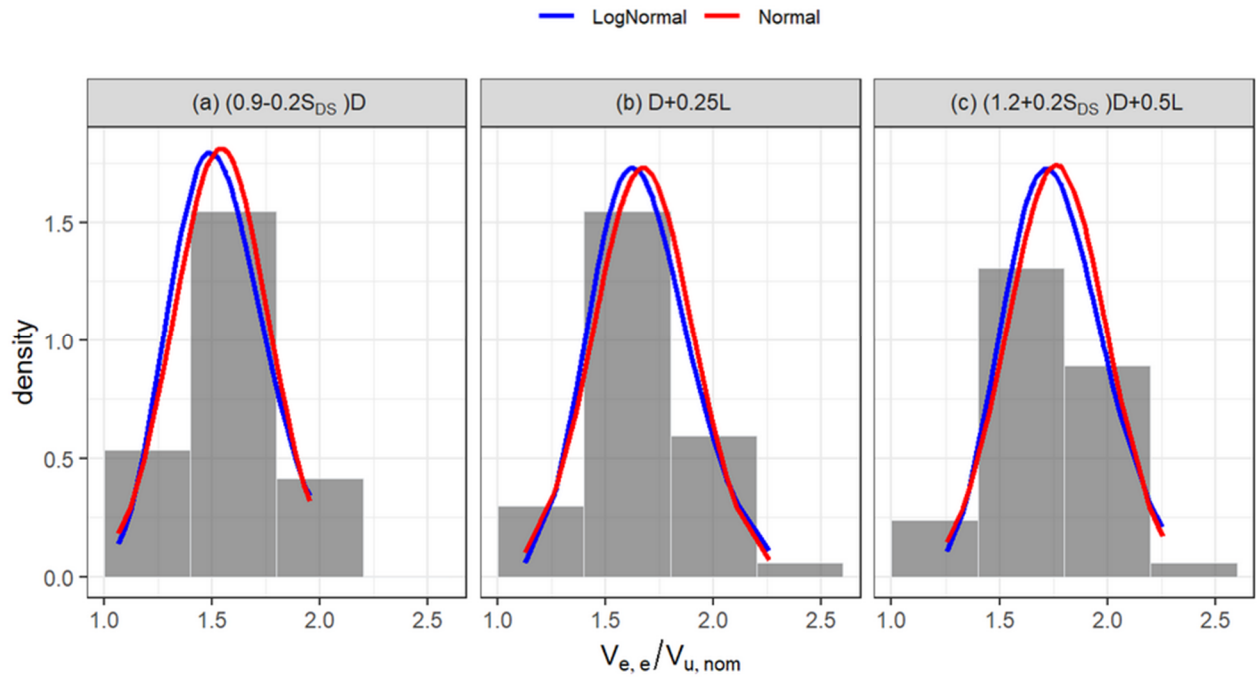

***Figure 10.8**: Density histograms and fitted distributions of the actual-to-nominal shear ratios, where nominal value is the demand V_u without amplification – 4-Story Archetype*

Even though similar histograms can be obtained for axial load and moment demands, it would not be representative to draw random samples from distributions based on those histograms when performing a Monte Carlo simulation to simulate the variability of these demands. The reason for this is because they are correlated with the lateral force imposed by the ground motion. Therefore, a relationship between these demands and the base shear is sought and found. **Figure 10.9** shows how the $P_{u,e}/P_{u,nom}$ ratio correlates with the $V_{e,e}/V_{e,nom}$ ratio for the different load combinations, while **Figure 10.10** does the same but between $M_{u,e}/M_{u,nom}$ and $V_{e,e}/V_{e,nom}$.

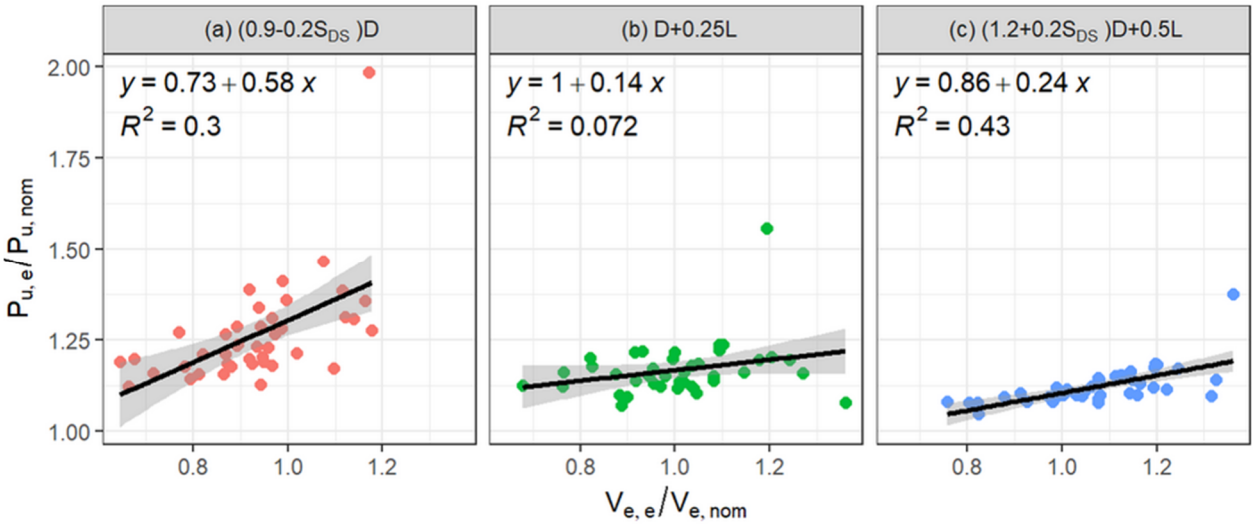

***Figure 10.9**: Relationship between actual-to-nominal axial load ratio and actual-to-nominal shear ratio – 4-Story Archetype*

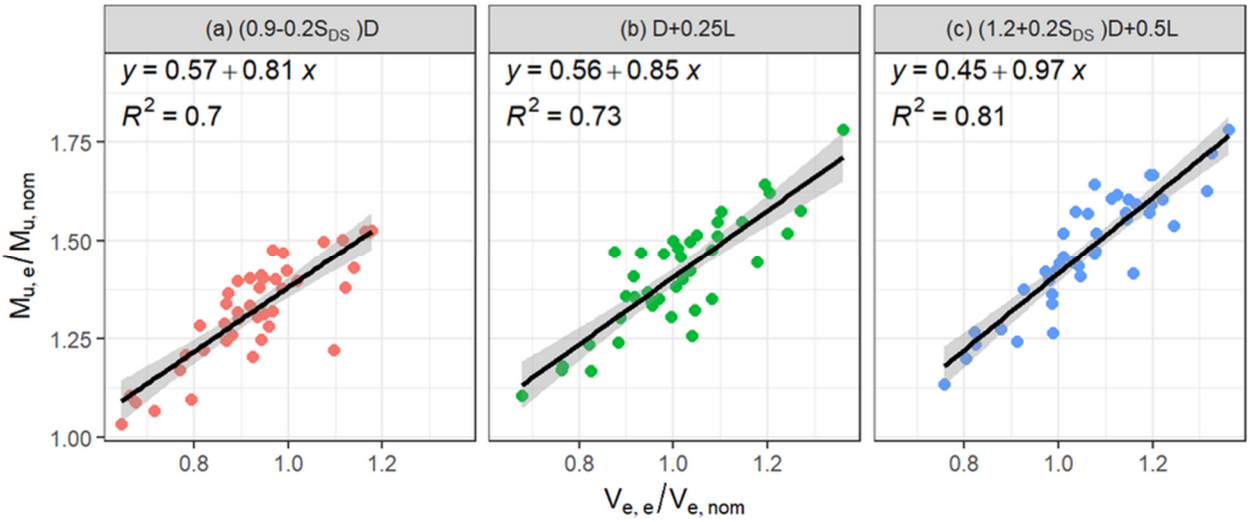

***Figure 10.10**: Relationship between actual-to-nominal moment ratio and actual-to-nominal shear ratio – 4-Story Archetype*

It is considered that a linear regression estimates these trends good enough. Therefore, the approach is to make the $P_{u,e}/P_{u,nom}$ to follow a normal distribution with a mean value that follows the linear regression in **Figure 10.9** for each load combination. Similarly, $M_{u,e}/M_{u,nom}$ is set to follow a normal distribution which mean value follows the linear regression in **Figure 10.10** for each load combination.

With the mean value of the distribution already defined, the standard deviation is the only parameter left to define for these distributions. The standard deviation of a sample around a mean value is obtained based on the differences between the samples and the mean value, as show in Eq. (10.2).

$$\sigma = \sqrt{\frac{\Sigma_{i=1}^{n}(x_i - \mu_x)^2}{n-1}} \tag{10.2}$$

By looking at Eq. (10.3), it is clear that the standard deviation is a measurement of the error when the values of a sample are estimated just by the sample mean. Similarly, the residuals

of a regression are the error between the observed (actual) value and the predicted one, i.e., $y_{i,obs} - y_{i,pred}$. The analogy is clear by looking at Eq. (10.4).

$$x_i = \mu_x + \varepsilon_i \tag{10.3}$$

$$x_i = \underbrace{\beta_0 + \beta_1 x_i}_{\mu_i} + \varepsilon_i \tag{10.4}$$

The residual standard error of a sample represented by a regression is defined on the same way that the standard deviation is defined for a sample represented by its mean. Thus, the standard deviation of a normal distribution which mean values follows a linear regression can be obtained using Eq. (10.5). In Eq. (10.5), instead of dividing by the sample size n, which gives us the root mean square error (RMSE), the denominator corresponds to the degrees of freedom (statistical concept, not the one used in structural engineering) because is works better in order to obtain an unbiased estimation. The statistical degree of freedom corresponds to the number of samples minus the number of parameters that are estimated, which are two in this case (intercept and slope of the linear regression).

$$\text{Residual Standard Error} = \sqrt{\frac{\Sigma_{i=1}^{n}\left(y_i - y_{i,pred}\right)^2}{n-2}} = \sqrt{\frac{\Sigma_{i=1}^{n}\left(y_i - (\beta_0 + \beta_1 x_i)\right)^2}{n-2}} \tag{10.5}$$

Figure 10.11 shows the residual and their corresponding residual standard error of the linear regression between $V_{e,e}/V_{e,nom}$ and $P_{u,e}/P_{u,nom}$ shown in **Figure 10.9**. Same thing is done in **Figure 10.12**.

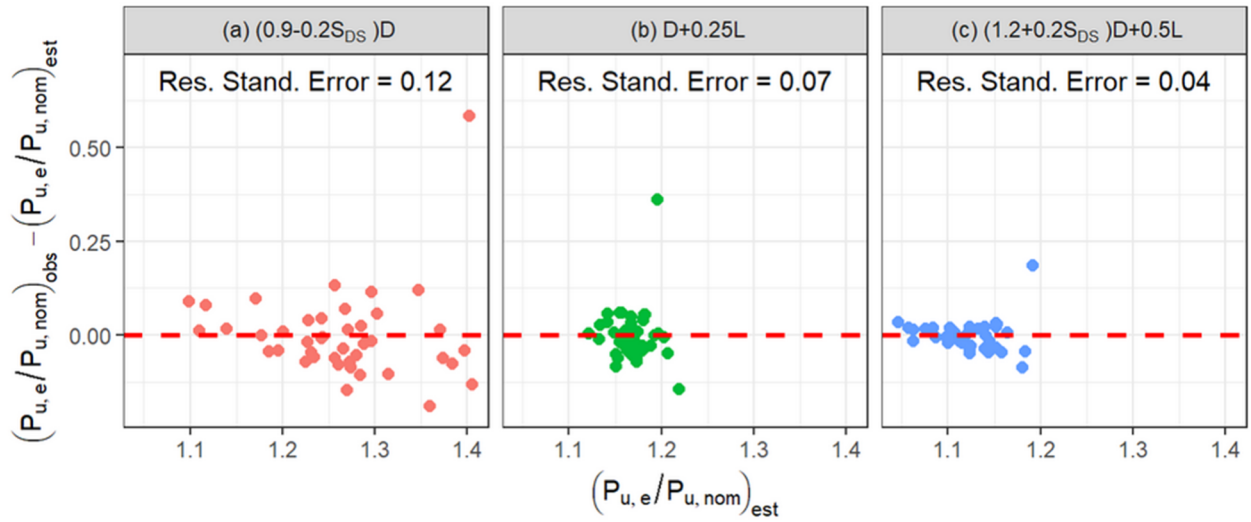

***Figure 10.11**: Residuals and residual standard deviations for actual-to-nominal axial demands – 4-Story Archetype*

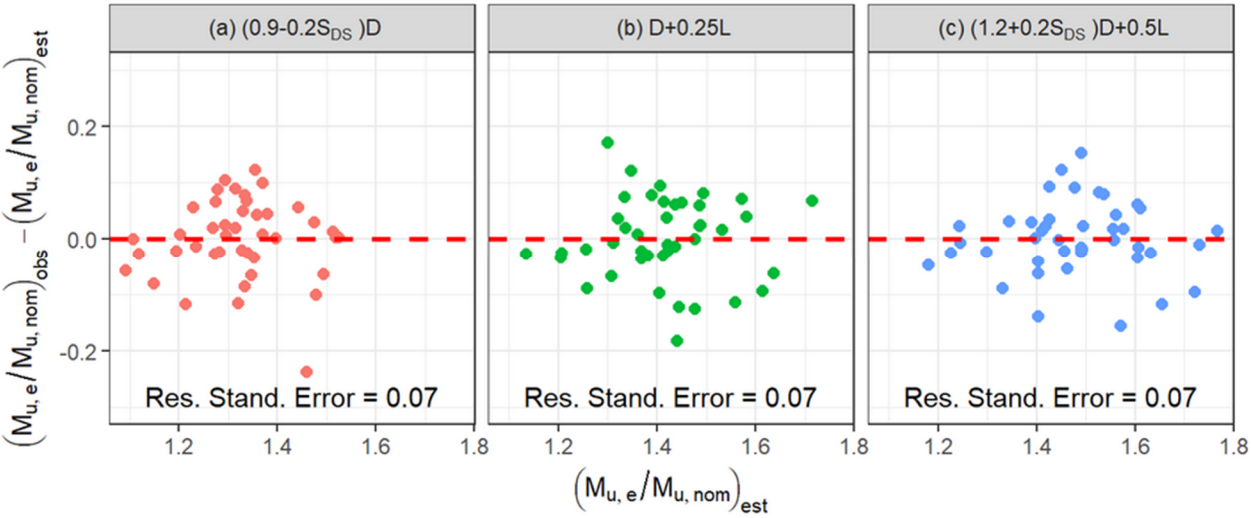

***Figure 10.12**: Residuals and residual standard deviations for actual-to-nominal moment demands – 4-Story Archetype*

Finally, by considering the actual-to-nominal shear demand distributions of **Figure 10.7** and **Figure 10.8**, the linear regressions shown in **Figure 10.9** and **Figure 10.10**, and the associated residual standard errors shown in **Figure 10.11** and **Figure 10.12**, the probability distributions representing the actual-to-nominal demands can be defined for this archetype. **Table 10.5** summarizes this information.

***Table 10.5**: Selected actual-to-nominal demand probability distributions for the 4-Story Archetype*

Load Combination	Variable	Distribution Type	Parameter 1	Parameter 2
(0.9-0.2S_{DS})D	$V_{e,e}/V_{e,\text{nom}}$	Log-Normal	$\mu_{log} = -0.08$	$\sigma_{log} = 0.15$
	$V_{e,e}/V_{u,\text{nom}}$	Log-Normal	$\mu_{log} = 0.42$	$\sigma_{log} = 0.15$
	$P_{u,e}/P_{u,\text{nom}}$	Normal	$\mu_i = 0.73 + 0.58\left(\frac{V_{e,e}}{V_{e,\text{nom}}}\right)_i$	$\sigma = 0.12$
	$M_{u,e}/M_{u,\text{nom}}$	Normal	$\mu_i = 0.57 + 0.81\left(\frac{V_{e,e}}{V_{e,\text{nom}}}\right)_i$	$\sigma = 0.07$
D+0.25L	$V_{e,e}/V_{e,\text{nom}}$	Log-Normal	$\mu_{log} = 0.00$	$\sigma_{log} = 0.14$
	$V_{e,e}/V_{u,\text{nom}}$	Log-Normal	$\mu_{log} = 0.50$	$\sigma_{log} = 0.14$
	$P_{u,e}/P_{u,\text{nom}}$	Normal	$\mu_i = 1.02 + 0.14\left(\frac{V_{e,e}}{V_{e,\text{nom}}}\right)_i$	$\sigma = 0.07$
	$M_{u,e}/M_{u,\text{nom}}$	Normal	$\mu_i = 0.56 + 0.85\left(\frac{V_{e,e}}{V_{e,\text{nom}}}\right)_i$	$\sigma = 0.07$
(1.2+0.2S_{DS})D+0.5L	$V_{e,e}/V_{e,\text{nom}}$	Log-Normal	$\mu_{log} = 0.05$	$\sigma_{log} = 0.13$
	$V_{e,e}/V_{u,\text{nom}}$	Log-Normal	$\mu_{log} = 0.56$	$\sigma_{log} = 0.13$
	$P_{u,e}/P_{u,\text{nom}}$	Normal	$\mu_i = 0.86 + 0.24\left(\frac{V_{e,e}}{V_{e,\text{nom}}}\right)_i$	$\sigma = 0.04$
	$M_{u,e}/M_{u,\text{nom}}$	Normal	$\mu_i = 0.45 + 0.97\left(\frac{V_{e,e}}{V_{e,\text{nom}}}\right)_i$	$\sigma = 0.07$

10.6.2 Monte Carlo Simulation Results

10.6.2.1 Verification of Correlation Between Demands

A Monte Carlo Simulation using 10,000 iterations is carried out for each load combination. The correlation of the simulated actual-to-nominal axial and moment demands with the actual-to-nominal shear ratios are first verified (see **Figure 10.13** and **Figure 10.14**, respectively).

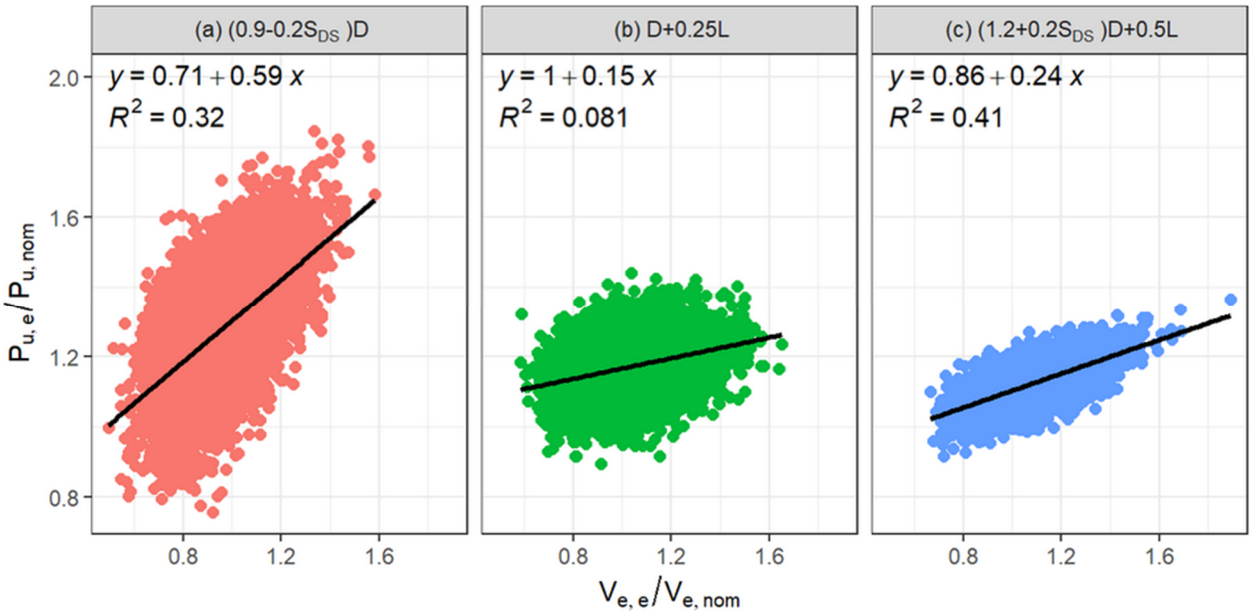

***Figure 10.13**: Relationship between simulated actual-to-nominal axial demands versus actual-to-nominal shear demands – 4-Story Archetype*

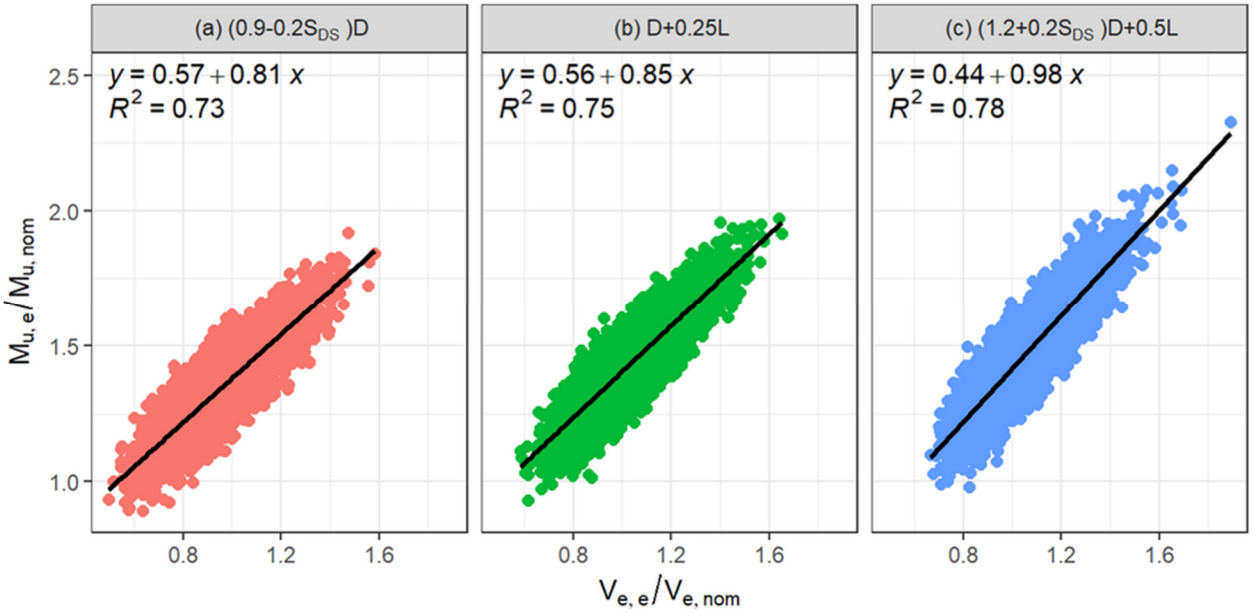

***Figure 10.14**: Relationship between simulated actual-to-nominal moment demands versus actual-to-nominal shear demands – 4-Story Archetype*

10.6.2.2 Reliability Results Expressed in Terms of $V_n - V_e$

Because the variables (strength and demand) are dependent, the plots are expressed only as a junction variable. In this case, is in terms of the difference between strength and demand ($V_n - V_e$), where the failure condition corresponds to $V_n - V_e \leq 0$. **Figure 10.15** presents the results when using the ACI 318-19 equation, whereas **Figure 10.16** does the same but using the proposed equation. It is relevant to recall that these archetypes are ACI 318-19 compliant walls. Therefore, the results obtained with the proposed equation (**Figure 10.16**) can be understood as a more accurate estimation, because the better performance of the proposed equation has already been demonstrated.

For the worse scenario, i.e., gravity load coming from the (1.2+0.2S_{DS})D+0.5L load combination, results say that ACI 318-19 estimates this archetype to have 0.8% of probability of failure, whereas the proposed equation says its probability of failure is actually closer to 7%. It is worth to highlight that the shear strength estimated with the proposed equation is $V_n^{(PropEq)} = 3{,}306\ kips$, which is equivalent to have used a strength reduction factor of only $\phi = V_e / V_n^{(PropEq)} = 0.90$ (see **Table 10.1**) in order to satisfy $\phi V_n^{(PropEq)} = V_e$.

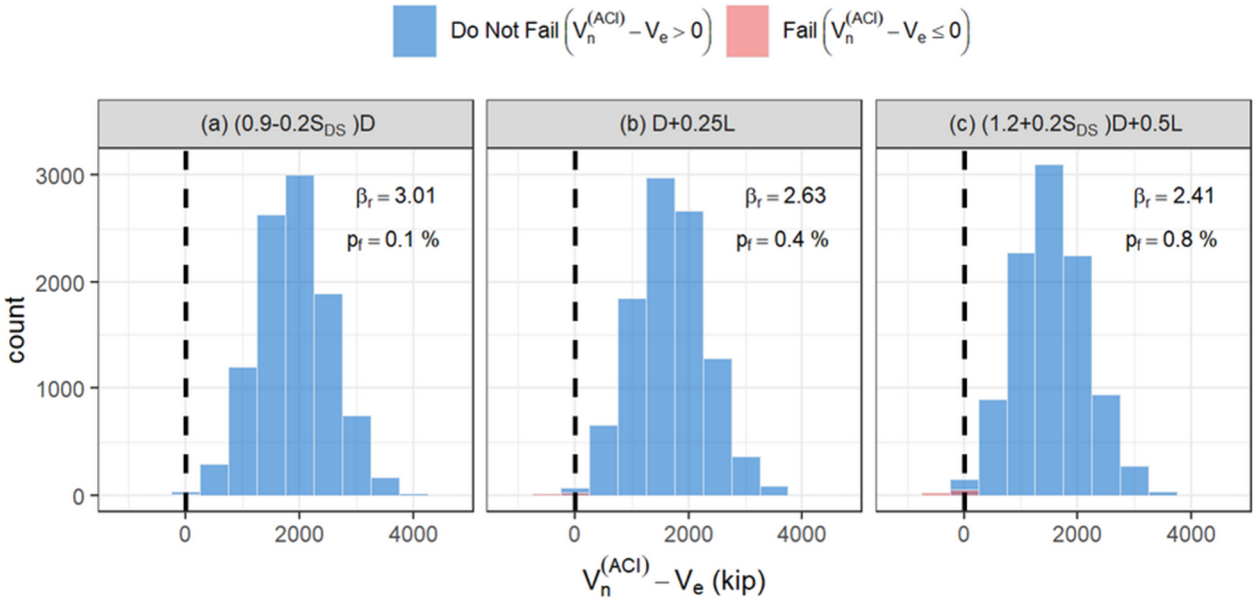

***Figure 10.15**: Reliability results using the ACI 318-19 equation, in terms of $V_n - V_e$, for the 4-Story Archetype*

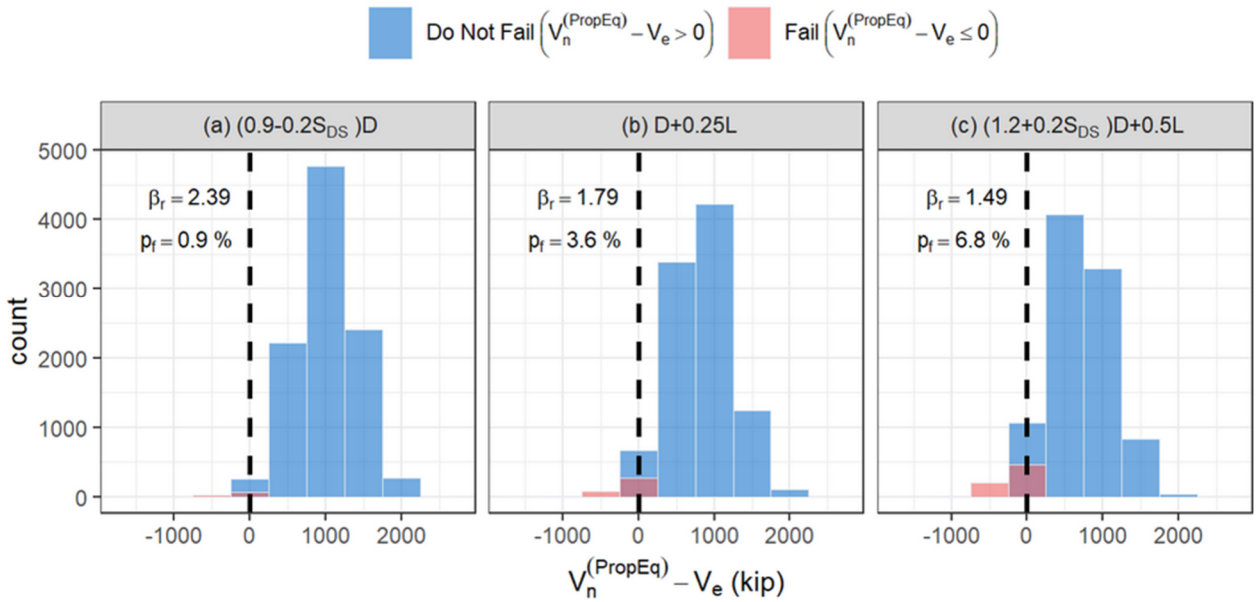

***Figure 10.16**: Reliability results using the proposed equation, in terms of $V_n - V_e$, for the 4-Story Archetype*

10.6.2.3 Reliability Results Expressed in Terms of V_e/V_n

The proposed equation estimates a much higher probability of failure for this ACI 318-19 compliant archetype respect to what the ACI 318-19 equation does.

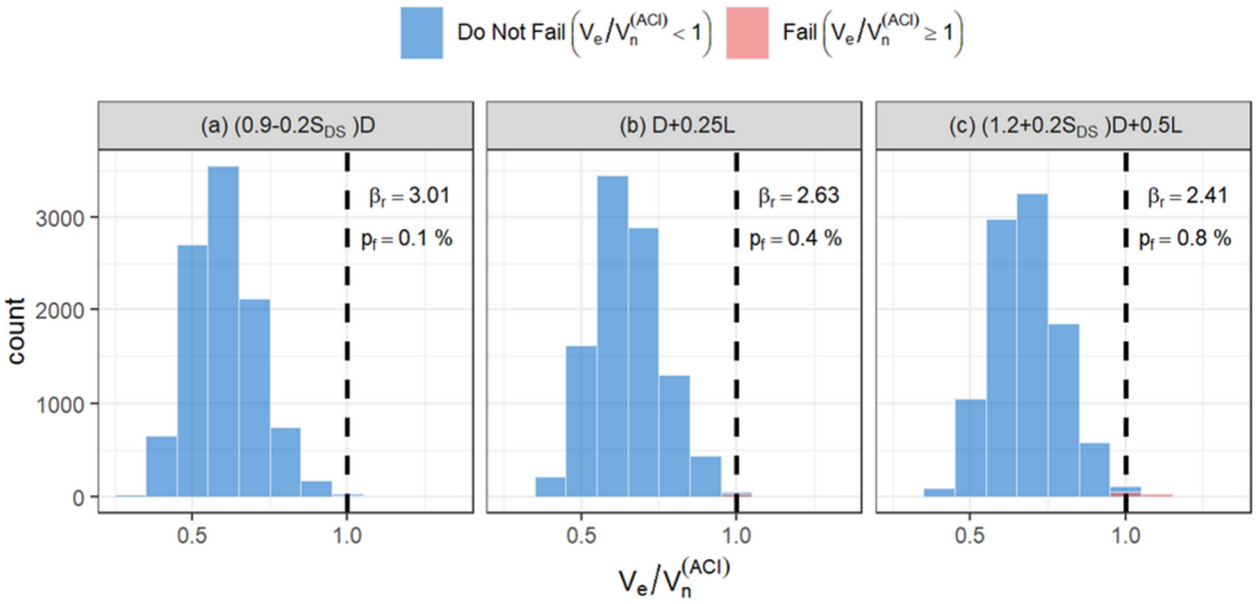

***Figure 10.17**: Reliability results using the ACI 318-19 equation, in terms of V_e/V_n, for the 4-Story Archetype*

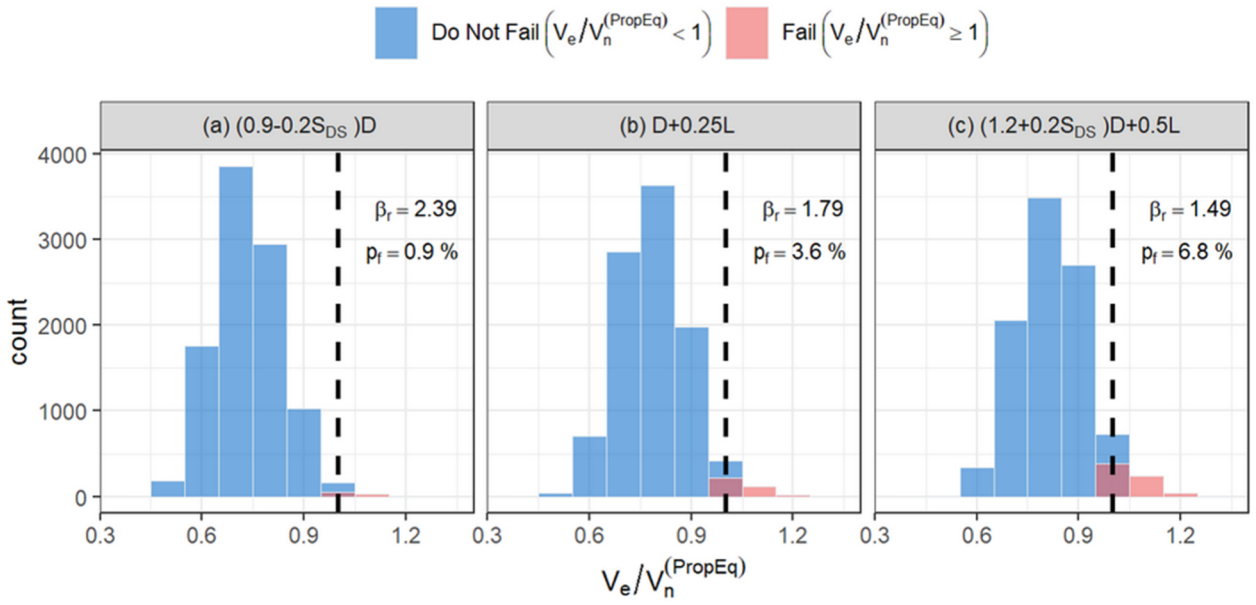

***Figure 10.18**: Reliability results using the proposed equation, in terms of V_e/V_n, for the 4-Story Archetype*

Even though expressing the results in terms of the V_e/V_n ratio instead of the difference $V_n - V_e$ says the same in terms of the reliability index and probability of failure, it provides a better understanding of the demand-to-strength relationship. This can also give a general view about the reduction factor associated with these actual values (demand and strength). **Table 10.6** indicates the mean values of the V_e/V_n distributions shown in **Figure 10.17** and **Figure 10.18**.

***Table 10.6**: Mean values of the actual shear demand over the actual shear strength*

Load Combination	$\left(\frac{V_e}{V_n^{(ACI)}}\right)_{\substack{Actual\\Mean}}$	$\left(\frac{V_e}{V_n^{(PropEq)}}\right)_{\substack{Actual\\Mean}}$
(0.9-0.2S_{DS})D	0.60	0.74
D+0.25L	0.65	0.79
(1.2+0.2S_{DS})D+0.5L	0.68	0.83

10.7 Reliability Analysis for the 8-Story Archetype

10.7.1 Probability Distribution for Actual-to-Nominal Demands Ratio

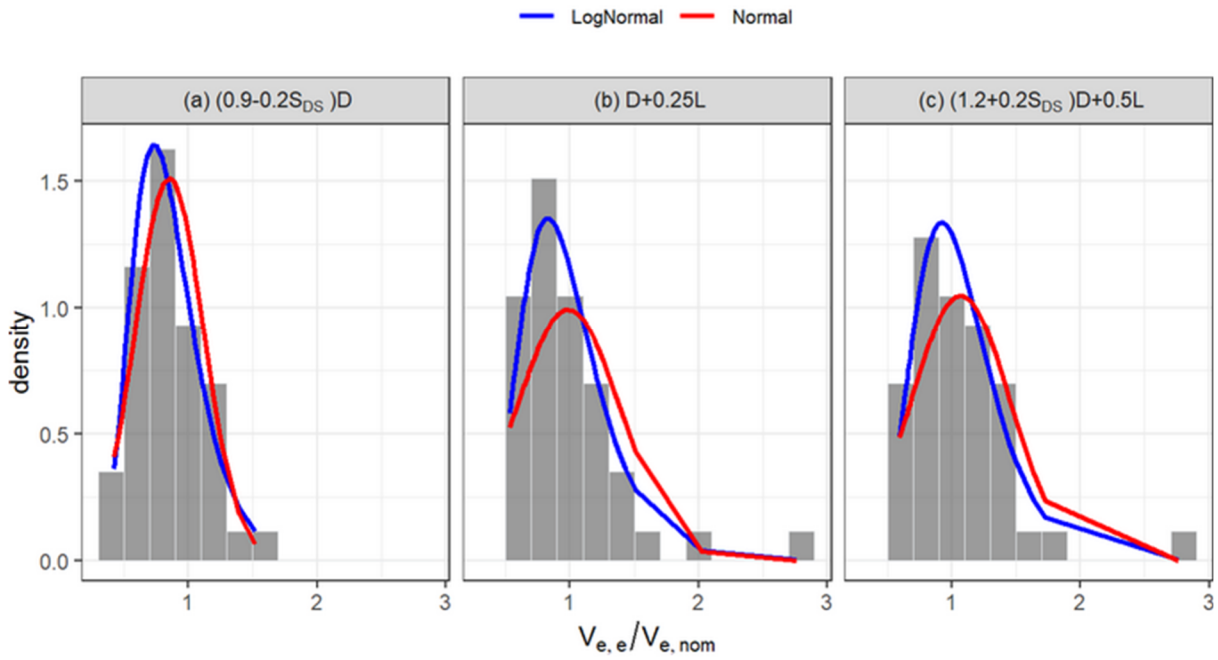

***Figure 10.19**: Density histograms and fitted distributions of the actual-to-demand shear ratios, where the nominal value is the amplified shear demand V_e obtained using ACI 318-10 provisions – 8-Story Archetype*

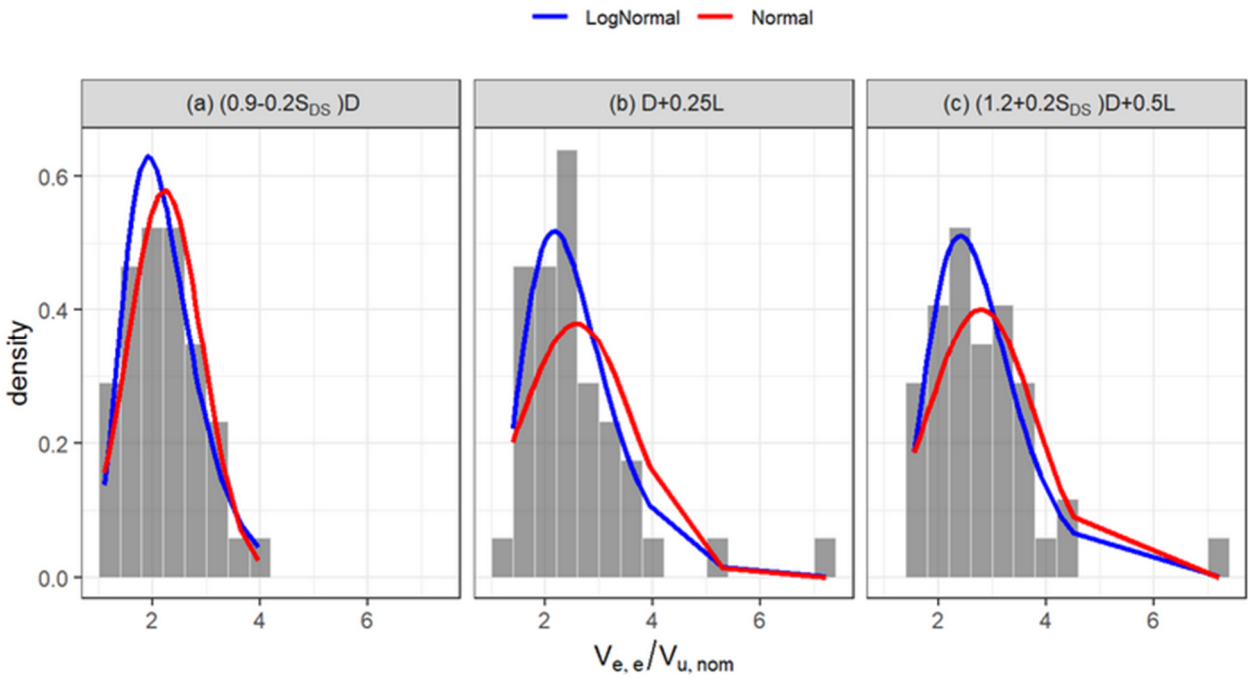

***Figure 10.20**: Density histograms and fitted distributions of the actual-to-nominal shear ratios, where nominal value is the demand V_u without amplification – 8-Story Archetype*

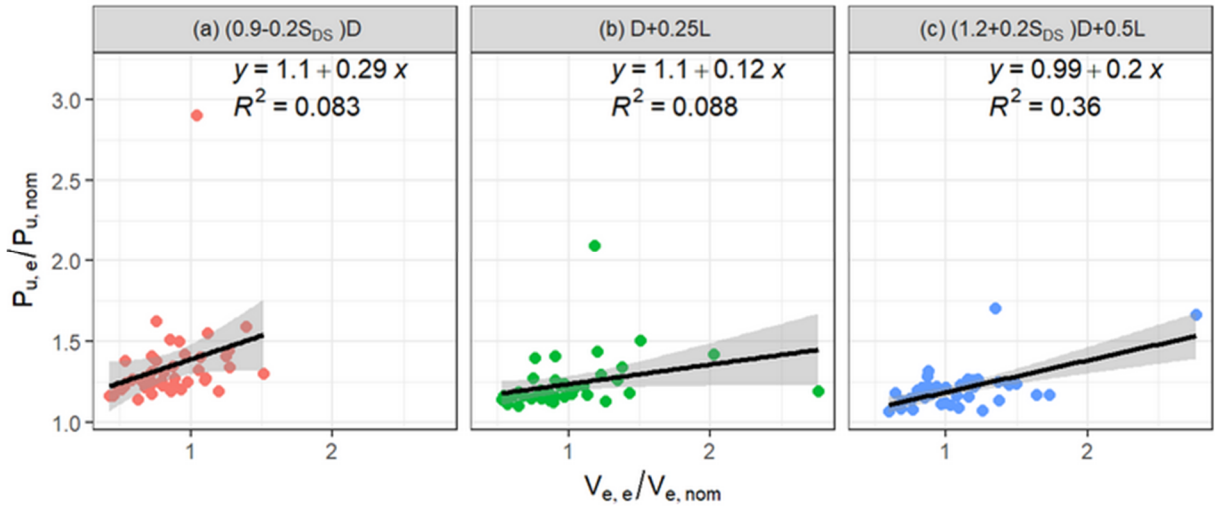

***Figure 10.21**: Relationship between actual-to-nominal axial load ratio and actual-to-nominal shear ratio – 8-Story Archetype*

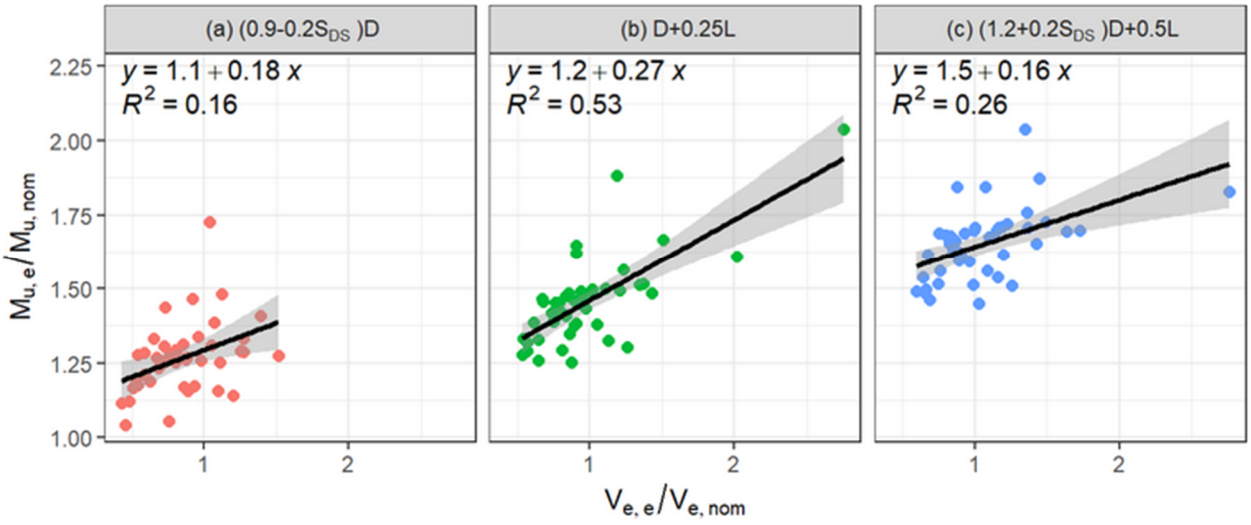

***Figure 10.22**: Relationship between actual-to-nominal moment ratio and actual-to-nominal shear ratio – 8-Story Archetype*

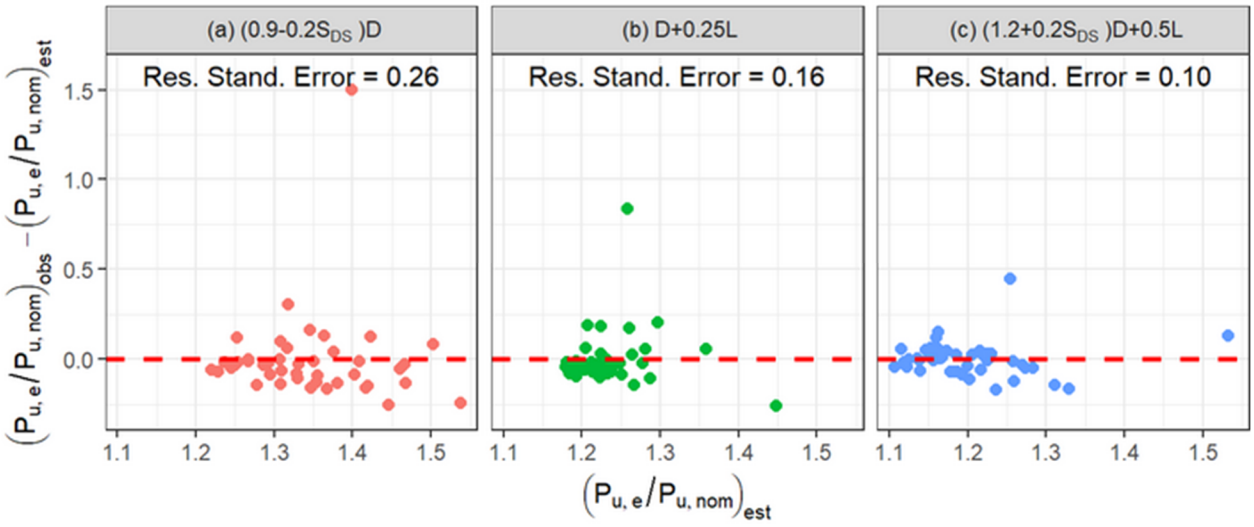

***Figure 10.23**: Residuals and residual standard deviations for actual-to-nominal axial demands – 8-Story Archetype*

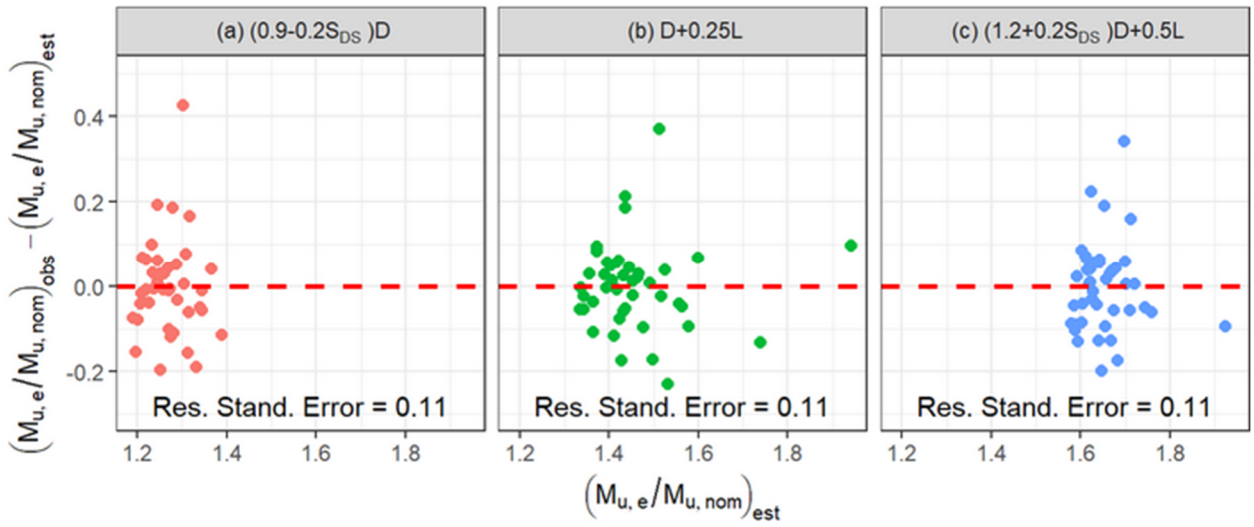

***Figure 10.24**: Residuals and residual standard deviations for actual-to-nominal moment demands – 8-Story Archetype*

***Table 10.7**: Selected actual-to-nominal demand probability distributions for the 8-Story Archetype*

Load Combination	Variable	Distribution Type	Parameter 1	Parameter 2
(0.9-0.2S_{DS})D	$V_{e,e}/V_{e,\text{nom}}$	Log-Normal	$\mu_{log} = -0.21$	$\sigma_{log} = 0.31$
	$V_{e,e}/V_{u,\text{nom}}$	Log-Normal	$\mu_{log} = 0.75$	$\sigma_{log} = 0.31$
	$P_{u,e}/P_{u,\text{nom}}$	Normal	$\mu_i = 1.10 + 0.29\left(\frac{V_{e,e}}{V_{e,\text{nom}}}\right)_i$	$\sigma = 0.26$
	$M_{u,e}/M_{u,\text{nom}}$	Normal	$\mu_i = 1.11 + 0.18\left(\frac{V_{e,e}}{V_{e,\text{nom}}}\right)_i$	$\sigma = 0.11$
D+0.25L	$V_{e,e}/V_{e,\text{nom}}$	Log-Normal	$\mu_{log} = -0.08$	$\sigma_{log} = 0.34$
	$V_{e,e}/V_{u,\text{nom}}$	Log-Normal	$\mu_{log} = 0.88$	$\sigma_{log} = 0.34$
	$P_{u,e}/P_{u,\text{nom}}$	Normal	$\mu_i = 1.11 + 0.12\left(\frac{V_{e,e}}{V_{e,\text{nom}}}\right)_i$	$\sigma = 0.16$
	$M_{u,e}/M_{u,\text{nom}}$	Normal	$\mu_i = 1.19 + 0.27\left(\frac{V_{e,e}}{V_{e,\text{nom}}}\right)_i$	$\sigma = 0.11$
(1.2+0.2S_{DS})D+0.5L	$V_{e,e}/V_{e,\text{nom}}$	Log-Normal	$\mu_{log} = 0.02$	$\sigma_{log} = 0.31$
	$V_{e,e}/V_{u,\text{nom}}$	Log-Normal	$\mu_{log} = 0.98$	$\sigma_{log} = 0.31$
	$P_{u,e}/P_{u,\text{nom}}$	Normal	$\mu_i = 0.99 + 0.20\left(\frac{V_{e,e}}{V_{e,\text{nom}}}\right)_i$	$\sigma = 0.10$
	$M_{u,e}/M_{u,\text{nom}}$	Normal	$\mu_i = 1.48 + 0.16\left(\frac{V_{e,e}}{V_{e,\text{nom}}}\right)_i$	$\sigma = 0.11$

10.7.2 Monte Carlo Simulation Results

10.7.2.1 Verification of Correlation Between Demands

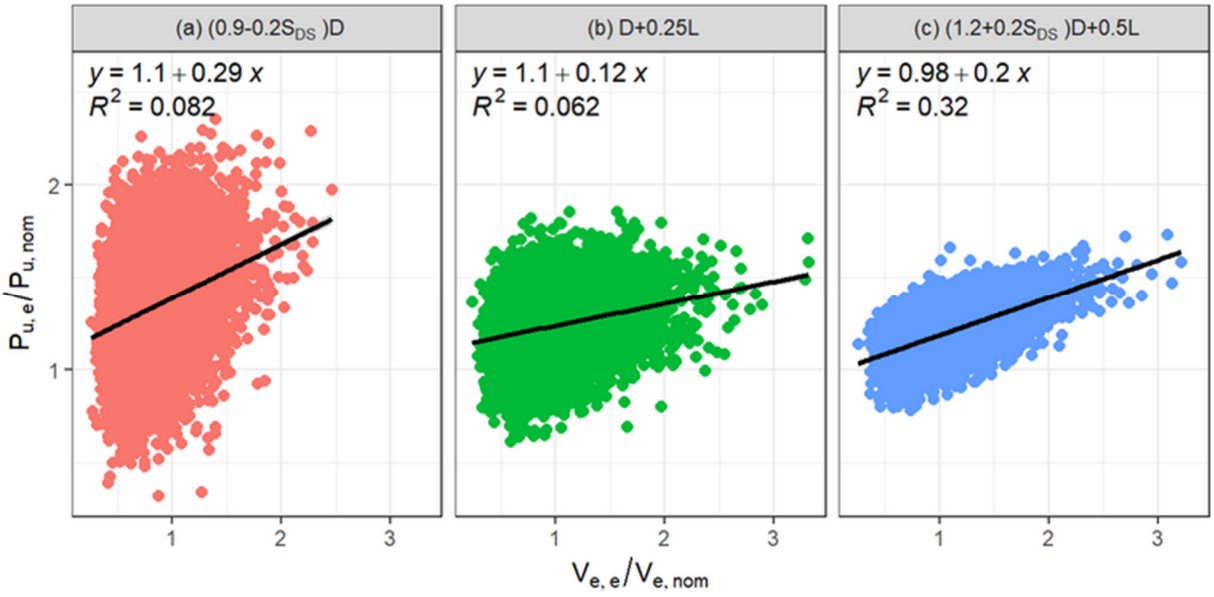

***Figure 10.25**: Relationship between simulated actual-to-nominal axial demands versus actual-to-nominal shear demands – 8-Story Archetype*

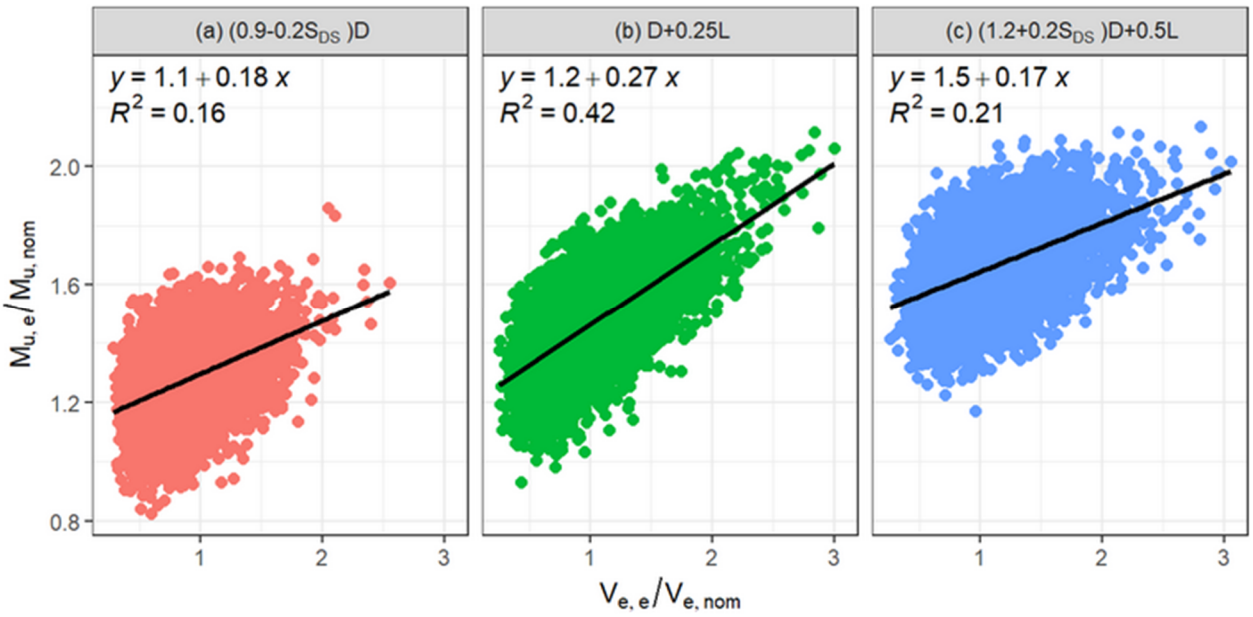

***Figure 10.26**: Relationship between simulated actual-to-nominal moment demands versus actual-to-nominal shear demands – 8-Story Archetype*

10.7.2.2 Reliability Results Expressed in Terms of $V_n - V_e$

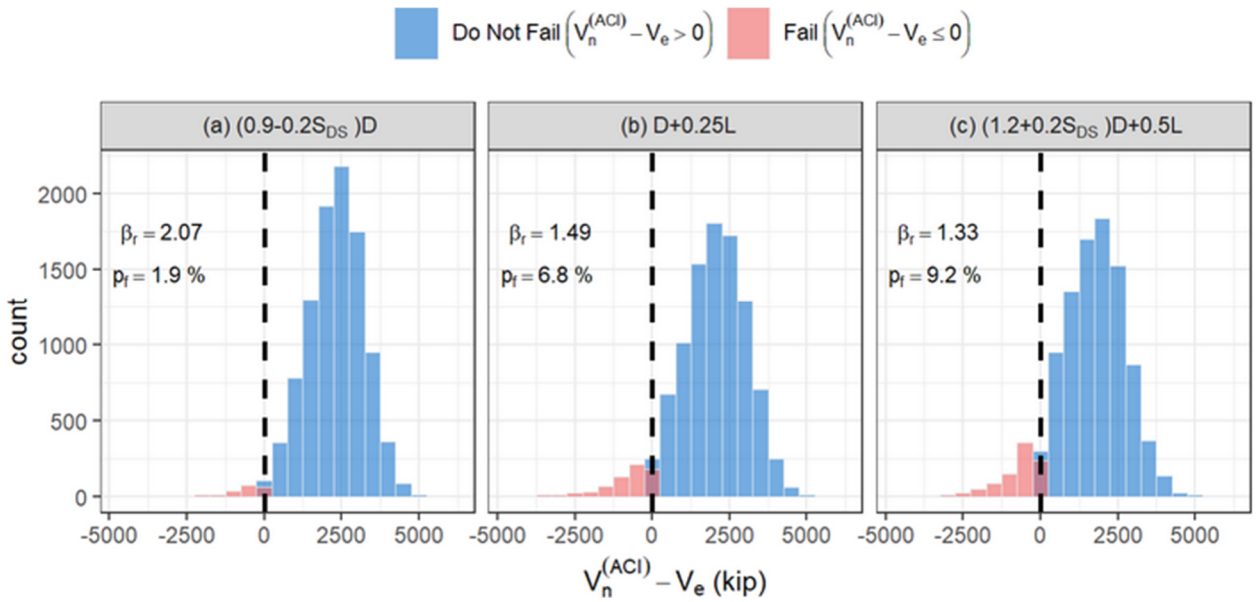

***Figure 10.27**: Reliability results using the ACI 318-19 equation, in terms of $V_n - V_e$, for the 8-Story Archetype*

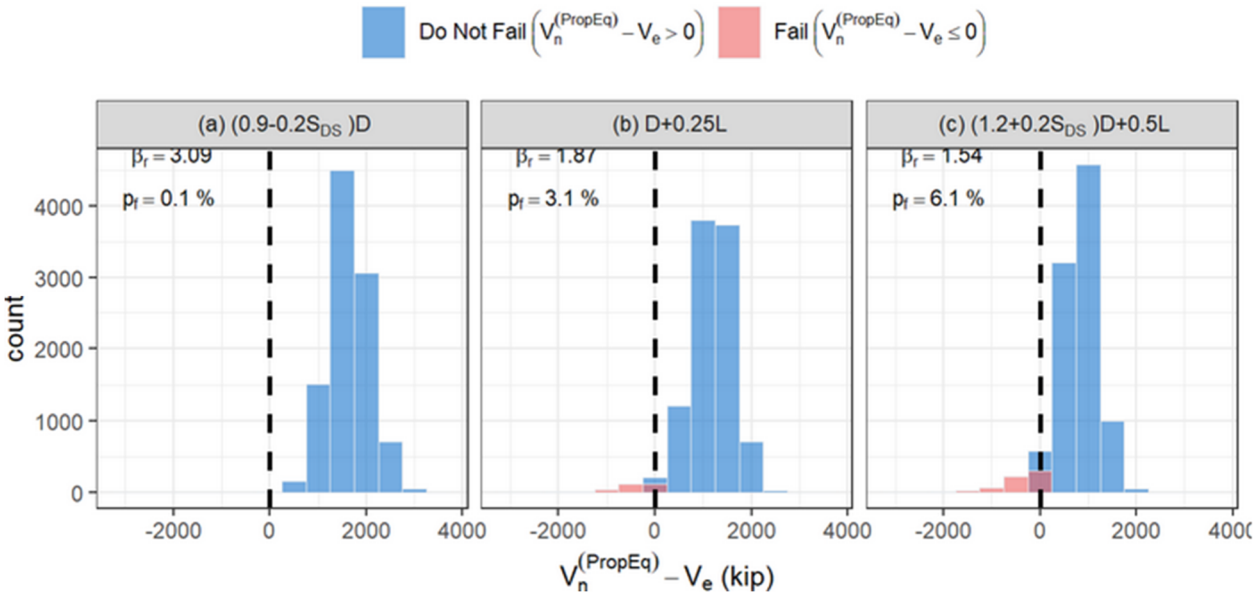

***Figure 10.28**: Reliability results using the proposed equation, in terms of $V_n - V_e$, for the 8-Story Archetype*

10.7.2.3 Reliability Results Expressed in Terms of V_e/V_n

The proposed equation estimates a moderate lower probability of failure for this ACI 318-19 compliant archetype respect to what the ACI 318-19 equation does.

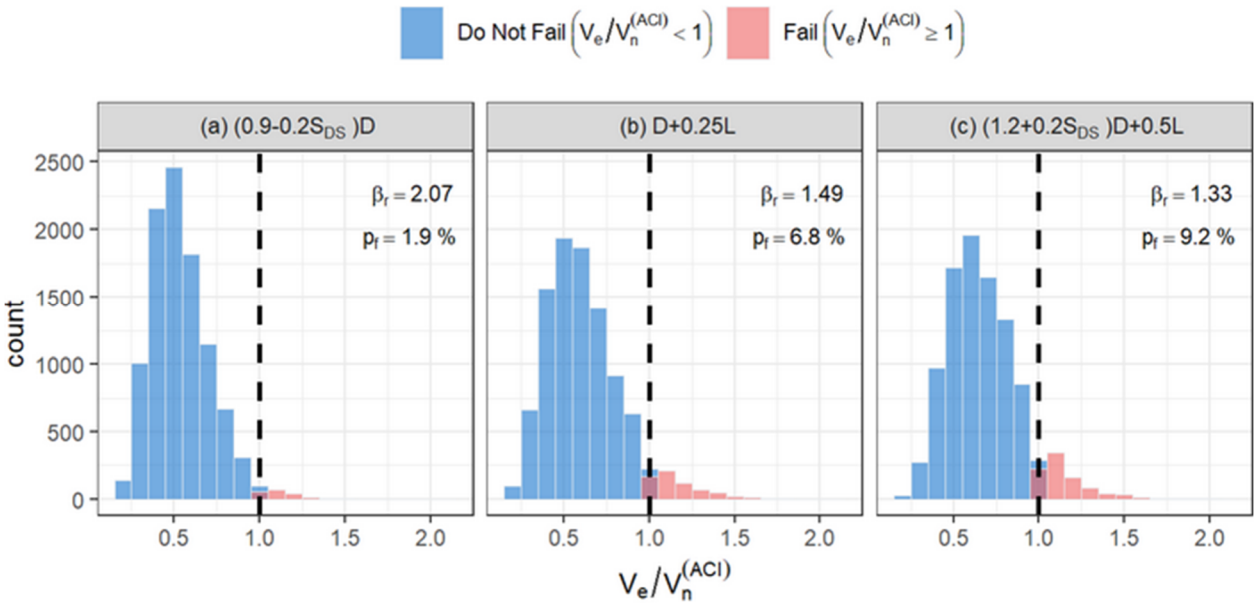

***Figure 10.29**: Reliability results using the ACI 318-19 equation, in terms of V_e/V_n, for the 8-Story Archetype*

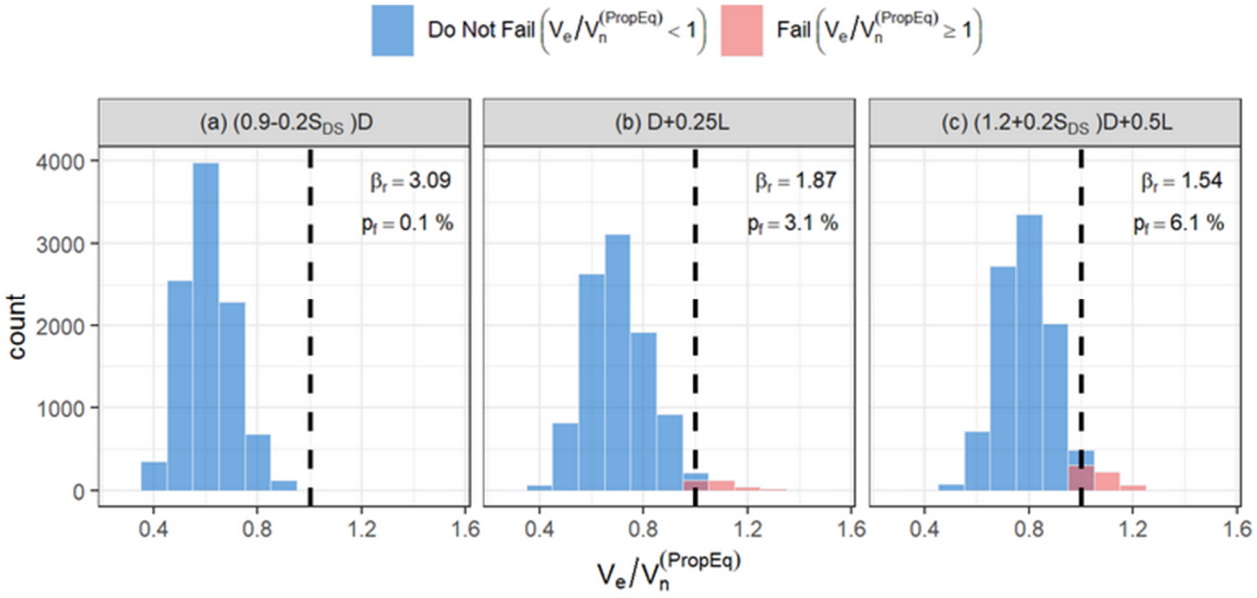

***Figure 10.30**: Reliability results using the proposed equation, in terms of V_e/V_n, for the 8-Story Archetype*

***Table 10.8**: Mean values of the actual shear demand over the actual shear strength – 8-Story Archetype*

Load Combination	$\left(\frac{V_e}{V_n^{(ACI)}}\right)_{\substack{Actual \\ Mean}}$	$\left(\frac{V_e}{V_n^{(PropEq)}}\right)_{\substack{Actual \\ Mean}}$
$(0.9-0.2S_{DS})D$	0.55	0.61
D+0.25L	0.63	0.71
$(1.2+0.2S_{DS})D+0.5L$	0.69	0.80

10.8 Reliability Analysis for the 12-Story Archetype

10.8.1 Probability Distribution for Actual-to-Nominal Demands Ratio

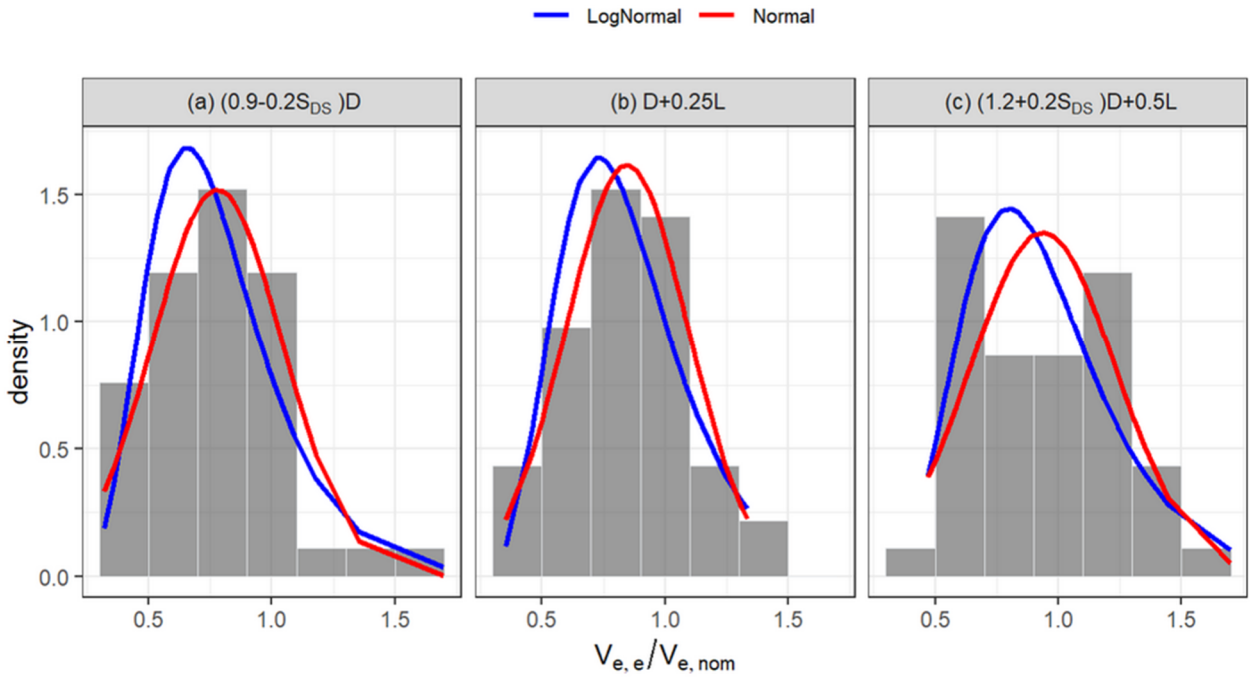

***Figure 10.31**: Density histograms and fitted distributions of the actual-to-demand shear ratios, where the nominal value is the amplified shear demand V_e obtained using ACI 318-10 provisions – 12-Story Archetype*

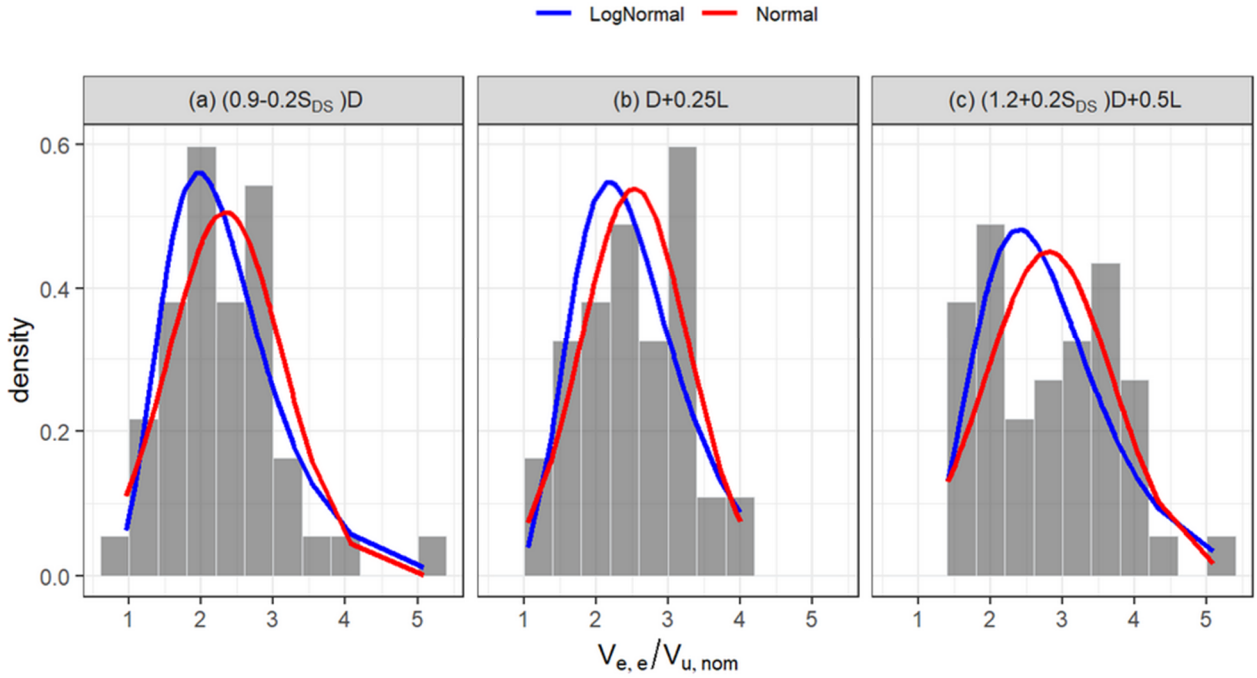

***Figure 10.32**: Density histograms and fitted distributions of the actual-to-nominal shear ratios, where nominal value is the demand V_u without amplification – 12-Story Archetype*

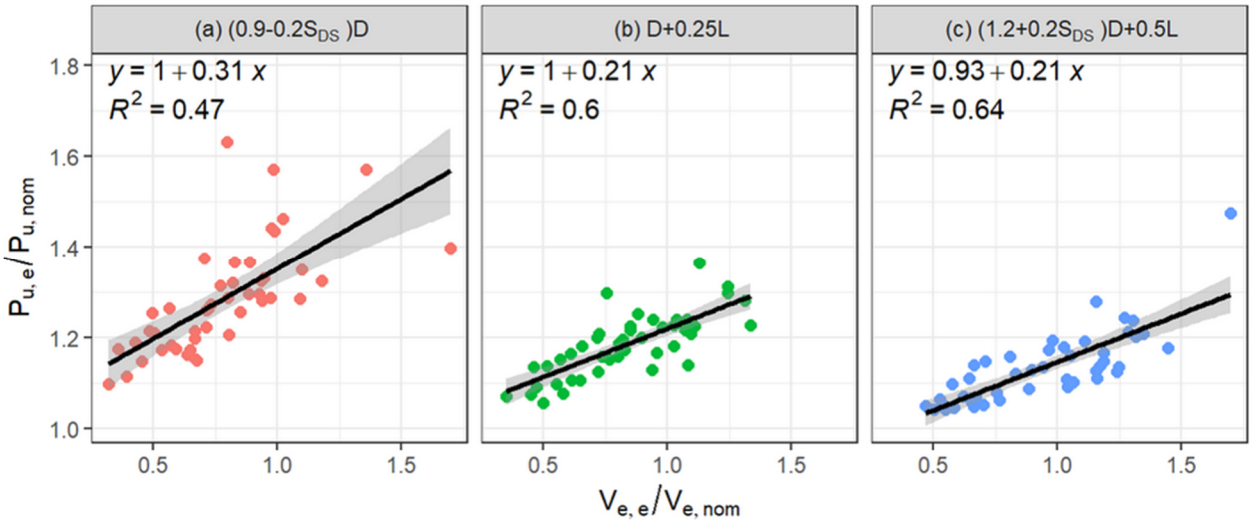

***Figure 10.33**: Relationship between actual-to-nominal axial load ratio and actual-to-nominal shear ratio – 12-Story Archetype*

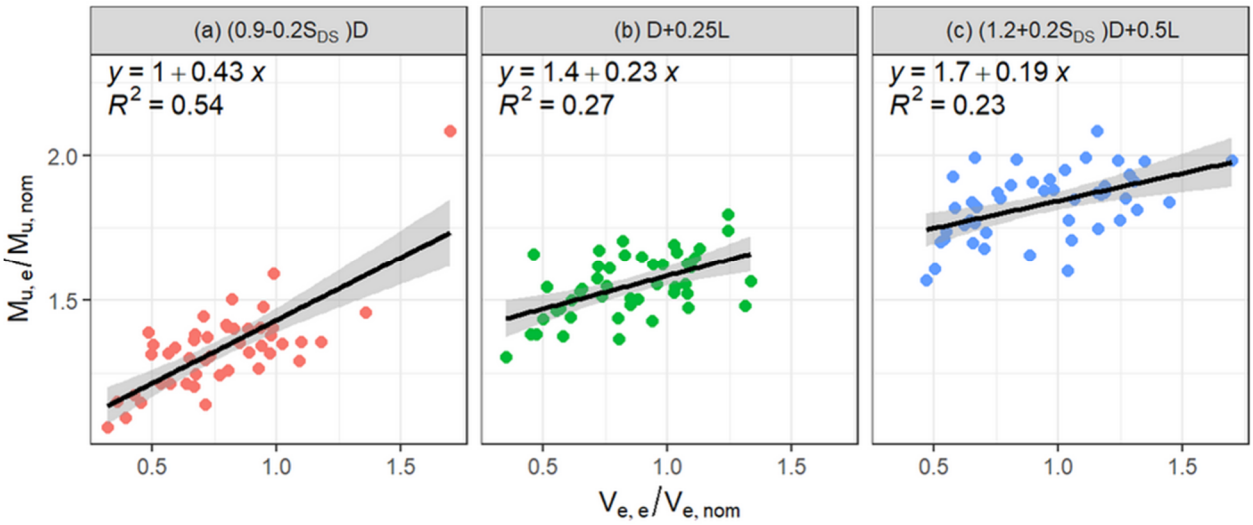

***Figure 10.34**: Relationship between actual-to-nominal moment ratio and actual-to-nominal shear ratio – 12-Story Archetype*

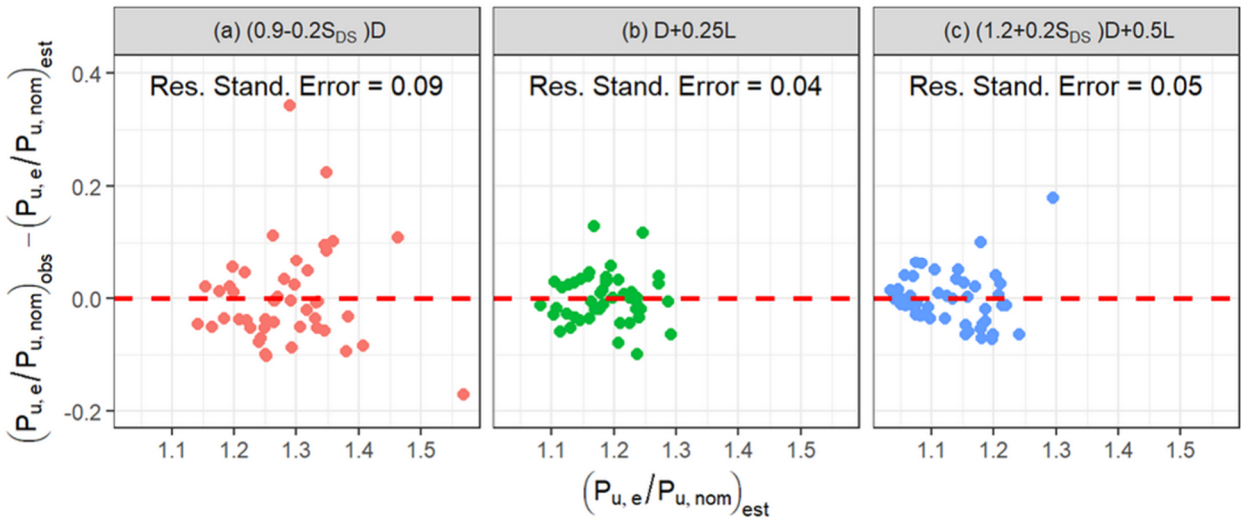

***Figure 10.35**: Residuals and residual standard deviations for actual-to-nominal axial demands – 12-Story Archetype*

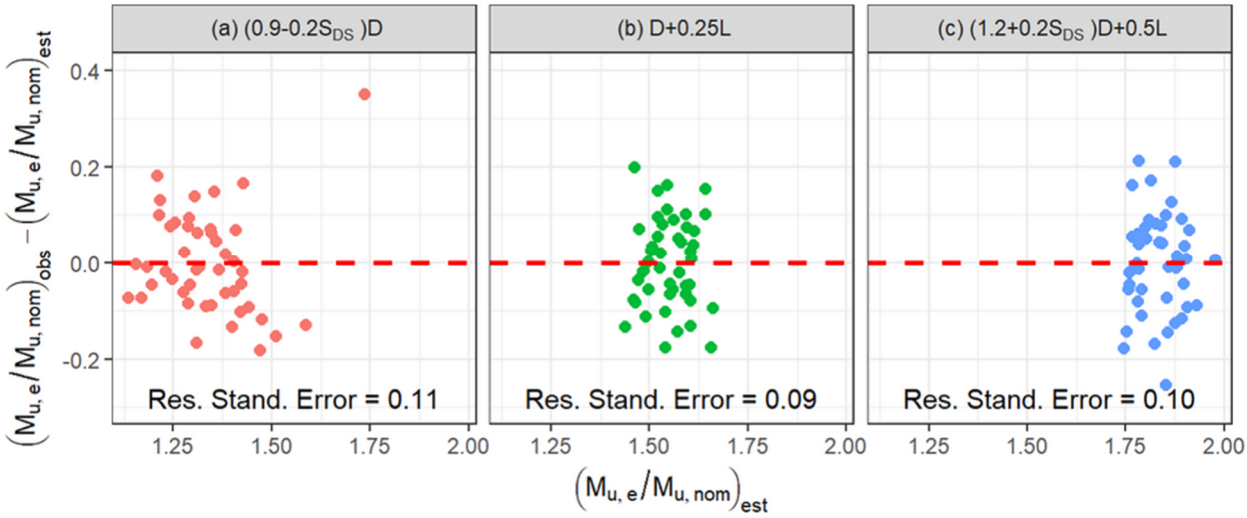

***Figure 10.36**: Residuals and residual standard deviations for actual-to-nominal moment demands – 12-Story Archetype*

***Table 10.9**: Selected actual-to-nominal demand probability distributions for the 12-Story Archetype*

Load Combination	Variable	Distribution Type	Parameter 1	Parameter 2
(0.9-0.2S_{DS})D	$V_{e,e}/V_{e,\text{nom}}$	Log-Normal	$\mu_{log} = -0.31$	$\sigma_{log} = 0.34$
	$V_{e,e}/V_{u,\text{nom}}$	Log-Normal	$\mu_{log} = 0.79$	$\sigma_{log} = 0.34$
	$P_{u,e}/P_{u,\text{nom}}$	Normal	$\mu_i = 1.04 + 0.31\left(\frac{V_{e,e}}{V_{e,\text{nom}}}\right)_i$	$\sigma = 0.09$
	$M_{u,e}/M_{u,\text{nom}}$	Normal	$\mu_i = 1.00 + 0.43\left(\frac{V_{e,e}}{V_{e,\text{nom}}}\right)_i$	$\sigma = 0.11$
D+0.25L	$V_{e,e}/V_{e,\text{nom}}$	Log-Normal	$\mu_{log} = -0.22$	$\sigma_{log} = 0.32$
	$V_{e,e}/V_{u,\text{nom}}$	Log-Normal	$\mu_{log} = 0.88$	$\sigma_{log} = 0.32$
	$P_{u,e}/P_{u,\text{nom}}$	Normal	$\mu_i = 1.01 + 0.21\left(\frac{V_{e,e}}{V_{e,\text{nom}}}\right)_i$	$\sigma = 0.04$
	$M_{u,e}/M_{u,\text{nom}}$	Normal	$\mu_i = 1.36 + 0.23\left(\frac{V_{e,e}}{V_{e,\text{nom}}}\right)_i$	$\sigma = 0.09$
(1.2+0.2S_{DS})D+0.5L	$V_{e,e}/V_{e,\text{nom}}$	Log-Normal	$\mu_{log} = -0.12$	$\sigma_{log} = 0.33$
	$V_{e,e}/V_{u,\text{nom}}$	Log-Normal	$\mu_{log} = 0.98$	$\sigma_{log} = 0.33$
	$P_{u,e}/P_{u,\text{nom}}$	Normal	$\mu_i = 0.93 + 0.21\left(\frac{V_{e,e}}{V_{e,\text{nom}}}\right)_i$	$\sigma = 0.05$
	$M_{u,e}/M_{u,\text{nom}}$	Normal	$\mu_i = 1.66 + 0.19\left(\frac{V_{e,e}}{V_{e,\text{nom}}}\right)_i$	$\sigma = 0.10$

10.8.2 Monte Carlo Simulation Results

10.8.2.1 Verification of Correlation Between Demands

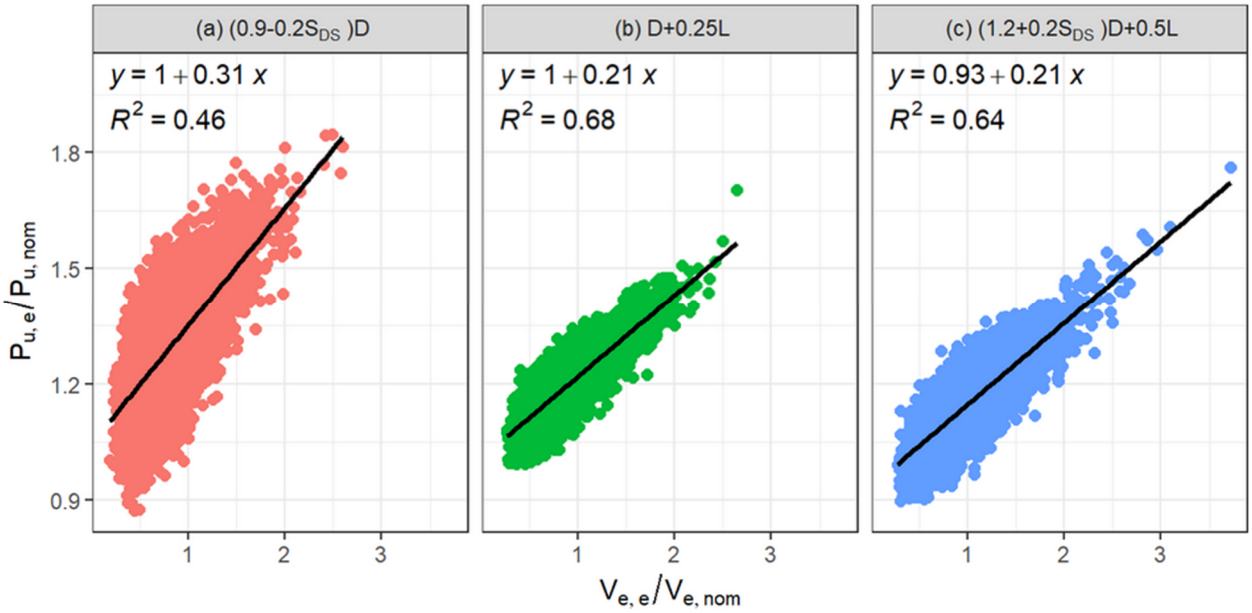

***Figure 10.37**: Relationship between simulated actual-to-nominal axial demands versus actual-to-nominal shear demands – 12-Story Archetype*

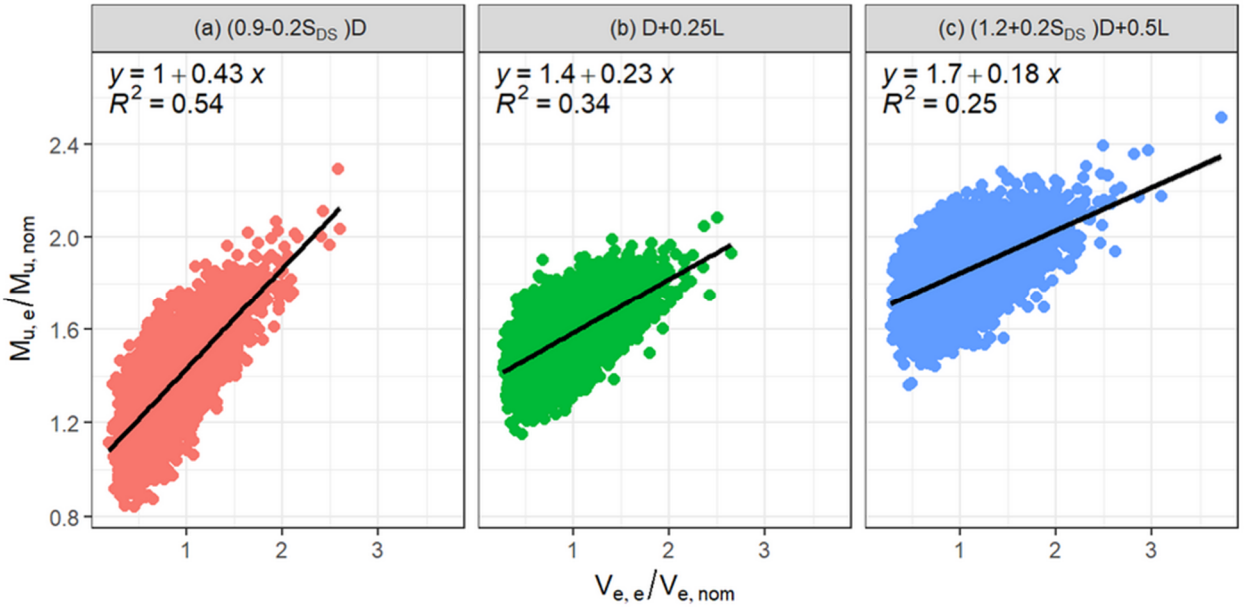

***Figure 10.38**: Relationship between simulated actual-to-nominal moment demands versus actual-to-nominal shear demands – 12-Story Archetype*

10.8.2.2 Reliability Results Expressed in Terms of $V_n - V_e$

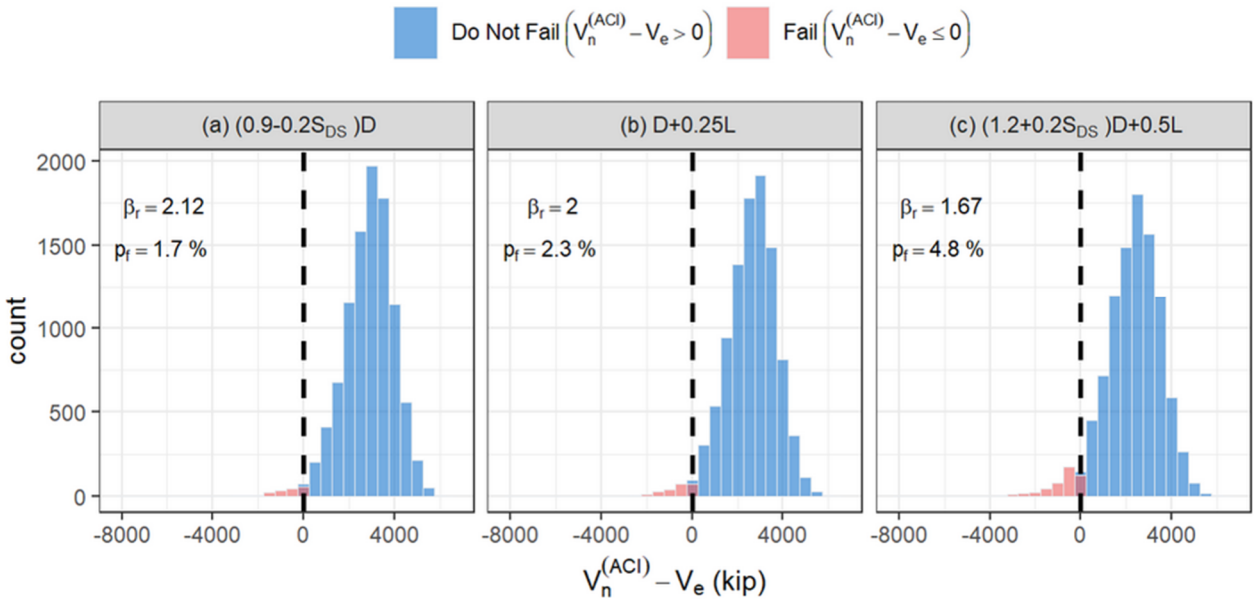

Figure 10.39*: Reliability results using the ACI 318-19 equation, in terms of $V_n - V_e$, for the 12-Story Archetype*

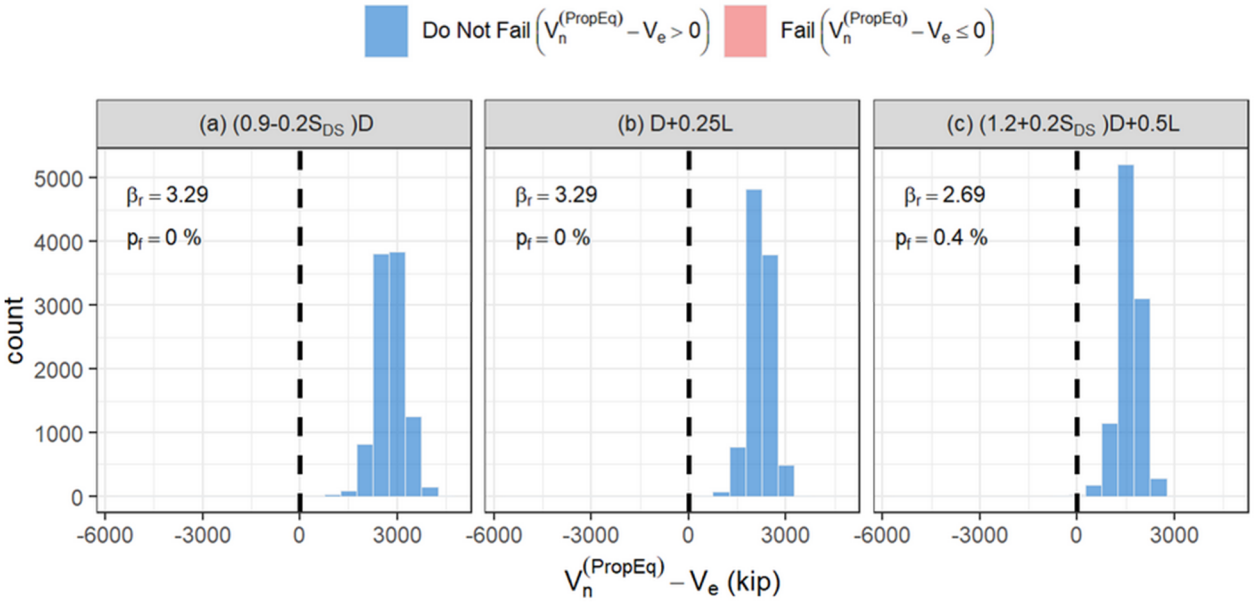

Figure 10.40*: Reliability results using the proposed equation, in terms of $V_n - V_e$, for the 12-Story Archetype*

10.8.2.3 Reliability Results Expressed in Terms of V_e/V_n

The proposed equation estimates a much lower probability of failure for this ACI 318-19 compliant archetype respect to what the ACI 318-19 equation does.

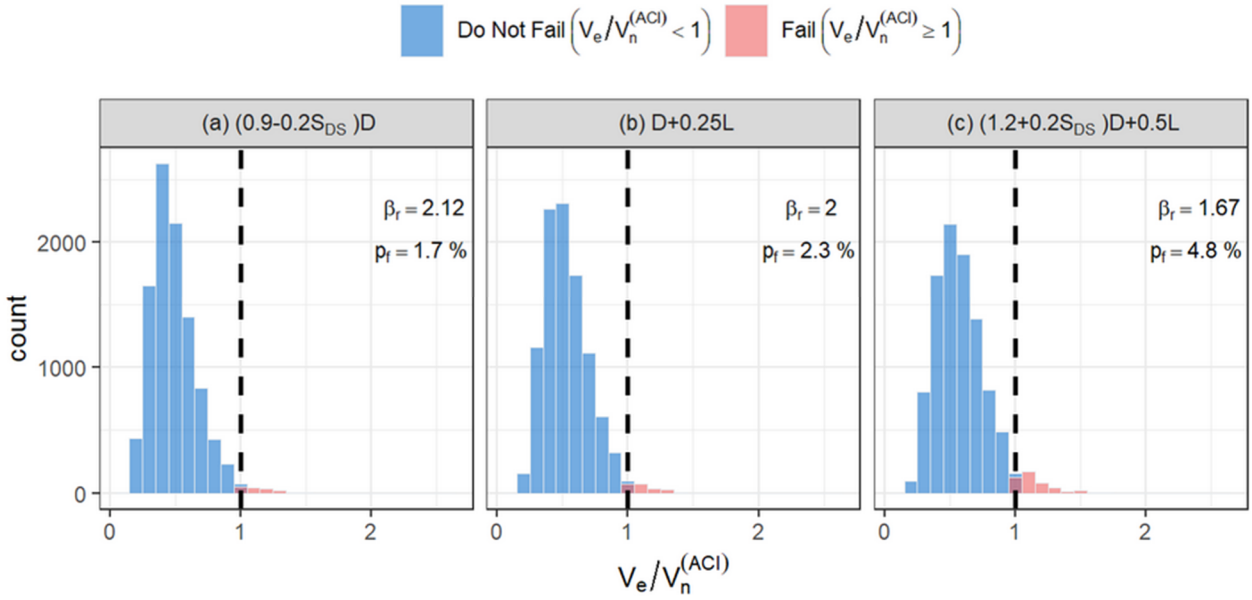

***Figure 10.41**: Reliability results using the ACI 318-19 equation, in terms of V_e/V_n, for the 12-Story Archetype*

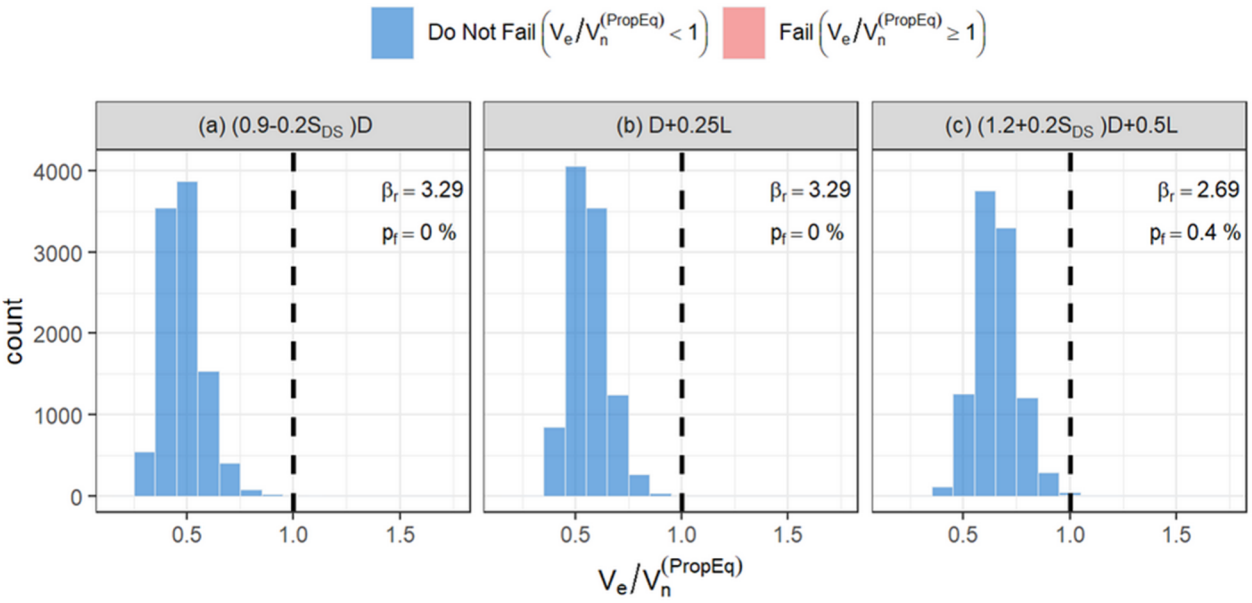

***Figure 10.42**: Reliability results using the proposed equation, in terms of V_e/V_n, for the 12-Story Archetype*

***Table 10.10**: Mean values of the actual shear demand over the actual shear strength*

Load Combination	$\left(\frac{V_e}{V_n^{(ACI)}}\right)_{\substack{Actual \\ Mean}}$	$\left(\frac{V_e}{V_n^{(PropEq)}}\right)_{\substack{Actual \\ Mean}}$
$(0.9\text{-}0.2S_{DS})D$	0.49	0.48
D+0.25L	0.54	0.56
$(1.2+0.2S_{DS})D+0.5L$	0.59	0.65

10.9 Further Assessment of the Archetypes Reliability Analyses Results

Even though the archetypes are ACI 318-19 compliant, a relationship between the probability of failure and the strength reduction factor when using the proposed equation can be obtained. Using the proposed equation, different shear strengths for the different load combinations can be estimated; for each axial load, the associated probable moment is obtained from the unreduced P-M diagram (obtained using $1.25f_y = 75$ ksi), and then the amplified shear demand is calculated accordingly with the resultant overstrength factor $\Omega_v = M_{pr}/M_u$. The α_c and α_s coefficients are calculated using its more generalized form, as shown in Eq. (10.6) and (10.7), respectively. Note that these expressions are equivalent to the ones presented before for the load combination producing the largest axial demand, unless $\omega_v \Omega_v \geq 3.0$.

$$\alpha_c = \frac{1}{100}\left(9\frac{\left(1+\frac{P_u}{A'_g f'_c}\right)^3}{\left(\frac{M_{pr}}{V_e l_w}\right)^{1/3}} - 6\right) \geq 0.010 \qquad (10.6)$$

$$\alpha_s = \frac{2}{5\left(\frac{M_{pr}}{V_e l_w}\right)^{1/3}} \geq 0.30 \qquad (10.7)$$

The demands and shear strength are shown in **Table 10.11**, where in addition of presenting the $V_e/V_n^{(PropEq)}$ ratio, an "equivalent strength reduction factor" (ϕ_{eq}) is included. This ϕ_{eq} represents the strength reduction factor that would have been applied if designing the archetype with the proposed equation in order to comply with the condition $\phi V_n \geq V_e$. The margin between ϕV_n and V_e is usually small, e.g., it is between 4% and 5% for the ACI 318-19 compliant archetypes of this study. Therefore, the factor ϕ_{eq} in **Table 10.11** is estimated as 1.05 $V_e/V_n^{(PropEq)}$. The probability of failure (p_f) obtained with the Monte Carlo simulation analysis is also tabulated.

***Table 10.11**: Shear strength $V_n^{(PropEq)}$ for each load combination and associated ϕ_{eq}*

Archetype	Load ** Combination	P_u (kip)	M_{pr} (kip-ft)	V_e (kip)	ALR (%)	SSR	$V_n^{(PropEq)}$ (kip)	$\frac{V_e}{V_n^{(PropEq)}}$	p_f (%)	ϕ_{eq}
4-Story Archetype	LC_min	684	110,572	2,692	1.6	1.37	3,031	0.89	0.9	0.93
	LC_avg	1,157	115,891	2,826	2.7	1.37	3,154	0.90	3.6	0.94
	LC_max	1,741	122,361	2,984	4.0	1.37	3,306	0.90	6.8	0.95
8-Story Archetype	LC_min	1,584	107,716	2,487	2.9	1.44	3,212	0.77	0.1	0.81
	LC_avg	2,674	120,058	2,772	5.0	1.44	3,493	0.79	3.1	0.83
	LC_max	4,018	134,678	3,110	7.4	1.44	3,855	0.81	6.1	0.85
12-Story Archetype	LC_min	2,426	117,283	2,716	4.5	1.44	3,961	0.69	0.0	0.72
	LC_avg	4,098	135,520	3,138	7.6	1.44	4,072	0.77	0.0	0.81
	LC_max	6,159	156,260	3,618	11.4	1.44	4,663	0.78	0.4	0.82
	LC_max*	6,159	156,260	3,474	11.4	1.50*	4,589	0.76	0.4	0.79

*The only difference in the calculation of the values in this row respect to the one above, is that the upper limit for the amplification factor was considered ($\boldsymbol{\omega_v \Omega_v \leq 3.0}$).

**LC_min = (0.9-S_{DS})D ; LC_avg = D+0.25L ; LC_max = (1.2+0.2S_{DS})D+0.5L

Figure 10.43(a) highlights the trends between the probability of failure and axial load ratio, **Figure 10.43(b)** associates probability of failure and the ratio of shear demand over the shear upper limit (note that $\alpha_{shape} = 1.0$ for rectangular walls). Naturally, with higher shear demand, the probability of failure increases. **Figure 10.43(c)** relates the probability of failure with the strength reduction factor ϕ_{eq}. From this plot it can be seen that values vary between approximate values of 0.75 and 0.95, keeping the probability of failure always below 10%, which is the threshold for MCE level defined in ASCE 7-16.

Since these archetypes are ACI 318-19 compliant, the results here show what was said before in Chapter 10. Shear strength for rectangular walls with low levels of axial load ratio is underestimated by the ACI 318-19 equation, which results in a larger probability of failure for the 4-Story Archetype in this case. However, it is relevant to acknowledge that the variation of axial load around the average value estimated from D+0.25L shows a positive correlation with the probability of failure (**Figure 10.43(a)**).

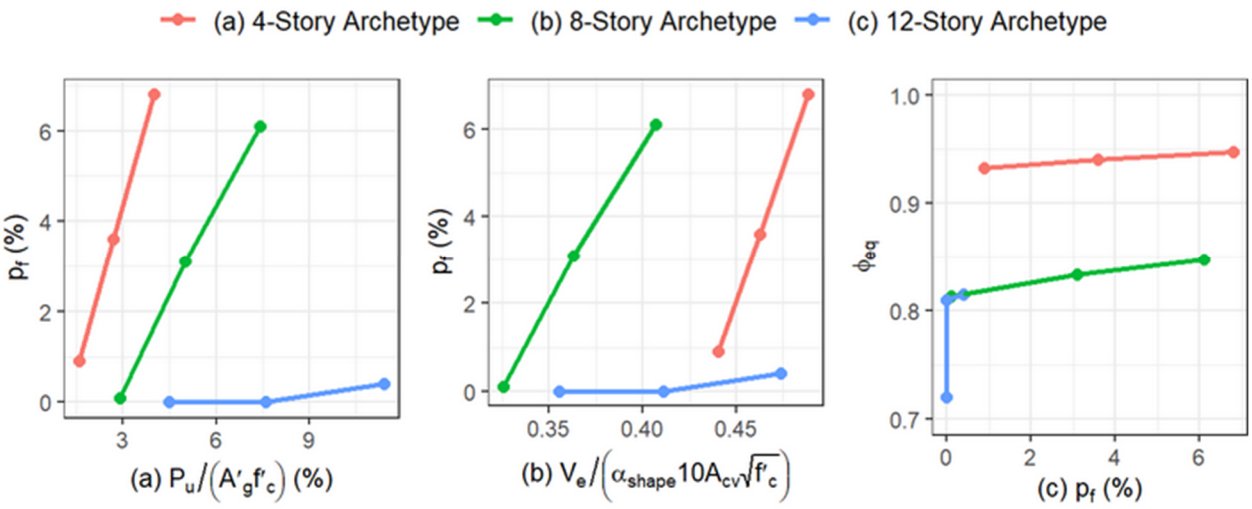

***Figure 10.43**: Probability of failure trends and its relationship with associated ϕ_{eq}*

Figure 10.43(c), computed without the upper limit for V_e currently considered in ACI 318-19, suggest that using $\phi \leq 0.80$ might result in probability of failures that are always very small (close to 0%). For values of $\phi > 0.80$ it can be seen that the probability of failure varies from ~0% to ~6% for the 8-story archetype, and from ~1% to ~7% for the 4-story archetype. In other words, the probability of failure for each archetype varies depending on the vertical load combination, thus defining a variability region for p_f, as shown in **Figure 10.44(a).** If the upper limit that ACI 318-19 currently has for the shear demand amplification factor is considered ($\omega_v \Omega_v \leq 3.0$), then the variability region for p_f increases, but around the portion related to lower ϕ factors and lower p_f (**Figure 10.44(b)**).

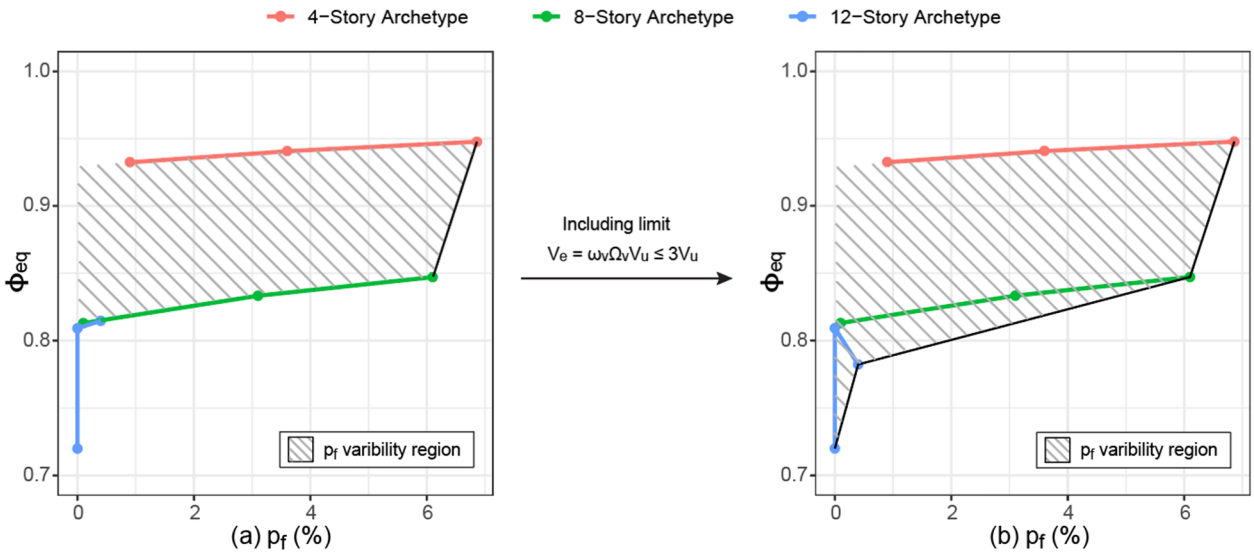

***Figure 10.44**: Relationship between p_f and ϕ_{eq} to assess selection of ϕ for the proposed equation*

Chapter 11. Conclusions

The performance of existing RC wall shear strength equations (used in building codes or standards or proposed in the literature) vary substantially when evaluated with different databases and generally perform poorly when evaluated against a common database (i.e., high error and/or high variance). Some of the more complex models reported in the literature indicate good performance by showing that the more complex model performance is better than simpler models, which is an unfair comparison because it is expected to obtain better predictions if the model is more complex. As well, comparisons between two models of similar model complexity level are not enough to say the one with better performance is a good model, because it can be the case that a third equivalent complexity model could have better performance. This led to pose the problem of establishing objective model performance criteria. The problem was addressed by implementing a systematic combined ML-Statistics methodology to establish target errors for different model complexity levels. The methodology was applied to the problem of RC walls shear strength prediction using a comprehensive database. Based on the results obtain with this framework, the following specific conclusions are drawn:

- The proposed methodology can be used as a framework to obtain relationships between target model performance for models with different complexity levels and can be particularly useful when addressing a mechanic-based problem with a small database.

- A comprehensive database of 333 RC walls reported to have failed in shear is obtained from the UCLA-RC Shear Walls Database. Each test includes approximately 30 variables, which enables a detailed assessment of how each variable influences wall shear strength. This database is large by structural engineering standards for large scale tests, but still relatively small to take advantage of ML approaches.
- The framework used in this study can be implemented as means to determine if a properly trained complex ML model can make a big difference in terms of predictive power respect to a simple linear regression model obtained from the ENMs analysis.
- When applied to the RC wall shear strength capacity estimation problem, the framework shows that a systematic methodology that recognizes the mechanics of the problem and the availability of limited data (compared to those databases with thousands or millions of samples available in fields where ML shows its greats potential) can produce simple models with performance as good as complex ML models.
- The proposed iterative sensitivity analysis enables clear ML hyper-parameters trends to be identified which made it easier to select the optimum set of hyper-parameter values. Including the standard deviation of the errors obtained for each hyper-parameter configuration in the trend plots helps to assess the underfitting-overfitting trade-off and it shows how a non-appropriate hyper-parameter selection could be made if only one iteration is run.
- When coming up with a new model (ML model or not), it is required to split the dataset into testing and training sets. Before using the entire database to refine the model, it is a requisite for the model to have similar predictive power against both

training and testing sets. This should be verified not only in terms of the error indicator selected for the optimization process, but also (at a minimum) in terms of mean of V_{true}/V_{pred} and its COV.

- Defining the starting features and the predicted variable as normalized (unitless) and mechanic-based is one of the key initial steps in the framework to make: (1) the database representative of full-scale test specimens, because structural laboratory tests are often conducted at less than full-scale; (2) the error indicator used in the optimization process more robust; (3) the ENMs better able to capture data trends.
- All ML models considered in this study at their optimum complexity level (ANN, RF Regression and LASSO model), result in very similar predictive performance. This result is taken as a validation for using underfitted models derived from the optimum LASSO model as a soft relaxation away from the optimum when looking for target model performance (errors) that fulfill user requirements for less complex models.
- Target performance of a model to predict reinforced concrete wall shear strength for implementation in codes and standards should achieve a V_{true}/V_{pred} mean ratio very close to 1.0 with a COV in the range of 0.16 to 0.19 when faced against the comprehensive database provided in this study (or a similar one). In addition, the training and testing errors should be within a margin of $\pm 10\%$ of the converging error (in terms, at least, of the error used in the optimization process and in terms of COV).
- Complex ML models are required to have a V_{true}/V_{pred} mean ratio of 1.0 (or very close to) with a COV of 0.12 or lower, and to verify a training and testing error within a margin of $\pm 20\%$ of the converging error (in terms, at least, of the error used in the optimization process and in terms of COV).

After applying the framework and established objective model performance criteria for the reinforced concrete wall shear strength problem, several existing models in codes, standards, and literature were studied. None of the existing code-oriented models meets the target performance for a simplified shear strength model, which suggested there is room for improvement in terms of code equation predictive performance.

Using a methodology, that involves statistical and ML approaches, applied to the same comprehensive and cleanse database of 333 walls that are reported to have failed in shear, a new wall shear strength equation is obtained. Also, a modification on the current shear stress upper limit is proposed.

- The proposed equation satisfies the target model performance for a code-oriented equations. A simplified version of the equation is obtained, and it also meets the target model performance objectives.
- The proposed equation applies to walls with rectangular, barbell, and flanged (C-, H-, T- and L-shaped) cross-sections, although the validation was limited for asymmetric cross-section shapes due to lack of data (database with only 13 samples).
- Unlike the ACI 318-19 equation, the proposed equation has practically the same performance (prior to application of a limiting shear stress) for walls with different cross-section shape, axial load ratio, shear-span ratio, or aspect ratio.
- Analyses of two companion tests groups indicate that the shear strength contribution coming from the terms of the proposed equation are more accurate than the contributions coming from the terms on the ACI 318-19 equation, which tends to

significantly underestimate and overestimate the contributions associated with concrete and horizontal web reinforcement, respectively.

- The coefficients on the equation are unitless, which provides a more natural use of the equation because it does not depend on the specific set of units the engineer is using.
- The proposed shear strength upper limit is simple and is designed to have the performance similar to the limit in ACI 318-19 for rectangular walls (most of walls not failing in diagonal-compression below the limit and about half of the walls failing in diagonal-compression above the limit), but for all walls. The proposed limit consists in including the α_{sh} factor (function of the cross-section area of the compressed flange over A_{cv}) to the current upper bound definition, which allows shear stresses ($v_n = V_n/A_{cv}$) up to $15\sqrt{f_c'}$ for walls with flanges.

Finally, a reliability analysis is performed through a Monte Carlo Simulation. Three ACI 318-19 compliant archetypes were studied, for which the shear strength was also estimated using the proposed equation. It is found that the shear strength reduction factor associated with the proposed equation can vary between approximately values of 0.75 and 0.95, keeping a probability of failure less than 10% for MCE level, and practically in 0% for ϕ values around 0.80 or less. Also, the reliability analysis presents results that are consistent with those obtained by performing comparisons of the proposed equation and the ACI 318-19 equation on the database; the ACI 318-19 equation underestimates the shear strength of rectangular walls and walls with low axial load ratio, and it overestimates it for barbell walls or walls with flanges, or walls with high axial load. Explicitly:

- The proposed equation estimates a much higher probability of failure for the 4-story rectangular wall respect to what the ACI 318-19 equation does.
- The proposed equation estimates a moderate lower probability of failure for the 8-story rectangular wall respect to what the ACI 318-19 equation does.
- The proposed equation estimates a much lower probability of failure for the 12-story rectangular wall respect to what the ACI 318-19 equation does.

Appendix A. Design and Analysis of 4-Story Archetype

Content

A.1 Analysis - Design Forces and Displacements

Building Information

- $n_s := 4$ stories.

- Story height of $h_{typ} := 13\ ft$, except for the 1st story which $h_b := 15\ ft$ high

- 120 ft x 120 ft every story

- $n_w := 4$ rectangular walls in each direction

- Center of mass and stiffness coincide (no eccentricity)

- Dead load = 175 psf (floors)
  = 140 psf (roof)

- Live load = 50 psf + 15 psf (partitions) = 65 psf (floors)
  = 20 psf + 0 psf (partitions) = 20 psf (floors)

- Risk Category II

- Site Class C

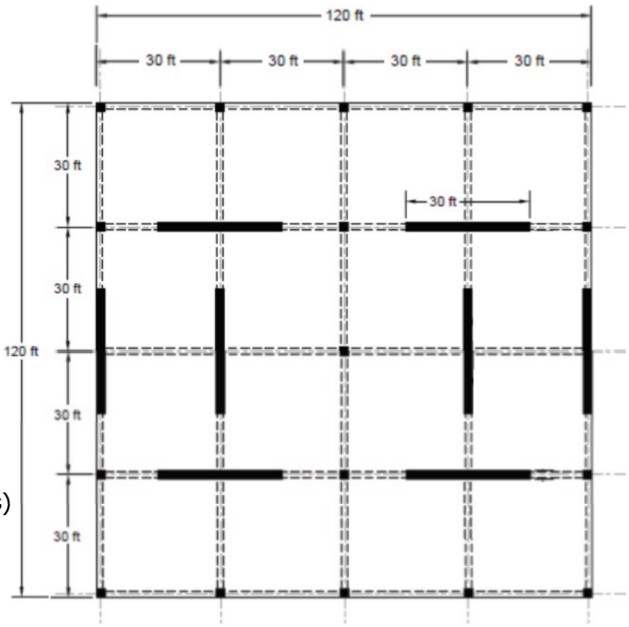

- Wall dimensions: $l_w := 30\ ft$, $t_w := 24\ in$, $t_{fl} := 0\ ft$, $b_{fl} := 0\ ft$

$$A_{cv} := l_w \cdot t_w = 8640\ in^2$$

$$A_g := t_w \cdot \left(l_w - 2 \cdot t_{fl}\right) + 2 \cdot b_{fl} \cdot t_{fl} = 8640\ in^2$$

$$A'_g := t_w \cdot \left(l_w - t_{fl}\right) + b_{fl} \cdot t_{fl} = 8640\ in^2$$

Determination of SDC

Mapped acceleration parameters

From USGS Hazard Tool Website:

Maximum considered earthquake spectral response acceleration at short periods. $S_s := 2.08\ g$

Maximum considered earthquake spectral response acceleration at a period of 1-sec. $S_1 := 0.64\ g$

Determine if the building is permitted to be automatically asigned to SDC A

Because $S_s = 2.08 > 0.15$ and $S_1 = 0.64 > 0.04$, the building is not permitted to be automatically assigned to SDC A.

Determine if the SDC is E or F

Because the Risk Category is II and $S_1 = 0.64 < 0.750$, the SDC is not E or F

Design acceleration parameters

According to ASCE 7-16:

Table 11.4-1 $F_a := 1.0$

Table 11.4-2 $F_v := 1.4$

Eq. 11.4-1 $S_{MS} := F_a \cdot S_s = 2.08$

Eq. 11.4-2 $S_{M1} := F_v \cdot S_1 = 0.90$

Eq. 11.4-3 $S_{DS} := \frac{2}{3} \cdot S_{MS} = 1.39$

Eq. 11.4-4 $S_{D1} := \frac{2}{3} \cdot S_{M1} = 0.60$

Check if the SDC can be determine by ASCE 7-16 Table 11.6-1 alone

Check if all four conditions in ASCE 7-16 11.6 are satisifed.

Structural height $h_n := \left(n_s \quad 1\right) \cdot h_{typ} + h_b = 54 \ ft$

From Table 12.8-2 $C_t := 0.02$, $x := 0.75$

Approximate fundamental period (Eq. 12.8-7) $T_a := C_t \cdot \left(\frac{h_n}{ft}\right)^x = 0.40$

T_s (S. 11.4.5) $T_s := \frac{S_{D1}}{S_{DS}} = 0.43$

Because $T_a = 0.40$ > $0.8\ T_s = 0.34$, the SDC cannot be determined by ASCE 7-16 Table 11.6-1 alone (1st condition is not satisfied)

Determine the SDC

From ASCE 7-16 Table 11.6-1 with $S_{DS} = 1.39$ > 0.50 and Risk Category II, the SDC is D.
From ASCE 7-16 Table 11.621 with $S_{D1} = 0.60$ > 0.20 and Risk Category II, the SDC is D.

Therefore, SDC is D.

Gravity Load and Mass Calculation

Gravity Load

Load combination 6 and 7 include the seismic load effects (ASCE 7-17, S. 2.3.6). These axial loads are; (LC6) 1.2D + Ev + Eh + L + 0.2S; (LC7) 0.9D - Ev + Eh. Exception No.1 of S. 2.3.6 allows the load factor on LL in LC6 to be taken as 0.5 when live load is less than 100psf. From ASCE 7-16 S. 12.4.2.2, the vertical seismic load effect shall be determined as $E_v = \left(0.2\ S_{DS}\right) \cdot DL$. Therefore:

Gravity load from LC6: $\left(1.2 + 0.2\ S_{DS}\right)\ DL + 0.5\ LL$ Gravity load from LC7: $\left(0.9 - 0.2\ S_{DS}\right)\ DL$

Tributary area of the wall: $A_{trib.wall} := 4 \cdot \left(56.25 \cdot 2 + 168.75\right)\ ft^2 - 28.125\ ft^2 = 1097\ ft^2$

Wall weigth:

$w_{w.r} := 0\ kip$ (in the upper story)

$w_{w.typ} := \left(150\ pcf\right) \cdot A_g \cdot h_{typ} = 117\ kip$ (in a typical story)

$w_{w.b} := \left(150\ pcf\right) \cdot A_g \cdot h_b = 135\ kip$ (in the bottom story)

Table 1. Wall gravity load

Level	DL (psf)	LL (psf)	D+0.25L (psf)	LC6 (psf)	LC7 (psf)	Applied Vertical Load D+0.25L (kips)	Applied Vertical Load LC6 (kips)	Applied Vertical Load LC7 (kips)	Wall Axial Load D+0.25L (kips)	Wall Axial Load LC6 (kips)	Wall Axial Load LC7 (kips)
Base	0	0	0	0	0	0	0	0	1,157	1,741	684
2	298	65	314	473	186	345	519	204	813	1,222	480
3	282	65	298	449	175	327	492	192	486	730	288
4	282	65	298	449	175	327	492	192	159	238	96
Roof	140	20	145	217	87	159	238	96	0	0	0

Seismic Weight of the Building

Seismic weight = dead + partitions = $175\ psf + 15\ psf = 190\ psf$ (floors)

= $140\ psf + 7.5\ psf = 147.5\ psf$ (roof)

Table 2. Seismic weight and mass of the building (considering wall self weight)

Story	DL (psf)	Area (ft^2)	Seismic Weight, W_i (kips)	Seismic Mass, m_i (kips-s^2/in)
1	190	14,400	3,744	9.70
2	190	14,400	3,672	9.51
3	190	14,400	3,672	9.51
4	147.5	14,400	2,592	6.71
		Sum	**13,680**	**35.43**

Values for the model (one quarter of the building only)

	Building	Associated to one Wall
Seismic weight:	$W_{building} = 13680\ kip$	$W_t := \frac{W_{building}}{n_w} = 3420\ kip$
Seismic mass:	$M_{building} = 35.43\ \frac{kip \cdot s^2}{in}$	$M_t := \frac{M_{building}}{n_w} = 8.86\ \frac{kip \cdot s^2}{in}$

Accidental Torsion Factor

Accordingly to ASCE 7-16 S. 12.8.4.2, accidental torsion shall be calculating by displacing the center of mass each way from its actual loaction by a distance equal to 5% of the dimension of the structure perpendicular to the direction of applied forces. In this case, the floor slabs are a square of 120 ft x 120 ft. The distance between each wall and the CM is $d_{wcm} := 30\ ft$. The (base or story) shear of the building is called V_{build}, while the (base or story) shear of the wall is called V_{wall}. Therefore:

Eccentricity	$e := 0.05 \cdot (120\ ft) = 6.00\ ft$
Distance between walls and actual CM	$d_{wcm} = 30\ ft$
Stiffness of one wall	k_w (no need to actually obtain this value now)

Moment due to acc. torsion
(V_{build} and V_{wall} are the building base shear and wall base shear w/o acc. torsion)

$$M_{at} = e \cdot V_{build} = e \cdot \left(4\ V_{wall}\right) = 6\ k_w d_{wcm} \theta d_{wcm} + 2\ k_w \left(2\ d_{wcm}\right)\ \theta\ \left(2\ d_{wcm}\right)$$

Rotation of the slab due to acc. torsion

$$\theta_{at} = \frac{M_{at}}{14\ k_w {d_{wcm}}^2}$$

Extra (+/-) shear in one wall due to acc. torsion

$$V_{at} = k_w \cdot \left(\theta_{at} d_{wcm}\right) = \frac{M_{at}}{14\ d_{wcm}} = \frac{e \cdot \left(4\ V_{wall}\right)}{14\ d_{wcm}} = \frac{2\ eV_{wall}}{7\ d_{wcm}}$$

Total shear in one wall due to acc. torsion

$$V_{Tot.Wall} = V_{wall} + \frac{2\ eV_{wall}}{7\ d_{wcm}} = \left(1 + \frac{2\ e}{7\ d_{wcm}}\right) V_{wall}$$

Factor to account for acc. torsion

$$k_{at} := 1 + \frac{2\ e}{7\ d_{wcm}} = 1.06$$

Base Shear of the Building (ELF)

Required parameters:

Response modifiation coefficient (Table 12.2-1)	$R := 5$
Deflection amplification factor (Table 12.2-1)	$C_d := 5$
Importance factor (Table 1.5-2)	$I_e := 1.0$
Long-period transition (Fig. 22-12)	$T_L := 8$
Approximate fundamental period (already calculated)	$T_a = 0.40$

Determine the fundamental period:

Fundamental period (from modal analysis)	$T := 0.24\ s$
Coefficient for upper limit for T (Table 12.8-1)	$C_u := 1.4$
Upper limit for T (S. 12.8.2)	$T_u := C_u \cdot T_a = 0.56\ \ s$
Therefore, the fundamental period to use is:	$T := min\left(T, T_u\right) = 0.24\ \ s$

Determine the seismic coefficient:

Seismic response coefficient (Eq. 12.8-2)

$$C_s := \frac{S_{DS}}{\frac{R}{I_e}} = 0.28$$

Upper limit for C_s, given that $T_a < T_L$ (Eq.12.8-3)

$$C_{s.max} := \frac{S_{D1}}{T \cdot \left(\frac{R}{I_e}\right)} = 0.50$$

Lower limit for C_s, given that $T_a < T_L$ (Eq.12.8-5 and -6)
(Eq. 12.8-6 applies when $S_1 \geq 0.6\ g$, which is the case now)

$$C_{s.min} := \max\left(0.044 \cdot S_{DS} \cdot I_e, \frac{0.5 \cdot S_1}{\frac{R}{I_e}}\right) = 0.064$$

Therefore:

Seismic coefficient to be used: $C_s := C_{s.max} = 0.50$

Seismic base shear of the wall: $V_b := C_s \cdot W_t = 1702\ \textit{kip}$

Seismic base shear of the wall accounting for acc. torsion: $V_b := k_{at} \cdot V_b = 1800\ \textit{kip}$

Modal Response Spectrum Analysis

Concrete strength $f'_c := 5000\ \textit{psi}$

Modulus of elasticity $E := 57000 \cdot \sqrt{f'_c \cdot \textit{psi}} = 4031\ \textit{ksi}$

Inertia $I_g := \frac{t_w \cdot (l_w - 2 \cdot t_{fl})^3}{12} + 2 \cdot \left(\frac{b_{fl} \cdot t_{fl}^3}{12} + b_{fl} \cdot t_{fl} \cdot \left(\frac{l_w}{2} \quad \frac{t_{fl}}{2} \right)^2 \right) = 4500\ \textit{ft}^4$

Eff. inertia $I_{eff} := 0.50 \cdot I_g = 2250\ \textit{ft}^4$

Modal periods $T := \frac{2\,\pi}{\omega_m}$ $T^{\mathrm{T}} = [0.24 \quad 0.04 \quad 0.01 \quad 0.01]$

Number of required modes to achieve more than 90% of the total mass $\frac{\sum_{j=1}^{3} M_{m.eff_j}}{M_t} = 0.98$

Base shear: $V_{b.MRSA} = 725\ \textit{kip}$

Because the base shear obtain with the modal analysis is less than the base hsear obtained by the ELF method ($V_{b.MRSA} = 725\ \textit{kip} < V_b = 1800\ \textit{kip}$), all forces and drifts are requried to be scaled with the factor $V_{ELF} / V_{ModalAnalysis}$ (ASCE 7-16, S. 12.9.1.4).

Factor for scaling of forces $k_{shear} := \frac{V_b}{V_{b.MRSA}} = 2.48$

Design Forces and Displacements - Summary

The lateral demands on the wall obtained from the Modal Response Spectrum Analysis are shown in the table below. The forces were scaled to acchieve 100% of the base shear calcualted by the ELF method. The table incorporates the wall gravity loads calculated before (see Table 1).

Table 3. Loads and displacement demands on the wall

Level	Height (ft)	Axial Load D+0.25L (kip)	Axial Load LC6 (kip)	Axial Load LC7 (kip)	Lateral Force (kip)	Story Shear (kip)	Overturning Moment (kip-ft)	Elastic Deflection (in)	Amplified Deflection (in)	Story Drift (%)
Base	0	1,157	1,741	684	0	1,800	73,815	0.00	0.00	0.00
2	15	813	1,222	480	233	1,661	47,271	0.06	0.32	0.18
3	28	486	730	288	435	1,314	26,051	0.20	0.98	0.42
4	41	159	238	96	651	702	9,132	0.37	1.83	0.55
Roof	54	0	0	0	702	0	0	0.55	2.76	0.60

The roof drift is: $\Delta_{roof} = 0.43\%$

Min. axial load: $P_{min} = 684\ \boldsymbol{kip}$

D+0.5L axial load: $P_{D.25L} = 1157\ \boldsymbol{kip}$

Max. axial load: $P_{max} = 1741\ \boldsymbol{kip}$

Shear demand: $V_u = 1800\ \boldsymbol{kip}$

Moment demand: $M_u = 73815\ \boldsymbol{kip \cdot ft}$

Axial load ratios:

$$ALR_{min} := \frac{P_{min}}{A'_g \cdot f'_c} = 1.6\%$$

$$ALR_{D.25L} := \frac{P_{D.25L}}{A'_g \cdot f'_c} = 2.7\%$$

$$ALR_{max} := \frac{P_{max}}{A'_g \cdot f'_c} = 4.0\%$$

A.2 Wall Design

Critical Section

Building Information

Number of stories	$n_s := 4$
Lightweight concrete	$\lambda := 1.0$
Concrete compressive strength	$f'_c := 5000\ psi$
Yield strength of steel bars	$f_y := 60\ ksi$
Height of the wall	$h_w := (n_s - 1) \cdot 13\ ft + 15\ ft = 54\ ft$
Length of the wall	$l_w := 30\ ft$
Thickness of the wall	$t_w := 24\ in$
Flange thickness	$t_{fl} := 0\ ft = 0.00\ in$
Flange total width	$b_{fl} := 0\ ft$
Gross Area	$A_g := t_w \cdot (l_w - 2\ t_{fl}) + 2\ b_{fl} \cdot t_{fl} = 8640\ in^2$
A_{cv} cross-section area	$A_{cv} := t_w \cdot l_w = 8640\ in^2$
Min., avg., and max. axial demand	$P_{min} := 684\ kip$ $P_{avg} := 1157\ kip$ $P_{max} := 1741\ kip$
Shear demand	$V_u := 1800\ kip$
Moment demand at critical section	$M_u := 73815\ kip \cdot ft$
Critical section at the bottom	$h_{wcs} := h_w = 54\ ft$

Provided longitudinal reinforcement in the critical section

Web Hor.: #5 @ 5.0

#4 rebar	$A_{\#5} := 0.31\ in^2$
Spacing	$s_{wh} := 5.0\ in$
Reinf. ratio	$\rho_{wh} := \frac{2 \cdot A_{\#5}}{s_{wh} \cdot t_w} = 0.52\%$

Web Ver.: #4 @ 6.6

#4 rebar	$A_{\#4} = 0.20\ in^2$
Spacing	$s_{wv} := 6.6\ in$
Reinf. ratio	$\rho_{wv} := \frac{2 \cdot A_{\#4}}{s_{wv} \cdot t_w} = 0.25\%$

Boundary Element: 36 #10

#10 rebar - area	$A_{\#10} = 1.27\ in^2$
#10 rebar - diam.	$d_{\#10} = 1.27\ in$ ($d_b := d_{\#10}$)
Length of BE	$l_{be} := 69.0\ in$
Width of BE	$b := t_w = 24.00\ in$
Reinf. ratio	$\rho_{be} := \frac{36 \cdot A_{\#10}}{(l_{be} + 3\ in) \cdot t_w} = 0.0265$
	$\rho_{sb} := \frac{36 \cdot A_{\#10}}{A_{cv}} = 0.0053$

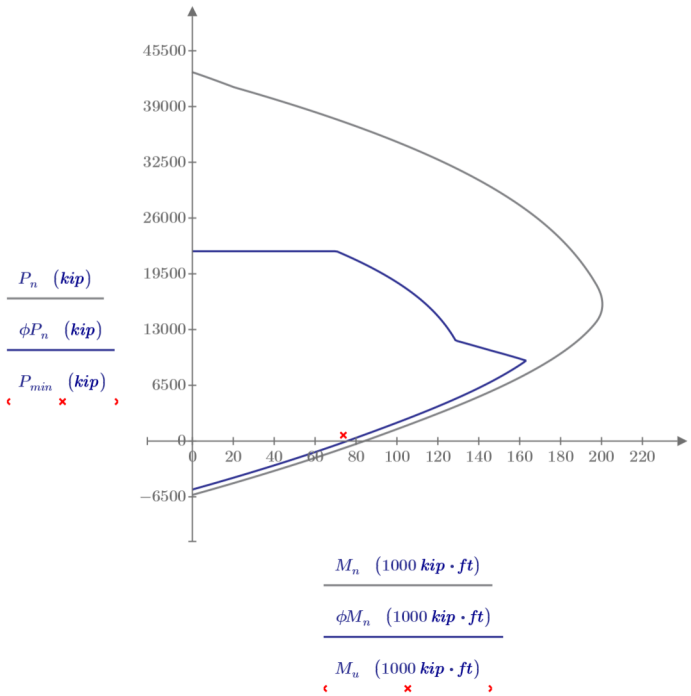

Minimum reinforcement ratios for the web

$A_{cv} := l_w \cdot t_w = 8640\ in^2$

Because $V_u = 1800\ kip > \lambda \sqrt{f'_c \cdot psi}\ A_{cv} = 611\ kip$, we can use $\rho_l := 0.0025$ and $\rho_t := 0.0025$ (ACI 18.10.2.1)

Number of curtains of reinforcement in the web (ACI 18.10.2.2)

Even though $\frac{h_w}{l_w} = 1.80$ < 2, 2 curtains of longitudinal and transverse reinforcement are provided in the web.

Required area of longitudinal reinforcement for flexure and axial forces

Longitudinal reinforcement ratio within $0.15\ l_w = 54.0\ in$ from the end of the wall, and over a width equal to the wall thickness, shall be at least $6 \frac{\sqrt{f'_c \cdot psi}}{f_y} = 0.0071$. Therefore, the requirements of ACI 318-19, 18.10.2.4(a) are satisfied.

The longitudinal reinforcement required by 18.10.2.4(a) shal extend vertically above and below the critical section at least the greater of $l_w = 30.0\ ft$ and $\frac{M_u}{3\ V_u} = 13.7\ ft$. This is satisfied becuase $\rho_{be} = 0.0265$ is provided in up to 2 feet above level 3, covering a height equal to $15\ ft + 13\ ft + 2\ ft = 30.0\ ft$

No more than 50 percent of the reinforcement required by 18.10.2.4(a) shall be terminated at any section. This means that outside the greater of l_w and $M_u / (3\ V_u)$ (which is $30\ ft$), we have:

Minimum long. reinf. ratio (within $0.15\ l_w = 54.0\ in$ from the end of the wall)	$\frac{1}{2}\left(6 \frac{\sqrt{f'_c \cdot psi}}{f_y}\right) = 0.0035$
Minimum amount of long. reinf. above cut-off point	$\frac{1}{2}\left(6 \frac{\sqrt{f'_c \cdot psi}}{f_y}\right) \cdot 0.15\ l_w \cdot t_w = 4.58\ in^2$

Maximum Probable Moment

P-M diagram obtained with $1.25\ f_y = 75\ ksi$ and $P_{max} = 1741\ kip$

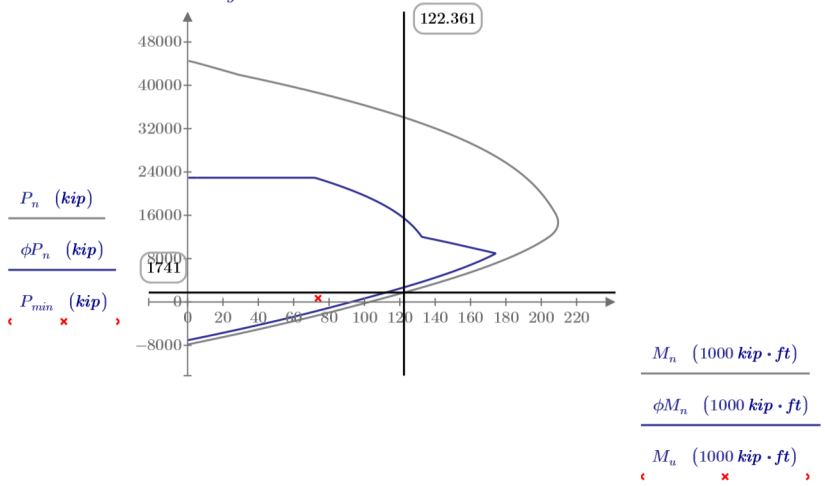

Design shear force

(a) Demand

Maximum probable moment (using P-M diagram obtained with $1.25\,f_y = 75\ ksi$) $M_{pr} = 122361\ kip \cdot ft$

Critical section at the bottom $h_{wcs} = 54\ ft$

Wall length $l_w = 30.0\ ft$

Shear demand $V_u = 1800\ kip$

Overstrength factor when $\frac{h_{wcs}}{l_w} = 1.80 > 1.5$: $\Omega_v := \max\left(\frac{M_{pr}}{M_u}, 1.5\right) = 1.66$

w_s when $\frac{h_{wcs}}{l_w} = 1.80 < 2.0$: $\omega_v := 1.0$

Therefore, accodring to ACI 318-19, 18.10.3.1:

$V_e := min\left(\Omega_v \cdot \omega_v \cdot V_u, 3\ V_u\right) = 2984\ kip$ ($\Omega_v \cdot \omega_v = 1.66$)

(b) Strength (**ACI 318-19**):

α_c coefficient

$$\alpha_{c.aci} := \begin{cases} 3.0 & \text{if } \frac{h_w}{l_w} \le 1.5 \\ 2.0 & \text{else if } \frac{h_w}{l_w} \ge 2.0 \\ 2 \cdot \left(3 - \frac{h_{wcs}}{l_w}\right) & \text{else} \end{cases} \qquad \alpha_{c.aci} = 2.40$$

Upper limit $V_{n.aci.lim} := 10 \cdot A_{cv} \cdot \sqrt{f'_c \cdot psi} = 6109\ kip$

Shear strength $V_{n.aci} := \left(\alpha_{c.aci} \cdot \lambda \cdot \sqrt{f'_c \cdot psi} + \rho_{wh} \cdot f_y\right) \cdot A_{cv} = 4145\ kip < V_{n.aci.lim} = 6109\ kip$

Thus: $\phi V_n := 0.75 \cdot V_{n.aci} = 3108\ kip > V_e = 2984\ kip$

The capacity (**Prop. Eq.**):

Ratio of long. steel boundary $\rho_{sb} = 0.53\%$

Axial load considered: $P_{max} = 1741\ kip$

α_c coefficient

$$\alpha_{c.p} := \frac{1}{100} \cdot \left(9 \cdot \frac{\left(1 + \frac{P_{max}}{A_{cv} \cdot f'_c}\right)^3}{\sqrt[3]{\frac{M_u}{\omega_v \cdot V_u \cdot l_w}}} - 6 \right) = 0.031$$

α_s coefficient $\quad \alpha_{s.p} := \dfrac{2}{5 \cdot \sqrt[3]{\dfrac{M_u}{\omega_v \cdot V_u \cdot l_w}}} = 0.36$

α_{shape} factor $\quad \alpha_{shape} := \min\left(\max\left(1, 0.7 \cdot \left(1 + \dfrac{t_{fl} \cdot b_{fl}}{A_{cv}}\right)^2\right), 1.5\right) = 1.00$

Upper limit $\quad V_{n.lim} := \alpha_{shape} \cdot 10 \cdot A_{cv} \cdot \sqrt{f'_c \cdot psi} = 6109\ kip$

Shear strength $\quad V_{n.prop} := \left(\alpha_{c.p} \cdot f'_c + \alpha_{s.p} \cdot \left(\rho_{sb} + \rho_{wh}\right) \cdot f_y\right) \cdot A_{cv} = 3306\ kip < V_{n.lim} = 6109\ kip$

Resultant DCR $\quad \dfrac{V_e}{V_{n.prop}} = 0.90$ (Remember we are not designing the wall with the proposed equation. We want to assess an ACI 318-19 compliant wall with it).

Determine if special boundary elemens are required

Since $\dfrac{h_w}{l_w} = 1.80 < 2.0$, Section 18.10.6.2 does not apply. Specification on Section 18.10.6.3 are used instead.

The maximum extreme fiber compressive stress is obtained as shown below. The results are shown in Table 1.

$$\sigma = \frac{M_u \cdot l_w}{2\ I_x} + \frac{P_{max}}{A_{cv}}$$

Table 3. Maximum compressive stress

Level	Height (ft)	Axial Load LC6 (kip)	Overturning Moment (kip-ft)	Stress (ksi)
Base	0	1,741	73,815	1.91
2	15	1,222	47,271	1.24
3	28	730	26,051	0.69
4	41	238	9,132	0.24
Roof	54	0	0	0.00

Because there are stresses > $\sigma_{max} := 0.2 \cdot f'_c = 1.00\ ksi$ at the base, special boundary element is required.

$\sigma_1 = 1.91\ ksi > \sigma_{max} = 1.00\ ksi$ --> Special Boundary Element

$\sigma_2 = 1.24\ ksi > \sigma_{max} = 1.00\ ksi$ --> Special Boundary Element

$\sigma_3 = 0.69\ ksi < 0.15 \cdot f'_c = 0.75\ ksi$ and $\rho_{l.end} > \dfrac{400\ psi}{f_y} = 0.0067$ --> Ties per 18.10.6.5

$\sigma_4 = 0.24\ ksi < 0.15 \cdot f'_c = 0.75\ ksi$ and $\rho_{l.end} < \dfrac{400\ psi}{f_y} = 0.0067$ --> No ties

To see how is the longitudinal reinforcement at the wall ends for stories 3 and 4, see the corresponding section later in this report.

Horizontal length of the Special BE

The neutral axis depth associated wih the maximum axial load is $c := c_{Pmax} = 51.5\ in$. According to ACI 318-19 18.10.6.4(a), the special boundary elements must extend horizontally from the extreme compression fiber a distance equal to the greater of the following:

Greater between $c - 0.1\ l_w = 15.49\ in$ and $\frac{c}{2} = 25.75\ in$

Therefore, using a BE length of $l_{be} = 69.0\ in$ satisfies this requirement.

Check the width of the flexural compression zone

The laterally unsupported wall height corresponds to the height of the 1st story $h_u := 15\ ft$

$b = 24.00\ in > \frac{h_u}{16} = 11.25\ in$ --> ACI 318-19 18.10.6.4(b) is satisfied

$\frac{c}{l_w} = 0.14 < \frac{3}{8} = 0.38$ --> ACI 318-19 18.10.6.4(c) does not apply

Transverse reinforcement in the Special BE

The provided vertical spacing is $s := 5.0\ in$, and the largest distance (centerline to centerline) between laterally restrained longitudinal bars is $h_x := 6.0\ in$.

First, we check the requirements of ACI 318-19 18.10.6.4(e). The maximum vertical spacing of the special boundary element transverse reinforcement is equal to the following:

s_{max} = lesser of

- $\frac{b}{3} = 8.0\ in$
- $\frac{l_{be}}{3} = 23.0\ in$
- For grade 80 bars, lesser of $5\ d_b = 6.35\ in$ or $6\ in$ --> use 6.0
- $s_o := 4 + \left(\frac{14 - \frac{h_x}{in}}{3}\right) = 6.67$ shall be within $[4\ in, 6\ in]$ --> use 6.0

Because $s = 5.00\ in$, ACI 318-19 18.10.6.4(e) is satisfied.

#5 perimetral hoop, one 135-degree #4 crosstie in the longitudinal direction and ten #4 crossties in the transvese direction. For #4 bars: $A_{\#4} := 0.20\ in^2$ and $d_{\#4} := 0.5\ in$; for #5 bars: $A_{\#5} := 0.31\ in^2$ and $d_{\#5} := 0.625\ in$.

$b = 24.00\ in$

$l_{be} = 69.00\ in$

$b_{c1} := l_{be} - 3\ in + 2 \cdot \left(d_{\#5} + \frac{d_{\#10}}{2}\right) = 68.52\ in$

$b_{c2} := b - 2 \cdot (3\ in) + 2 \cdot \left(d_{\#5} + \frac{d_{\#10}}{2}\right) = 20.52\ in$

$$A_{g.be} := b \cdot l_{be} = 1656.00\ in^2$$
$$A_{ch} := b_{c1} \cdot b_{c2} = 1406.03\ in^2$$

According to ACI 318-19 18.10.6.4(g), the minimum amount of transverse reinforcement is:

$$\frac{A_{sh}}{s \cdot b_c} = \text{greater of} \begin{cases} 0.3 \cdot \left(\frac{A_{g.be}}{A_{ch}} - 1 \right) \cdot \frac{f'_c}{f_y} = 0.00444 \\ 0.09 \cdot \frac{f'_c}{f_y} = 0.00750 \end{cases}$$

Therefore, the minimum BE transverse reinforcements are:

When doing a X-X cut: $A_{sh.minXX} := 0.0075 \cdot s \cdot b_{c1} = 2.57\ in^2$

When doing a Y-Y cut: $A_{sh.minYY} := 0.0075 \cdot s \cdot b_{c2} = 0.77\ in^2$

And the provided BE transverse reinforcements are:

When doing a X-X cut: $A_{sh.XX} := 2 \cdot A_{\#5} + 10 \cdot A_{\#4} = 2.62\ in^2$

When doing a Y-Y cut: $A_{sh.YY} := 2 \cdot A_{\#5} + A_{\#4} = 0.82\ in^2$

Thus, the minimum requirements for the amount of transverse reinforcement in the BE are satisfied.

Flexural Strength Verification - Story 3

Demand

Minimum axial load: $P_{min} := 288\ kip$

Maximum axial load: $P_{max} := 730\ kip$

Shear: $V_u := 1314\ kip$

Moment: $M_u := 26051\ kip \cdot ft$

Web: #4 @ 6.4 in both directions

#4 rebar $A_{\#4} = 0.20\ in^2$

Spacing $s_w := 6.6\ in$

Reinf. ratio $\rho_w := \frac{2 \cdot A_{\#4}}{s_w \cdot t_w} = 0.25\%$

Boundary Element: 18 #10

#10 rebar - area $A_{\#10} = 1.27\ in^2$

#10 rebar - diam. $d_{\#10} = 1.27\ in$ ($d_b := d_{\#10}$)

Length of BE $l_{be} := 33\ in$

Width of BE $b := t_w = 24.00\ in$

Reinf. ratio $\rho_{l.end} := \frac{18 \cdot A_{\#10}}{(l_{be} + 3\ in) \cdot t_w} = 0.0265$

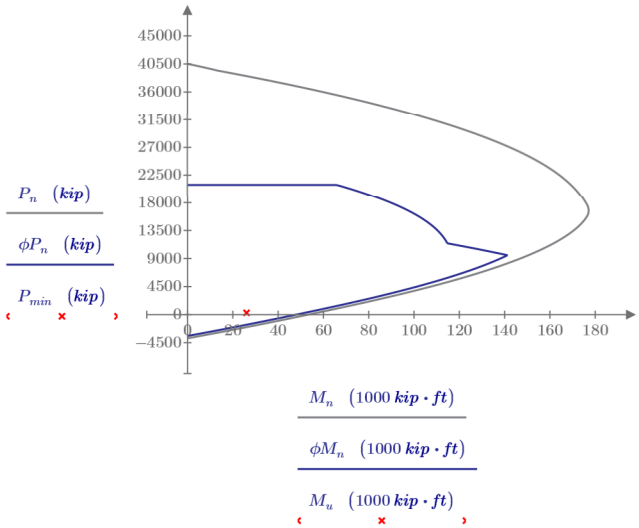

Verification of flexural strength for $P_{min} = 288\ kip$ and $M_u = 26051\ kip \cdot ft$

From the sectional analysis, the largest neutral axis depth is $c := c_{Pmax} = 51.5\ in$.

Becasue $\rho_{l.end} = 0.0265$ > $\frac{400\ psi}{f_y} = 0.0067$, the transverse reinforcement in accordance with ACI 18.10.6.5 is required at the ends of the wall:

> Boundary transverse reinforcement shall satisfy the requirements 18.7.5.2(a) through (e) over the greater of $c - 0.1\ l_w = 15.49\ in$ and $\frac{c}{2} = 26\ in$
>
> Because the section above the 2th story there is no yield expected (i.e., outside the length of the plastic hinge length calculated before), the maximum spacing of the transverse reinforcement is equal to the lesser of the following for Grade 80 reinforcement:
>
> $s_{max} := min(6\ d_b, 6\ in) = 6.00\ in$

Following transversal reinforcement over an horizontal wall segment of $l_{be} = 33\ in$ satisfies all above requirements:

One #4 perimetral hoop
One #4 crosstie inthe longitudinal direcction
Six #4 crossties in the transvese direction

Also, above the cut-off point we have that $\rho_{l.end} = 0.0265$ > $\frac{1}{2}\left(6\frac{\sqrt{f'_c \cdot psi}}{f_y}\right) = 0.0035$. Therefore, S. 18.19.2.4 (c) is satisfied.

Because $V_u = 1314\ kip < \lambda \cdot \sqrt{f'_c \cdot psi} \cdot A_{cv} = 611\ kip$, ACI 18.10.6.5 needs to be satisfied, i.e., the horizontal reinforcement shall be terminate with hooks.

Flexural Strength Verification - Story 4

Demand

Minimum axial load: $P_{min} := 96\ kip$

Maximum axial load: $P_{max} := 238\ kip$

Shear: $V_u := 702\ kip$

Moment: $M_u := 9132\ kip \cdot ft$

Web: #4 @ 6.6 in both directions

#4 rebar $A_{\#4} = 0.20\ in^2$

Spacing $s_w = 6.60\ in$

Reinf. ratio $\rho_w = 0.25\%$

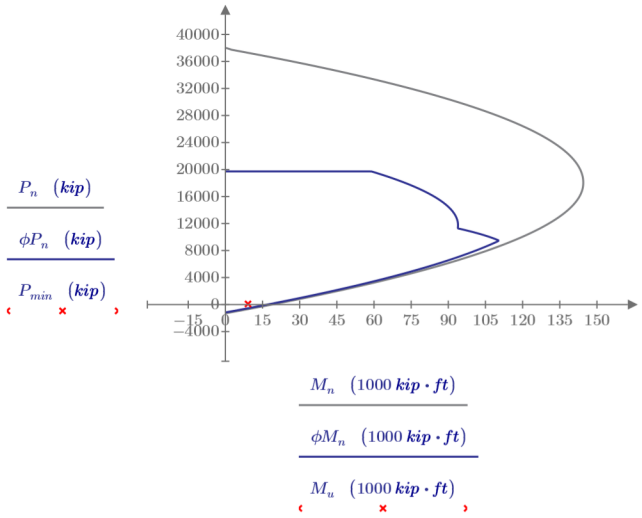

Verification of flexural strength for $P_{min} = 96\ kip$ and $M_u = 9132\ kip \cdot ft$

Becasue $\rho_w = 0.0025$ < $\frac{400\ psi}{f_y} = 0.0067$, the transverse reinforcement in accordance with ACI 18.10.6.5(b) is not required.

Because $V_u = 702\ kip > \lambda \cdot \sqrt{f'_c \cdot psi} \cdot A_{cv} = 611\ kip$, ACI 18.10.6.5 needs to be satisfied, i.e., the horizontal reinforcement in the last story shall be terminated with hooks.

A.3 Wall Sketches

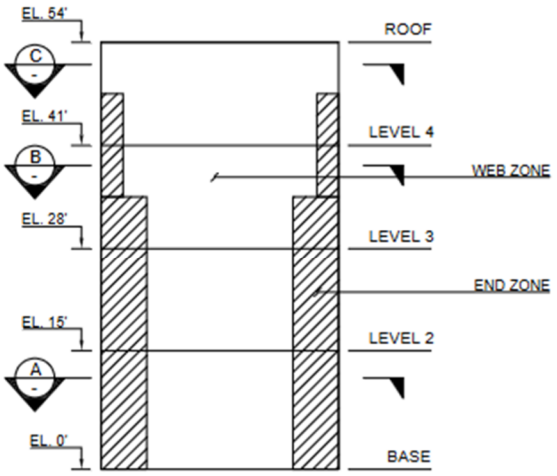

WALL - SCHEMATIC ELEVATION VIEW

LEVEL	STORY	HEIGHT (FT)	WEB ZONE	WALL END ZONE
ROOF	4	54	2-#4 @ 6.6" V 2-#4 @ 6.6" H	-
4	3	41	2-#4 @ 6.6" V 2-#4 @ 6.6" H	33" x 24" 18 - #9 HOOPS AND CROSSTIES @ 6.0"
3	2	28	2-#4 @ 6.6" V 2-#5 @ 5.0" H	69" x 24" 36 - #10 HOOPS AND CROSSTIES @ 5.0"
2	1	15		

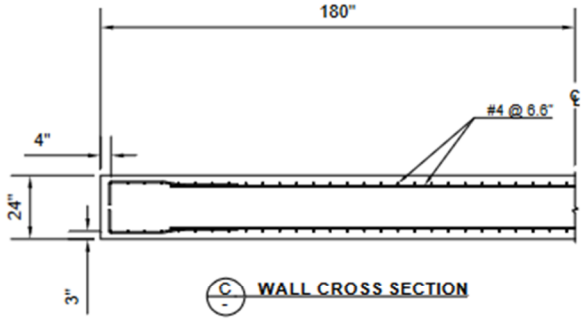

C - WALL CROSS SECTION

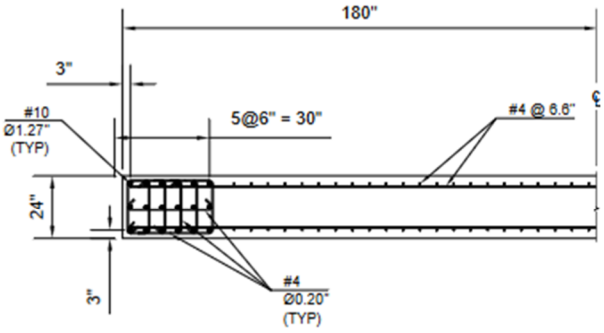

B - WALL CROSS SECTION

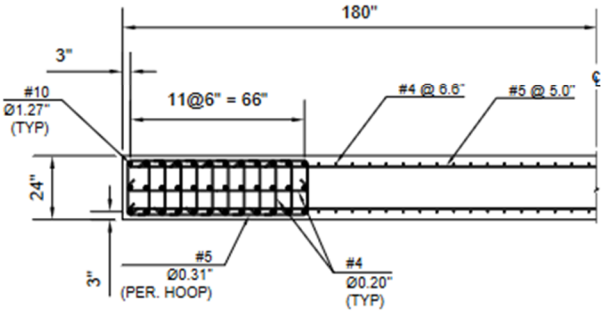

A - WALL CROSS SECTION

NOTES:

CROSSTIES IN THE WEB ARE NOT SHOWN

THE DRAWING OF THE DETAILING OF THE BOUNDARY ELEMENT MIGHT NOT SATISFY ALL ACI 318-19 REQUIREMENTS, HOWEVER THE PURPOSE OF PROVIDING ENOUGH TRANSVERSE STEEL AND ESTIMATE THE CORRESPONDING CONFINEMENT IS MET.

A.4 Expected Concrete Stress-Strain Relationship

Materials

#4 and #5 Hoops and Crossties:

Diameter: $d_{bt.n4} := 0.5\ in$ $d_{bt.n5} := 0.625\ in$

Area: $A_{st.n4} := 0.2\ in^2$ $A_{st.n5} := 0.31\ in^2$

Expected yield Stress: $f_{yt} := 70\ ksi$

Steel for Longitudinal Bars (#10)

Diameter: $d_{b1} := 1.27\ in$

Area: $A_{s1} := 1.27\ in^2$

Yield Stress: $f_{y1} := 70\ ksi$

Concrete

Expected unconfined concrete strength $f'_{co} := 1.3 \cdot 5000\ psi = 6500\ psi$

Modulus of elasticity $E_c := 57000 \cdot \sqrt{f'_{co} \cdot psi} = 4595\ ksi$

Strain related to f'_c $\varepsilon_{co} := \frac{2 \cdot f'_{co}}{E_c} = 0.0028$

Saatciougly & Razvi Model

(a) Unconfined Concrete

Strain at maximum concrete compressive strength $\varepsilon_{01} := \varepsilon_{co} = 0.0028$

When specific information is not available, the authors of this model reccomend to use $\varepsilon_{085} := 0.0038$

Strain at which the descending branch touches the X axis $\varepsilon_{cf} := \frac{(\varepsilon_{085} - \varepsilon_{co})}{0.15} + \varepsilon_{co}$ $\varepsilon_{cf} = 0.0093$

Stress-strain relation for confined concrete
(This also recovers the Hognestad expression)

$$f_{c.SR.1}(\varepsilon_c) := \begin{cases} \text{if } 0 \le \varepsilon_c \le \varepsilon_{01} \\ \quad f'_{co} \cdot \left(\frac{2 \cdot \varepsilon_c}{\varepsilon_{01}} - \left(\frac{\varepsilon_c}{\varepsilon_{01}} \right)^2 \right) \\ \text{else if } \varepsilon_{01} < \varepsilon_c \le \varepsilon_{cf} \\ \quad f'_{co} \cdot \left(1 - 0.15 \cdot \frac{\varepsilon_c - \varepsilon_{01}}{\varepsilon_{085} - \varepsilon_{01}} \right) \\ \text{else} \\ \quad 0 \end{cases}$$

(b) Confined Concrete in Stories 1 & 2

Dimension to centerline of outermost hoop, in X direction

$b_{cx} := 69\ in + d_{b1} + d_{bt.n5}$ $\quad b_{cx} = 70.9\ in$

Dimension to centerline of outermost hoop, in Y direction

$b_{cy} := 24\ in - 2 \cdot 3\ in + d_{b1} + d_{bt.n5}$ $\quad b_{cy} = 19.9\ in$

Dimension between laterally supported vertical bars, in X dir.

$s_{lx} := 6.0\ in$ $\quad s_{lx} = 6\ in$

Dimension between laterally supported vertical bars, in Y dir.

$s_{ly} := \frac{24\ in - 2 \cdot 3\ in}{2}$ $\quad s_{ly} = 9\ in$

Vertical spacing of hoops

$s := 5.0\ in$

# of hoops or crossties that appear when doing a X-X cut

$n_{y.n4} := 10$ $\quad n_{y.n5} := 2$

# of hoops or crossties that appear when doing a Y-Y cut

$n_{x.n5} := 2$ $\quad n_{x.n4} := 1$

More parameters required to obtained the maximum confined stress:

$f_{lx} := \frac{\left(n_{y.n4} \cdot A_{st.n4} + n_{y.n5} \cdot A_{st.n5}\right) \cdot f_{yt}}{s \cdot b_{cx}}$ $\quad f_{lx} = 0.517\ ksi$

$f_{ly} := \frac{\left(n_{x.n5} \cdot A_{st.n5} + n_{x.n4} \cdot A_{st.n4}\right) \cdot f_{yt}}{s \cdot b_{cy}}$ $\quad f_{ly} = 0.577\ ksi$

$k_{2x} := min\left(0.099 \cdot \sqrt[2]{\frac{{b_{cx}}^2}{s \cdot s_{lx} \cdot \frac{f_{lx}}{ksi}}}, 1\right)$ $\quad k_{2x} = 1$

$k_{2y} := min\left(0.099 \cdot \sqrt[2]{\frac{{b_{cy}}^2}{s \cdot s_{ly} \cdot \frac{f_{ly}}{ksi}}}, 1\right)$ $\quad k_{2y} = 0.387$

$f_{lex} := k_{2x} \cdot f_{lx}$ $\quad f_{lex} = 0.517\ ksi$

$f_{ley} := k_{2y} \cdot f_{ly}$ $\quad f_{ley} = 0.223\ ksi$

$f_{le} := \frac{f_{lex} \cdot b_{cx} + f_{ley} \cdot b_{cy}}{b_{cx} + b_{cy}}$ $\quad f_{le} = 0.453\ ksi$

$k_1 := 4.825 \cdot \left(\frac{f_{le}}{ksi}\right)^{-0.17}$ $\quad k_1 = 5.521$

Maximum confined stress

$f'_{cc} := f'_{co} + k_1 \cdot f_{le}$ $\quad f'_{cc} = 9\ ksi$

More parameters required to obtain the confined stress-strain curve:

$K := k_1 \cdot \frac{f_{le}}{f'_{co}}$ $\quad K = 0.385$

Volumetric ratio

$\rho := \frac{n_{y.n4} \cdot A_{st.n4} + n_{y.n5} \cdot A_{st.n5} + n_{x.n5} \cdot A_{st.n5}}{s \cdot \left(b_{cx} + b_{cy}\right)}$ $\quad \rho = 0.007$

$$\varepsilon_1 := \varepsilon_{01} \cdot (1 + 5 \cdot K) \qquad \varepsilon_1 = 0.00827$$

$$\varepsilon_{85} := 260 \cdot \rho \cdot \varepsilon_1 + \varepsilon_{085} \qquad \varepsilon_{85} = 0.0191$$

Strain at which is reached the residual stress

$$\varepsilon_{c.res} := \frac{0.8 \cdot (\varepsilon_{85} - \varepsilon_1)}{0.15} + \varepsilon_1 \qquad \varepsilon_{c.res} = 0.0663$$

Residual Stress

$$f_{res} := 0.2 \cdot f'_{cc} \qquad f_{res} = 1.8\ ksi$$

Stress-strain relation for confined concrete

$$f_{cc.SR.1}(\varepsilon_c) := \begin{cases} \text{if } 0 \le \varepsilon_c \le \varepsilon_1 \\ \quad f'_{cc} \cdot \left(\dfrac{2 \cdot \varepsilon_c}{\varepsilon_1} - \left(\dfrac{\varepsilon_c}{\varepsilon_1} \right)^2 \right)^{\frac{1}{1+2 \cdot K}} \\ \text{else if } \varepsilon_1 < \varepsilon_c \le \varepsilon_{c.res} \\ \quad f'_{cc} \cdot \left(1 - 0.15 \cdot \dfrac{\varepsilon_c - \varepsilon_1}{\varepsilon_{85} - \varepsilon_1} \right) \\ \text{else} \\ \quad f_{res} \end{cases}$$

(c) Confined Concrete in Story 3

Dimension to centerline of outermost hoop, in X direction

$$b_{cx} := 69\ in + d_{b1} + d_{bt.n4} \qquad b_{cx} = 70.77\ in$$

Dimension to centerline of outermost hoop, in Y direction

$$b_{cy} := 24\ in - 2 \cdot 3\ in + d_{b1} + d_{bt.n4} \qquad b_{cy} = 19.77\ in$$

Dimension between laterally supported vertical bars, in X dir.

$$s_{lx} := 6.0\ in \qquad s_{lx} = 6\ in$$

Dimension between laterally supported vertical bars, in Y dir.

$$s_{ly} := \frac{24\ in - 2 \cdot 3\ in}{2} \qquad s_{ly} = 9\ in$$

Vertical spacing of hoops

$$s := 6.0\ in$$

# of hoops or crossties that appear when doing a X-X cut

$$n_y := 6$$

# of hoops or crossties that appear when doing a Y-Y cut

$$n_x := 3$$

More parameters required to obtained the maximum confined stress:

$$f_{lx} := \frac{n_y \cdot A_{st.n4} \cdot f_{yt}}{s \cdot b_{cx}} \qquad f_{lx} = 0.198\ ksi$$

$$f_{ly} := \frac{n_x \cdot A_{st.n4} \cdot f_{yt}}{s \cdot b_{cy}} \qquad f_{ly} = 0.354\ ksi$$

$$k_{2x} := min\left(0.099 \cdot \sqrt[2]{\frac{{b_{cx}}^2}{s \cdot s_{lx} \cdot \frac{f_{lx}}{ksi}}}, 1 \right) \qquad k_{2x} = 1$$

$$k_{2y} := min\left(0.099 \cdot \sqrt[2]{\frac{b_{cy}^{\,2}}{s \cdot s_{ly} \cdot \frac{f_{ly}}{ksi}}}, 1\right) \qquad k_{2y} = 0.448$$

$$f_{lex} := k_{2x} \cdot f_{lx} \qquad f_{lex} = 0.198\ ksi$$

$$f_{ley} := k_{2y} \cdot f_{ly} \qquad f_{ley} = 0.158\ ksi$$

$$f_{le} := \frac{f_{lex} \cdot b_{cx} + f_{ley} \cdot b_{cy}}{b_{cx} + b_{cy}} \qquad f_{le} = 0.189\ ksi$$

$$k_1 := 4.825 \cdot \left(\frac{f_{le}}{ksi}\right)^{-0.17} \qquad k_1 = 6.403$$

Maximum confined stress

$$f'_{cc} := f'_{co} + k_1 \cdot f_{le} \qquad f'_{cc} = 7.712\ ksi$$

More parameters required to obtain the confined stress-strain curve:

$$K := k_1 \cdot \frac{f_{le}}{f'_{co}} \qquad K = 0.186$$

Volumetric ratio

$$\rho := \frac{(n_y + n_x) \cdot A_{st.n4}}{s \cdot (b_{cx} + b_{cy})} \qquad \rho = 0.003$$

$$\varepsilon_1 := \varepsilon_{01} \cdot (1 + 5 \cdot K) \qquad \varepsilon_1 = 0.00547$$

$$\varepsilon_{85} := 260 \cdot \rho \cdot \varepsilon_1 + \varepsilon_{085} \qquad \varepsilon_{85} = 0.0085$$

$$\varepsilon_{c.res} := \frac{0.8\ (\varepsilon_{85} - \varepsilon_1)}{0.15} + \varepsilon_1 \qquad \varepsilon_{c.res} = 0.0217$$

Strain at which is reached the residual stress

$$f_{res} := 0.2 \cdot f'_{cc} \qquad f_{res} = 1.542\ ksi$$

Residual Stress

Stress-strain relation for confined concrete

$$f_{cc.SR.2}(\varepsilon_c) := \begin{cases} \text{if } 0 \le \varepsilon_c \le \varepsilon_1 \\ \quad f'_{cc} \cdot \left(\frac{2 \cdot \varepsilon_c}{\varepsilon_1} - \left(\frac{\varepsilon_c}{\varepsilon_1}\right)^2\right)^{\frac{1}{1 + 2 \cdot K}} \\ \text{else if } \varepsilon_1 < \varepsilon_c \le \varepsilon_{c.res} \\ \quad f'_{cc} \cdot \left(1 - 0.15 \cdot \frac{\varepsilon_c - \varepsilon_1}{\varepsilon_{85} - \varepsilon_1}\right) \\ \text{else} \\ \quad f_{res} \end{cases}$$

Plots

# of points $i := 1 .. 100$

Concrete strain values $\varepsilon_{c_i} := 0.002 \cdot (i - 1)$

Unconfined concrete strength $f_{c.unc_i} := f_{c.SR.1}\left(\varepsilon_{c_i}\right)$

Confined concrete strength (stories 1 & 2) $f_{c.conf1_i} := f_{cc.SR.1}\left(\varepsilon_{c_i}\right)$

Confined concrete strength (story 3) $f_{c.conf2_i} := f_{cc.SR.2}\left(\varepsilon_{c_i}\right)$

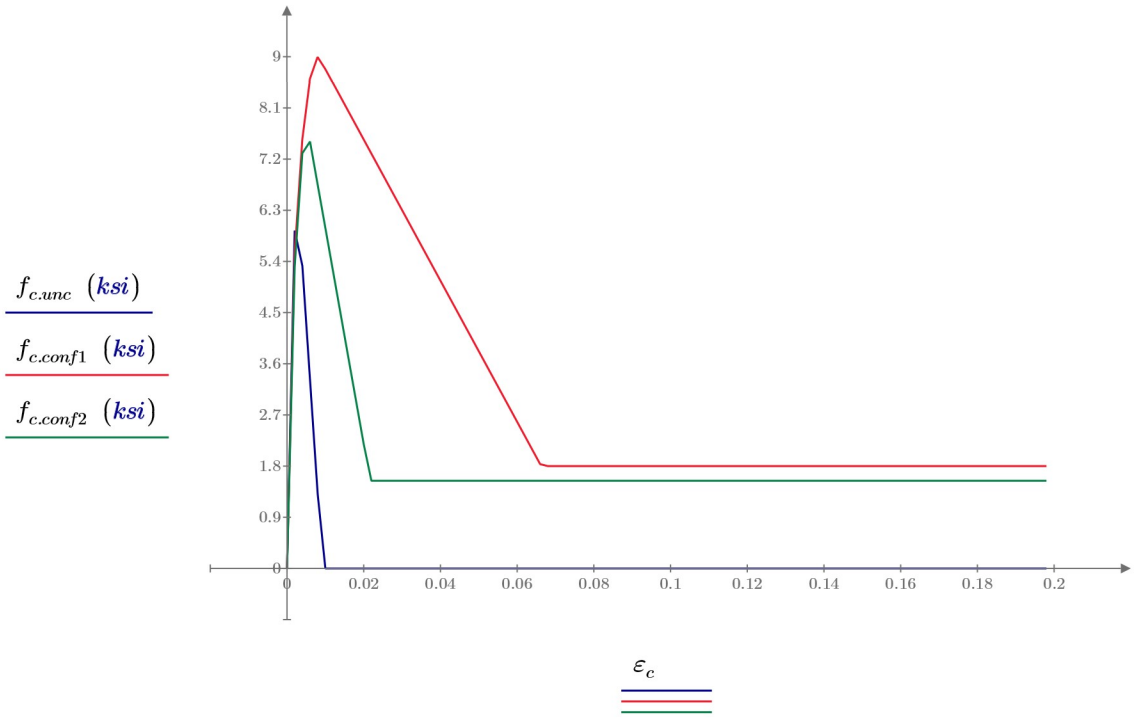

A.5 Sectional Analysis with Expected Material Properties and Δ_{roof} Capacity

Expected Material Properties

Unconfined Concrete

Max. compressive stress $f'_{c.unc} := 6.5\ ksi$

Strain at max. comp. stress $\varepsilon_{c.unc} := 0.003$

$\varepsilon_{085} := 0.0038$

Strain at which the descending branch touches the X axis $\varepsilon_{cf.unc} := \frac{(\varepsilon_{085} - \varepsilon_{c.unc})}{0.15} + \varepsilon_{c.unc}$

$$f_{c.unc}(\varepsilon_c) := \begin{cases} f'_{c.unc} \cdot \left(\frac{2 \cdot \varepsilon_c}{\varepsilon_{c.unc}} - \left(\frac{\varepsilon_c}{\varepsilon_{c.unc}}\right)^2\right) & \text{if } 0 \le \varepsilon_c \le \varepsilon_{c.unc} \\ f'_{c.unc} \cdot \left(1 - 0.15 \cdot \frac{\varepsilon_c - \varepsilon_{c.unc}}{\varepsilon_{085} - \varepsilon_{c.unc}}\right) & \text{if } \varepsilon_{c.unc} < \varepsilon_c \le \varepsilon_{cf.unc} \\ 0 & \text{otherwise} \end{cases}$$

Confined Concrete

Length of BE $l_{be} := 69.0\ in$

Concrete peak stress $f'_c := 9.00\ ksi$

Strain at Concrete Peak Stress $\varepsilon_{cu} := 0.0083$

Rresidual stress $f_{res} := 0.2 \cdot f'_c$

Strain at residual stress $\varepsilon_{c.res} := 0.0663$

Other parameters (S&R model) $K := 0.39$

$\varepsilon_{c85} := 0.0191$

$$f_c(\varepsilon_c) := \begin{cases} f'_c \cdot \left(\frac{2 \cdot \varepsilon_c}{\varepsilon_{cu}} - \left(\frac{\varepsilon_c}{\varepsilon_{cu}}\right)^2\right)^{\frac{1}{1+2 \cdot K}} & \text{if } 0 \le \varepsilon_c \le \varepsilon_{cu} \\ f'_c \cdot \left(1 - 0.15 \cdot \frac{\varepsilon_c - \varepsilon_{cu}}{\varepsilon_{c85} - \varepsilon_{cu}}\right) & \text{if } \varepsilon_{cu} < \varepsilon_c \le \varepsilon_{c.res} \\ f_{res} & \text{if } \varepsilon_{c.res} \le \varepsilon_c \\ 0 & \text{otherwise} \end{cases}$$

Steel

Steel yielding stress $f_y := 70\ ksi$

Elastic modulus of steel $E_s := 29000\ ksi$

Yielding Strain $\varepsilon_y := \frac{f_y}{E_s} = 0.00241$

Post-yielding slope $E_{sh} := 0.01 \cdot E_s = 290.00\ ksi$

$\varepsilon_{sh} := \varepsilon_y$

$$f_s(\varepsilon_s) := \begin{cases} E_s \cdot \varepsilon_s & \text{if } 0 \le |\varepsilon_s| \le \varepsilon_y \\ \text{sign}(\varepsilon_s) \cdot f_y & \text{if } \varepsilon_y < |\varepsilon_s| \le \varepsilon_{sh} \\ \text{sign}(\varepsilon_s) \cdot (f_y + (|\varepsilon_s| - \varepsilon_{sh}) \cdot E_{sh}) & \text{if } \varepsilon_{sh} < |\varepsilon_s| \le 0.3 \\ \text{sign}(\varepsilon_s) \cdot (f_y + (0.8 - \varepsilon_{sh}) \cdot E_{sh}) & \text{if } 0.3 < |\varepsilon_s| \le 0.80 \\ 0 & \text{otherwise} \end{cases}$$

LRFD Reduction Factor

$$\phi(\varepsilon_t) := \begin{cases} 0.65 & \text{if } |\varepsilon_t| \le \varepsilon_y \\ 0.9 & \text{if } |\varepsilon_t| \ge 0.005 \\ 0.65 + \frac{0.9 - 0.65}{0.005 - \varepsilon_y} \cdot (|\varepsilon_t| - \varepsilon_y) & \text{otherwise} \end{cases}$$

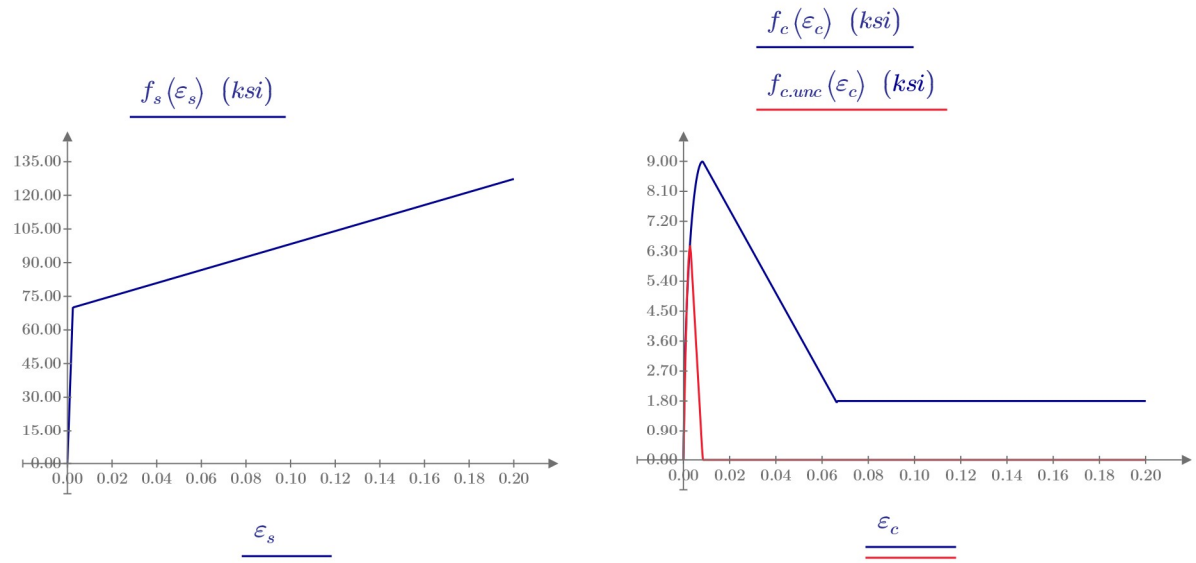

P-M Diagram & Critical Demand

Wall length	$l_w := 30\ ft$ ($h := l_w$)
Web width	$b := 24\ in$
Flange thickness	$t_{fl} := 0\ ft = 0.00\ in$
Flange total width	$b_{fl} := 0\ ft$

Moment demand: $M_u := 73815\ kip \cdot ft$

Axial demands: $P_{min} := 684\ kip$

$P_{avg} := 1157\ kip$

$P_{max} := 1741\ kip$

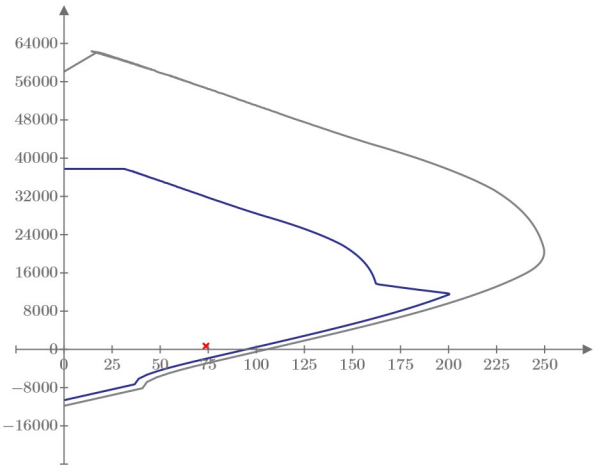

Web Ver.: #4 @ 6.6

#4 rebar	$A_{\#4} = 0.20\ in^2$
Spacing	$s_{wv} := 6.6\ in$
Reinf. ratio	$\rho_{wv} := \frac{2 \cdot A_{\#4}}{s_{wv} \cdot b} = 0.25\%$

Boundary Element: 36 #10

#10 rebar - area	$A_{\#10} = 1.27\ in^2$
#10 rebar - diam.	$d_{\#10} = 1.27\ in$ ($d_b := d_{\#10}$)
Length of BE	$l_{be} := 69.0\ in$
Width of BE	$b = 24.00\ in$
Reinf. ratio	$\rho_{be} := \frac{36 \cdot A_{\#10}}{(l_{be} + 3\ in) \cdot b} = 2.65\%$
	$\rho_{sb} := \frac{36 \cdot A_{\#10}}{A_{cv}} = 0.53\%$

Maximum Probable Moment

Sectional analysis using expected material properties and P_{max}, which comes from (1.2+0.2SDS)DL + 0.5LL

Story 1: Neutral axis depth $c := 47.683\ in$ (Iterate until obtain $P_{max} = 1741\ kip$)

P-M Capacity

$P_{np} := \sum_l F_{cp_l} + \sum_i F_{sp_i}$ $\quad P_{np} = 1741\ kip$

$M_{pr} := \sum_l F_{cp_l} \cdot \left(h - y_{cp_l}\right) + \sum_i F_{sp_i} \cdot \left(h - d_i\right) - P_{np} \cdot \frac{h}{2}$ $\quad M_{pr} = 124046\ kip \cdot ft$

Moment and Curvature at Yielding

Sectional analysis using expected material properties and expected axial load (DL + 0.25LL Condition)

$E_c := 57000 \cdot \sqrt{f'_c \cdot psi} = 5407.49\ ksi$

Story 1: Neutral axis depth $y := 62.37\ in$ (Iterate until obtain $P_{avg} = 1157\ kip$)

P-M Capacity

$P_{np} := \sum_l F_{cp_l} + \sum_i F_{sp_i}$ $\quad P_{np} = 1157\ kip$

$M_{np} := \sum_l F_{cp_l} \cdot \left(h - y_{cp_l}\right) + \sum_i F_{sp_i} \cdot \left(h - d_i\right) - P_{np} \cdot \frac{h}{2}$ $\quad M_{np} = 89958\ kip \cdot ft$

$\phi_y := \frac{\varepsilon_y}{d_{N_i} - y}$ $\quad \phi_y = \left(9.831 \cdot 10^{-5}\right) \frac{1}{ft}$

Expected Capacity

Sectional analysis using expected material properties and expected axial load (DL + 0.25LL Condition)

Story 1: Neutral axis depth $c := 44.503\ in$ (Iterate until obtain $P_{avg} = 1157\ kip$)

P-M Capacity

$P_{np} := \sum_l F_{cp_l} + \sum_i F_{sp_i}$ $\quad P_{np} = 1157\ kip$

$M_{np} := \sum_l F_{cp_l} \cdot \left(h - y_{cp_l}\right) + \sum_i F_{sp_i} \cdot \left(h - d_i\right) - P_{np} \cdot \frac{h}{2}$ $\quad M_{np} = 117814\ kip \cdot ft$

Design shear force with amplification factors

Maximum probable moment
(expected material properties and highest axial load) $M_{pr} = 124046\ kip \cdot ft$

Critical section at the bottom $h_{wcs} := 54\ ft$

Wall length $l_w = 30.0\ ft$

Shear demand $V_u := 1800\ kip$

Overstrength factor when $\frac{h_{wcs}}{l_w} = 1.80 \ > \ 1.5$: $\Omega_v := \max\left(\frac{M_{pr}}{M_u}, 1.5\right) = 1.68$

w_s when $\frac{h_{wcs}}{l_w} = 1.80 \ < \ 2.0$: $\omega_v := 1.0$

Therefore, accodring to ACI 318-19, 18.10.3.1:

$V_e := min\left(\Omega_v \cdot \omega_v \cdot V_u, 3\ V_u\right) = 3025\ kip$ ($\Omega_v \cdot \omega_v = 1.68$)

Predicted Drift Capacity

Wall length $l_w = 30.00\ ft$

Width of wall cross section $b = 24.00\ in$

Web cross-sectional area $A_{cv} := l_w \cdot b = 8640\ in^2$

Neutral axis depth at expected demand $c_e := 44.5\ in$

Maximum expected shear demand $V_e = 3025\ kip$

Nominal shear stress $v_{max} := \frac{V_e}{A_{cv}} = 350.10\ psi$

λ_b parameter $\lambda_b := \frac{l_w \cdot c_e}{b^2} = 27.81$

α parameter for combination of a single perimeter hoop with supplemental crossties $\alpha := 45$

Expected unconfined concrete strength $f'_{c.unc} = 6.50\ ksi$

Height of the wall $h_w := 54\ ft$

Roof drift capacity $\frac{\delta_c}{h_w} = 3.85 - \frac{\lambda_b}{\alpha} - \frac{v_{max}}{8 \cdot \sqrt{f'_{c.unc} \cdot psi}} = 2.69\ \%$

Deformation capcity $\delta_c := 0.027 \cdot h_w = 17\ in$

A.6 Selection of MCE Level Ground Motions

The methodology described by Baker and Lee (2018) was implemented. The scripts developed by the authors are available in Baker's GitHub repository (link here). The period used as the input T_{cond} in **Table A.1** corresponds to the fundamental period obtained with the OpenSees model. The spectral acceleration used as target when computing the conditional spectrum, $S_a(T_{cond})$ in **Table A.1**, was obtained by interpolating T_{cond} in the Uniform Hazard Response Spectrum of the site (shown in **Figure 10.3**).

***Table A.1**: Input values used in "Main_select_motions.m" script by Baker and Lee (2018)*

Parameter	Value
Tcond	0.18
Tmin	0.01
Tmax	5
SaTcond	0.57
rup.M_bar	6.92
rup..Rjb	8.4
rup.eps_bar	1.31
rup.Vs30	760
rup.z1	999
rup.region	1
rup.Fault_Type	1
rup.Rrup	4.60
rup.Rx	4.60
rup.W	11
rup.Ztor	0
rup.Zbot	11
rup.dip	90
allowedRecs.Vs30	[560 1130]
allowedRecs.Mag	[6.2 8.2]
allowRecs.D	[0 50]

***Table A.2**: Selected ground motions for the 4-Story Archetype MCE level analysis*

Tag	RSN*	Earthquake Name	Year	Horizontal Acc. Filename Utilized	Scale Factor
EQ 401	1012	"Northridge-01"	1994	RSN1012_NORTHR_LA0270.AT2	2.8
EQ 402	1020	"Northridge-01"	1994	RSN1020_NORTHR_H12090.AT2	3.94
EQ 403	1023	"Northridge-01"	1994	RSN1023_NORTHR_L09090.AT2	2.21
EQ 404	1078	"Northridge-01"	1994	RSN1078_NORTHR_SSU090.AT2	1.77
EQ 405	1126	"Kozani_ Greece-01"	1995	RSN1126_KOZANI_KOZ--L.AT2	3.32
EQ 406	1350	"Chi-Chi_ Taiwan"	1999	RSN1350_CHICHI_ILA067-N.AT2	3.7
EQ 407	1520	"Chi-Chi_ Taiwan"	1999	RSN1520_CHICHI_TCU088-E.AT2	2.63
EQ 408	1633	"Manjil_ Iran"	1990	RSN1633_MANJIL_ABBAR--L.AT2	1.04
EQ 409	288	"Irpinia_ Italy-01"	1980	RSN288_ITALY_A-BRZ270.AT2	3.62
EQ 410	3943	"Tottori_ Japan"	2000	RSN3943_TOTTORI_SMN015EW.AT2	2.84
EQ 411	4213	"Niigata_ Japan"	2004	RSN4213_NIIGATA_NIG023EW.AT2	2.09
EQ 412	4227	"Niigata_ Japan"	2004	RSN4227_NIIGATA_NIGH10NS.AT2	3.43
EQ 413	4229	"Niigata_ Japan"	2004	RSN4229_NIIGATA_NIGH12NS.AT2	2.44
EQ 414	4231	"Niigata_ Japan"	2004	RSN4231_NIIGATA_NIGH15EW.AT2	4.95
EQ 415	4455	"Montenegro_ Yugoslavia"	1979	RSN4455_MONTENE.GRO_HRZ000.AT2	2.71
EQ 416	4483	"L'Aquila_ Italy"	2009	RSN4483_L-AQUILA_AM043YLN.AT2	3.09
EQ 417	4842	"Chuetsu-oki_ Japan"	2007	RSN4842_CHUETSU_65005EW.AT2	1.41
EQ 418	4845	"Chuetsu-oki_ Japan"	2007	RSN4845_CHUETSU_65008NS.AT2	1.4
EQ 419	4858	"Chuetsu-oki_ Japan"	2007	RSN4858_CHUETSU_65028EW.AT2	3.99
EQ 420	4867	"Chuetsu-oki_ Japan"	2007	RSN4867_CHUETSU_65040NS.AT2	2.4
EQ 421	4869	"Chuetsu-oki_ Japan"	2007	RSN4869_CHUETSU_65042EW.AT2	3.53
EQ 422	4873	"Chuetsu-oki_ Japan"	2007	RSN4873_CHUETSU_65056EW.AT2	1.96
EQ 423	495	"Nahanni_ Canada"	1985	RSN495_NAHANNI_S1280.AT2	0.83
EQ 424	5285	"Chuetsu-oki_ Japan"	2007	RSN5285_CHUETSU_NIGH12EW.AT2	2.67
EQ 425	5474	"Iwate_ Japan"	2008	RSN5474_IWATE_AKT019EW.AT2	3.46
EQ 426	5623	"Iwate_ Japan"	2008	RSN5623_IWATE_IWT015EW.AT2	3.69
EQ 427	5807	"Iwate_ Japan"	2008	RSN5807_IWATE_55462NS.AT2	4.15
EQ 428	5809	"Iwate_ Japan"	2008	RSN5809_IWATE_55465NS.AT2	3.37
EQ 429	5819	"Iwate_ Japan"	2008	RSN5819_IWATE_4CA71NS.AT2	2.98
EQ 430	6928	"Darfield_ New Zealand"	2010	RSN6928_DARFIELD_LPCCN80E.AT2	2.6
EQ 431	71	"San Fernando"	1971	RSN71_SFERN_L12021.AT2	1.42
EQ 432	72	"San Fernando"	1971	RSN72_SFERN_L04201.AT2	3.46
EQ 433	763	"Loma Prieta"	1989	RSN763_LOMAP_GIL337.AT2	1.78
EQ 434	801	"Loma Prieta"	1989	RSN801_LOMAP_SJTE315.AT2	3.4
EQ 435	809	"Loma Prieta"	1989	RSN809_LOMAP_UC2000.AT2	2.27
EQ 436	80	"San Fernando"	1971	RSN80_SFERN_PSL270.AT2	4.39
EQ 437	810	"Loma Prieta"	1989	RSN810_LOMAP_LOB090.AT2	1.86
EQ 438	8164	"Duzce_ Turkey"	1999	RSN8164_DUZCE_487-NS.AT2	2.55
EQ 439	8165	"Duzce_ Turkey"	1999	RSN8165_DUZCE_496-EW.AT2	0.63
EQ 440	825	"Cape Mendocino"	1992	RSN825_CAPEMEND_CPM000.AT2	0.76
EQ 441	87	"San Fernando"	1971	RSN87_SFERN_SAD003.AT2	4.92
EQ 442	957	"Northridge-01"	1994	RSN957_NORTHR_HOW330.AT2	4.13
*Record Sequential Number of the PEER NGA-West2 database					

A.7 OpenSees Analysis Results

A.7.1 Model with Expected Material Properties and Expected Axial Load

This model uses the expected material properties defined by the application of the Saatcioglu and Razvi (1992) model. The applied gravity load comes from the load combination D+0.25L.

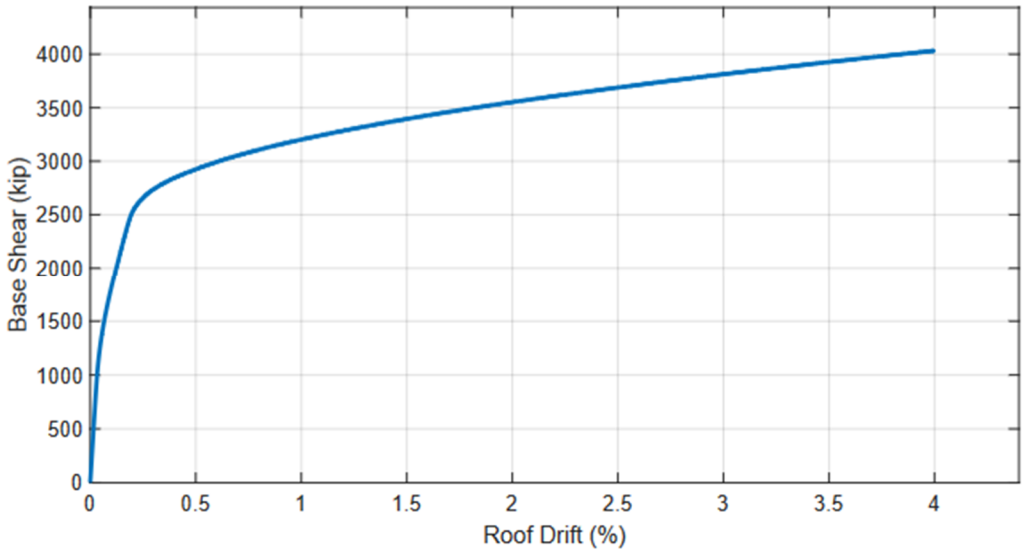

***Figure A.1**: Base shear versus roof drift – Monotonic Pushover with P_{avg} and w/o modification to expected material properties (4-Story Archetype)*

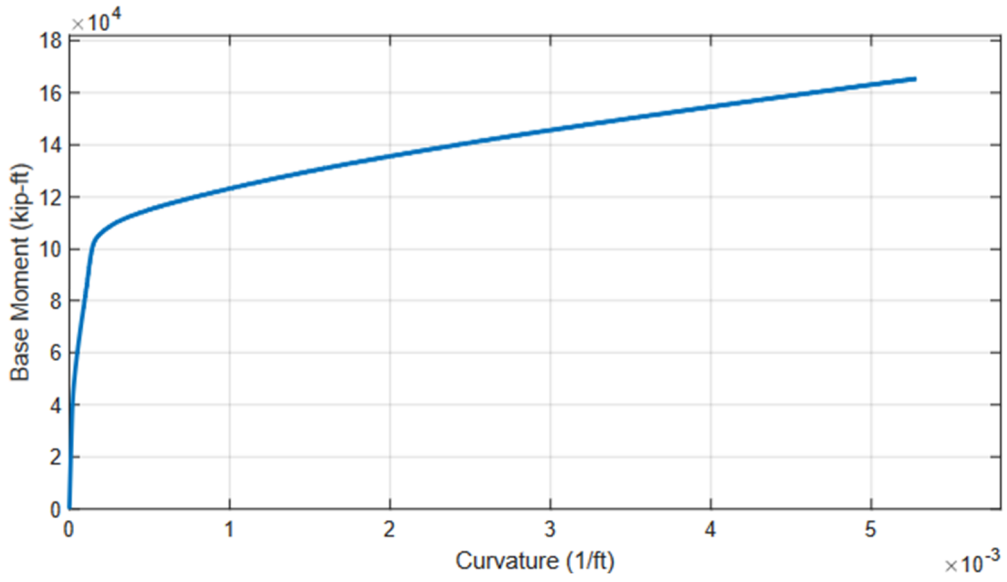

***Figure A.2**: Base moment versus curvature – Monotonic Pushover with P_{avg} and w/o modification to expected material properties (4-Story Archetype)*

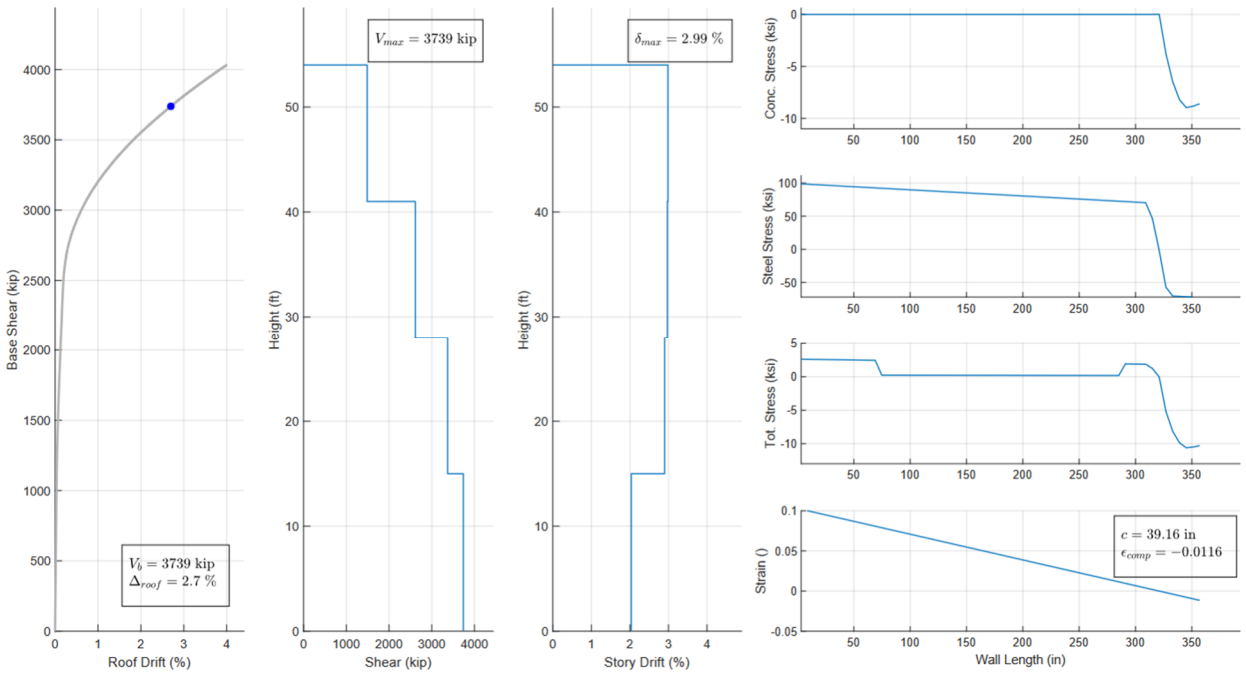

***Figure A.3**: Monotonic pushover results at predicted roof drift capacity (4-Story Archetype)*

A.7.2 Model with Modified Expected Material Properties and Expected Axial Load

A.7.2.1 Monotonic Pushover Results

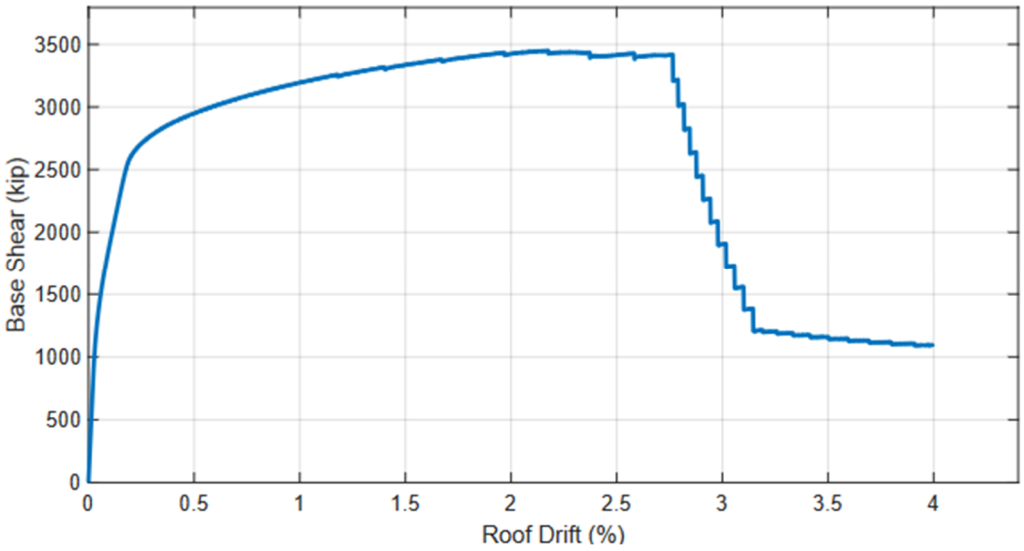

***Figure A.4**: Base shear versus roof drift – Monotonic Pushover with P_{avg} and modified expected material properties (4-Story Archetype)*

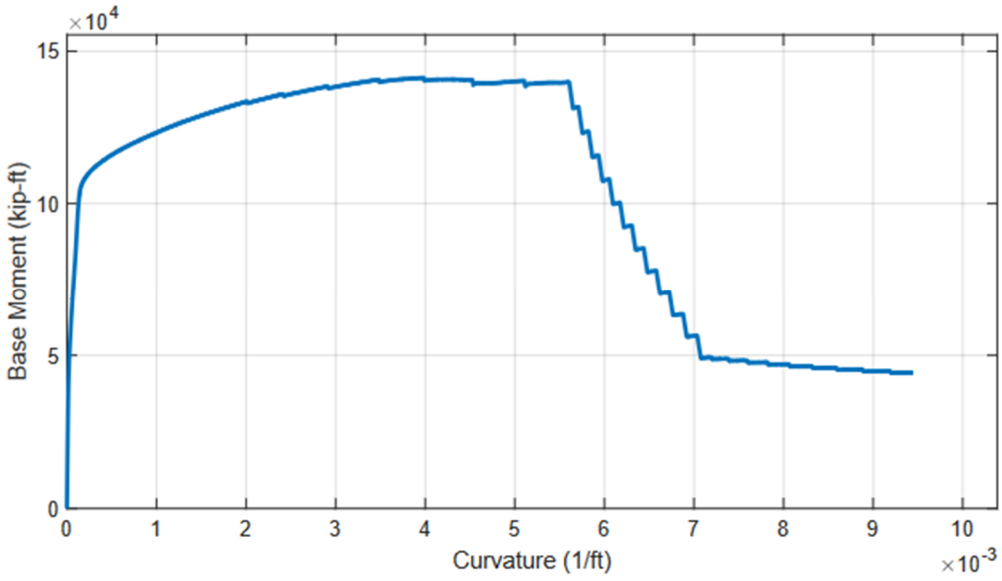

***Figure A.5**: Base moment versus curvature – Monotonic Pushover with P_{avg} and modified expected material properties (4-Story Archetype)*

A.7.2.2 Cyclic Pushover Results

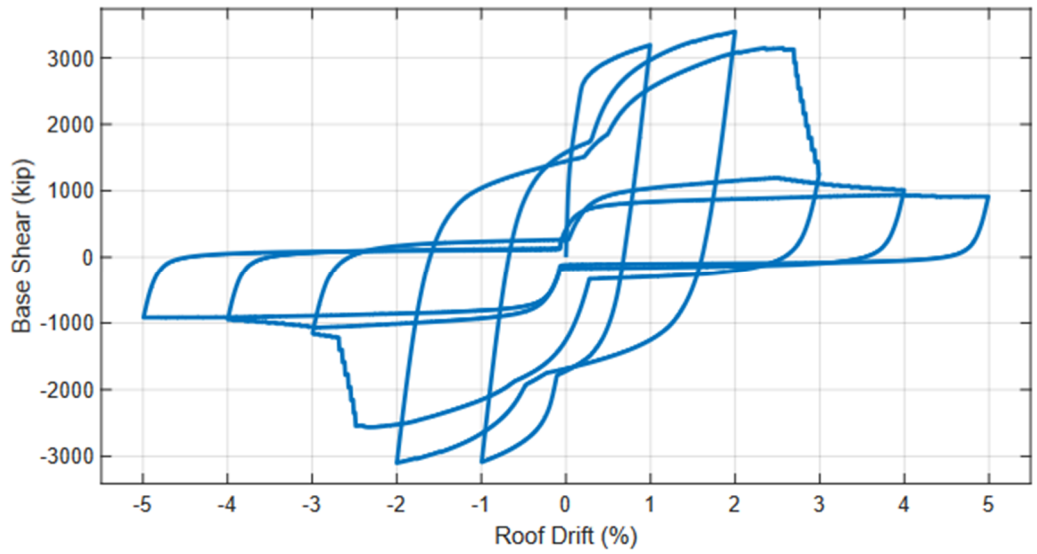

***Figure A.6**: Base shear versus roof drift – Cyclic Pushover with P_{avg} and modified expected material properties (4-Story Archetype)*

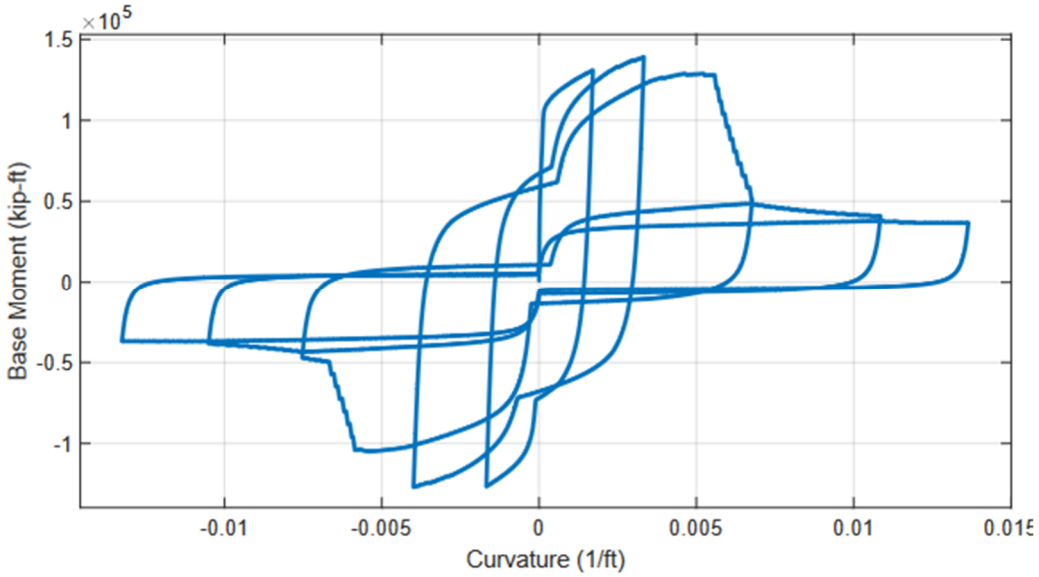

***Figure A.7**: Base moment versus Curvature – Cyclic Pushover with P_{avg} and modified expected material properties (4-Story Archetype)*

A.7.2.3 Dynamic Analysis Results – LC: (1.2+0.2S_{DS})D+0.25L

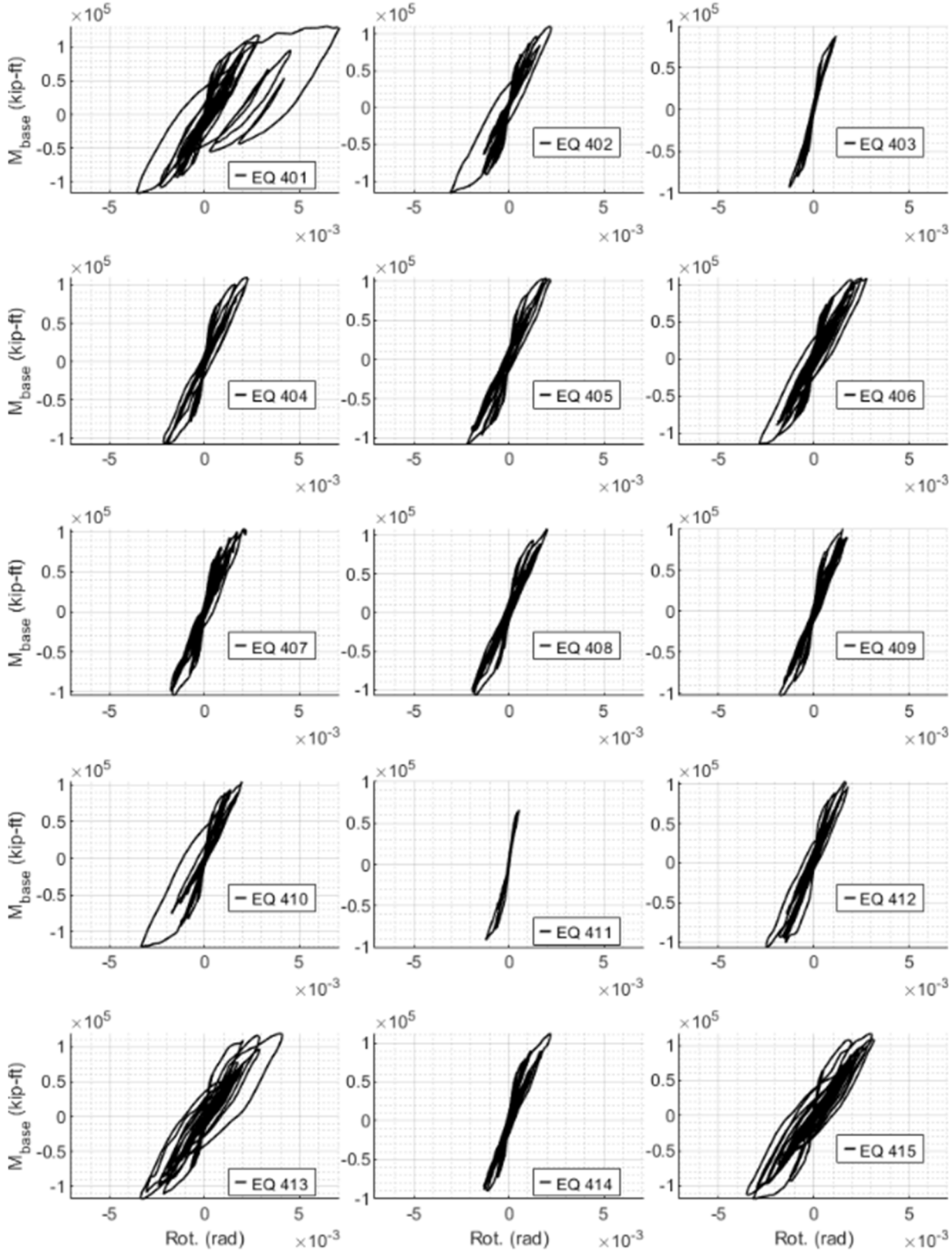

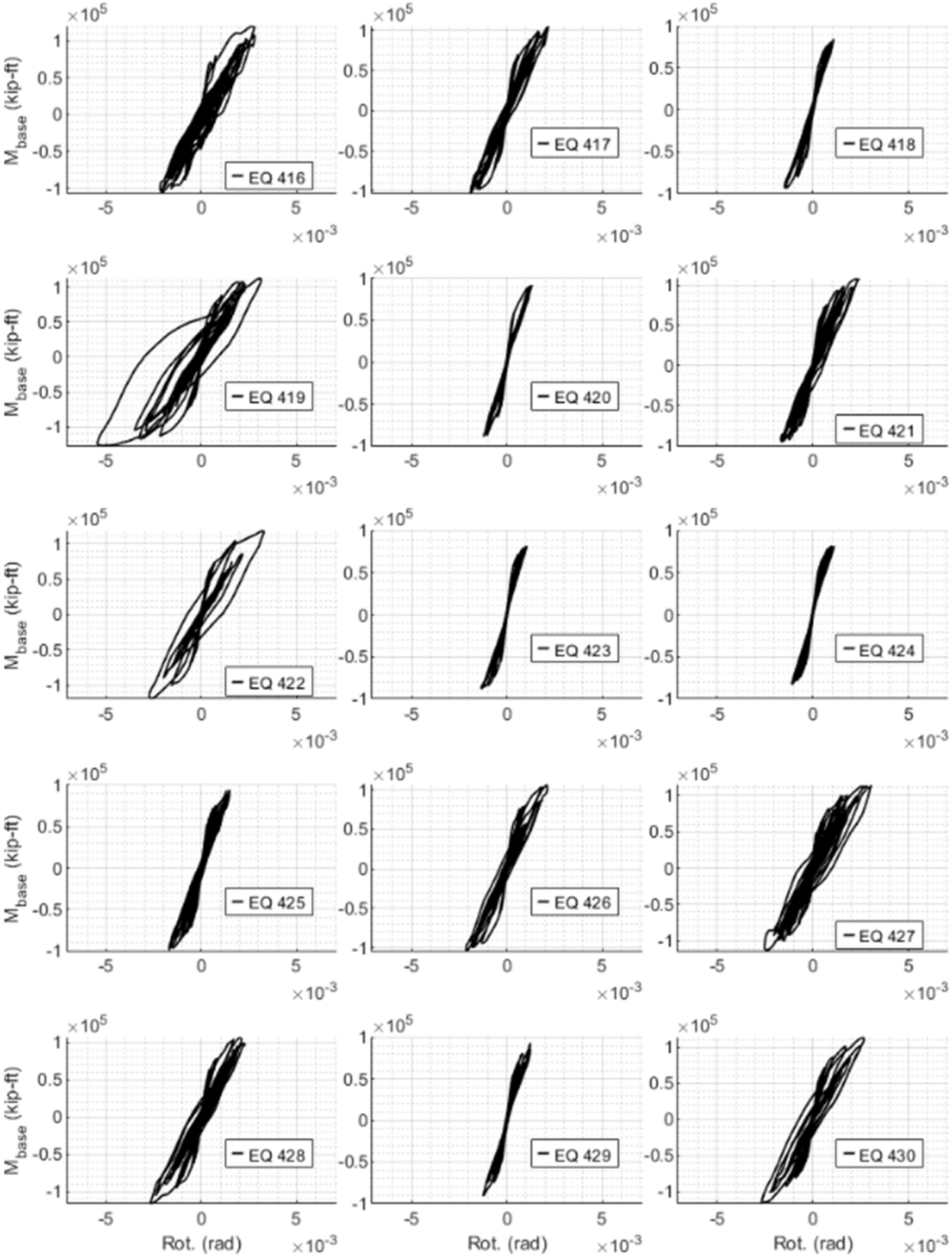
EQ 416
EQ 417
EQ 418
EQ 419
EQ 420
EQ 421
EQ 422
EQ 423
EQ 424
EQ 425
EQ 426
EQ 427
EQ 428
EQ 429
EQ 430
M_base (kip-ft)
Rot. (rad)
×10^5
×10^-3

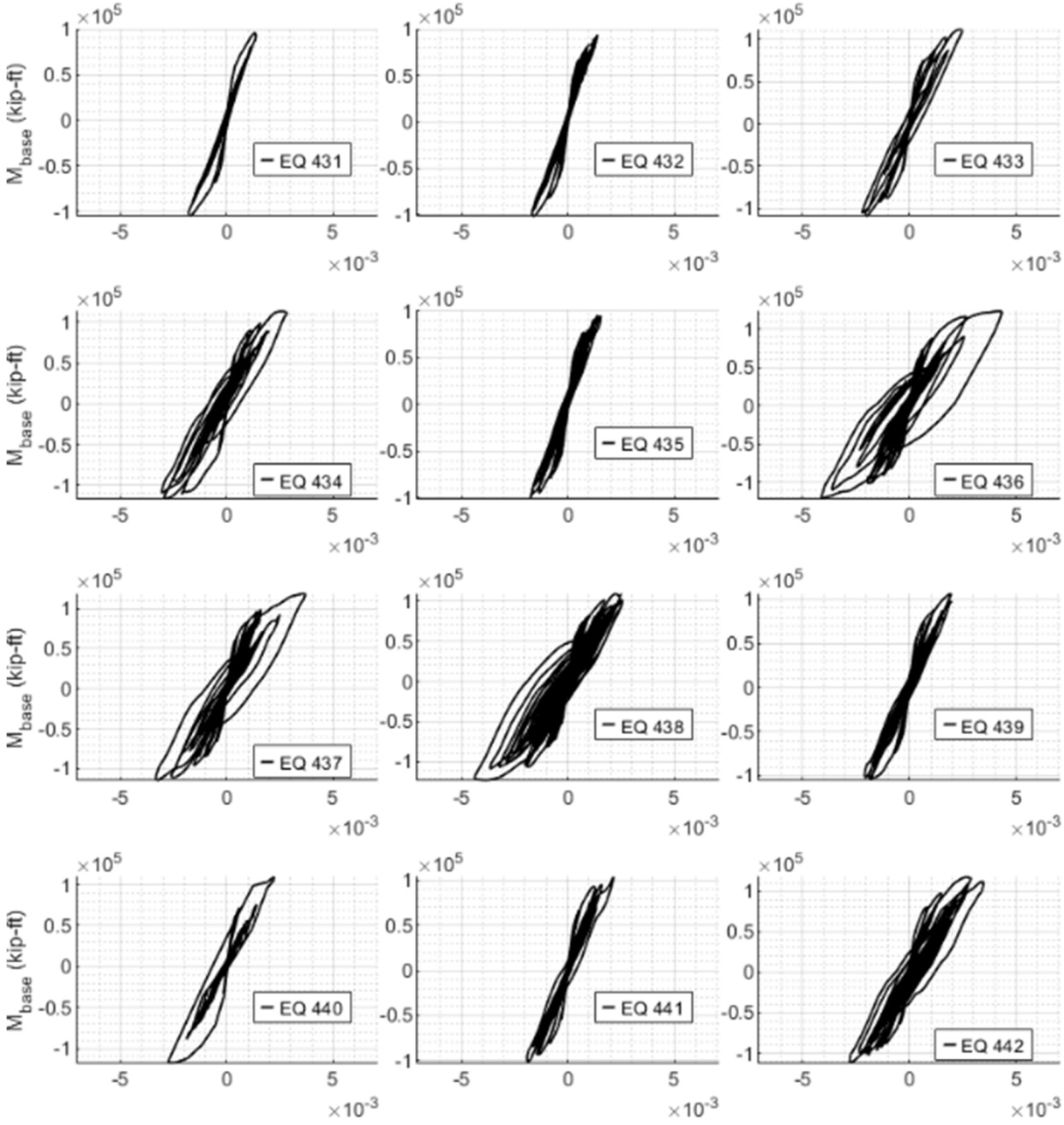
M_base (kip-ft)
×10^5
×10^-3
EQ 431
EQ 432
EQ 433
EQ 434
EQ 435
EQ 436
EQ 437
EQ 438
EQ 439
EQ 440
EQ 441
EQ 442

Appendix B. Design and Analysis of 8-Story Archetype

Content

B.1 Analysis - Design Forces and Displacements

Building Information

- $n_s := 8$ stories.

- Story height of $h_{typ} := 13\ ft$, except for the 1st story which $h_b := 15\ ft$ high

- 120 ft x 120 ft every story

- $n_w := 4$ rectangular walls in each direction

- Center of mass and stiffness coincide (no eccentricity)

- Dead load = 175 psf (floors)
  = 140 psf (roof)

- Live load = 50 psf + 15 psf (partitions) = 65 psf (floors)
  = 20 psf + 0 psf (partitions) = 20 psf (floors)

- Risk Category II

- Site Class C

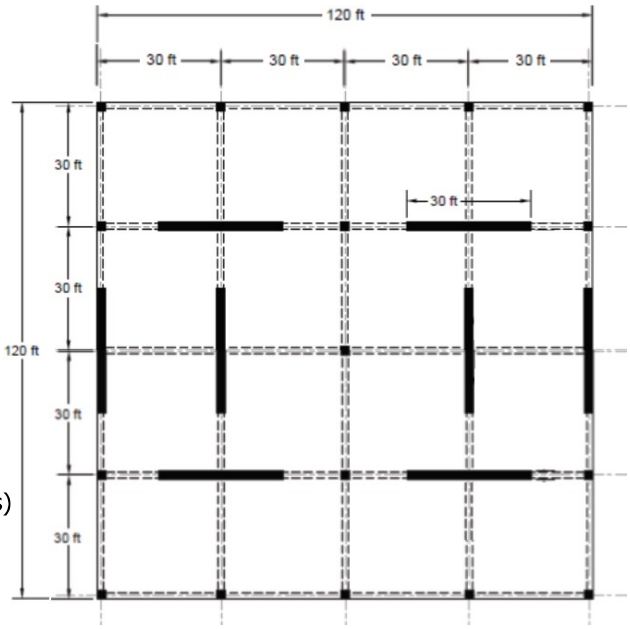

- Wall dimensions: $l_w := 30\ ft$, $t_w := 30\ in$, $t_{fl} := 0\ ft$, $b_{fl} := 0\ ft$

$$A_{cv} := l_w \cdot t_w = 10800\ in^2$$

$$A_g := t_w \cdot (l_w - 2 \cdot t_{fl}) + 2 \cdot b_{fl} \cdot t_{fl} = 10800\ in^2$$

$$A'_g := t_w \cdot (l_w - t_{fl}) + b_{fl} \cdot t_{fl} = 10800\ in^2$$

Determination of SDC

Mapped acceleration parameters

From USGS Hazard Tool Website:

Maximum considered earthquake spectral response acceleration at short periods. $S_s := 2.08\ g$

Maximum considered earthquake spectral response acceleration at a period of 1-sec. $S_1 := 0.64\ g$

Determine if the building is permitted to be automatically asigned to SDC A

Because $S_s = 2.08 > 0.15$ and $S_1 = 0.64 > 0.04$, the building is not permitted to be automatically assigned to SDC A.

Determine if the SDC is E or F

Because the Risk Category is II and $S_1 = 0.64 < 0.750$, the SDC is not E or F

Design acceleration parameters

According to ASCE 7-16:

Table 11.4-1 $F_a := 1.0$

Table 11.4-2 $F_v := 1.4$

Eq. 11.4-1 $S_{MS} := F_a \cdot S_s = 2.08$

Eq. 11.4-2 $S_{M1} := F_v \cdot S_1 = 0.90$

Eq. 11.4-3 $S_{DS} := \frac{2}{3} \cdot S_{MS} = 1.39$

Eq. 11.4-4 $S_{D1} := \frac{2}{3} \cdot S_{M1} = 0.60$

Check if the SDC can be determine by ASCE 7-16 Table 11.6-1 alone

Check if all four conditions in ASCE 7-16 11.6 are satisifed.

Structural height $h_n := (n_s - 1) \cdot h_{typ} + h_b = 106\ \textbf{ft}$

From Table 12.8-2 $C_t := 0.02$, $x := 0.75$

Approximate fundamental period (Eq. 12.8-7) $T_a := C_t \cdot \left(\frac{h_n}{\textbf{ft}}\right)^x = 0.66$

T_s (S. 11.4.5) $T_s := \frac{S_{D1}}{S_{DS}} = 0.43$

Because $T_a = 0.66$ > $0.8\ T_s = 0.34$, the SDC cannot be determined by ASCE 7-16 Table 11.6-1 alone (1st condition is not satisfied)

Determine the SDC

From ASCE 7-16 Table 11.6-1 with $S_{DS} = 1.39$ > 0.50 and Risk Category II, the SDC is D.
From ASCE 7-16 Table 11.621 with $S_{D1} = 0.60$ > 0.20 and Risk Category II, the SDC is D.

Therefore, SDC is D.

Gravity Load and Mass Calculation

Gravity Load

Load combination 6 and 7 include the seismic load effects (ASCE 7-17, S. 2.3.6). These axial loads are; (LC6) 1.2D + Ev + Eh + L + 0.2S; (LC7) 0.9D - Ev + Eh. Exception No.1 of S. 2.3.6 allows the load factor on LL in LC6 to be taken as 0.5 when live load is less than 100psf. From ASCE 7-16 S. 12.4.2.2, the vertical seismic load effect shall be determined as $E_v = (0.2\ S_{DS}) \cdot DL$. Therefore:

Gravity load from LC6: $(1.2 + 0.2\ S_{DS})\ DL + 0.5\ LL$ Gravity load from LC7: $(0.9 - 0.2\ S_{DS})\ DL$

Tributary area of the wall: $A_{trib.wall} := 4 \cdot (56.25 \cdot 2 + 168.75)\ \textbf{ft}^2 - 28.125\ \textbf{ft}^2 = 1097\ \textbf{ft}^2$

Wall weigth:

$w_{w.r} := 0\ \textbf{kip}$ (in the upper story)

$w_{w.typ} := (150\ \textbf{pcf}) \cdot A_g \cdot h_{typ} = 146\ \textbf{kip}$ (in a typical story)

$w_{w.b} := (150\ \textbf{pcf}) \cdot A_g \cdot h_b = 169\ \textbf{kip}$ (in the bottom story)

Table 1. Wall gravity load

Level	DL (psf)	LL (psf)	D+0.25L (psf)	LC6 (psf)	LC7 (psf)	Applied Vertical Load D+0.25L (kips)	Applied Vertical Load LC6 (kips)	Applied Vertical Load LC7 (kips)	Wall Axial Load D+0.25L (kips)	Wall Axial Load LC6 (kips)	Wall Axial Load LC7 (kips)
Base	0	0	0	0	0	0	0	0	2,674	4,018	1,584
2	329	65	345	518	205	379	569	225	2,295	3,450	1,359
3	308	65	325	488	192	356	535	211	1,939	2,914	1,149
4	308	65	325	488	192	356	535	211	1,583	2,379	938
5	308	65	325	488	192	356	535	211	1,227	1,844	727
6	308	65	325	488	192	356	535	211	871	1,308	517
7	308	65	325	488	192	356	535	211	515	773	306
8	308	65	325	488	192	356	535	211	159	238	96
Roof	140	20	145	217	87	159	238	96	0	0	0

Seismic Weight of the Building

Seismic weight = dead + partitions = $175\ \boldsymbol{psf} + 15\ \boldsymbol{psf} = 190\ \boldsymbol{psf}$ (floors)

= $140\ \boldsymbol{psf} + 7.5\ \boldsymbol{psf} = 147.5\ \boldsymbol{psf}$ (roof)

Table 2. Seismic weight and mass of the building (considering wall self weight)

Story	DL (psf)	Area (ft^2)	Seismic Weight, W_i (kips)	Seismic Mass, m_i (kips-s^2/in)
1	190	14,400	3,996	10.35
2	190	14,400	3,906	10.12
3	190	14,400	3,906	10.12
4	190	14,400	3,906	10.12
5	190	14,400	3,906	10.12
6	190	14,400	3,906	10.12
7	190	14,400	3,906	10.12
8	147.5	14,400	2,709	7.02
		Sum	**30,141**	**78.07**

Values for the model (one quarter of the building only)

	Building	Associated to one Wall
Seismic weight:	$W_{building} = 30141\ \boldsymbol{kip}$	$W_t := \frac{W_{building}}{n_w} = 7535\ \boldsymbol{kip}$
Seismic mass:	$M_{building} = 78.07\ \frac{\boldsymbol{kip \cdot s^2}}{\boldsymbol{in}}$	$M_t := \frac{M_{building}}{n_w} = 19.52\ \frac{\boldsymbol{kip \cdot s^2}}{\boldsymbol{in}}$

Accidental Torsion Factor

Accordingly to ASCE 7-16 S. 12.8.4.2, accidental torsion shall be calculating by displacing the center of mass each way from its actual loaction by a distance equal to 5% of the dimension of the structure perpendicular to the direction of applied forces. In this case, the floor slabs are a square of 120 ft x 120 ft. The distance between each wall and the CM is $d_{wcm} := 30\ ft$. The (base or story) shear of the building is called V_{build}, while the (base or story) shear of the wall is called V_{wall}. Therefore:

Eccentricity $e := 0.05 \cdot (120\ ft) = 6.00\ ft$

Distance between walls and actual CM $d_{wcm} = 30\ ft$

Stiffness of one wall k_w (no need to actually obtain this value now)

Moment due to acc. torsion (V_{build} and V_{wall} are the building base shear and wall base shear w/o acc. torsion)

$$M_{at} = e \cdot V_{build} = e \cdot (4\ V_{wall}) = 6\ k_w d_{wcm} \theta d_{wcm} + 2\ k_w (2\ d_{wcm})\ \theta\ (2\ d_{wcm})$$

Rotation of the slab due to acc. torsion

$$\theta_{at} = \frac{M_{at}}{14\ k_w {d_{wcm}}^2}$$

Extra (+/-) shear in one wall due to acc. torsion

$$V_{at} = k_w \cdot (\theta_{at} d_{wcm}) = \frac{M_{at}}{14\ d_{wcm}} = \frac{e \cdot (4\ V_{wall})}{14\ d_{wcm}} = \frac{2\ eV_{wall}}{7\ d_{wcm}}$$

Total shear in one wall due to acc. torsion

$$V_{Tot.Wall} = V_{wall} + \frac{2\ eV_{wall}}{7\ d_{wcm}} = \left(1 + \frac{2\ e}{7\ d_{wcm}}\right) V_{wall}$$

Factor to account for acc. torsion

$$k_{at} := 1 + \frac{2\ e}{7\ d_{wcm}} = 1.06$$

Base Shear of the Building (ELF)

Required parameters:

Response modifiation coefficient (Table 12.2-1) $R := 5$

Deflection amplification factor (Table 12.2-1) $C_d := 5$

Importance factor (Table 1.5-2) $I_e := 1.0$

Long-period transition (Fig. 22-12) $T_L := 8$

Approximate fundamental period (already calculated) $T_a = 0.66$

Determine the fundamental period:

Fundamental period (from modal analysis) $T := 0.80\ s$

Coefficient for upper limit for T (Table 12.8-1) $C_u := 1.4$

Upper limit for T (S. 12.8.2) $T_u := C_u \cdot T_a = 0.92\ \ s$

Therefore, the fundamental period to use is: $T := min(T, T_u) = 0.80\ \ s$

Determine the seismic coefficient:

Seismic response coefficient (Eq. 12.8-2) $C_s := \frac{S_{DS}}{\frac{R}{I_e}} = 0.28$

Upper limit for C_s, given that $T_a < T_L$ (Eq.12.8-3) $C_{s.max} := \frac{S_{D1}}{T \cdot \left(\frac{R}{I_e}\right)} = 0.15$

Lower limit for C_s, given that $T_a < T_L$ (Eq.12.8-5 and -6) $C_{s.min} := \max\left(0.044 \cdot S_{DS} \cdot I_e, \frac{0.5 \cdot S_1}{\frac{R}{I_e}}\right) = 0.064$

(Eq. 12.8-6 applies when $S_1 \geq 0.6\ g$, which is the case now)

Therefore:

Seismic coefficient to be used: $C_s := C_{s.max} = 0.15$

Seismic base shear of the wall: $V_b := C_s \cdot W_t = 1125\ \textbf{\textit{kip}}$

Seismic base shear of the wall accounting for acc. torsion: $V_b := k_{at} \cdot V_b = 1190\ \textbf{\textit{kip}}$

Modal Response Spectrum Analysis

Concrete strength $f'_c := 5000\ \textbf{\textit{psi}}$

Modulus of elasticity $E := 57000 \cdot \sqrt{f'_c \cdot \textbf{\textit{psi}}} = 4031\ \textbf{\textit{ksi}}$

Inertia $I_g := \frac{t_w \cdot \left(l_w - 2 \cdot t_{fl}\right)^3}{12} + 2 \cdot \left(\frac{b_{fl} \cdot {t_{fl}}^3}{12} + b_{fl} \cdot t_{fl} \cdot \left(\frac{l_w}{2} - \frac{t_{fl}}{2}\right)^2\right) = 5625\ \textbf{\textit{ft}}^4$

Eff. inertia $I_{eff} := 0.50 \cdot I_g = 2813\ \textbf{\textit{ft}}^4$

Modal periods $T := \frac{2\ \pi}{\omega_m}$ $T^{\mathrm{T}} = \begin{bmatrix} 0.80 & 0.13 & 0.05 & 0.02 & 0.01 & 0.01 & 0.01 & 0.01 \end{bmatrix}$

Number of required modes to achieve more than 90% of the total mass $\frac{\sum_{j=1}^{3} M_{m.eff_j}}{M_t} = 0.93$

Base shear: $V_{b.MRSA} = 912\ \textbf{\textit{kip}}$

Because the base shear obtain with the modal analysis is less than the base hsear obtained by the ELF method ($V_{b.MRSA} = 912\ \textbf{\textit{kip}} < V_b = 1190\ \textbf{\textit{kip}}$), all forces and drifts are requried to be scaled with the factor $V_{ELF}/V_{ModalAnalysis}$ (ASCE 7-16, S. 12.9.1.4).

Factor for scaling of forces $k_{shear} := \frac{V_b}{V_{b.MRSA}} = 1.30$

Design Forces and Displacements - Summary

The lateral demands on the wall obtained from the Modal Response Spectrum Analysis are shown in the table below. The forces were scaled to acchieve 100% of the base shear calcualted by the ELF method. The table incorporates the wall gravity loads calculated before (see Table 1).

Table 3. Loads and displacement demands on the wall

Level	Height (ft)	Axial Load D+0.25L (kip)	Axial Load LC6 (kip)	Axial Load LC7 (kip)	Lateral Force (kip)	Story Shear (kip)	Overturning Moment (kip-ft)	Elastic Deflection (in)	Amplified Deflection (in)	Story Drift (%)
Base	0	2,674	4,018	1,584	0	1,190	82,299	0.0	0.0	0.00
2	15	2,295	3,450	1,359	75	1,150	65,958	0.1	0.3	0.17
3	28	1,939	2,914	1,149	173	1,059	52,668	0.2	1.0	0.44
4	41	1,583	2,379	938	235	941	40,530	0.4	2.0	0.63
5	54	1,227	1,844	727	253	820	29,571	0.6	3.2	0.78
6	67	871	1,308	517	245	700	19,670	0.9	4.6	0.89
7	80	515	773	306	227	548	10,879	1.2	6.1	0.96
8	93	159	238	96	270	294	3,824	1.5	7.6	0.99
Roof	106	0	0	0	294	0	0	1.8	9.2	1.00

The roof drift is: $\Delta_{roof} = 0.72\%$

Min. axial load: $P_{min} = 1584\ \boldsymbol{kip}$

D+0.25L axial load: $P_{D.25L} = 2674\ \boldsymbol{kip}$

Max. axial load: $P_{max} = 4018\ \boldsymbol{kip}$

Shear demand: $V_u = 1190\ \boldsymbol{kip}$

Moment demand: $M_u = 82299\ \boldsymbol{kip \cdot ft}$

Axial load ratios:

$$ALR_{min} := \frac{P_{min}}{A'_g \cdot f'_c} = 2.9\%$$

$$ALR_{D.25L} := \frac{P_{D.25L}}{A'_g \cdot f'_c} = 5.0\%$$

$$ALR_{max} := \frac{P_{max}}{A'_g \cdot f'_c} = 7.4\%$$

B.2 Wall Design

Critical Section

Building Information

Number of stories	$n_s := 8$
Lightweight concrete	$\lambda := 1.0$
Concrete compressive strength	$f'_c := 5000\ psi$
Yield strength of steel bars	$f_y := 60\ ksi$
Height of the wall	$h_w := (n_s - 1) \cdot 13\ ft + 15\ ft = 106\ ft$
Length of the wall	$l_w := 30\ ft$
Thickness of the wall	$t_w := 30\ in$
Flange thickness	$t_{fl} := 0\ ft = 0.00\ in$
Flange total width	$b_{fl} := 0\ ft$
Gross Area	$A_g := t_w \cdot (l_w - 2\ t_{fl}) + 2\ b_{fl} \cdot t_{fl} = 10800\ in^2$
A_{cv} cross-section area	$A_{cv} := t_w \cdot l_w = 10800\ in^2$
Min., avg., and max. axial demand	$P_{min} := 1584\ kip$ $P_{avg} := 2674\ kip$ $P_{max} := 4018\ kip$
Shear demand	$V_u := 1190\ kip$
Moment demand at critical section	$M_u := 82299\ kip \cdot ft$
Critical section at the bottom	$h_{wcs} := h_w = 106\ ft$

Provided longitudinal reinforcement in the critical section

Web Hor.: #5 @ 4.75

#4 rebar	$A_{\#5} := 0.31\ in^2$
Spacing	$s_{wh} := 4.75\ in$
Reinf. ratio	$\rho_{wh} := \frac{2 \cdot A_{\#5}}{s_{wh} \cdot t_w} = 0.44\%$

Web Ver.: #4 @ 5.3

#4 rebar	$A_{\#4} := 0.20\ in^2$
Spacing	$s_{wv} := 5.3\ in$
Reinf. ratio	$\rho_{wv} := \frac{2 \cdot A_{\#4}}{s_{wv} \cdot t_w} = 0.25\%$

Boundary Element: 36 #9

#9 rebar - area	$A_{\#9} = 1.00\ in^2$
#9 rebar - diam.	$d_{\#9} = 1.128\ in$ ($d_b := d_{\#9}$)
Length of BE	$l_{be} := 69.0\ in$
Width of BE	$b := t_w = 30.00\ in$
Reinf. ratio	$\rho_{be} := \frac{36 \cdot A_{\#9}}{(l_{be} + 3\ in) \cdot t_w} = 1.67\%$
	$\rho_{sb} := \frac{36 \cdot A_{\#9}}{A_{cv}} = 0.33\%$

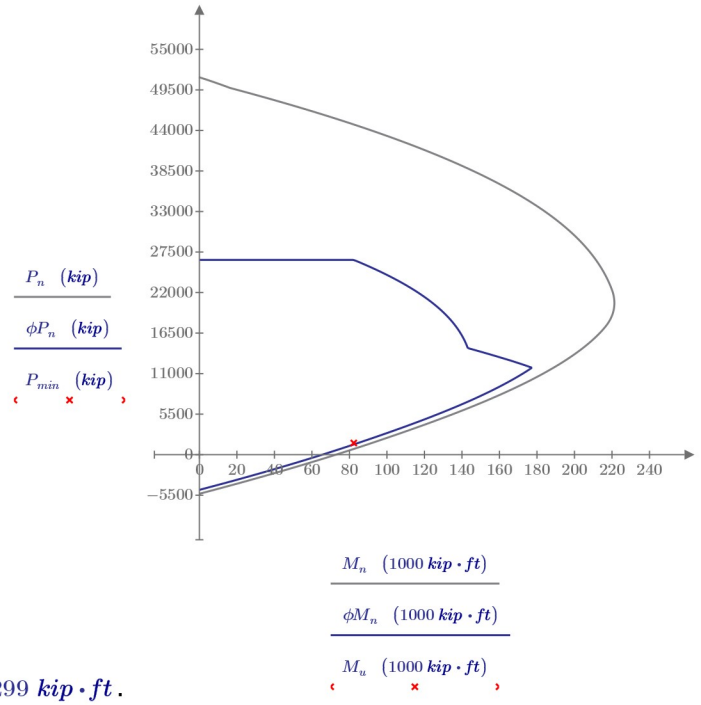

Verification for $P_{min} = 1584\ kip$ and $M_u = 82299\ kip \cdot ft$.

Minimum reinforcement ratios for the web

$A_{cv} := l_w \cdot t_w = 10800\ in^2$

Because $V_u = 1190\ kip > \lambda \sqrt{f'_c \cdot psi}\ A_{cv} = 764\ kip$, we can use $\rho_l := 0.0025$ and $\rho_t := 0.0025$ (ACI 18.10.2.1)

Number of curtains of reinforcement in the web

Because $\frac{h_w}{l_w} = 3.53 > 2$, 2 curtains of longitudinal and transverse reinforcement are required in the web (ACI 18.10.2.2)

Required area of longitudinal reinforcement for flexure and axial forces

Longitudinal reinforcement ratio within $0.15\ l_w = 54.0\ in$ from the end of the wall, and over a width equal to the wall thickness, shall be at least $6 \frac{\sqrt{f'_c \cdot psi}}{f_y} = 0.0071$. Therefore, the requirements of ACI 318-19, 18.10.2.4(a) are satisfied.

The longitudinal reinforcement required by 18.10.2.4(a) shal extend vertically above and below the critical section at least the greater of $l_w = 30.0\ ft$ and $\frac{M_u}{3\ V_u} = 23.1\ ft$. This is satisfied becuase $\rho_{be} = 0.0167$ is provided in the first 4 stories, covering a height equal to $15\ ft + 3 \cdot 13\ ft = 54.0\ ft$

No more than 50 percent of the reinforcement required by 18.10.2.4(a) shall be terminated at any section. This means that outside the greater of l_w and $M_u / (3\ V_u)$ (which is $30\ ft$), we have:

Minimum long. reinf. ratio (within $0.15\ l_w = 54.0\ in$ from the end of the wall)	$\frac{1}{2}\left(6 \frac{\sqrt{f'_c \cdot psi}}{f_y}\right) = 0.0035$
Minimum amount of long. reinf. above cut-off point	$\frac{1}{2}\left(6 \frac{\sqrt{f'_c \cdot psi}}{f_y}\right) \cdot 0.15\ l_w \cdot t_w = 5.73\ in^2$

Maximum Probable Moment

P-M diagram obtained with $1.25\ f_y = 75\ ksi$ and $P_{max} = 4018\ kip$

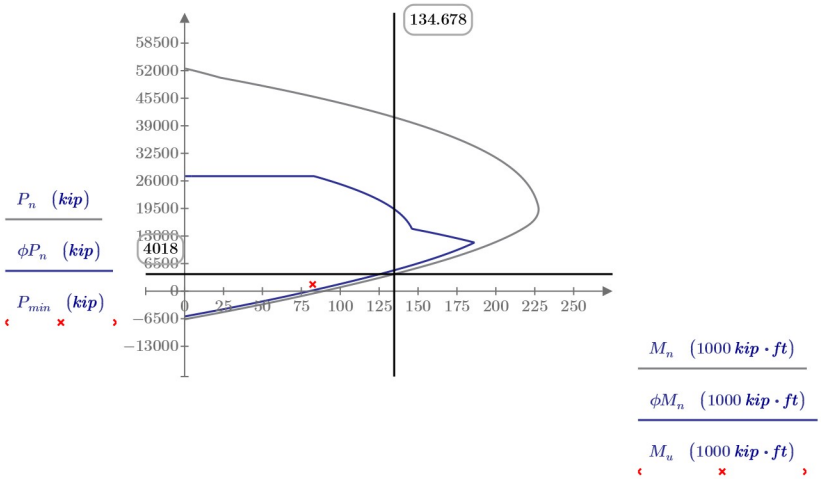

Design shear force

(a) Demand

Maximum probable moment (using P-M diagram obtained with $1.25\,f_y = 75\ ksi$) $M_{pr} = 134678\ kip \cdot ft$

Critical section at the bottom $h_{wcs} = 106\ ft$

Wall length $l_w = 30.0\ ft$

Shear demand $V_u = 1190\ kip$

Overstrength factor when $\frac{h_{wcs}}{l_w} = 3.53 > 1.5$: $\Omega_v := \max\left(\frac{M_{pr}}{M_u}, 1.5\right) = 1.64$

ω_v when $\frac{h_{wcs}}{l_w} = 3.53 > 2.0$ and $n_s := \max\left(8, 0.007 \cdot \frac{h_{wcs}}{in}\right) = 8.90 > 6$: $\omega_v := min\left(1.3 + \frac{n_s}{30}, 1.8\right)$

$\omega_v = 1.60$

Therefore, accodring to ACI 318-19, 18.10.3.1:

$V_e := min\left(\Omega_v \cdot \omega_v \cdot V_u, 3\ V_u\right) = 3110\ kip$ $\quad (\Omega_v \cdot \omega_v = 2.61)$

Strength (**ACI 318-19**):

α_c coefficient

$$\alpha_{c.aci} := \begin{cases} 3.0 & \text{if } \frac{h_w}{l_w} \le 1.5 \\ 2.0 & \text{else if } \frac{h_w}{l_w} \ge 2.0 \\ 2 \cdot \left(3 - \frac{h_{wcs}}{l_w}\right) & \text{else} \end{cases} \qquad \alpha_{c.aci} = 2.00$$

Upper limit $V_{n.aci.lim} := 8 \cdot A_{cv} \cdot \sqrt{f'_c \cdot psi} = 6109\ kip$

Shear strength $V_{n.aci} := \left(\alpha_{c.aci} \cdot \lambda \cdot \sqrt{f'_c \cdot psi} + \rho_{wh} \cdot f_y\right) \cdot A_{cv} = 4347\ kip < V_{n.aci.lim} = 6109\ kip$

Thus: $\phi V_n := 0.75 \cdot V_{n.aci} = 3260\ kip > V_e = 3110\ kip$

The capacity (**Prop. Eq.**):

Ratio of long. steel boundary $\rho_{sb} = 0.33\%$

Axial load considered: $P_{max} = 4018\ kip$

α_c coefficient

$$\alpha_{c.p} := \frac{1}{100} \cdot \left(9 \cdot \frac{\left(1 + \frac{P_{max}}{A_{cv} \cdot f'_c}\right)^3}{\sqrt[3]{\frac{M_u}{\omega_v \cdot V_u \cdot l_w}}} - 6\right) = 0.039$$

α_s coefficient $\alpha_{s.p} := \frac{2}{5 \cdot \sqrt[3]{\frac{M_u}{\omega_v \cdot V_u \cdot l_w}}} = 0.35$

α_{shape} factor $\alpha_{shape} := min\left(\max\left(1, 0.7 \cdot \left(1 + \frac{t_{fl} \cdot b_{fl}}{A_{cv}}\right)^2\right), 1.5\right) = 1.00$

Upper limit $V_{n.lim} := \alpha_{shape} \cdot 8 \cdot A_{cv} \cdot \sqrt{f'_c \cdot psi} = 6109\ kip$

Shear strength $V_{n.prop} := \left(\alpha_{c.p} \cdot f'_c + \alpha_{s.p} \cdot \left(\rho_{sb} + \rho_{wh}\right) \cdot f_y\right) \cdot A_{cv} = 3855\ kip < V_{n.lim} = 6109\ kip$

Resultant DCR $\frac{V_e}{V_{n.prop}} = 0.81$ (Remember we are not designing the wall with the proposed equation. We want to assess an ACI 318-19 compliant wall with it).

Determine if special boundary elemens are required

Special boundary elements are required where the following equation is satisfied (ACI 18.10.6.2):

$$\frac{1.5\ \delta_u}{h_{wcs}} \geq \frac{l_w}{600\ c}$$

From the analysis, the elastic displacement at the top of the building is $\delta_{xe} := 1.84\ in$. Also, from ASCE 7-16 Table 12.2-1 we have $C_d := 5$ for a Seismic Force-Resisting System consisting in special reinforced concrete shear walls. In addition, $I_e := 1.0$ for Risk Category II (ASCE 7-16 Tabe 1.5-2). Therefore:

$$\delta_u := \frac{C_d \cdot \delta_{xe}}{I_e} = 9.20\ in$$

Ratio δ_u / h_{wcs} shall not be taken less than 0.005. But in this case, $\frac{\delta_u}{h_{wcs}} = 0.007$

From the sectional analysis, the largest neutral axis depth is $c := c_{Pmax} = 59.0\ in$. Thus:

$$\frac{1.5\ \delta_u}{h_{wcs}} = 0.0108 > \frac{l_w}{600\ c} = 0.0102$$

Therefore, special boundary elements are required at the ends of the wall

Vertical extent of the special BE transverse reinforcement

According to ACI 318-19, 18.10.6.2(b)(i), provide special boundary element transverse reinforcement vertically over at least the greater of the following lengths from the critical wall section:

$l_w = 30.00\ ft$ and $\frac{M_u}{4\ V_u} = 17.3\ ft$

The special BE transverse reinforcement is provided along the first 4 stories (i.e., $15\ ft + 3 \cdot 13\ ft = 54.00\ ft$). BE transverse reinforcement in stories 5 and 6 has a vertical spacing of $6\ in$, satisfying the requirements of Table 18.10.6.5(b).

Check if ACI 18.10.6.2(b)(ii) or (iii) is satisfied

$b = 30.00\ in > \sqrt{0.025 \cdot c \cdot l_w} = 23.05\ in$ Cond. (b)(ii) is satisfied

$$\frac{\delta_c}{h_{wcs}} = \max\left(\frac{1}{100}\cdot\left(4 - \frac{1}{50}\left(\frac{l_w}{b}\right)\left(\frac{c}{b}\right) - \frac{V_e}{\left(8\sqrt{psi}\right)\cdot\sqrt{f'_c}\cdot A_{cv}}\right), 0.015\right) = 0.030 \quad > \quad \frac{1.5\ \delta_u}{h_{wcs}} = 0.011$$

Cond. (b)(iii) is satisfied

At least one of the above shall be satisfied. Therefore, ACI 18.10.6.2(b) is satisfied.

Horizontal length of the Special BE

According to ACI 318-19 18.10.6.4(a), the special boundary elements must extend horizontally from the extreme compression fiber a distance equal to the greater of the following:

Greater between $c - 0.1\ l_w = 23.01\ in$ and $\frac{c}{2} = 29.51\ in$

Therefore, using a BE length of $l_{be} = 69.0\ in$ satisfies this requirement.

Check the width of the flexural compression zone

The laterally unsupported wall height corresponds to the eight of the 1st story $h_u := 15\ ft$

$b = 30.00\ in > \frac{h_u}{16} = 11.25\ in$ --> ACI 318-19 18.10.6.4(b) is satisfied

$\frac{c}{l_w} = 0.16 < \frac{3}{8} = 0.38$ --> ACI 318-19 18.10.6.4(c) does not apply

Transverse reinforcement in the Special BE

The provided vertical spacing is $s := 3.5\ in$, and the largest distance (centerline to centerline) between laterally restrained longitudinal bars is $h_x := 6.0\ in$.

First, we check the requirements of ACI 318-19 18.10.6.4(e). The maximum vertical spacing of the special boundary element transverse reinforcement is equal to the following:

s_{max} = lesser of

- $\frac{b}{3} = 10.0\ in$
- $\frac{l_{be}}{3} = 23.0\ in$
- For grade 80 bars, lesser of $5\ d_b = 5.64\ in$ or $6\ in$ --> use 5.6
- $s_o := 4 + \left(\frac{14 - \frac{h_x}{in}}{3}\right) = 6.67$ shall be within $[4\ in, 6\ in]$ --> use 6.0

Because $s = 3.50\ in$, ACI 318-19 18.10.6.4(e) is satisfied.

#5 perimetral hoop, one 135-degree #4 crosstie in the longitudinal direction and ten #4 crossties in the transvese direction. For #4 bars: $A_{\#4} = 0.20\ in^2$ and $d_{\#4} := 0.5\ in$; for #5 bars: $A_{\#5} := 0.31\ in^2$ and $d_{\#5} := 0.625\ in$.

$b = 30.00\ in$

$l_{be} = 69.00\ in$

$b_{c1} := l_{be} - 3\ in + 2 \cdot \left(d_{\#5} + \frac{d_{\#9}}{2} \right) = 68.38\ in$

$b_{c2} := b - 2 \cdot (3\ in) + 2 \cdot \left(d_{\#5} + \frac{d_{\#9}}{2} \right) = 26.38\ in$

$A_{g.be} := b \cdot l_{be} = 2070.00\ in^2$

$A_{ch} := b_{c1} \cdot b_{c2} = 1803.67\ in^2$

According to ACI 318-19 18.10.6.4(g), the minimum amount of transverse reinforcement is:

$\frac{A_{sh}}{s \cdot b_c}$ = greater of $\begin{cases} 0.3 \cdot \left(\frac{A_{g.be}}{A_{ch}} - 1 \right) \cdot \frac{f'_c}{f_y} = 0.00369 \\ 0.09 \cdot \frac{f'_c}{f_y} = 0.00750 \end{cases}$

Therefore, the minimum BE transverse reinforcements are:

When doing a X-X cut: $A_{sh.minXX} := 0.0075 \cdot s \cdot b_{c1} = 1.79\ in^2$

When doing a Y-Y cut: $A_{sh.minYY} := 0.0075 \cdot s \cdot b_{c2} = 0.69\ in^2$

And the provided BE transverse reinforcements are:

When doing a X-X cut: $A_{sh.XX} := 2 \cdot A_{\#5} + 10 \cdot A_{\#4} = 2.62\ in^2$

When doing a Y-Y cut: $A_{sh.YY} := 2 \cdot A_{\#5} + A_{\#4} = 0.82\ in^2$

Thus, the minimum requirements for the amount of transverse reinforcement in the BE are satisfied.

Flexural Strength Verification - Stories 5 & 6

Demand

Minimum axial load: $P_{min} := 938\ kip$

Maximum axial load: $P_{max} := 2379\ kip$

Shear: $V_u := 570\ kip$

Moment: $M_u := 29496\ kip \cdot ft$

Web: #4 @ 5.3 in both directions

#4 rebar $A_{\#4} = 0.20\ in^2$

Spacing $s_w := 5.3\ in$

Reinf. ratio $\rho_w := \frac{2 \cdot A_{\#4}}{s_w \cdot t_w} = 0.25\%$

Boundary Element: 18 #9

#9 rebar - area $A_{\#9} = 1.00\ in^2$

#9 rebar - diam. $d_{\#9} = 1.128\ in$ ($d_b := d_{\#9}$)

Length of BE $l_{be} = 39.00\ in$

Width of BE $b := t_w = 30.00\ in$

Reinf. ratio $\rho_{l.end} := \frac{18 \cdot A_{\#9}}{(l_{be} + 3\ in) \cdot t_w} = 1.43\%$

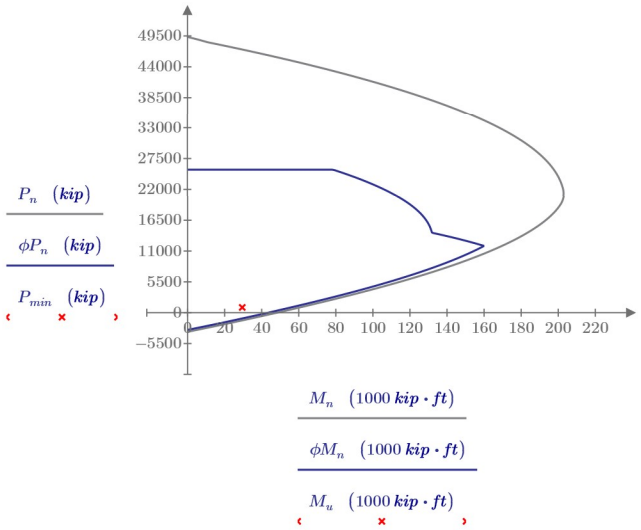

Verification of flexural strength for $P_{min} = 938\ kip$ and $M_u = 29496\ kip \cdot ft$

From the sectional analysis, the largest neutral axis depth (associated with the largest axial load) is $c := c_{Pmax} = 59.0\ in$ at the critical section.

Becasue $\rho_{l.end} = 0.0143$ > $\frac{400\ psi}{f_y} = 0.0067$, the transverse reinforcement in accordance with ACI 18.10.6.5 is required at the ends of the wall:

> Boundary transverse reinforcement shall satisfy the requirements 18.7.5.2(a) through (e) over the greater of $c - 0.1\ l_w = 23.01\ in$ and $\frac{c}{2} = 30\ in$
>
> Because the section above the 7th story is not expected to yield (i.e., outside the length of the plastic hinge length calculated before), the maximum spacing of the transverse reinforcement is equal to the lesser of the following for Grade 80 reinforcement:
>
> $s_{max} := min(6\ d_b, 6\ in) = 6.00\ in$

Following transversal reinforcement over an horizontal wall segment of $l_{be} = 39\ in$ satisfies all above requirements:

> One #4 perimetral hoop
> One #4 crosstie inthe longitudinal direcction
> Four #4 crossties in the transvese direction

Also, above the cut-off point we have that $\rho_{l.end} = 0.0143$ > $\frac{1}{2}\left(6\frac{\sqrt{f'_c \cdot psi}}{f_y}\right) = 0.0035$. Therefore, S. 18.19.2.4(c) is satisfied.

Because $V_u = 570\ kip < \lambda \cdot \sqrt{f'_c \cdot psi} \cdot A_{cv} = 764\ kip$, ACI 18.10.6.5 does not need to be satisfied, i.e., the horizontal reinforcement does not need to terminate with hook.

Flexural Strength Verification - Stories 7 & 8

Demand

Minimum axial load: $P_{min} := 306\ kip$

Maximum axial load: $P_{max} := 773\ kip$

Shear: $V_u := 548\ kip$

Moment: $M_u := 10879\ kip \cdot ft$

Web: #4 @ 5.3 in both directions

#4 rebar $A_{\#4} = 0.20\ in^2$

Spacing $s_w = 0.13\ m$

Reinf. ratio $\rho_w = 0.25\%$

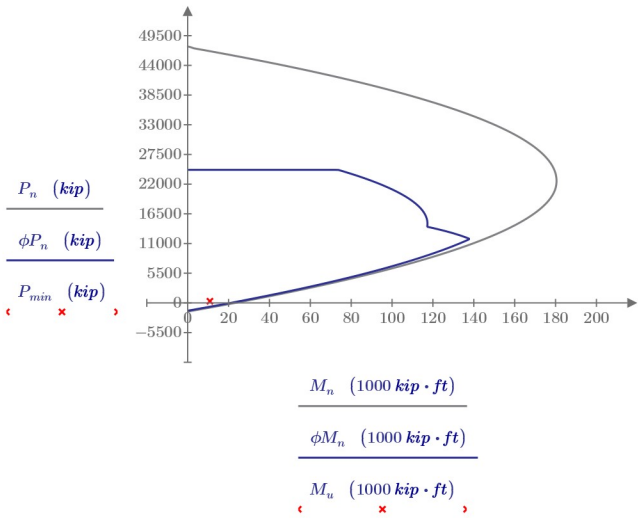

Verification of flexural strength for $P_{min} = 306\ kip$ and $M_u = 10879\ kip \cdot ft$

Because $\rho_w = 0.0025$ < $\frac{400\ psi}{f_y} = 0.0067$, the transverse reinforcement in accordance with ACI 18.10.6.5(b) is not required.

Because $V_u = 548\ kip < \lambda \cdot \sqrt{f'_c \cdot psi} \cdot A_{cv} = 764\ kip$, ACI 18.10.6.5 does not need to be satisfied, i.e., the horizontal reinforcement in the last story does not need to terminate with hook.

B.3 Wall Sketches

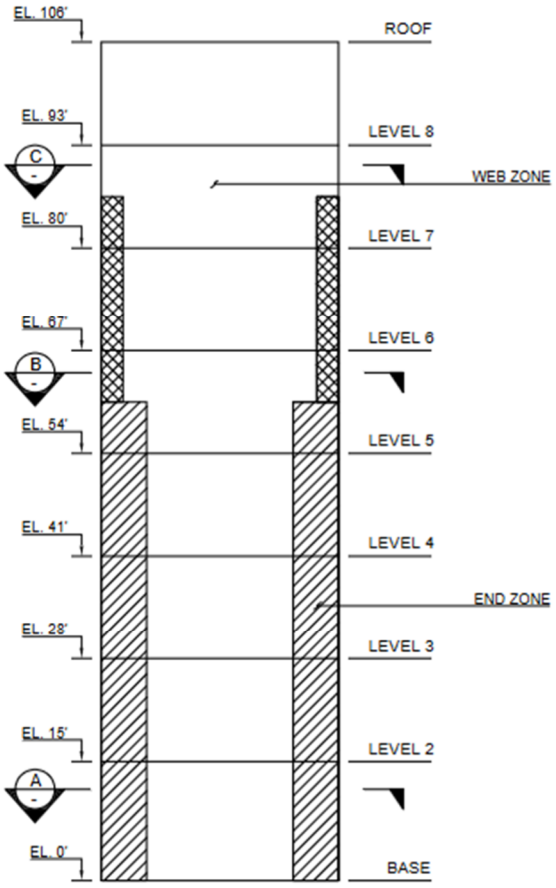

WALL - SCHEMATIC ELEVATION VIEW

LEVEL	STORY	HEIGHT (FT)	WEB ZONE	WALL END ZONE
ROOF	8	106	2-#4 @ 5.3" V 2-#4 @ 5.3" H	-
8	7	93		
7	6	80	2-#4 @ 5.3" V 2-#4 @ 5.3" H	39" x 24" 18 - #9 HOOPS AND CROSSTIES @ 6.0"
6	5	67		
5	4	54	2-#4 @ 5.3" V 2-#5 @ 4.75" H	69" x 30" 36 - #9 HOOPS AND CROSSTIES @ 3.5"
4	3	41		
3	2	28		
2	1	15		

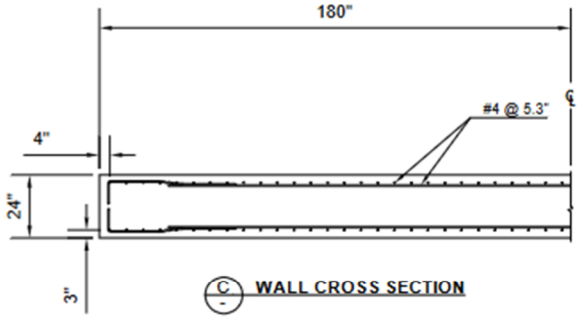

C WALL CROSS SECTION

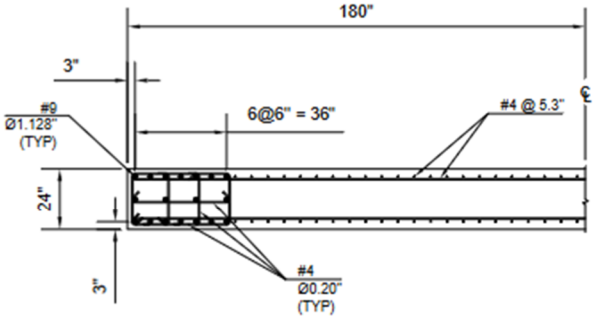

B WALL CROSS SECTION

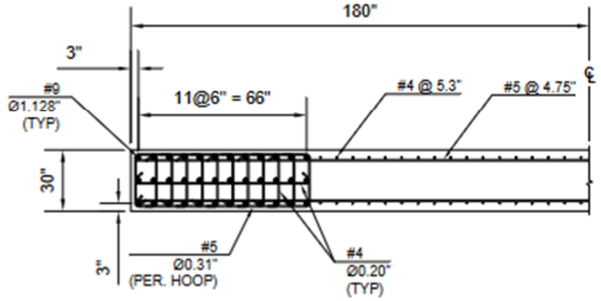

A WALL CROSS SECTION

NOTES:

CROSSTIES IN THE WEB ARE NOT SHOWN

THE DRAWING OF THE DETAILING OF THE BOUNDARY ELEMENT MIGHT NOT SATISFY ALL ACI 318-19 REQUIREMENTS, HOWEVER THE PURPOSE OF PROVIDING ENOUGH TRANSVERSE STEEL AND ESTIMATE THE CORRESPONDING CONFINEMENT IS MET.

B.4 Expected Concrete Stress-Strain Relationship

Materials

#4 and #5 Hoops and Crossties:

Diameter: $d_{bt.n4} := 0.5\ in$ $d_{bt.n5} := 0.625\ in$

Area: $A_{st.n4} := 0.2\ in^2$ $A_{st.n5} := 0.31\ in^2$

Expected yield Stress: $f_{yt} := 70\ ksi$

Steel for Longitudinal Bars (#9)

Diameter: $d_{b1} := 1.128\ in$

Area: $A_{s1} := 1.00\ in^2$

Yield Stress: $f_{y1} := 70\ ksi$

Concrete

Expected unconfined concrete strength $f'_{co} := 1.3 \cdot 5000\ psi = 6500\ psi$

Modulus of elasticity $E_c := 57000 \cdot \sqrt{f'_{co} \cdot psi} = 4595\ ksi$

Strain related to f'_c $\varepsilon_{co} := \frac{2 \cdot f'_{co}}{E_c} = 0.0028$

Saatciougly & Razvi Model

(a) Unconfined Concrete

Strain at maximum concrete compressive strength $\varepsilon_{01} := \varepsilon_{co} = 0.0028$

When specific information is not available, the authors of this model reccomend to use $\varepsilon_{085} := 0.0038$

Strain at which the descending branch touches the X axis $\varepsilon_{cf} := \frac{(\varepsilon_{085} - \varepsilon_{co})}{0.15} + \varepsilon_{co}$ $\varepsilon_{cf} = 0.0093$

Stress-strain relation for confined concrete
(This also recovers the Hognestad expression)

$$f_{c.SR.1}(\varepsilon_c) := \begin{cases} f'_{co} \cdot \left(\frac{2 \cdot \varepsilon_c}{\varepsilon_{01}} - \left(\frac{\varepsilon_c}{\varepsilon_{01}}\right)^2\right) & \text{if } 0 \le \varepsilon_c \le \varepsilon_{01} \\ f'_{co} \cdot \left(1 - 0.15 \cdot \frac{\varepsilon_c - \varepsilon_{01}}{\varepsilon_{085} - \varepsilon_{01}}\right) & \text{else if } \varepsilon_{01} < \varepsilon_c \le \varepsilon_{cf} \\ 0 & \text{else} \end{cases}$$

(b) Confined Concrete in Stories 1, 2, 3 & 4

Dimension to centerline of outermost hoop, in X direction

$b_{cx} := 69\ in + d_{b1} + d_{bt.n5}$ $\quad b_{cx} = 70.75\ in$

Dimension to centerline of outermost hoop, in Y direction

$b_{cy} := 30\ in - 2 \cdot 3\ in + d_{b1} + d_{bt.n5}$ $\quad b_{cy} = 25.75\ in$

Dimension between laterally supported vertical bars, in X dir.

$s_{lx} := 6.0\ in$ $\quad s_{lx} = 6\ in$

Dimension between laterally supported vertical bars, in Y dir.

$s_{ly} := \frac{30\ in - 2 \cdot 3\ in}{2}$ $\quad s_{ly} = 12\ in$

Vertical spacing of hoops

$s := 3.5\ in$

# of hoops or crossties that appear when doing a X-X cut

$n_{y.n4} := 10$ $\quad n_{y.n5} := 2$

# of hoops or crossties that appear when doing a Y-Y cut

$n_{x.n4} := 1$ $\quad n_{x.n5} := 2$

More parameters required to obtained the maximum confined stress:

$f_{lx} := \frac{\left(n_{y.n4} \cdot A_{st.n4} + n_{y.n5} \cdot A_{st.n5}\right) \cdot f_{yt}}{s \cdot b_{cx}}$ $\quad f_{lx} = 0.741\ ksi$

$f_{ly} := \frac{\left(n_{x.n5} \cdot A_{st.n5} + n_{x.n4} \cdot A_{st.n4}\right) \cdot f_{yt}}{s \cdot b_{cy}}$ $\quad f_{ly} = 0.637\ ksi$

$k_{2x} := min\left(0.099 \cdot \sqrt[2]{\frac{{b_{cx}}^2}{s \cdot s_{lx} \cdot \frac{f_{lx}}{ksi}}}, 1\right)$ $\quad k_{2x} = 1$

$k_{2y} := min\left(0.099 \cdot \sqrt[2]{\frac{{b_{cy}}^2}{s \cdot s_{ly} \cdot \frac{f_{ly}}{ksi}}}, 1\right)$ $\quad k_{2y} = 0.493$

$f_{lex} := k_{2x} \cdot f_{lx}$ $\quad f_{lex} = 0.741\ ksi$

$f_{ley} := k_{2y} \cdot f_{ly}$ $\quad f_{ley} = 0.314\ ksi$

$f_{le} := \frac{f_{lex} \cdot b_{cx} + f_{ley} \cdot b_{cy}}{b_{cx} + b_{cy}}$ $\quad f_{le} = 0.627\ ksi$

$k_1 := 4.825 \cdot \left(\frac{f_{le}}{ksi}\right)^{-0.17}$ $\quad k_1 = 5.224$

Maximum confined stress

$f'_{cc} := f'_{co} + k_1 \cdot f_{le}$ $\quad f'_{cc} = 9.774\ ksi$

More parameters required to obtain the confined stress-strain curve:

$K := k_1 \cdot \frac{f_{le}}{f'_{co}}$ $\quad K = 0.504$

Volumetric ratio

$\rho := \frac{n_{y.n4} \cdot A_{st.n4} + n_{y.n5} \cdot A_{st.n5} + n_{x.n5} \cdot A_{st.n5}}{s \cdot \left(b_{cx} + b_{cy}\right)}$ $\quad \rho = 0.01$

$$\varepsilon_1 := \varepsilon_{01} \cdot (1 + 5 \cdot K) \qquad \varepsilon_1 = 0.00995$$

$$\varepsilon_{85} := 260 \cdot \rho \cdot \varepsilon_1 + \varepsilon_{085} \qquad \varepsilon_{85} = 0.0286$$

Strain at which is reached the residual stress

$$\varepsilon_{c.res} := \frac{0.8\ (\varepsilon_{85} - \varepsilon_1)}{0.15} + \varepsilon_1 \qquad \varepsilon_{c.res} = 0.1095$$

Residual Stress

$$f_{res} := 0.2 \cdot f'_{cc} \qquad f_{res} = 1.955\ ksi$$

Stress-strain relation for confined concrete

$$f_{cc.SR.1}(\varepsilon_c) := \begin{cases} \text{if } 0 \le \varepsilon_c \le \varepsilon_1 \\ \quad f'_{cc} \cdot \left(\dfrac{2 \cdot \varepsilon_c}{\varepsilon_1} - \left(\dfrac{\varepsilon_c}{\varepsilon_1} \right)^2 \right)^{\frac{1}{1 + 2 \cdot K}} \\ \text{else if } \varepsilon_1 < \varepsilon_c \le \varepsilon_{c.res} \\ \quad f'_{cc} \cdot \left(1 - 0.15 \cdot \dfrac{\varepsilon_c - \varepsilon_1}{\varepsilon_{85} - \varepsilon_1} \right) \\ \text{else} \\ \quad f_{res} \end{cases}$$

(c) Confined Concrete in Stories 5 & 6

Dimension to centerline of outermost hoop, in X direction

$$b_{cx} := 39\ in + d_{b1} + d_{bt.n4} \qquad b_{cx} = 40.63\ in$$

Dimension to centerline of outermost hoop, in Y direction

$$b_{cy} := 30\ in - 2 \cdot 3\ in + d_{b1} + d_{bt.n4} \qquad b_{cy} = 25.63\ in$$

Dimension between laterally supported vertical bars, in X dir.

$$s_{lx} := 12.0\ in \qquad s_{lx} = 12\ in$$

Dimension between laterally supported vertical bars, in Y dir.

$$s_{ly} := \frac{30\ in - 2 \cdot 3\ in}{2} \qquad s_{ly} = 12\ in$$

Vertical spacing of hoops

$$s := 6.0\ in$$

# of hoops or crossties that appear when doing a X-X cut

$$n_y := 4$$

# of hoops or crossties that appear when doing a Y-Y cut

$$n_x := 3$$

More parameters required to obtained the maximum confined stress:

$$f_{lx} := \frac{n_y \cdot A_{st.n4} \cdot f_{yt}}{s \cdot b_{cx}} \qquad f_{lx} = 0.23\ ksi$$

$$f_{ly} := \frac{n_x \cdot A_{st.n4} \cdot f_{yt}}{s \cdot b_{cy}} \qquad f_{ly} = 0.273\ ksi$$

$$k_{2x} := min\left(0.099 \cdot \sqrt[2]{\frac{{b_{cx}}^2}{s \cdot s_{lx} \cdot \frac{f_{lx}}{ksi}}}, 1 \right) \qquad k_{2x} = 0.989$$

$$k_{2y} := min\left(0.099 \cdot \sqrt[2]{\frac{{b_{cy}}^2}{s \cdot s_{ly} \cdot \frac{f_{ly}}{ksi}}}, 1\right) \qquad k_{2y} = 0.572$$

$$f_{lex} := k_{2x} \cdot f_{lx} \qquad f_{lex} = 0.227\ ksi$$

$$f_{ley} := k_{2y} \cdot f_{ly} \qquad f_{ley} = 0.156\ ksi$$

$$f_{le} := \frac{f_{lex} \cdot b_{cx} + f_{ley} \cdot b_{cy}}{b_{cx} + b_{cy}} \qquad f_{le} = 0.2\ ksi$$

$$k_1 := 4.825 \cdot \left(\frac{f_{le}}{ksi}\right)^{-0.17} \qquad k_1 = 6.345$$

Maximum confined stress

$$f'_{cc} := f'_{co} + k_1 \cdot f_{le} \qquad f'_{cc} = 7.767\ ksi$$

More parameters required to obtain the confined stress-strain curve:

$$K := k_1 \cdot \frac{f_{le}}{f'_{co}} \qquad K = 0.195$$

Volumetric ratio

$$\rho := \frac{(n_y + n_x) \cdot A_{st.n4}}{s \cdot (b_{cx} + b_{cy})} \qquad \rho = 0.004$$

$$\varepsilon_1 := \varepsilon_{01} \cdot (1 + 5 \cdot K) \qquad \varepsilon_1 = 0.00559$$

$$\varepsilon_{85} := 260 \cdot \rho \cdot \varepsilon_1 + \varepsilon_{085} \qquad \varepsilon_{85} = 0.0089$$

Strain at which is reached the residual stress

$$\varepsilon_{c.res} := \frac{0.8\ (\varepsilon_{85} - \varepsilon_1)}{0.15} + \varepsilon_1 \qquad \varepsilon_{c.res} = 0.0233$$

Residual Stress

$$f_{res} := 0.2 \cdot f'_{cc} \qquad f_{res} = 1.553\ ksi$$

Stress-strain relation for confined concrete

$$f_{cc.SR.2}(\varepsilon_c) := \begin{array}{l} \text{if } 0 \le \varepsilon_c \le \varepsilon_1 \\ \quad \left\| f'_{cc} \cdot \left(\frac{2 \cdot \varepsilon_c}{\varepsilon_1} - \left(\frac{\varepsilon_c}{\varepsilon_1}\right)^2\right)^{\frac{1}{1 + 2 \cdot K}} \right. \\ \text{else if } \varepsilon_1 < \varepsilon_c \le \varepsilon_{c.res} \\ \quad \left\| f'_{cc} \cdot \left(1 - 0.15 \cdot \frac{\varepsilon_c - \varepsilon_1}{\varepsilon_{85} - \varepsilon_1}\right) \right. \\ \text{else} \\ \quad \left\| f_{res} \right. \end{array}$$

Plots

# of points $i := 1 .. 100$

Concrete strain values $\varepsilon_{c_i} := 0.002 \cdot (i - 1)$

Unconfined concrete strength $f_{c.unc_i} := f_{c.SR.1}\left(\varepsilon_{c_i}\right)$

Confined concrete strength (stories 1, 2, 3 & 4) $f_{c.conf1_i} := f_{cc.SR.1}\left(\varepsilon_{c_i}\right)$

Confined concrete strength (stories 5 & 6) $f_{c.conf2_i} := f_{cc.SR.2}\left(\varepsilon_{c_i}\right)$

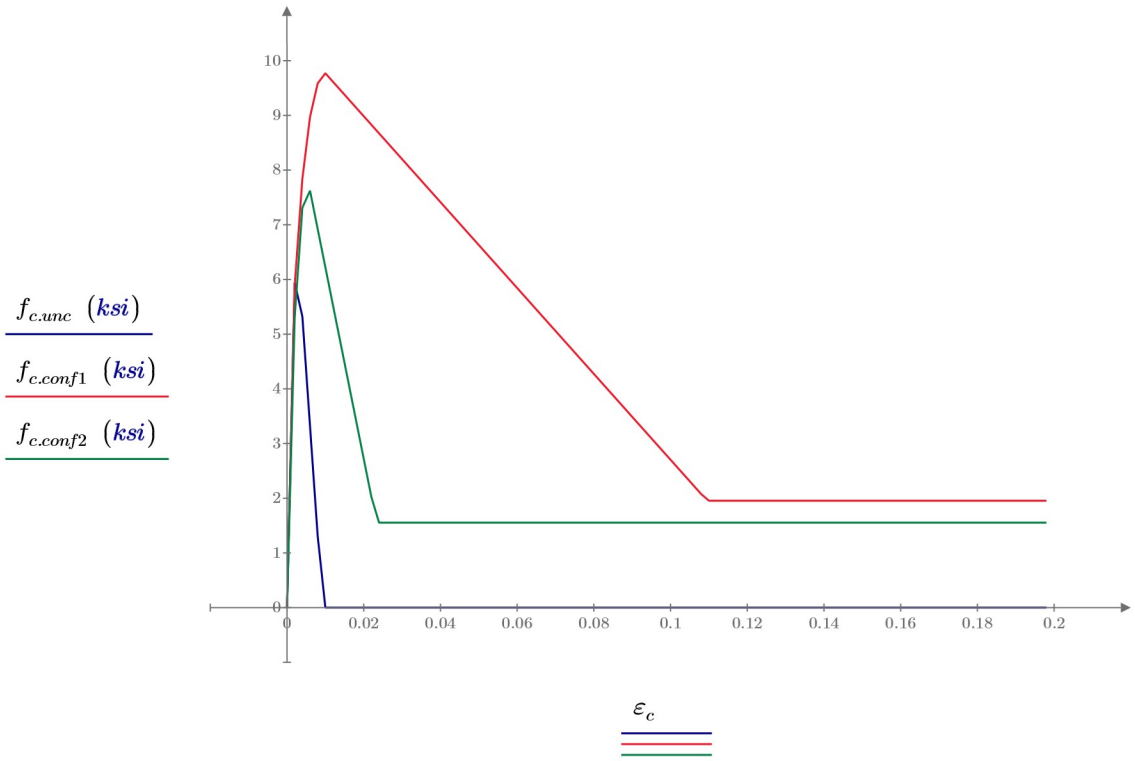

B.5 Sectional Analysis with Expected Material Properties and Δ_{roof} Capacity

Expected Material Properties

Unconfined Concrete

Max. compressive stress $f'_{c.unc} := 6.5\ ksi$

Strain at max. comp. stress $\varepsilon_{c.unc} := 0.003$

$\varepsilon_{085} := 0.0038$

Strain at which the descending branch touches the X axis $\varepsilon_{cf.unc} := \frac{(\varepsilon_{085} - \varepsilon_{c.unc})}{0.15} + \varepsilon_{c.unc}$

$$f_{c.unc}(\varepsilon_c) := \begin{cases} \text{if } 0 \le \varepsilon_c \le \varepsilon_{c.unc} \\ \quad f'_{c.unc} \cdot \left(\frac{2 \cdot \varepsilon_c}{\varepsilon_{c.unc}} - \left(\frac{\varepsilon_c}{\varepsilon_{c.unc}} \right)^2 \right) \\ \text{else if } \varepsilon_{c.unc} < \varepsilon_c \le \varepsilon_{cf.unc} \\ \quad f'_{c.unc} \cdot \left(1 - 0.15 \cdot \frac{\varepsilon_c - \varepsilon_{c.unc}}{\varepsilon_{085} - \varepsilon_{c.unc}} \right) \\ \text{else} \\ \quad 0 \end{cases}$$

Confined Concrete

Length of BE $l_{be} := 69.0\ in$

Concrete peak stress $f'_c := 9.77\ ksi$

Strain at Concrete Peak Stress $\varepsilon_{cu} := 0.0100$

Rresidual stress $f_{res} := 0.2 \cdot f'_c$

Strain at residual stress $\varepsilon_{c.res} := 0.1095$

Other parameters (S&R model) $K := 0.50$

$\varepsilon_{c85} := 0.029$

$$f_c(\varepsilon_c) := \begin{cases} \text{if } 0 \le \varepsilon_c \le \varepsilon_{cu} \\ \quad f'_c \cdot \left(\frac{2 \cdot \varepsilon_c}{\varepsilon_{cu}} - \left(\frac{\varepsilon_c}{\varepsilon_{cu}} \right)^2 \right)^{\frac{1}{1+2 \cdot K}} \\ \text{else if } \varepsilon_{cu} < \varepsilon_c \le \varepsilon_{c.res} \\ \quad f'_c \cdot \left(1 - 0.15 \cdot \frac{\varepsilon_c - \varepsilon_{cu}}{\varepsilon_{c85} - \varepsilon_{cu}} \right) \\ \text{else if } \varepsilon_{c.res} \le \varepsilon_c \\ \quad f_{res} \\ \text{else} \\ \quad 0 \end{cases}$$

Steel

Steel yielding stress $f_y := 70\ ksi$

Elastic modulus of steel $E_s := 29000\ ksi$

Yielding Strain $\varepsilon_y := \frac{f_y}{E_s} = 0.00241$

Post-yielding slope $E_{sh} := 0.01 \cdot E_s = 290.00\ ksi$

$\varepsilon_{sh} := \varepsilon_y$

$$f_s(\varepsilon_s) := \begin{cases} \text{if } 0 \le |\varepsilon_s| \le \varepsilon_y \\ \quad E_s \cdot \varepsilon_s \\ \text{else if } \varepsilon_y < |\varepsilon_s| \le \varepsilon_{sh} \\ \quad \text{sign}(\varepsilon_s) \cdot f_y \\ \text{else if } \varepsilon_{sh} < |\varepsilon_s| \le 0.3 \\ \quad \text{sign}(\varepsilon_s) \cdot (f_y + (|\varepsilon_s| - \varepsilon_{sh}) \cdot E_{sh}) \\ \text{else if } 0.3 < |\varepsilon_s| \le 0.80 \\ \quad \text{sign}(\varepsilon_s) \cdot (f_y + (0.8 - \varepsilon_{sh}) \cdot E_{sh}) \\ \text{else} \\ \quad 0 \end{cases}$$

LRFD Reduction Factor

$$\phi(\varepsilon_t) := \begin{cases} \text{if } |\varepsilon_t| \le \varepsilon_y \\ \quad 0.65 \\ \text{else if } |\varepsilon_t| \ge 0.005 \\ \quad 0.9 \\ \text{else} \\ \quad 0.65 + \frac{0.9 - 0.65}{0.005 - \varepsilon_y} \cdot (|\varepsilon_t| - \varepsilon_y) \end{cases}$$

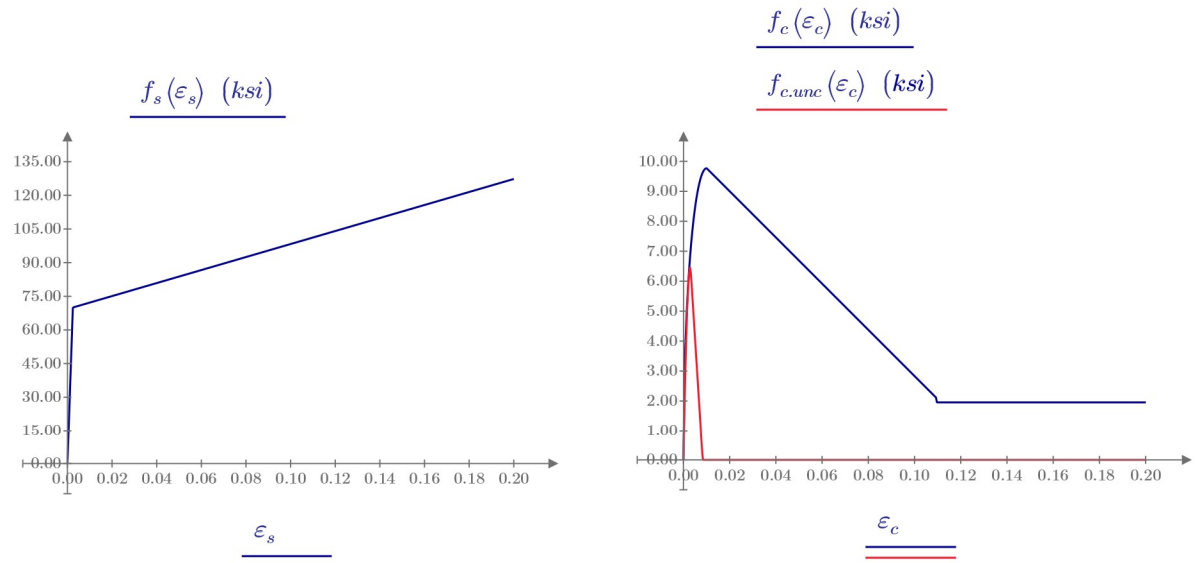

P-M Diagram & Critical Demand

Wall length	$l_w := 30\ ft$ ($h := l_w$)
Web width	$b := 30\ in$
Flange thickness	$t_{fl} := 0\ ft = 0.00\ in$
Flange total width	$b_{fl} := 0\ ft$

Moment demand: $M_u := 82299\ kip \cdot ft$

Axial demands: $P_{min} := 1584\ kip$

$P_{avg} := 2674\ kip$

$P_{max} := 4018\ kip$

Web Ver.: #4 @ 5.3

#4 rebar $A_{\#4} = 0.20\ in^2$

Spacing $s_{wv} := 5.3\ in$

Reinf. ratio $\rho_{wv} := \dfrac{2 \cdot A_{\#4}}{s_{wv} \cdot b} = 0.25\%$

Boundary Element: 36 #9

#9 rebar - area $A_{\#9} = 1.00\ in^2$

Length of BE $l_{be} = 69.00\ in$

Width of BE $b = 30.00\ in$

Reinf. ratio $\rho_{be} := \dfrac{36 \cdot A_{\#9}}{(l_{be} + 3\ in) \cdot b} = 1.67\%$

$\rho_{sb} := \dfrac{36 \cdot A_{\#9}}{A_{cv}} = 0.33\%$

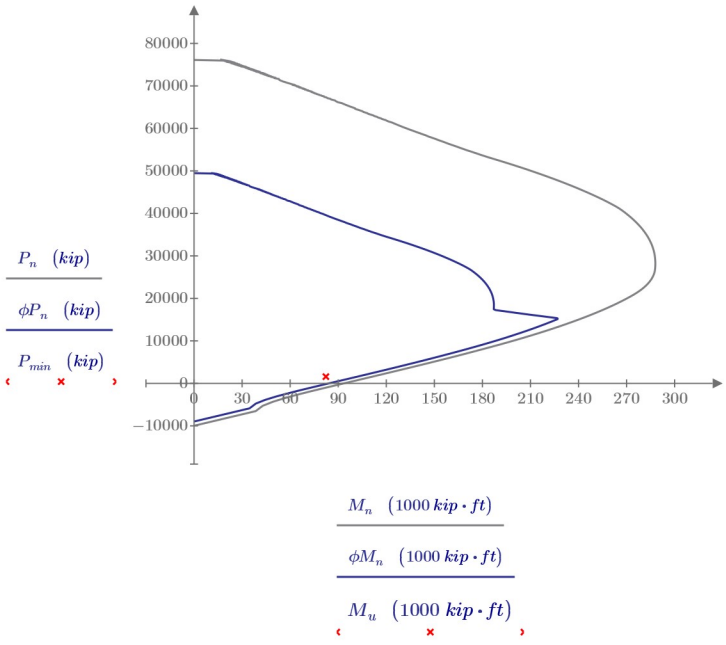

Maximum Probable Moment

Sectional analysis using expected material properties and P_{max}, which comes from (1.2+0.2SDS)DL + 0.5LL.

Story 1: Neutral axis depth $c := 48.886\ in$ (Iterate until obtain $P_{max} = 4018\ kip$)

P-M Capacity

$$P_{np} := \sum_l F_{cp_l} + \sum_i F_{sp_i} \qquad P_{np} = 4018\ kip$$

$$M_{pr} := \sum_l F_{cp_l} \cdot \left(h - y_{cp_l}\right) + \sum_i F_{sp_i} \cdot \left(h - d_i\right) - P_{np} \cdot \frac{h}{2} \qquad M_{pr} = 138168\ kip \cdot ft$$

Moment and Curvature at Yielding

Sectional analysis using expected material properties and expected axial load (DL + 0.25LL Condition)

$E_c := 57000 \cdot \sqrt{f'_c \cdot psi} = 5634.07\ ksi$

Story 1: Neutral axis depth $y := 58.38\ in$ (Iterate until obtain $P_{avg} = 2674\ kip$)

P-M Capacity

$$P_{np} := \sum_l F_{cp_l} + \sum_i F_{sp_i} \qquad P_{np} = 2674\ kip$$

$$M_{np} := \sum_l F_{cp_l} \cdot \left(h - y_{cp_l}\right) + \sum_i F_{sp_i} \cdot \left(h - d_i\right) - P_{np} \cdot \frac{h}{2} \qquad M_{np} = 96308\ kip \cdot ft$$

$$\phi_y := \frac{\varepsilon_y}{d_{N_i} - y} \qquad \phi_y = \left(9.700 \cdot 10^{-5}\right) \frac{1}{ft}$$

Expected Capacity

Sectional analysis using expected material properties and expected axial load (DL + 0.25LL Condition)

Story 1: Neutral axis depth $c := 42.384\ in$ (Iterate until obtain $P_{avg} = 2674\ kip$)

P-M Capacity

$$P_{np} := \sum_l F_{cp_l} + \sum_i F_{sp_i} \qquad P_{np} = 2674\ kip$$

$$M_{np} := \sum_l F_{cp_l} \cdot \left(h - y_{cp_l}\right) + \sum_i F_{sp_i} \cdot \left(h - d_i\right) - P_{np} \cdot \frac{h}{2} \qquad M_{np} = 123425\ kip \cdot ft$$

Design shear force with amplification factors

Maximum probable moment
(expected material properties and highest axial load) $M_{pr} = 138168\ kip \cdot ft$

Critical section at the bottom $h_{wcs} := 106\ ft$

Wall length $l_w := 30\ ft$

Shear demand $V_u := 1190\ kip$

Overstrength factor when $\frac{h_{wcs}}{l_w} = 3.53 > 1.5$: $\Omega_v := \max\left(\frac{M_{pr}}{M_u}, 1.5\right) = 1.68$

w_s when $\frac{h_{wcs}}{l_w} = 3.53 > 2.0$ and $n_s := \max\left(8, 0.007 \cdot \frac{h_{wcs}}{in}\right) = 8.90 > 6$: $\omega_v := min\left(1.3 + \frac{n_s}{30}, 1.8\right)$

$\omega_v = 1.60$

Therefore, accodring to ACI 318-19, 18.10.3.1:

$V_e := min\left(\Omega_v \cdot \omega_v \cdot V_u, 3\ V_u\right) = 3190\ kip$ $(\Omega_v \cdot \omega_v = 2.68)$

Predicted Drift Capacity

Wall length $l_w = 30.00\ ft$

Width of wall cross section $b = 30.00\ in$

Web cross-sectional area $A_{cv} := l_w \cdot b = 10800\ in^2$

Neutral axis depth at expected demand $c_e := 42.38\ in$

Maximum expected shear demand $V_e = 3190\ kip$

Nominal shear stress $v_{max} := \frac{V_e}{A_{cv}} = 295.38\ psi$

λ_b parameter $\lambda_b := \frac{l_w \cdot c_e}{b^2} = 16.95$

α parameter for combination of a single perimeter hoop with supplemental crossties $\alpha := 45$

Expected unconfined concrete strength $f'_{c.unc} = 6.50\ ksi$

Height of the wall $h_w := 106\ ft$

Roof drift capacity $\frac{\delta_c}{h_w} = 3.85 - \frac{\lambda_b}{\alpha} - \frac{v_{max}}{8 \cdot \sqrt{f'_{c.unc} \cdot psi}} = 3.02\ \%$

Deformation capcity $\delta_c := 0.0302 \cdot h_w = 38\ in$

B.6 Selection of MCE Level Ground Motions

The methodology described by Baker and Lee (2018) was implemented. The scripts developed by the authors are available in Baker's GitHub repository (link here). The period used as the input T_{cond} in **Table A.1** corresponds to the fundamental period obtained with the OpenSees model. The spectral acceleration used as target when computing the conditional spectrum, $S_a(T_{cond})$ in **Table A.1**, was obtained by interpolating T_{cond} in the Uniform Hazard Response Spectrum of the site (shown in **Figure 10.3**).

***Table B.1**: Input values used in "Main_select_motions.m" script by Baker and Lee (2018)*

Parameter	Value
Tcond	0.52
Tmin	0.01
Tmax	5
SaTcond	0.57
rup.M_bar	6.92
rup..Rjb	8.4
rup.eps_bar	1.31
rup.Vs30	760
rup.z1	999
rup.region	1
rup.Fault_Type	1
rup.Rrup	4.60
rup.Rx	4.60
rup.W	11
rup.Ztor	0
rup.Zbot	11
rup.dip	90
allowedRecs.Vs30	[560 1130]
allowedRecs.Mag	[6.2 8.2]
allowRecs.D	[0 50]

***Table B.2**: Selected ground motions for the 8-Story Archetype MCE level analysis*

Tag	RSN*	Earthquake Name	Year	Horizontal Acc. Filename Utilized	Scale Factor
EQ 801	1012	"Northridge-01"	1994	RSN1012_NORTHR_LA0180.AT2	1.72
EQ 802	1078	"Northridge-01"	1994	RSN1078_NORTHR_SSU000.AT2	2.49
EQ 803	1091	"Northridge-01"	1994	RSN1091_NORTHR_VAS090.AT2	3.87
EQ 804	1111	"Kobe_ Japan"	1995	RSN1111_KOBE_NIS000.AT2	0.6
EQ 805	1211	"Chi-Chi_ Taiwan"	1999	RSN1211_CHICHI_CHY052-N.AT2	2.52
EQ 806	1234	"Chi-Chi_ Taiwan"	1999	RSN1234_CHICHI_CHY086-E.AT2	3.05
EQ 807	1281	"Chi-Chi_ Taiwan"	1999	RSN1281_CHICHI_HWA032-N.AT2	5
EQ 808	1485	"Chi-Chi_ Taiwan"	1999	RSN1485_CHICHI_TCU045-E.AT2	0.93
EQ 809	1492	"Chi-Chi_ Taiwan"	1999	RSN1492_CHICHI_TCU052-E.AT2	2.14
EQ 810	1618	"Duzce_ Turkey"	1999	RSN1618_DUZCE_531-E.AT2	2.89
EQ 811	291	"Irpinia_ Italy-01"	1980	RSN291_ITALY_A-VLT000.AT2	4.7
EQ 812	3472	"Chi-Chi_ Taiwan-06"	1999	RSN3472_CHICHI.06_TCU076E.AT2	4.46
EQ 813	3943	"Tottori_ Japan"	2000	RSN3943_TOTTORI_SMN015NS.AT2	2.79
EQ 814	4213	"Niigata_ Japan"	2004	RSN4213_NIIGATA_NIG023NS.AT2	1.73
EQ 815	4227	"Niigata_ Japan"	2004	RSN4227_NIIGATA_NIGH10NS.AT2	3.53
EQ 816	4229	"Niigata_ Japan"	2004	RSN4229_NIIGATA_NIGH12EW.AT2	2.17
EQ 817	4455	"Montenegro_ Yugoslavia"	1979	RSN4455_MONTENE.GRO_HRZ090.AT2	4.74
EQ 818	4481	"L'Aquila_ Italy"	2009	RSN4481_L-AQUILA_FA030XTE.AT2	2.23
EQ 819	4483	"L'Aquila_ Italy"	2009	RSN4483_L-AQUILA_AM043YLN.AT2	2.72
EQ 820	4841	"Chuetsu-oki_ Japan"	2007	RSN4841_CHUETSU_65004EW.AT2	2.4
EQ 821	4842	"Chuetsu-oki_ Japan"	2007	RSN4842_CHUETSU_65005EW.AT2	2.12
EQ 822	4843	"Chuetsu-oki_ Japan"	2007	RSN4843_CHUETSU_65006EW.AT2	1.92
EQ 823	4845	"Chuetsu-oki_ Japan"	2007	RSN4845_CHUETSU_65008EW.AT2	2.8
EQ 824	4846	"Chuetsu-oki_ Japan"	2007	RSN4846_CHUETSU_65009EW.AT2	1.76
EQ 825	4854	"Chuetsu-oki_ Japan"	2007	RSN4854_CHUETSU_65020NS.AT2	4.36
EQ 826	4858	"Chuetsu-oki_ Japan"	2007	RSN4858_CHUETSU_65028NS.AT2	2.72
EQ 827	4864	"Chuetsu-oki_ Japan"	2007	RSN4864_CHUETSU_65037NS.AT2	1.59
EQ 828	4865	"Chuetsu-oki_ Japan"	2007	RSN4865_CHUETSU_65038EW.AT2	2.2
EQ 829	4868	"Chuetsu-oki_ Japan"	2007	RSN4868_CHUETSU_65041NS.AT2	1.37
EQ 830	4869	"Chuetsu-oki_ Japan"	2007	RSN4869_CHUETSU_65042EW.AT2	3.8
EQ 831	4874	"Chuetsu-oki_ Japan"	2007	RSN4874_CHUETSU_65057EW.AT2	0.72
EQ 832	4887	"Chuetsu-oki_ Japan"	2007	RSN4887_CHUETSU_6CB61EW.AT2	3.99
EQ 833	495	"Nahanni_ Canada"	1985	RSN495_NAHANNI_S1280.AT2	1.45
EQ 834	5623	"Iwate_ Japan"	2008	RSN5623_IWATE_IWT015EW.AT2	2.63
EQ 835	5806	"Iwate_ Japan"	2008	RSN5806_IWATE_55461NS.AT2	2.05
EQ 836	6928	"Darfield_ New Zealand"	2010	RSN6928_DARFIELD_LPCCN80E.AT2	2.14
EQ 837	748	"Loma Prieta"	1989	RSN748_LOMAP_BES345.AT2	3.73
EQ 838	763	"Loma Prieta"	1989	RSN763_LOMAP_GIL337.AT2	2.09
EQ 839	801	"Loma Prieta"	1989	RSN801_LOMAP_SJTE315.AT2	2.54
EQ 840	809	"Loma Prieta"	1989	RSN809_LOMAP_UC2000.AT2	4.44
EQ 841	8164	"Duzce_ Turkey"	1999	RSN8164_DUZCE_487-NS.AT2	2.36
EQ 842	957	"Northridge-01"	1994	RSN957_NORTHR_HOW060.AT2	4.11
EQ 843	989	"Northridge-01"	1994	RSN989_NORTHR_CHL070.AT2	2.04
*Record Sequential Number of the PEER NGA-West2 database					

B.7 OpenSees Analysis Results

B.7.1 Model with Expected Material Properties and Expected Axial Load

This model uses the expected material properties defined by the application of the Saatcioglu and Razvi (1992) model. The applied gravity load comes from the load combination D+0.25L.

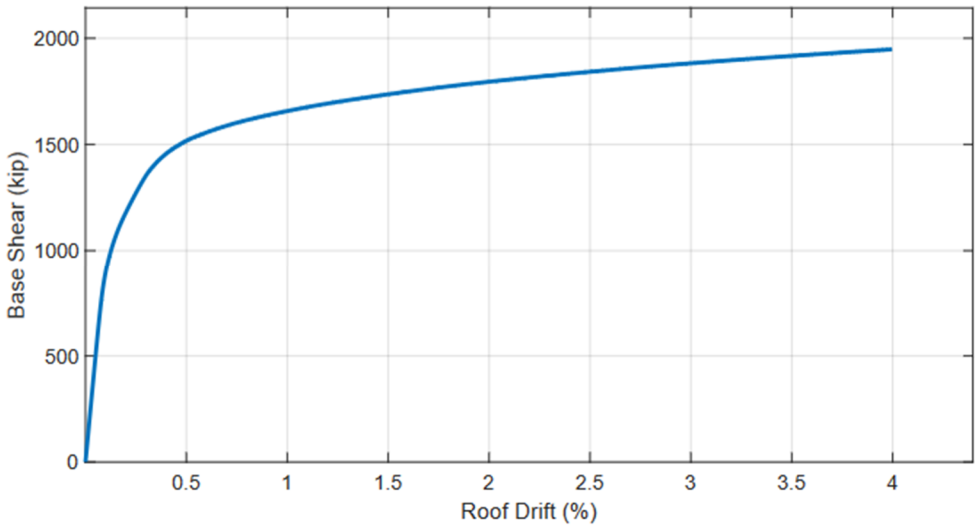

***Figure B.1**: Base shear versus roof drift – Monotonic Pushover with P_{avg} and w/o modification to expected material properties (8-Story Archetype)*

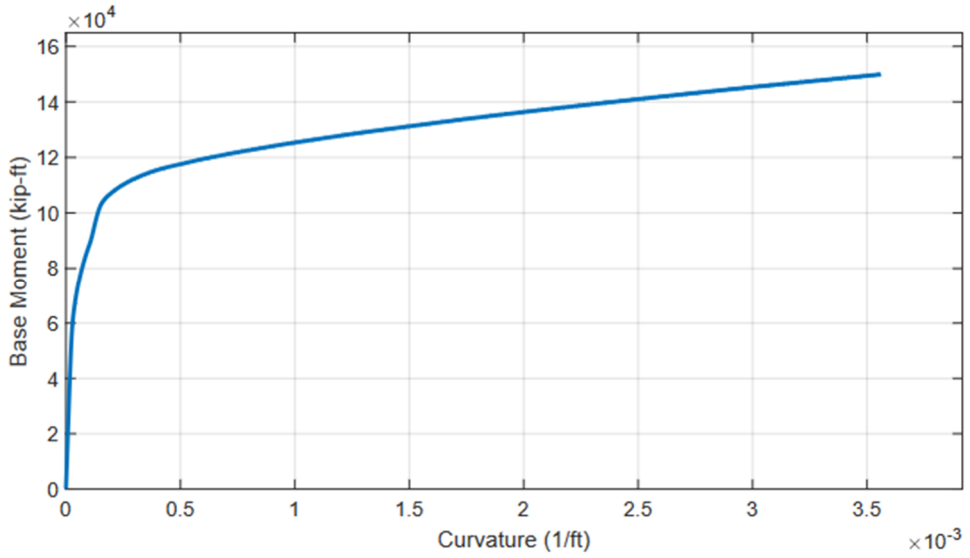

***Figure B.2**: Base moment versus curvature – Monotonic Pushover with P_{avg} and w/o modification to expected material properties (8-Story Archetype)*

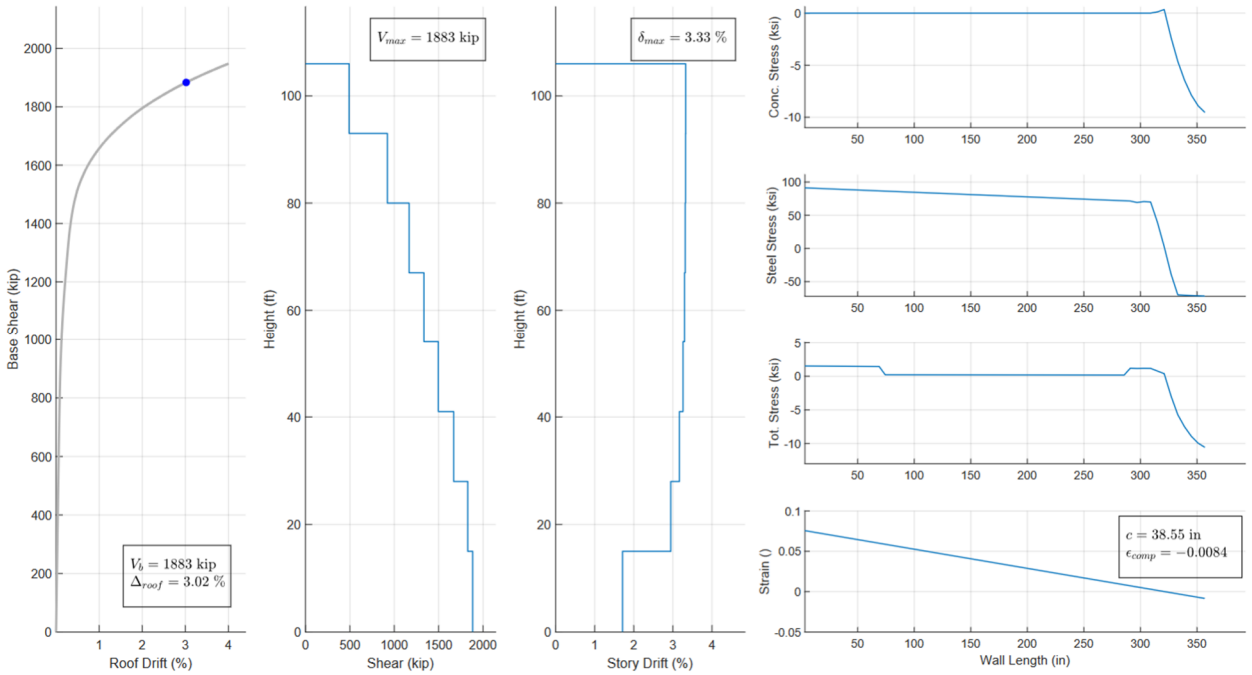

***Figure B.3**: Monotonic pushover results at predicted roof drift capacity (8-Story Archetype)*

B.7.2 Model with Modified Expected Material Properties and Expected Axial Load

B.7.2.1 Monotonic Pushover Results

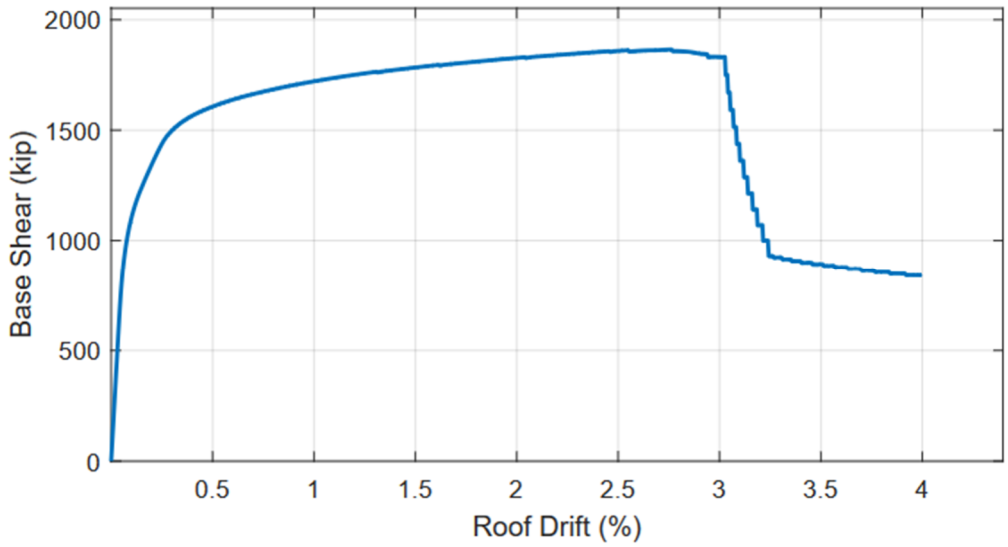

***Figure B.4**: Base shear versus roof drift – Monotonic Pushover with P_{avg} and modified expected material properties (8-Story Archetype)*

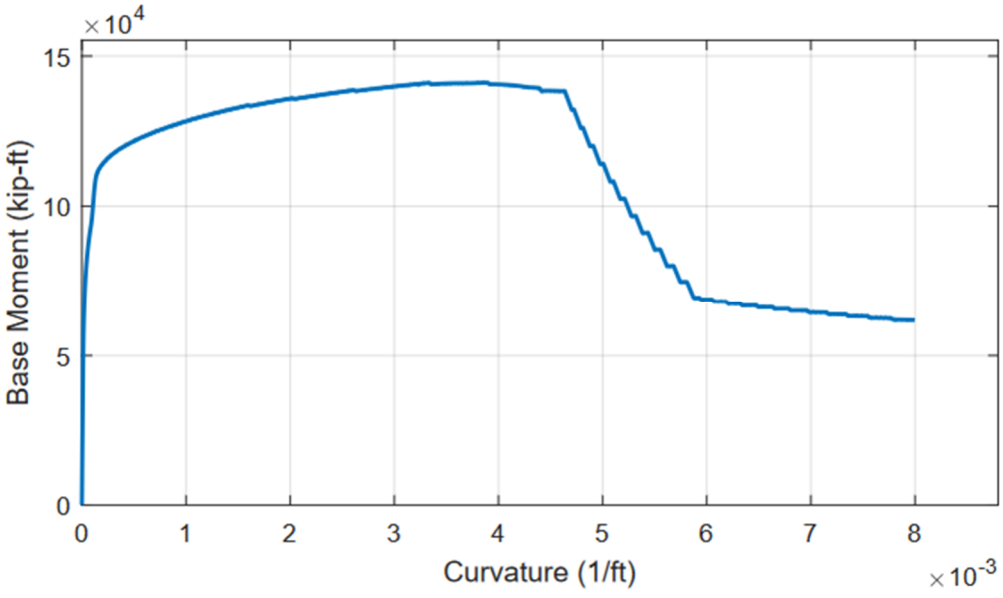

***Figure B.5**: Base moment versus curvature – Monotonic Pushover with P_{avg} and modified expected material properties (8-Story Archetype)*

B.7.2.2 Cyclic Pushover Results

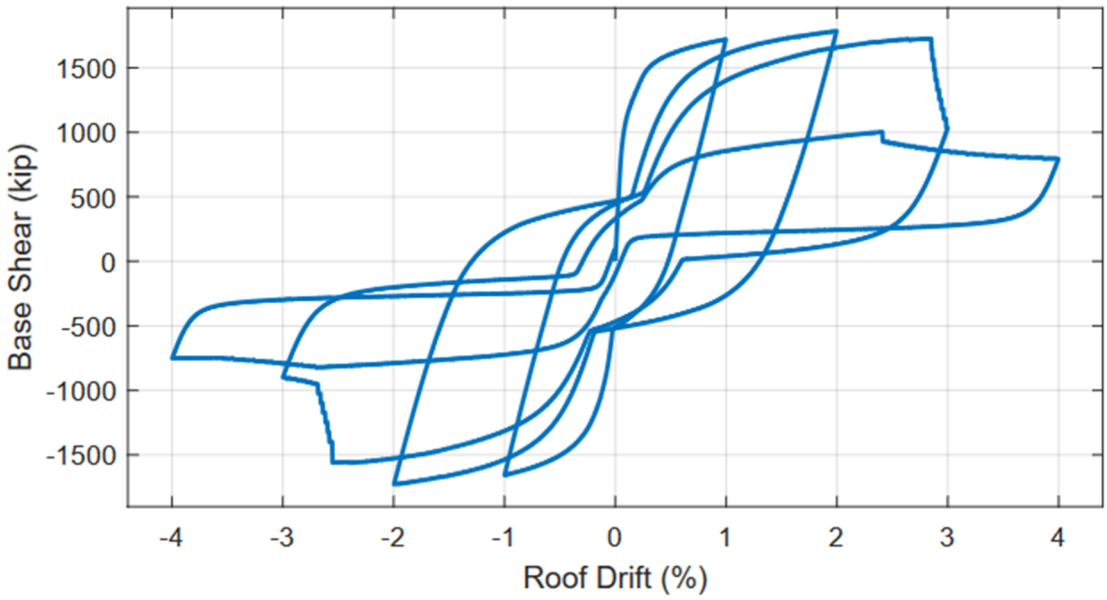

***Figure B.6**: Base shear versus roof drift – Cyclic Pushover with P_{avg} and modified expected material properties (8-Story Archetype)*

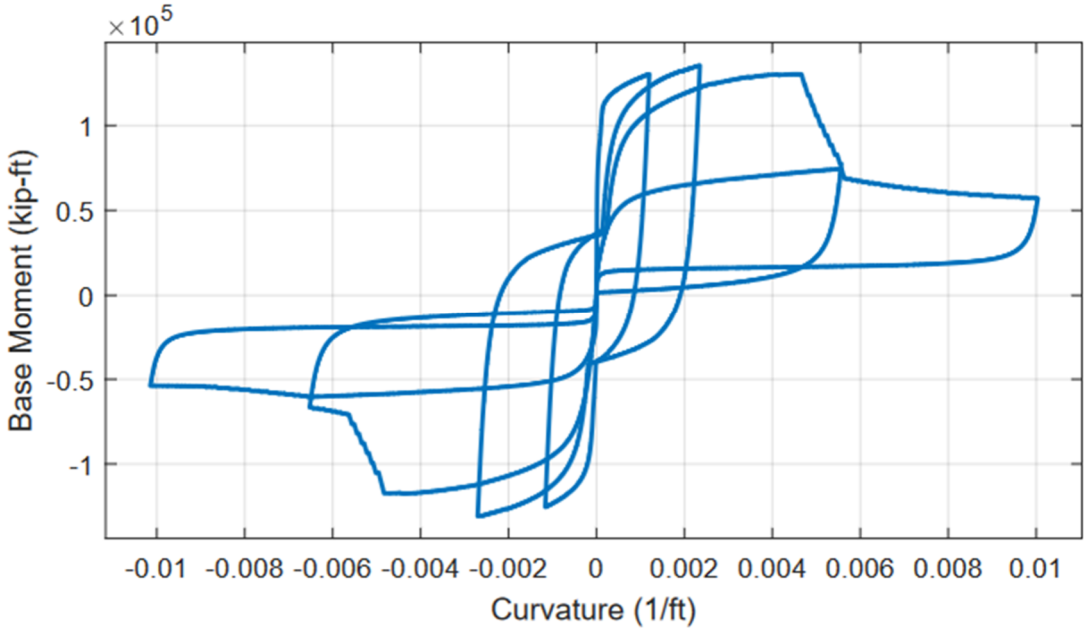

***Figure B.7**: Base moment versus Curvature – Cyclic Pushover with P_{avg} and modified expected material properties (8-Story Archetype)*

B.7.2.3 Dynamic Analysis Results – LC: (1.2+0.2SDS)D+0.25L

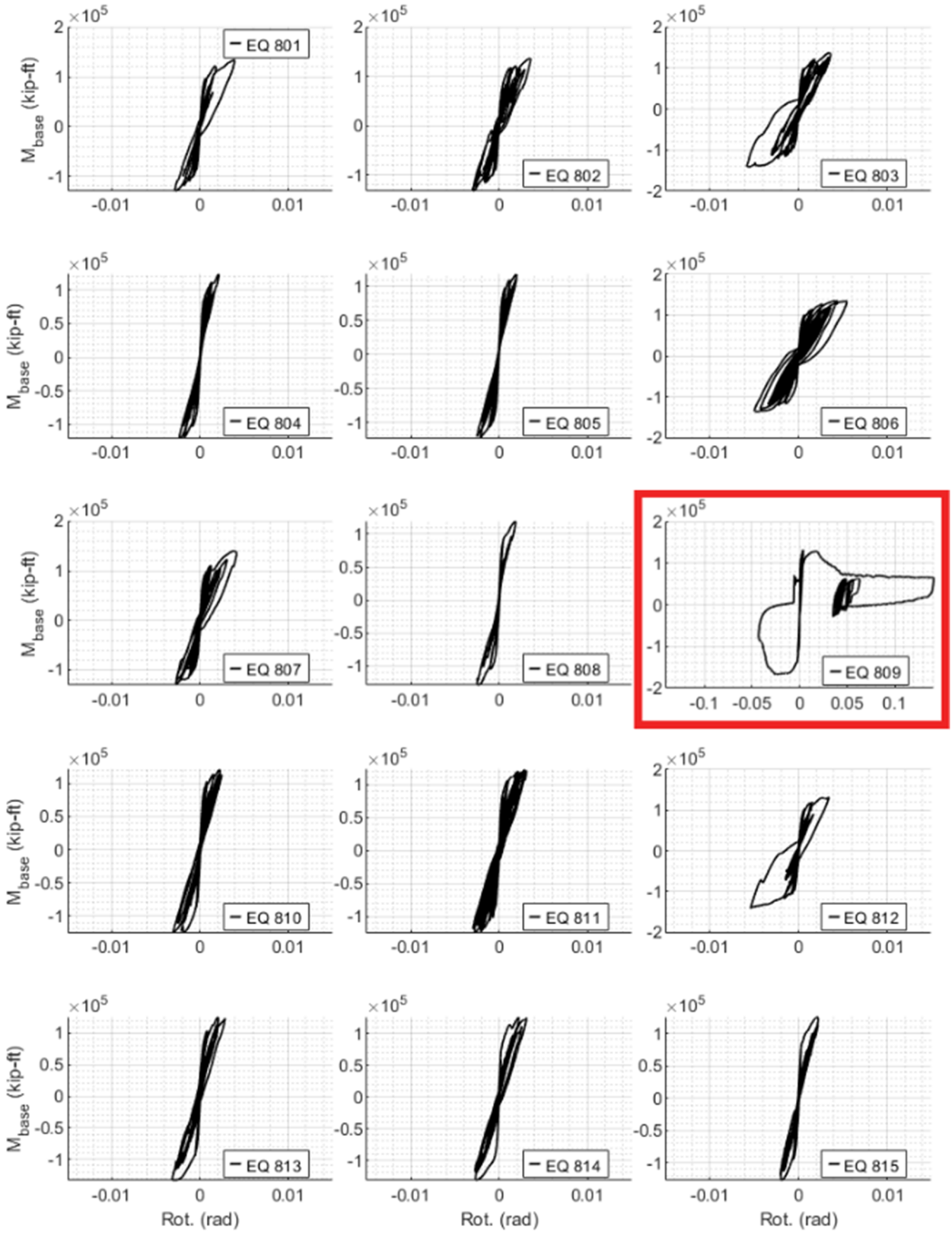

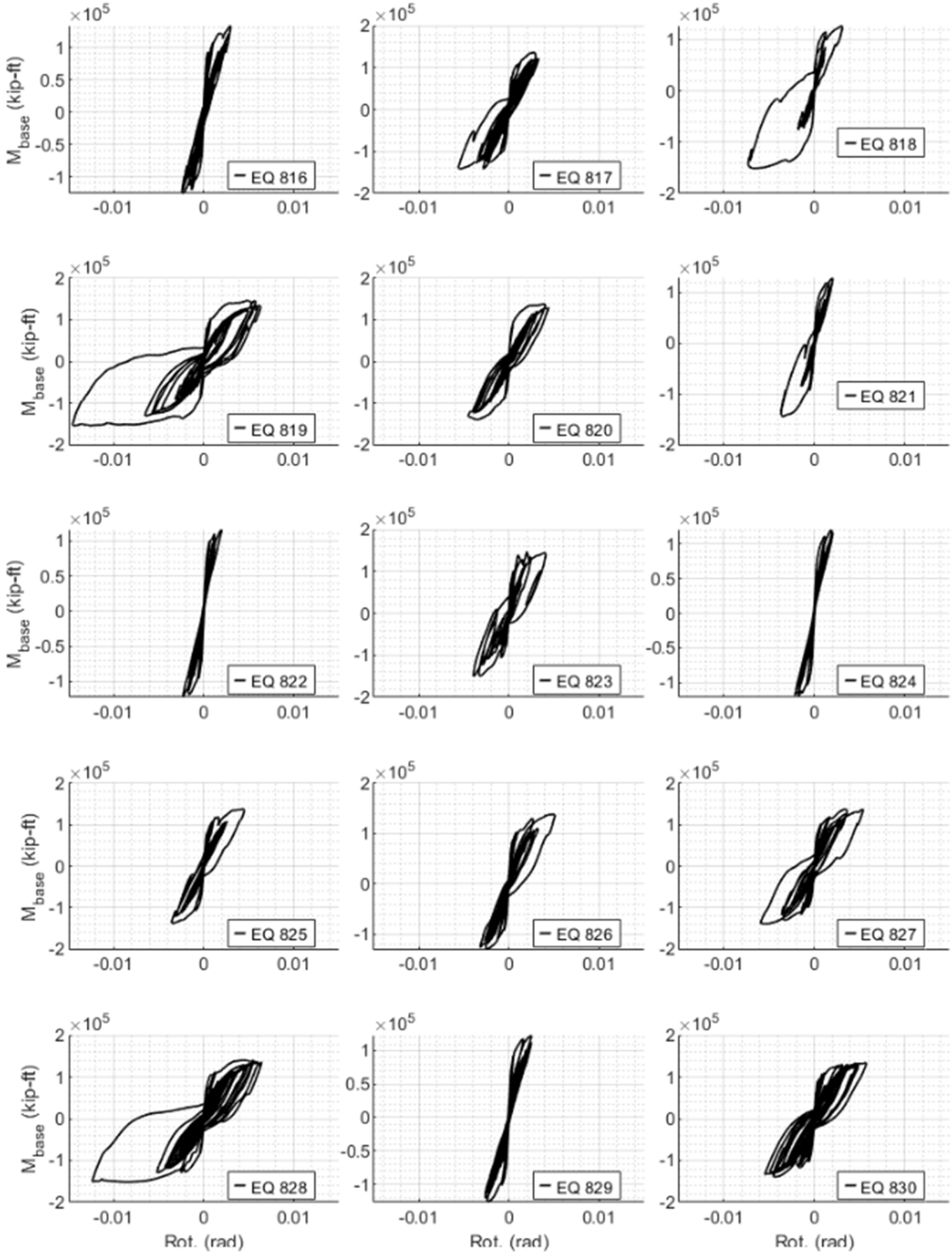
EQ 816
EQ 817
EQ 818
EQ 819
EQ 820
EQ 821
EQ 822
EQ 823
EQ 824
EQ 825
EQ 826
EQ 827
EQ 828
EQ 829
EQ 830
M_base (kip-ft)
Rot. (rad)
×10^5

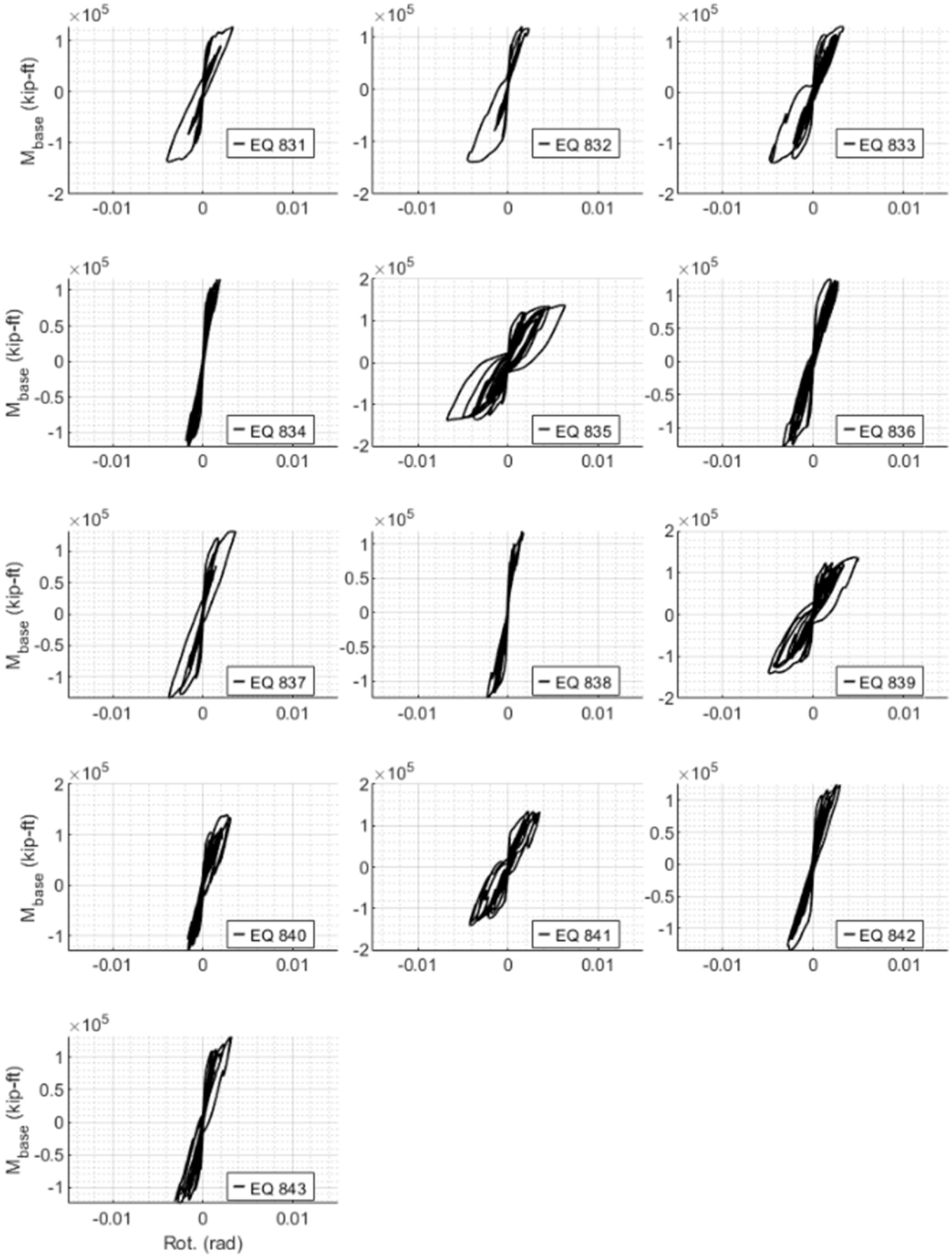
EQ 831
EQ 832
EQ 833
EQ 834
EQ 835
EQ 836
EQ 837
EQ 838
EQ 839
EQ 840
EQ 841
EQ 842
EQ 843
M_base (kip-ft)
Rot. (rad)
×10^5

Appendix C. Design and Analysis of 12-Story Archetype

Content

C.1 Analysis - Design Forces and Displacements

Building Information

- $n_s := 12$ stories.

- Story height of $h_{typ} := 13\ ft$, except for the 1st story which $h_b := 15\ ft$ high

- 120 ft x 120 ft every story

- $n_w := 4$ rectangular walls in each direction

- Center of mass and stiffness coincide (no eccentricity)

- Dead load = 175 psf (floors)
  = 140 psf (roof)

- Live load = 50 psf + 15 psf (partitions) = 65 psf (floors)
  = 20 psf + 0 psf (partitions) = 20 psf (floors)

- Risk Category II

- Site Class C

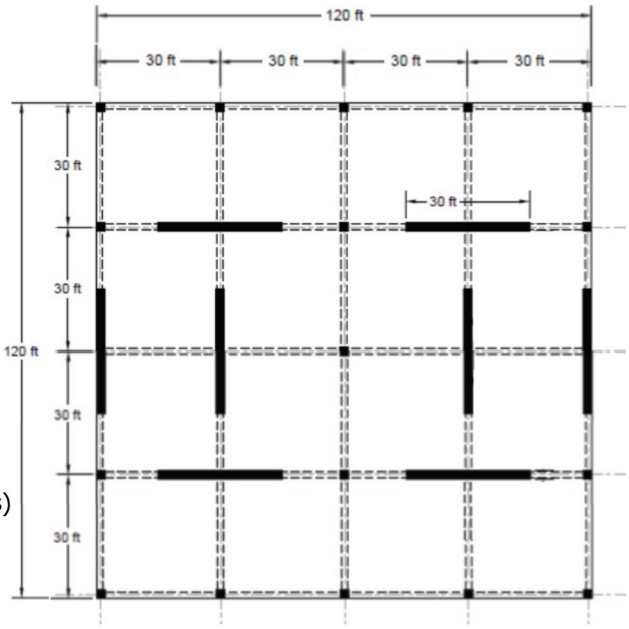

- Wall dimensions: $l_w := 30\ ft$, $t_w := 30\ in$, $t_{fl} := 0\ ft$, $b_{fl} := 0\ ft$

$$A_{cv} := l_w \cdot t_w = 10800\ in^2$$

$$A_g := t_w \cdot (l_w - 2 \cdot t_{fl}) + 2 \cdot b_{fl} \cdot t_{fl} = 10800\ in^2$$

$$A'_g := t_w \cdot (l_w - t_{fl}) + b_{fl} \cdot t_{fl} = 10800\ in^2$$

Determination of SDC

Mapped acceleration parameters

From USGS Hazard Tool Website:

Maximum considered earthquake spectral response acceleration at short periods. $S_s := 2.08\ g$

Maximum considered earthquake spectral response acceleration at a period of 1-sec. $S_1 := 0.64\ g$

Determine if the building is permitted to be automatically asigned to SDC A

Because $S_s = 2.08 > 0.15$ and $S_1 = 0.64 > 0.04$, the building is not permitted to be automatically assigned to SDC A.

Determine if the SDC is E or F

Because the Risk Category is II and $S_1 = 0.64 < 0.750$, the SDC is not E or F

Design acceleration parameters

According to ASCE 7-16:

Table 11.4-1 $F_a := 1.0$

Table 11.4-2 $F_v := 1.4$

Eq. 11.4-1 $S_{MS} := F_a \cdot S_s = 2.08$

Eq. 11.4-2 $S_{M1} := F_v \cdot S_1 = 0.90$

Eq. 11.4-3 $S_{DS} := \frac{2}{3} \cdot S_{MS} = 1.39$

Eq. 11.4-4 $S_{D1} := \frac{2}{3} \cdot S_{M1} = 0.60$

Check if the SDC can be determine by ASCE 7-16 Table 11.6-1 alone

Check if all four conditions in ASCE 7-16 11.6 are satisifed.

Structural height $h_n := \left(n_s \quad 1\right) \cdot h_{typ} + h_b = 158 \ ft$

From Table 12.8-2 $C_t := 0.02$, $x := 0.75$

Approximate fundamental period (Eq. 12.8-7) $T_a := C_t \cdot \left(\frac{h_n}{ft}\right)^x = 0.89$

T_s (S. 11.4.5) $T_s := \frac{S_{D1}}{S_{DS}} = 0.43$

Because $T_a = 0.89 \ > \ 0.8 \ T_s = 0.34$, the SDC cannot be determined by ASCE 7-16 Table 11.6-1 alone (1st condition is not satisfied)

Determine the SDC

From ASCE 7-16 Table 11.6-1 with $S_{DS} = 1.39 \ > 0.50$ and Risk Category II, the SDC is D.
From ASCE 7-16 Table 11.621 with $S_{D1} = 0.60 \ > 0.20$ and Risk Category II, the SDC is D.

Therefore, SDC is D.

Gravity Load and Mass Calculation

Gravity Load

Load combination 6 and 7 include the seismic load effects (ASCE 7-17, S. 2.3.6). These axial loads are; (LC6) 1.2D + Ev + Eh + L + 0.2S; (LC7) 0.9D - Ev + Eh. Exception No.1 of S. 2.3.6 allows the load factor on LL in LC6 to be taken as 0.5 when live load is less than 100psf. From ASCE 7-16 S. 12.4.2.2, the vertical seismic load effect shall be determined as $E_v = \left(0.2 \ S_{DS}\right) \cdot DL$. Therefore:

Gravity load from LC6: $\left(1.2 + 0.2 \ S_{DS}\right) \ DL + 0.5 \ LL$ Gravity load from LC7: $\left(0.9 - 0.2 \ S_{DS}\right) \ DL$

Tributary area of the wall: $A_{trib.wall} := 4 \cdot \left(56.25 \cdot 2 + 168.75\right) \ ft^2 - 28.125 \ ft^2 = 1097 \ ft^2$

Wall weigth:

$w_{w.r} := 0 \ kip$ (in the upper story)

$w_{w.typ} := \left(150 \ pcf\right) \cdot A_g \cdot h_{typ} = 146 \ kip$ (in a typical story)

$w_{w.b} := \left(150 \ pcf\right) \cdot A_g \cdot h_b = 169 \ kip$ (in the bottom story)

Table 1. Wall gravity load

Level	DL (psf)	LL (psf)	D+0.25L (psf)	LC6 (psf)	LC7 (psf)	Applied Vertical Load D+0.25L (kips)	Applied Vertical Load LC6 (kips)	Applied Vertical Load LC7 (kips)	Wall Axial Load D+0.25L (kips)	Wall Axial Load LC6 (kips)	Wall Axial Load LC7 (kips)
Base	0	0	0	0	0	0	0	0	4,098	6,159	2,426
2	329	65	345	518	205	379	569	225	3,719	5,591	2,201
3	308	65	325	488	192	356	535	211	3,363	5,055	1,991
4	308	65	325	488	192	356	535	211	3,007	4,520	1,780
5	308	65	325	488	192	356	535	211	2,651	3,985	1,570
6	308	65	325	488	192	356	535	211	2,295	3,450	1,359
7	308	65	325	488	192	356	535	211	1,939	2,914	1,149
8	308	65	325	488	192	356	535	211	1,583	2,379	938
9	308	65	325	488	192	356	535	211	1,227	1,844	727
10	308	65	325	488	192	356	535	211	871	1,308	517
11	308	65	325	488	192	356	535	211	515	773	306
12	308	65	325	488	192	356	535	211	159	238	96
Roof	140	20	145	217	87	159	238	96	0	0	0

Seismic Weight of the Building

Seismic weight = dead + partitions = $175\ psf + 15\ psf = 190\ psf$ (floors)

= $140\ psf + 7.5\ psf = 147.5\ psf$ (roof)

Table 2. Seismic weight and mass of the building (considering wall self weight)

Story	DL (psf)	Area (ft^2)	Seismic Weight, W_i (kips)	Seismic Mass, m_i (kips-s^2/in)
1	190	14,400	3,996	10.35
2	190	14,400	3,906	10.12
3	190	14,400	3,906	10.12
4	190	14,400	3,906	10.12
5	190	14,400	3,906	10.12
6	190	14,400	3,906	10.12
7	190	14,400	3,906	10.12
8	190	14,400	3,906	10.12
9	190	14,400	3,906	10.12
10	190	14,400	3,906	10.12
11	190	14,400	3,906	10.12
12	147.5	14,400	2,709	7.02
		Sum	**45,765**	**118.53**

Values for the model (one quarter of the building only)

	Building	Associated to one Wall
Seismic weight:	$W_{building} = 45765\ kip$	$W_t := \frac{W_{building}}{n_w} = 11441\ kip$
Seismic mass:	$M_{building} = 118.53\ \frac{kip \cdot s^2}{in}$	$M_t := \frac{M_{building}}{n_w} = 29.63\ \frac{kip \cdot s^2}{in}$

Accidental Torsion Factor

Accordingly to ASCE 7-16 S. 12.8.4.2, accidental torsion shall be calculating by displacing the center of mass each way from its actual loaction by a distance equal to 5% of the dimension of the structure perpendicular to the direction of applied forces. In this case, the floor slabs are a square of 120 ft x 120 ft. The distance between each wall and the CM is $d_{wcm} := 30\ ft$. The (base or story) shear of the building is called V_{build}, while the (base or story) shear of the wall is called V_{wall}. Therefore:

Eccentricity	$e := 0.05 \cdot (120\ ft) = 6.00\ ft$
Distance between walls and actual CM	$d_{wcm} = 30\ ft$
Stiffness of one wall	k_w (no need to actually obtain this value now)
Moment due to acc. torsion (V_{build} and V_{wall} are the building base shear and wall base shear w/o acc. torsion)	$M_{at} = e \cdot V_{build} = e \cdot (4\ V_{wall}) = 6\ k_w d_{wcm} \theta d_{wcm} + 2\ k_w (2\ d_{wcm})\ \theta\ (2\ d_{wcm})$
Rotation of the slab due to acc. torsion	$\theta_{at} = \frac{M_{at}}{14\ k_w {d_{wcm}}^2}$
Extra (+/-) shear in one wall due to acc. torsion	$V_{at} = k_w \cdot (\theta_{at} d_{wcm}) = \frac{M_{at}}{14\ d_{wcm}} = \frac{e \cdot (4\ V_{wall})}{14\ d_{wcm}} = \frac{2\ eV_{wall}}{7\ d_{wcm}}$
Total shear in one wall due to acc. torsion	$V_{Tot.Wall} = V_{wall} + \frac{2\ eV_{wall}}{7\ d_{wcm}} = \left(1 + \frac{2\ e}{7\ d_{wcm}}\right) V_{wall}$
Factor to account for acc. torsion	$k_{at} := 1 + \frac{2\ e}{7\ d_{wcm}} = 1.06$

Base Shear of the Building (ELF)

Required parameters:

Response modifiation coefficient (Table 12.2-1)	$R := 5$
Deflection amplification factor (Table 12.2-1)	$C_d := 5$
Importance factor (Table 1.5-2)	$I_e := 1.0$
Long-period transition (Fig. 22-12)	$T_L := 8$
Approximate fundamental period (already calculated)	$T_a = 0.89$

Determine the fundamental period:

Fundamental period (from modal analysis) $T := 1.75\ s$

Coefficient for upper limit for T (Table 12.8-1) $C_u := 1.4$

Upper limit for T (S. 12.8.2) $T_u := C_u \cdot T_a = 1.25\ \ s$

Therefore, the fundamental period to use is: $T := min\left(T, T_u\right) = 1.25\ \ s$

Determine the seismic coefficient:

Seismic response coefficient (Eq. 12.8-2) $C_s := \dfrac{S_{DS}}{\dfrac{R}{I_e}} = 0.28$

Upper limit for C_s, given that $T_a < T_L$ (Eq.12.8-3) $C_{s.max} := \dfrac{S_{D1}}{T \cdot \left(\dfrac{R}{I_e}\right)} = 0.10$

Lower limit for C_s, given that $T_a < T_L$ (Eq.12.8-5 and -6) $C_{s.min} := \max\left(0.044 \cdot S_{DS} \cdot I_e, \dfrac{0.5 \cdot S_1}{\dfrac{R}{I_e}}\right) = 0.064$

(Eq. 12.8-6 applies when $S_1 \geq 0.6\ g$, which is the case now)

Therefore:

Seismic coefficient to be used: $C_s := C_{s.max} = 0.10$

Seismic base shear of the wall: $V_b := C_s \cdot W_t = 1095\ \ \boldsymbol{kip}$

Seismic base shear of the wall accounting for acc. torsion: $V_b := k_{at} \cdot V_b = 1158\ \ \boldsymbol{kip}$

Modal Response Spectrum Analysis

Concrete strength $f'_c := 5000\ \ \boldsymbol{psi}$

Modulus of elasticity $E := 57000 \cdot \sqrt{f'_c \cdot \boldsymbol{psi}} = 4031\ \ \boldsymbol{ksi}$

Inertia $I_g := \dfrac{t_w \cdot \left(l_w - 2 \cdot t_{fl}\right)^3}{12} + 2 \cdot \left(\dfrac{b_{fl} \cdot {t_{fl}}^3}{12} + b_{fl} \cdot t_{fl} \cdot \left(\dfrac{l_w}{2} - \dfrac{t_{fl}}{2}\right)^2\right) = 5625\ \ \boldsymbol{ft}^4$

Eff. inertia $I_{eff} := 0.50 \cdot I_g = 2813\ \ \boldsymbol{ft}^4$

Modal periods $T := \dfrac{2\,\pi}{\omega_m}$ $T^{\mathrm{T}} = \left[1.75\ \ 0.28\ \ 0.10\ \ 0.05\ \ 0.03\ \ 0.02\ \ 0.02\ \ 0.01\ \ 0.01\ \ 0.01\ \ \ldots\right]$

Number of required modes to achieve more than 90% of the total mass $\dfrac{\sum_{j=1}^{3} M_{m.eff_j}}{M_t} = 0.91$

Base shear: $V_{b.MRSA} = 883\ \ \boldsymbol{kip}$

Because the base shear obtain with the modal analysis is less than the base hsear obtained by the ELF method ($V_{b.MRSA} = 883\ \ \boldsymbol{kip} < V_b = 1158\ \ \boldsymbol{kip}$), all forces and drifts are requried to be scaled with the factor $V_{ELF} / V_{ModalAnalysis}$ (ASCE 7-16, S. 12.9.1.4).

Factor for scaling of forces $k_{shear} := \dfrac{V_b}{V_{b.MRSA}} = 1.31$

Design Forces and Displacements - Summary

The lateral demands on the wall obtained from the Modal Response Spectrum Analysis are shown in the table below. The forces were scaled to acchieve 100% of the base shear calcualted by the ELF method. The table incorporates the wall gravity loads calculated before (see Table 1).

Table 3. Loads and displacement demands on the wall

Level	Height (ft)	Axial Load D+0.25L (kip)	Axial Load LC6 (kip)	Axial Load LC7 (kip)	Lateral Force (kip)	Story Shear (kip)	Overturning Moment (kip-ft)	Elastic Deflection (in)	Amplified Deflection (in)	Story Drift (%)
Base	0	4,098	6,159	2,426	0	1,158	87,139	0.0	0.0	0.00
2	15	3,719	5,591	2,201	48	1,127	73,156	0.1	0.3	0.18
3	28	3,363	5,055	1,991	125	1,045	62,471	0.2	1.1	0.48
4	41	3,007	4,520	1,780	197	924	53,579	0.4	2.2	0.71
5	54	2,651	3,985	1,570	237	792	46,447	0.7	3.6	0.90
6	67	2,295	3,450	1,359	245	681	40,541	1.0	5.2	1.06
7	80	1,939	2,914	1,149	237	605	35,114	1.4	7.1	1.19
8	93	1,583	2,379	938	226	570	29,496	1.8	9.1	1.29
9	106	1,227	1,844	727	203	566	23,260	2.2	11.2	1.37
10	119	871	1,308	517	159	551	16,365	2.7	13.5	1.43
11	132	515	773	306	133	465	9,326	3.2	15.8	1.47
12	145	159	238	96	217	254	3,302	3.6	18.1	1.49
Roof	158	0	0	0	254	0	0	4.1	20.4	1.50

The roof drift is: $\Delta_{roof} = 1.08\%$

Min. axial load: $P_{min} = 2426\ \boldsymbol{kip}$

D+0.25L axial load: $P_{D.25L} = 4098\ \boldsymbol{kip}$

Max. axial load: $P_{max} = 6159\ \boldsymbol{kip}$

Shear demand: $V_u = 1158\ \boldsymbol{kip}$

Moment demand: $M_u = 87139\ \boldsymbol{kip \cdot ft}$

Axial load ratios: $ALR_{min} := \frac{P_{min}}{A'_g \cdot f'_c} = 4.5\%$

$$ALR_{D.25L} := \frac{P_{D.25L}}{A'_g \cdot f'_c} = 7.6\%$$

$$ALR_{max} := \frac{P_{max}}{A'_g \cdot f'_c} = 11.4\%$$

C.2 Wall Design

Critical Section

Building Information

Number of stories	$n_s := 12$
Lightweight concrete	$\lambda := 1.0$
Concrete compressive strength	$f'_c := 5000\ psi$
Yield strength of steel bars	$f_y := 60\ ksi$
Height of the wall	$h_w := (n_s - 1) \cdot 13\ ft + 15\ ft = 158\ ft$
Length of the wall	$l_w := 30\ ft$
Thickness of the wall	$t_w := 30\ in$
Flange thickness	$t_{fl} := 0\ ft = 0.00\ in$
Flange total width	$b_{fl} := 0\ ft$
Gross Area	$A_g := t_w \cdot (l_w - 2\ t_{fl}) + 2\ b_{fl} \cdot t_{fl} = 10800\ in^2$
A_{cv} cross-section area	$A_{cv} := t_w \cdot l_w = 10800\ in^2$
Min., avg., and max. axial demand	$P_{min} := 2426\ kip$ $P_{avg} := 4098\ kip$ $P_{max} := 6159\ kip$
Shear demand	$V_u := 1158\ kip$
Moment demand at critical section	$M_u := 87139\ kip \cdot ft$
Critical section at the bottom	$h_{wcs} := h_w = 158\ ft$

Provided longitudinal reinforcement in the critical section

Web Hor.: #5 @ 4.0

#4 rebar	$A_{\#5} := 0.31\ in^2$
Spacing	$s_{wh} := 4.0\ in$
Reinf. ratio	$\rho_{wh} := \frac{2 \cdot A_{\#5}}{s_{wh} \cdot t_w} = 0.52\%$

Web Ver.: #4 @ 5.3

#4 rebar	$A_{\#4} = 0.20\ in^2$
Spacing	$s_{wv} := 5.3\ in$
Reinf. ratio	$\rho_{wv} := \frac{2 \cdot A_{\#4}}{s_{wv} \cdot t_w} = 0.25\%$

Boundary Element: 36 #8

#9 rebar - area	$A_{\#9} = 1.00\ in^2$
#9 rebar - diam.	$d_{\#9} = 1.128\ in$ ($d_b := d_{\#9}$)
Length of BE	$l_{be} = 69.00\ in$
Width of BE	$b := t_w = 30.00\ in$
Reinf. ratio	$\rho_{be} := \frac{36 \cdot A_{\#9}}{(l_{be} + 3\ in) \cdot t_w} = 1.67\%$
	$\rho_{sb} := \frac{36 \cdot A_{\#9}}{A_{cv}} = 0.33\%$

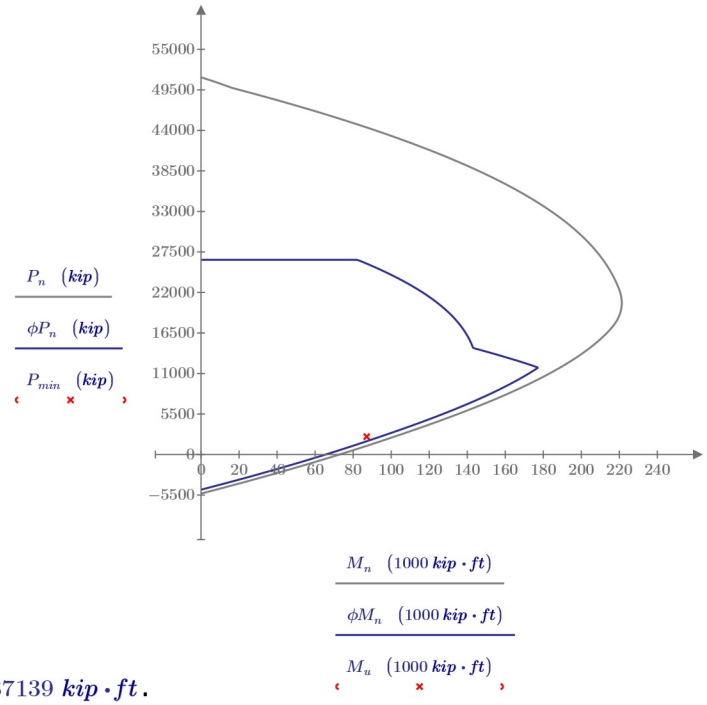

Verification for $P_{min} = 2426\ kip$ and $M_u = 87139\ kip \cdot ft$.

Minimum reinforcement ratios for the web

$A_{cv} := l_w \cdot t_w = 10800\ in^2$

Because $V_u = 1158\ kip > \lambda \sqrt{f'_c \cdot psi}\ A_{cv} = 764\ kip$, we can use $\rho_l := 0.0025$ and $\rho_t := 0.0025$ (ACI 18.10.2.1)

Number of curtains of reinforcement in the web

Because $\frac{h_w}{l_w} = 5.27 > 2$, 2 curtains of longitudinal and transverse reinforcement are required in the web (ACI 18.10.2.2)

Required area of longitudinal reinforcement for flexure and axial forces

Longitudinal reinforcement ratio within $0.15\ l_w = 54.0\ in$ from the end of the wall, and over a width equal to the wall thickness, shall be at least $6 \frac{\sqrt{f'_c \cdot psi}}{f_y} = 0.0071$. Therefore, the requirements of ACI 318-19, 18.10.2.4(a) are satisfied.

The longitudinal reinforcement required by 18.10.2.4(a) shal extend vertically above and below the critical section at least the greater of $l_w = 30.0\ ft$ and $\frac{M_u}{3\ V_u} = 25.1\ ft$. This is satisfied becuase $\rho_{be} = 0.0167$ is provided in the first 6 stories, covering a height equal to $15\ ft + 5 \cdot 13\ ft = 80.0\ ft$

No more than 50 percent of the reinforcement required by 18.10.2.4(a) shall be terminated at any section. This means that outside the greater of l_w and $M_u / (3\ V_u)$ (which is $30\ ft$), we have:

Minimum long. reinf. ratio (within $0.15\ l_w = 54.0\ in$ from the end of the wall)	$\frac{1}{2}\left(6 \frac{\sqrt{f'_c \cdot psi}}{f_y}\right) = 0.0035$
Minimum amount of long. reinf. above cut-off point	$\frac{1}{2}\left(6 \frac{\sqrt{f'_c \cdot psi}}{f_y}\right) \cdot 0.15\ l_w \cdot t_w = 5.73\ in^2$

Maximum Probable Moment

P-M diagram obtained with $1.25\ f_y = 75\ ksi$ and $P_{max} = 6159\ kip$

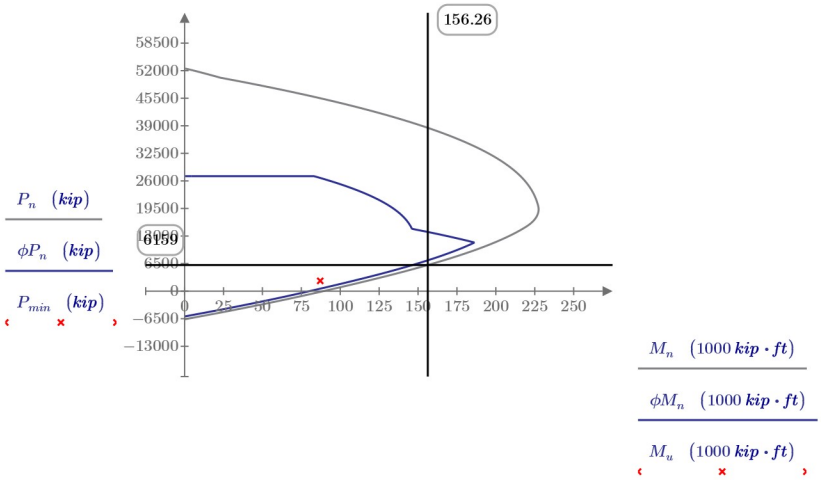

Design shear force

(a) Demand

Maximum probable moment (using P-M diagram obtained with $1.25\,f_y = 75\ ksi$) $M_{pr} = 156260\ kip \cdot ft$

Critical section at the bottom $h_{wcs} = 158\ ft$

Wall length $l_w = 30.0\ ft$

Shear demand $V_u = 1158\ kip$

Overstrength factor when $\frac{h_{wcs}}{l_w} = 5.27 > 1.5$: $\Omega_v := \max\left(\frac{M_{pr}}{M_u}, 1.5\right) = 1.79$

ω_v when $\frac{h_{wcs}}{l_w} = 5.27 > 2.0$ and $n_s := \max\left(12, 0.007 \cdot \frac{h_{wcs}}{in}\right) = 13.27 > 6$: $\omega_v := min\left(1.3 + \frac{n_s}{30}, 1.8\right)$

$\omega_v = 1.74$

Therefore, accodring to ACI 318-19, 18.10.3.1:

$V_e := min\left(\Omega_v \cdot \omega_v \cdot V_u, 3\ V_u\right) = 3474\ kip$ $\quad (\Omega_v \cdot \omega_v = 3.12)$

Strength (**ACI 318-19**):

α_c coefficient

$$\alpha_{c.aci} := \begin{cases} 3.0 & \text{if } \frac{h_w}{l_w} \le 1.5 \\ 2.0 & \text{else if } \frac{h_w}{l_w} \ge 2.0 \\ 2 \cdot \left(3 - \frac{h_{wcs}}{l_w}\right) & \text{else} \end{cases} \qquad \alpha_{c.aci} = 2.00$$

Upper limit $V_{n.aci.lim} := 8 \cdot A_{cv} \cdot \sqrt{f'_c \cdot psi} = 6109\ kip$

Shear strength $V_{n.aci} := \left(\alpha_{c.aci} \cdot \lambda \cdot \sqrt{f'_c \cdot psi} + \rho_{wh} \cdot f_y\right) \cdot A_{cv} = 4875\ kip < V_{n.aci.lim} = 6109\ kip$

Thus: $\phi V_n := 0.75 \cdot V_{n.aci} = 3657\ kip > V_e = 3474\ kip$

The capacity (**Prop. Eq.**):

Ratio of long. steel boundary $\rho_{sb} = 0.33\%$

Axial load considered: $P_{max} = 6159\ kip$

α_c coefficient

$$\alpha_{c.p} := \frac{1}{100} \cdot \left(9 \cdot \frac{\left(1 + \frac{P_{max}}{A_{cv} \cdot f'_c}\right)^3}{\sqrt[3]{\frac{M_u}{\omega_v \cdot V_u \cdot l_w}}} - 6 \right) = 0.050$$

α_s coefficient $\alpha_{s.p} := \frac{2}{5 \cdot \sqrt[3]{\frac{M_u}{\omega_v \cdot V_u \cdot l_w}}} = 0.35$

α_{shape} factor $\alpha_{shape} := \min\left(\max\left(1, 0.7 \cdot \left(1 + \frac{t_{fl} \cdot b_{fl}}{A_{cv}}\right)^2\right), 1.5\right) = 1.00$

Upper limit $V_{n.lim} := \alpha_{shape} \cdot 8 \cdot A_{cv} \cdot \sqrt{f'_c \cdot psi} = 6109\ kip$

Shear strength $V_{n.prop} := \left(\alpha_{c.p} \cdot f'_c + \alpha_{s.p} \cdot \left(\rho_{sb} + \rho_{wh}\right) \cdot f_y\right) \cdot A_{cv} = 4663\ kip < V_{n.lim} = 6109\ kip$

Resultant DCR $\frac{V_e}{V_{n.prop}} = 0.75$ (Remember we are not designing the wall with the proposed equation. We want to assess an ACI 318-19 compliant wall with it).

Determine if special boundary elemens are required

Special boundary elements are required where the following equation is satisfied (ACI 18.10.6.2):

$$\frac{1.5\ \delta_u}{h_{wcs}} \geq \frac{l_w}{600\ c}$$

From the analysis, the elastic displacement at the top of the building is $\delta_{xe} := 4.3\ in$. Also, from ASCE 7-16 Table 12.2-1 we have $C_d := 5$ for a Seismic Force-Resisting System consisting in special reinforced concrete shear walls. In addition, $I_e := 1.0$ for Risk Category II (ASCE 7-16 Tabe 1.5-2). Therefore:

$$\delta_u := \frac{C_d \cdot \delta_{xe}}{I_e} = 21.50\ in$$

Ratio δ_u / h_{wcs} shall not be taken less than 0.005. But in this case, $\frac{\delta_u}{h_{wcs}} = 0.011$

From the sectional analysis, the largest neutral axis depth is $c := c_{Pmax} = 75.4\ in$. Thus:

$$\frac{1.5\ \delta_u}{h_{wcs}} = 0.0170 > \frac{l_w}{600\ c} = 0.0080$$

Therefore, special boundary elements are required at the ends of the wall.

Vertical extent of the special BE transverse reinforcement

According to ACI 318-19, 18.10.6.2(b)(i), provide special boundary element transverse reinforcement vertically over at least the greater of the following lengths from the critical wall section:

$l_w = 30.00\ ft$ and $\frac{M_u}{4\ V_u} = 18.8\ ft$

The special BE transverse reinforcement is provided along the first 3 stories (i.e., $15\ ft + 2 \cdot 13\ ft = 41.00\ ft$). BE transverse reinforcement in stories 4, 5 and 6 has a vertical spacing of $6\ in$, satisfying the requirements of Table 18.10.6.5(b).

Check if ACI 18.10.6.2(b)(ii) or (iii) is satisfied

$b = 30.00\ in > \sqrt{0.025 \cdot c \cdot l_w} = 26.05\ in$ Cond. (b)(ii) is satisfied

$$\frac{\delta_c}{h_{wcs}} = \max\left(\frac{1}{100}\cdot\left(4 - \frac{1}{50}\left(\frac{l_w}{b}\right)\left(\frac{c}{b}\right) - \frac{V_e}{\left(8\sqrt{psi}\right)\cdot\sqrt{f'_c}\cdot A_{cv}}\right), 0.015\right) = 0.028 \quad > \quad \frac{1.5\ \delta_u}{h_{wcs}} = 0.017$$

Cond. (b)(iii) is satisfied

At least one of the above shall be satisfied. Therefore, ACI 18.10.6.2(b) is satisfied.

Horizontal length of the Special BE

According to ACI 318-19 18.10.6.4(a), the special boundary elements must extend horizontally from the extreme compression fiber a distance equal to the greater of the following:

Greater between $c - 0.1\ l_w = 39.37\ in$ and $\frac{c}{2} = 37.69\ in$

Therefore, using a BE length of $l_{be} = 69.0\ in$ satisfies this requirement.

Check the width of the flexural compression zone

The laterally unsupported wall height corresponds to the eight of the 1st story $h_u := 15\ ft$

$b = 30.00\ in > \frac{h_u}{16} = 11.25\ in$ --> ACI 318-19 18.10.6.4(b) is satisfied

$\frac{c}{l_w} = 0.21 \quad < \quad \frac{3}{8} = 0.38$ --> ACI 318-19 18.10.6.4(c) does not apply

Transverse reinforcement in the Special BE

The provided vertical spacing is $s := 3.5\ in$, and the largest distance (centerline to centerline) between laterally restrained longitudinal bars is $h_x := 6.0\ in$.

First, we check the requirements of ACI 318-19 18.10.6.4(e). The maximum vertical spacing of the special boundary element transverse reinforcement is equal to the following:

s_{max} = lesser of

- $\frac{b}{3} = 10.0\ in$
- $\frac{l_{be}}{3} = 23.0\ in$
- For grade 80 bars, lesser of $5\ d_b = 5.64\ in$ or $6\ in$ --> use 5.6
- $s_o := 4 + \left(\frac{14 - \frac{h_x}{in}}{3}\right) = 6.67$ shall be within $[4\ in, 6\ in]$ --> use 6.0

Because $s = 3.50\ in$, ACI 318-19 18.10.6.4(e) is satisfied.

#5 perimetral hoop, one 135-degree #4 crosstie in the longitudinal direction and ten #4 crossties in the transvese direction. For #4 bars: $A_{\#4} = 0.20\ in^2$ and $d_{\#4} := 0.5\ in$; for #5 bars: $A_{\#5} = 0.31\ in^2$ and $d_{\#5} := 0.625\ in$.

$$b = 30.00\ in$$

$$l_{be} = 69.00\ in$$

$$b_{c1} := l_{be} - 3\ in + 2 \cdot \left(d_{\#5} + \frac{d_{\#9}}{2} \right) = 68.38\ in$$

$$b_{c2} := b - 2 \cdot (3\ in) + 2 \cdot \left(d_{\#5} + \frac{d_{\#9}}{2} \right) = 26.38\ in$$

$$A_{g.be} := b \cdot l_{be} = 2070.00\ in^2$$

$$A_{ch} := b_{c1} \cdot b_{c2} = 1803.67\ in^2$$

According to ACI 318-19 18.10.6.4(g), the minimum amount of transverse reinforcement is:

$$\frac{A_{sh}}{s \cdot b_c} = \text{greater of} \begin{cases} 0.3 \cdot \left(\frac{A_{g.be}}{A_{ch}} - 1 \right) \cdot \frac{f'_c}{f_y} = 0.00369 \\ 0.09 \cdot \frac{f'_c}{f_y} = 0.00750 \end{cases}$$

Therefore, the minimum BE transverse reinforcements are:

When doing a X-X cut: $A_{sh.minXX} := 0.0075 \cdot s \cdot b_{c1} = 1.79\ in^2$

When doing a Y-Y cut: $A_{sh.minYY} := 0.0075 \cdot s \cdot b_{c2} = 0.69\ in^2$

And the provided BE transverse reinforcements are:

When doing a X-X cut: $A_{sh.XX} := 2 \cdot A_{\#5} + 10 \cdot A_{\#4} = 2.62\ in^2$

When doing a Y-Y cut: $A_{sh.YY} := 2 \cdot A_{\#5} + A_{\#4} = 0.82\ in^2$

Thus, the minimum requirements for the amount of transverse reinforcement in the BE are satisfied.

Flexural Strength Verification - Stories 7 & 8

Demand

Minimum axial load: $P_{min} := 938\ kip$

Maximum axial load: $P_{max} := 2379\ kip$

Shear: $V_u := 570\ kip$

Moment: $M_u := 29496\ kip \cdot ft$

Web: #4 @ 5.3 in both directions

#4 rebar $A_{\#4} = 0.20\ in^2$

Spacing $s_w := 5.3\ in$

Reinf. ratio $\rho_w := \frac{2 \cdot A_{\#4}}{s_w \cdot t_w} = 0.25\%$

Boundary Element: 28 #9

#9 rebar - area $A_{\#9} = 1.00\ in^2$

#9 rebar - diam. $d_{\#9} = 1.128\ in$ ($d_b := d_{\#9}$)

Length of BE $l_{be} = 69.00\ in$

Width of BE $b := t_w = 30.00\ in$

Reinf. ratio $\rho_{l.end} := \frac{28 \cdot A_{\#9}}{(l_{be} + 3\ in) \cdot t_w} = 1.30\%$

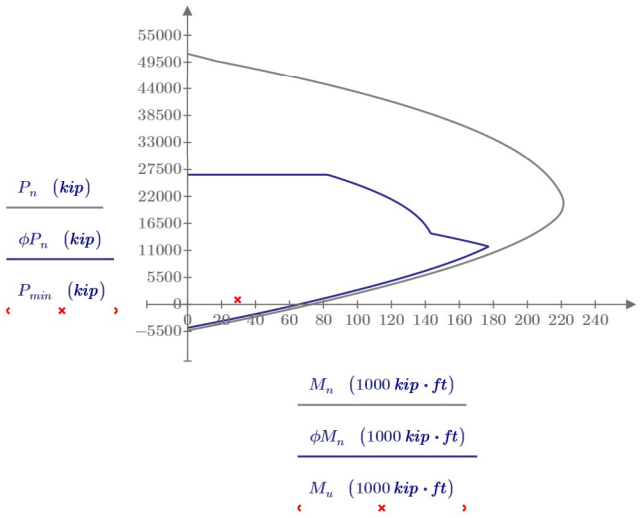

Verification of flexural strength for $P_{min} = 938\ kip$ and $M_u = 29496\ kip \cdot ft$

From the sectional analysis, the largest neutral axis depth (associated with the largest axial load) is $c := c_{Pmax} = 75.4\ in$ at the critical section.

Becasue $\rho_{l.end} = 0.0130$ > $\frac{400\ psi}{f_y} = 0.0067$, the transverse reinforcement in accordance with ACI 18.10.6.5 is required at the ends of the wall:

> Boundary transverse reinforcement shall satisfy the requirements 18.7.5.2(a) through (e) over the greater of $c - 0.1\ l_w = 39.37\ in$ and $\frac{c}{2} = 38\ in$
>
> Because the section above the 7th story is not expected to yield (i.e., outside the length of the plastic hinge length calculated before), the maximum spacing of the transverse reinforcement is equal to the lesser of the following for Grade 80 reinforcement:
>
> $s_{max} := min\left(6\ d_b, 6\ in\right) = 6.00\ in$

Following transversal reinforcement over an horizontal wall segment of $l_{be} = 69\ in$ satisfies all above requirements:

> One #4 perimetral hoop
> One #4 crosstie inthe longitudinal direcction
> Ten #4 crossties in the transvese direction

Because above the cut-off $\rho_{l.end} = 0.0130$ > $\frac{1}{2}\left(6\frac{\sqrt{f'_c \cdot psi}}{f_y}\right) = 0.0035$, S. 18.19.2.4(c) is satisfied.

Because $V_u = 570\ kip < \lambda \cdot \sqrt{f'_c \cdot psi} \cdot A_{cv} = 764\ kip$, ACI 18.10.6.5 does not need to be satisfied, i.e., the horizontal reinforcement does not need to terminate with hook.

Flexural Strength Verification - Story 9 & 10

Demand

Minimum axial load: $P_{min} := 517\ kip$

Maximum axial load: $P_{max} := 1308\ kip$

Shear: $V_u := 551\ kip$

Moment: $M_u := 16365\ kip \cdot ft$

Web: #4 @ 5.3 in both directions

#4 rebar $A_{\#4} = 0.20\ in^2$

Spacing $s_w = 0.13\ m$

Reinf. ratio $\rho_w := \frac{2 \cdot A_{\#4}}{s_w \cdot t_w} = 0.25\%$

Boundary Element: 14 #9

#9 rebar - area $A_{\#9} = 1.00\ in^2$

#9 rebar - diam. $d_{\#9} = 1.128\ in$ ($d_b := d_{\#9}$)

Length of BE $l_{be} := 39\ in$

Width of BE $b := t_w = 30.00\ in$

Reinf. ratio $\rho_{l.end} := \frac{14 \cdot A_{\#9}}{(l_{be} + 3\ in) \cdot t_w} = 1.11\%$

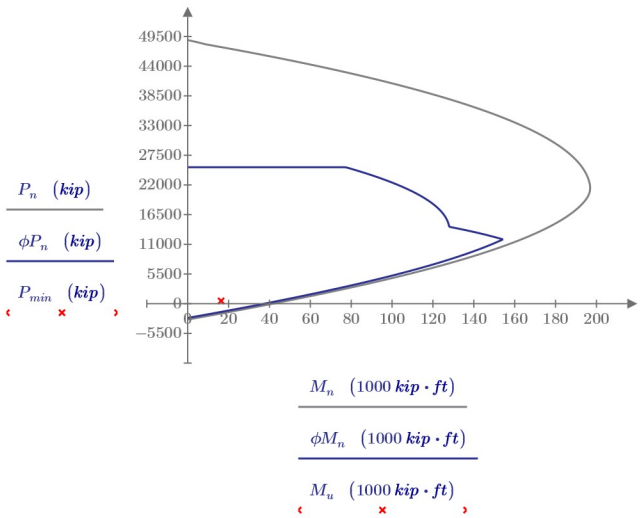

Verification of flexural strength for $P_{min} = 517\ kip$ and $M_u = 16365\ kip \cdot ft$

From the sectional analysis, the largest neutral axis depth (associated with the largest axial load) is $c := c_{Pmax} = 75.37\ in$ at the critical section.

Becasue $\rho_{l.end} = 0.0111$ > $\frac{400\ psi}{f_y} = 0.0067$, the transverse reinforcement in accordance with ACI 18.10.6.5 is required at the ends of the wall:

> Boundary transverse reinforcement shall satisfy the requirements 18.7.5.2(a) through (e) over the greater of
>
> $c - 0.1\ l_w = 39.37\ in$ and $\frac{c}{2} = 38\ in$
>
> Because the section above the 5th story is not expected to yield (i.e., outside the length of the plastic hinge length calculated before), the maximum spacing of the transverse reinforcement is equal to the lesser of the following for Grade 80 reinforcement:
>
> $s_{max} := min\left(6\ d_b, 6\ in\right) = 6.00\ in$

Following transversal reinforcement over an horizontal wall segment of $l_{be} = 39\ in$ satisfies all above requirements:

One #4 perimetral hoop
One #4 crosstie in the longitudinal direction
Four #4 crossties in the transvese direction

Because above cut-off point $\rho_{l.end} = 0.0111$ > $\frac{1}{2}\left(6\frac{\sqrt{f'_c \cdot psi}}{f_y}\right) = 0.0035$, S. 18.10.2.4(c) is satisfied.

Because $V_u = 551\ kip < \lambda \cdot \sqrt{f'_c \cdot psi} \cdot A_{cv} = 764\ kip$, ACI 18.10.6.5 does not need to be satisfied, i.e., the horizontal reinforcement in the last story does not need to terminate with hook.

Flexural Strength Verification - Stories 11 & 12

Demand

Minimum axial load: $P_{min} := 306\ kip$

Maximum axial load: $P_{max} := 773\ kip$

Shear: $V_u := 465\ kip$

Moment: $M_u := 9326\ kip \cdot ft$

Web: #4 @ 5.3 in both directions

#4 rebar $A_{\#4} = 0.20\ in^2$

Spacing $s_w = 0.13\ m$

Reinf. ratio $\rho_w = 0.25\%$

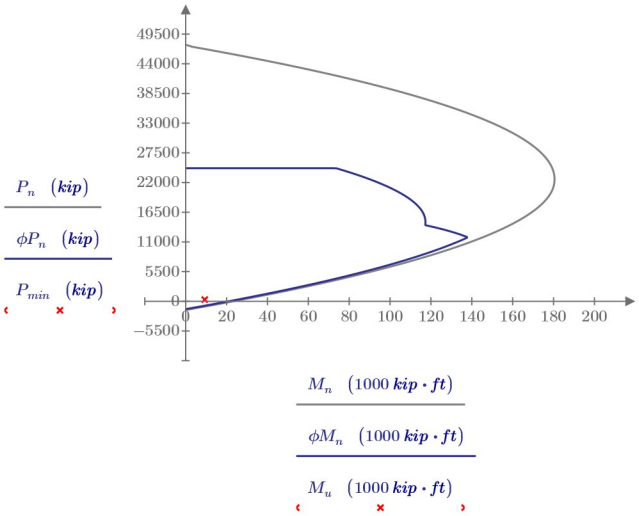

Verification of flexural strength for $P_{min} = 306\ kip$ and $M_u = 9326\ kip \cdot ft$

Becasue $\rho_w = 0.0025$ < $\frac{400\ psi}{f_y} = 0.0067$, the transverse reinforcement in accordance with ACI 18.10.6.5(b) is not required.

Because $V_u = 465\ kip < \lambda \cdot \sqrt{f'_c \cdot psi} \cdot A_{cv} = 764\ kip$, ACI 18.10.6.5 does not need to be satisfied, i.e., the horizontal reinforcement in the last story does not need to terminate with hook.

C.3 Wall Sketches

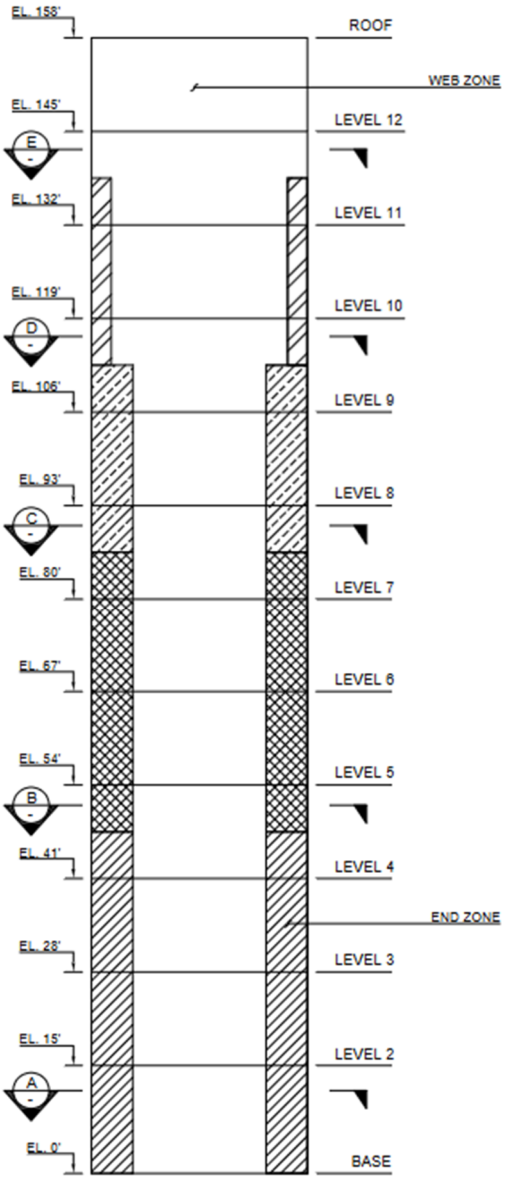

WALL - SCHEMATIC ELEVATION VIEW

LEVEL	STORY	HEIGHT (FT)	WEB ZONE	WALL END ZONE
ROOF	12	158	2-#4 @ 5.3" V 2-#4 @ 5.3" H	-
12	11	145		
11	10	132	2-#4 @ 5.3" V 2-#4 @ 5.3" H	39" x 30" 14 - #9 HOOPS AND CROSSTIES @ 6.0"
10	9	119		
9	8	106	2-#4 @ 5.3" V 2-#4 @ 5.3" H	69" x 30" 28 - #9 HOOPS AND CROSSTIES @ 6.0"
8	7	93		
7	6	80	2-#4 @ 5.3" V 2-#4 @ 5.3" H	69" x 30" 36 - #9 HOOPS AND CROSSTIES @ 6.0"
6	5	67		
5	4	54		
4	3	41	2-#4 @ 5.3" V 2-#5 @ 4.0" H	69" x 30" 36 - #9 HOOPS AND CROSSTIES @ 3.5"
3	2	28		
2	1	15		

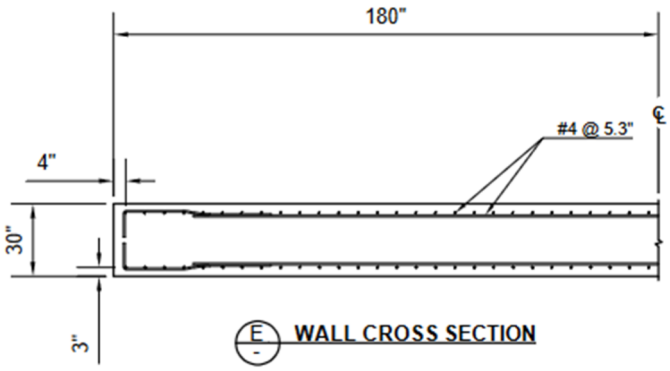

E - WALL CROSS SECTION

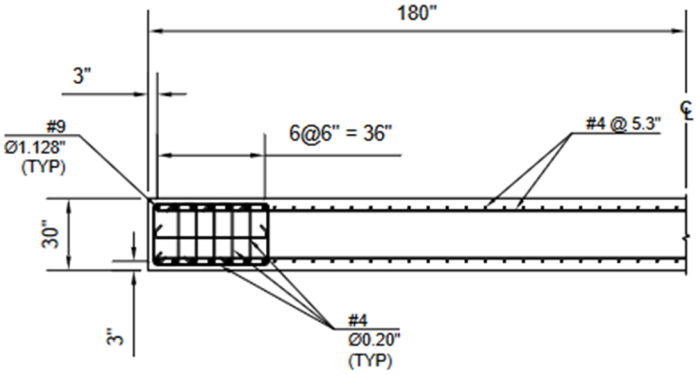

D - WALL CROSS SECTION

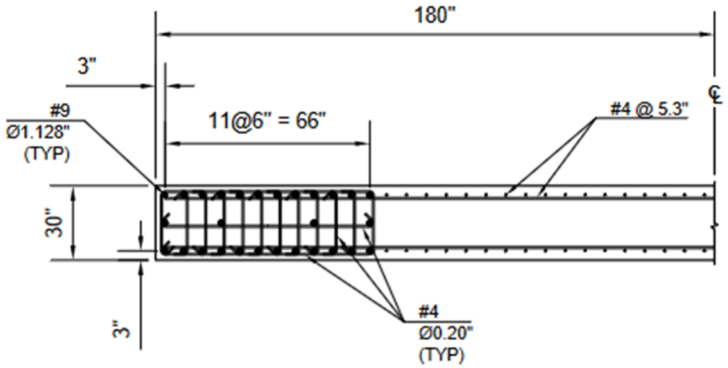

C WALL CROSS SECTION

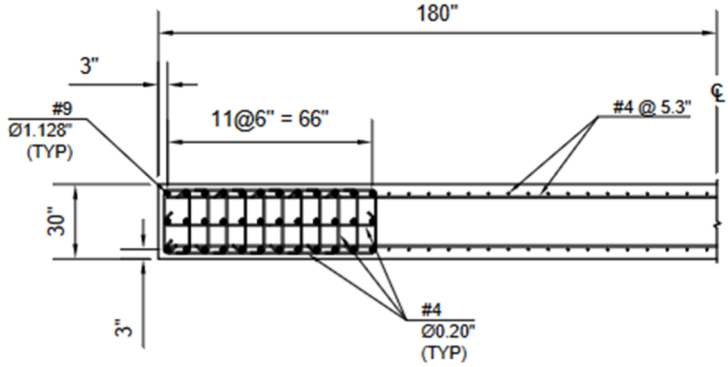

B WALL CROSS SECTION

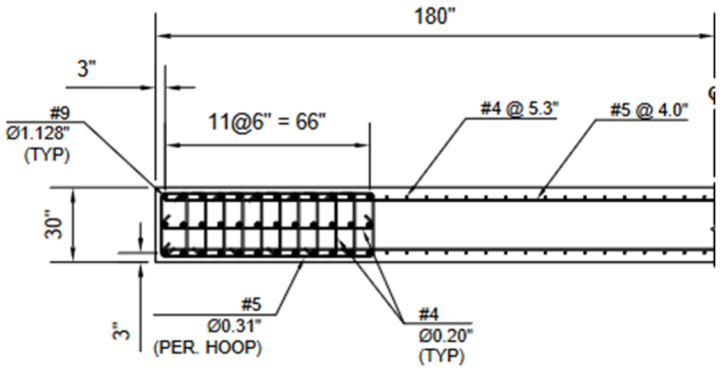

A WALL CROSS SECTION

NOTES:

CROSSTIES IN THE WEB ARE NOT SHOWN

THE DRAWING OF THE DETAILING OF THE BOUNDARY ELEMENT MIGHT NOT SATISFY ALL ACI 318-19 REQUIREMENTS, HOWEVER THE PURPOSE OF PROVIDING ENOUGH TRANSVERSE STEEL AND ESTIMATE THE CORRESPONDING CONFINEMENT IS MET.

C.4 Expected Concrete Stress-Strain Relationship

Materials

#4 and #5 Hoops and Crossties:

Diameter: $d_{bt.n4} := 0.5\ in$ $d_{bt.n5} := 0.625\ in$

Area: $A_{st.n4} := 0.2\ in^2$ $A_{st.n5} := 0.31\ in^2$

Expected yield Stress: $f_{yt} := 70\ ksi$

Steel for Longitudinal Bars (#9)

Diameter: $d_{b1} := 1.128\ in$

Area: $A_{s1} := 1.00\ in^2$

Yield Stress: $f_{y1} := 70\ ksi$

Concrete

Expected unconfined concrete strength $f'_{co} := 1.3 \cdot 5000\ psi = 6500\ psi$

Modulus of elasticity $E_c := 57000 \cdot \sqrt{f'_{co} \cdot psi} = 4595\ ksi$

Strain related to f'_c $\varepsilon_{co} := \frac{2 \cdot f'_{co}}{E_c} = 0.0028$

Saatciougly & Razvi Model

(a) Unconfined Concrete

Strain at maximum concrete compressive strength $\varepsilon_{01} := \varepsilon_{co} = 0.0028$

When specific information is not available, the authors of this model reccomend to use $\varepsilon_{085} := 0.0038$

Strain at which the descending branch touches the X axis $\varepsilon_{cf} := \frac{(\varepsilon_{085} - \varepsilon_{co})}{0.15} + \varepsilon_{co}$ $\varepsilon_{cf} = 0.0093$

Stress-strain relation for confined concrete
(This also recovers the Hognestad expression)

$$f_{c.SR.1}(\varepsilon_c) := \begin{cases} f'_{co} \cdot \left(\frac{2 \cdot \varepsilon_c}{\varepsilon_{01}} - \left(\frac{\varepsilon_c}{\varepsilon_{01}} \right)^2 \right) & \text{if } 0 \le \varepsilon_c \le \varepsilon_{01} \\ f'_{co} \cdot \left(1 - 0.15 \cdot \frac{\varepsilon_c - \varepsilon_{01}}{\varepsilon_{085} - \varepsilon_{01}} \right) & \text{else if } \varepsilon_{01} < \varepsilon_c \le \varepsilon_{cf} \\ 0 & \text{else} \end{cases}$$

(b) Confined Concrete in Stories 1, 2 & 3

Dimension to centerline of outermost hoop, in X direction

$b_{cx} := 69\ in + d_{b1} + d_{bt.n5}$ $\quad b_{cx} = 70.75\ in$

Dimension to centerline of outermost hoop, in Y direction

$b_{cy} := 30\ in - 2 \cdot 3\ in + d_{b1} + d_{bt.n5}$ $\quad b_{cy} = 25.75\ in$

Dimension between laterally supported vertical bars, in X dir.

$s_{lx} := 6.0\ in$ $\quad s_{lx} = 6\ in$

Dimension between laterally supported vertical bars, in Y dir.

$s_{ly} := \frac{30\ in - 2 \cdot 3\ in}{2}$ $\quad s_{ly} = 12\ in$

Vertical spacing of hoops

$s := 3.5\ in$

# of hoops or crossties that appear when doing a X-X cut

$n_{y.n4} := 10$ $\quad n_{y.n5} := 2$

# of hoops or crossties that appear when doing a Y-Y cut

$n_{x.n4} := 1$ $\quad n_{x.n5} := 2$

More parameters required to obtained the maximum confined stress:

$f_{lx} := \frac{\left(n_{y.n4} \cdot A_{st.n4} + n_{y.n5} \cdot A_{st.n5}\right) \cdot f_{yt}}{s \cdot b_{cx}}$ $\quad f_{lx} = 0.741\ ksi$

$f_{ly} := \frac{\left(n_{x.n5} \cdot A_{st.n5} + n_{x.n4} \cdot A_{st.n4}\right) \cdot f_{yt}}{s \cdot b_{cy}}$ $\quad f_{ly} = 0.637\ ksi$

$k_{2x} := min\left(0.099 \cdot \sqrt[2]{\frac{{b_{cx}}^2}{s \cdot s_{lx} \cdot \frac{f_{lx}}{ksi}}}, 1\right)$ $\quad k_{2x} = 1$

$k_{2y} := min\left(0.099 \cdot \sqrt[2]{\frac{{b_{cy}}^2}{s \cdot s_{ly} \cdot \frac{f_{ly}}{ksi}}}, 1\right)$ $\quad k_{2y} = 0.493$

$f_{lex} := k_{2x} \cdot f_{lx}$ $\quad f_{lex} = 0.741\ ksi$

$f_{ley} := k_{2y} \cdot f_{ly}$ $\quad f_{ley} = 0.314\ ksi$

$f_{le} := \frac{f_{lex} \cdot b_{cx} + f_{ley} \cdot b_{cy}}{b_{cx} + b_{cy}}$ $\quad f_{le} = 0.627\ ksi$

$k_1 := 4.825 \cdot \left(\frac{f_{le}}{ksi}\right)^{-0.17}$ $\quad k_1 = 5.224$

Maximum confined stress

$f'_{cc} := f'_{co} + k_1 \cdot f_{le}$ $\quad f'_{cc} = 9.774\ ksi$

More parameters required to obtain the confined stress-strain curve:

$K := k_1 \cdot \frac{f_{le}}{f'_{co}}$ $\quad K = 0.504$

Volumetric ratio

$\rho := \frac{n_{y.n4} \cdot A_{st.n4} + n_{y.n5} \cdot A_{st.n5} + n_{x.n5} \cdot A_{st.n5}}{s \cdot \left(b_{cx} + b_{cy}\right)}$ $\quad \rho = 0.01$

$$\varepsilon_1 := \varepsilon_{01} \cdot (1 + 5 \cdot K) \qquad \varepsilon_1 = 0.00995$$

$$\varepsilon_{85} := 260 \cdot \rho \cdot \varepsilon_1 + \varepsilon_{085} \qquad \varepsilon_{85} = 0.0286$$

Strain at which is reached the residual stress

$$\varepsilon_{c.res} := \frac{0.8\ (\varepsilon_{85} - \varepsilon_1)}{0.15} + \varepsilon_1 \qquad \varepsilon_{c.res} = 0.1095$$

Residual Stress

$$f_{res} := 0.2 \cdot f'_{cc} \qquad f_{res} = 1.955\ ksi$$

Stress-strain relation for confined concrete

$$f_{cc.SR.1}(\varepsilon_c) := \begin{cases} \text{if } 0 \le \varepsilon_c \le \varepsilon_1 \\ \quad f'_{cc} \cdot \left(\dfrac{2 \cdot \varepsilon_c}{\varepsilon_1} - \left(\dfrac{\varepsilon_c}{\varepsilon_1} \right)^2 \right)^{\frac{1}{1+2 \cdot K}} \\ \text{else if } \varepsilon_1 < \varepsilon_c \le \varepsilon_{c.res} \\ \quad f'_{cc} \cdot \left(1 - 0.15 \cdot \dfrac{\varepsilon_c - \varepsilon_1}{\varepsilon_{85} - \varepsilon_1} \right) \\ \text{else} \\ \quad f_{res} \end{cases}$$

(c) Confined Concrete in Stories 4, 5 & 6

Dimension to centerline of outermost hoop, in X direction

$$b_{cx} := 69\ in + d_{b1} + d_{bt.n4} \qquad b_{cx} = 70.63\ in$$

Dimension to centerline of outermost hoop, in Y direction

$$b_{cy} := 30\ in - 2 \cdot 3\ in + d_{b1} + d_{bt.n4} \qquad b_{cy} = 25.63\ in$$

Dimension between laterally supported vertical bars, in X dir.

$$s_{lx} := 6.0\ in \qquad s_{lx} = 6\ in$$

Dimension between laterally supported vertical bars, in Y dir.

$$s_{ly} := \frac{30\ in - 2 \cdot 3\ in}{2} \qquad s_{ly} = 12\ in$$

Vertical spacing of hoops

$$s := 6.0\ in$$

# of hoops or crossties that appear when doing a X-X cut

$$n_y := 12$$

# of hoops or crossties that appear when doing a Y-Y cut

$$n_x := 3$$

More parameters required to obtained the maximum confined stress:

$$f_{lx} := \frac{n_y \cdot A_{st.n4} \cdot f_{yt}}{s \cdot b_{cx}} \qquad f_{lx} = 0.396\ ksi$$

$$f_{ly} := \frac{n_x \cdot A_{st.n4} \cdot f_{yt}}{s \cdot b_{cy}} \qquad f_{ly} = 0.273\ ksi$$

$$k_{2x} := min\left(0.099 \cdot \sqrt[2]{\frac{{b_{cx}}^2}{s \cdot s_{lx} \cdot \frac{f_{lx}}{ksi}}}, 1 \right) \qquad k_{2x} = 1$$

$$k_{2y} := min\left(0.099 \cdot \sqrt[2]{\frac{b_{cy}^{\,2}}{s \cdot s_{ly} \cdot \frac{f_{ly}}{ksi}}}, 1\right) \qquad k_{2y} = 0.572$$

$$f_{lex} := k_{2x} \cdot f_{lx} \qquad f_{lex} = 0.396\ ksi$$

$$f_{ley} := k_{2y} \cdot f_{ly} \qquad f_{ley} = 0.156\ ksi$$

$$f_{le} := \frac{f_{lex} \cdot b_{cx} + f_{ley} \cdot b_{cy}}{b_{cx} + b_{cy}} \qquad f_{le} = 0.332\ ksi$$

$$k_1 := 4.825 \cdot \left(\frac{f_{le}}{ksi}\right)^{-0.17} \qquad k_1 = 5.818$$

Maximum confined stress

$$f'_{cc} := f'_{co} + k_1 \cdot f_{le} \qquad f'_{cc} = 8.435\ ksi$$

More parameters required to obtain the confined stress-strain curve:

$$K := k_1 \cdot \frac{f_{le}}{f'_{co}} \qquad K = 0.298$$

Volumetric ratio

$$\rho := \frac{(n_y + n_x) \cdot A_{st.n4}}{s \cdot (b_{cx} + b_{cy})} \qquad \rho = 0.005$$

$$\varepsilon_1 := \varepsilon_{01} \cdot (1 + 5 \cdot K) \qquad \varepsilon_1 = 0.00704$$

$$\varepsilon_{85} := 260 \cdot \rho \cdot \varepsilon_1 + \varepsilon_{085} \qquad \varepsilon_{85} = 0.0133$$

Strain at which is reached the residual stress

$$\varepsilon_{c.res} := \frac{0.8\ (\varepsilon_{85} - \varepsilon_1)}{0.15} + \varepsilon_1 \qquad \varepsilon_{c.res} = 0.0405$$

Residual Stress

$$f_{res} := 0.2 \cdot f'_{cc} \qquad f_{res} = 1.687\ ksi$$

Stress-strain relation for confined concrete

$$f_{cc.SR.2}(\varepsilon_c) := \begin{cases} \text{if } 0 \le \varepsilon_c \le \varepsilon_1 \\ \quad f'_{cc} \cdot \left(\frac{2 \cdot \varepsilon_c}{\varepsilon_1} - \left(\frac{\varepsilon_c}{\varepsilon_1}\right)^2\right)^{\frac{1}{1+2 \cdot K}} \\ \text{else if } \varepsilon_1 < \varepsilon_c \le \varepsilon_{c.res} \\ \quad f'_{cc} \cdot \left(1 - 0.15 \cdot \frac{\varepsilon_c - \varepsilon_1}{\varepsilon_{85} - \varepsilon_1}\right) \\ \text{else} \\ \quad f_{res} \end{cases}$$

(d) Confined Concrete in Stories 7 & 8

Dimension to centerline of outermost hoop, in X direction

$$b_{cx} := 69\ in + d_{b1} + d_{bt.n4} \qquad b_{cx} = 70.63\ in$$

Dimension to centerline of outermost hoop, in Y direction

$$b_{cy} := 30\ in - 2 \cdot 3\ in + d_{b1} + d_{bt.n4} \qquad b_{cy} = 25.63\ in$$

Dimension between laterally supported vertical bars, in X dir.

$$s_{lx} := 6\ in \qquad s_{lx} = 6\ in$$

Dimension between laterally supported vertical bars, in Y dir.

$$s_{ly} := \frac{4}{12} \cdot \left(\frac{30\ in - 2 \cdot 3\ in}{2} \right) + \frac{8}{12} \cdot (30\ in - 2 \cdot 3\ in) \qquad s_{ly} = 20\ in$$

Vertical spacing of hoops

$$s := 6.0\ in$$

# of hoops or crossties that appear when doing a X-X cut

$$n_y := 10$$

# of hoops or crossties that appear when doing a Y-Y cut

$$n_x := 3$$

More parameters required to obtained the maximum confined stress:

$$f_{lx} := \frac{n_y \cdot A_{st.n4} \cdot f_{yt}}{s \cdot b_{cx}} \qquad f_{lx} = 0.33\ ksi$$

$$f_{ly} := \frac{n_x \cdot A_{st.n4} \cdot f_{yt}}{s \cdot b_{cy}} \qquad f_{ly} = 0.273\ ksi$$

$$k_{2x} := min\left(0.099 \cdot \sqrt[2]{\frac{b_{cx}^{\,2}}{s \cdot s_{lx} \cdot \frac{f_{lx}}{ksi}}}, 1 \right) \qquad k_{2x} = 1$$

$$k_{2y} := min\left(0.099 \cdot \sqrt[2]{\frac{b_{cy}^{\,2}}{s \cdot s_{ly} \cdot \frac{f_{ly}}{ksi}}}, 1 \right) \qquad k_{2y} = 0.443$$

$$f_{lex} := k_{2x} \cdot f_{lx} \qquad f_{lex} = 0.33\ ksi$$

$$f_{ley} := k_{2y} \cdot f_{ly} \qquad f_{ley} = 0.121\ ksi$$

$$f_{le} := \frac{f_{lex} \cdot b_{cx} + f_{ley} \cdot b_{cy}}{b_{cx} + b_{cy}} \qquad f_{le} = 0.275\ ksi$$

$$k_1 := 4.825 \cdot \left(\frac{f_{le}}{ksi} \right)^{-0.17} \qquad k_1 = 6.01$$

Maximum confined stress

$$f'_{cc} := f'_{co} + k_1 \cdot f_{le} \qquad f'_{cc} = 8.151\ ksi$$

More parameters required to obtain the confined stress-strain curve:

$$K := k_1 \cdot \frac{f_{le}}{f'_{co}} \qquad K = 0.254$$

Volumetric ratio

$$\rho := \frac{(n_y + n_x) \cdot A_{st.n4}}{s \cdot (b_{cx} + b_{cy})} \qquad \rho = 0.005$$

$$\varepsilon_1 := \varepsilon_{01} \cdot (1 + 5 \cdot K) \qquad \varepsilon_1 = 0.00642$$

$$\varepsilon_{85} := 260 \cdot \rho \cdot \varepsilon_1 + \varepsilon_{085} \qquad \varepsilon_{85} = 0.0113$$

Strain at which is reached the residual stress

$$\varepsilon_{c.res} := \frac{0.8 \cdot (\varepsilon_{85} - \varepsilon_1)}{0.15} + \varepsilon_1 \qquad \varepsilon_{c.res} = 0.0325$$

Residual Stress

$$f_{res} := 0.2 \cdot f'_{cc} \qquad f_{res} = 1.63\ ksi$$

Stress-strain relation for confined concrete

$$f_{cc.SR.3}(\varepsilon_c) := \begin{cases} \text{if } 0 \le \varepsilon_c \le \varepsilon_1 \\ \quad f'_{cc} \cdot \left(\dfrac{2 \cdot \varepsilon_c}{\varepsilon_1} - \left(\dfrac{\varepsilon_c}{\varepsilon_1} \right)^2 \right)^{\frac{1}{1+2 \cdot K}} \\ \text{else if } \varepsilon_1 < \varepsilon_c \le \varepsilon_{c.res} \\ \quad f'_{cc} \cdot \left(1 - 0.15 \cdot \dfrac{\varepsilon_c - \varepsilon_1}{\varepsilon_{85} - \varepsilon_1} \right) \\ \text{else} \\ \quad f_{res} \end{cases}$$

(e) Confined Concrete in Stories 9 & 10

Dimension to centerline of outermost hoop, in X direction

$$b_{cx} := 39\ in + d_{b1} + d_{bt.n4} \qquad b_{cx} = 40.63\ in$$

Dimension to centerline of outermost hoop, in Y direction

$$b_{cy} := 30\ in - 2 \cdot 3\ in + d_{b1} + d_{bt.n4} \qquad b_{cy} = 25.63\ in$$

Dimension between laterally supported vertical bars, in X dir.

$$s_{lx} := 9.6\ in \qquad s_{lx} = 9.6\ in$$

Dimension between laterally supported vertical bars, in Y dir.

$$s_{ly} := 24\ in - 2 \cdot 3\ in \qquad s_{ly} = 18\ in$$

Vertical spacing of hoops

$$s := 6.0\ in$$

# of hoops or crossties that appear when doing a X-X cut

$$n_y := 7$$

# of hoops or crossties that appear when doing a Y-Y cut

$$n_x := 3$$

More parameters required to obtained the maximum confined stress:

$$f_{lx} := \frac{n_y \cdot A_{st.n4} \cdot f_{yt}}{s \cdot b_{cx}} \qquad f_{lx} = 0.402\ ksi$$

$$f_{ly} := \frac{n_x \cdot A_{st.n4} \cdot f_{yt}}{s \cdot b_{cy}} \qquad f_{ly} = 0.273\ ksi$$

$$k_{2x} := min\left(0.099 \cdot \sqrt[2]{\frac{b_{cx}^{\,2}}{s \cdot s_{lx} \cdot \frac{f_{lx}}{ksi}}}, 1 \right) \qquad k_{2x} = 0.836$$

$$k_{2y} := min\left(0.099 \cdot \sqrt[2]{\frac{b_{cy}^{\,2}}{s \cdot s_{ly} \cdot \frac{f_{ly}}{ksi}}}, 1 \right) \qquad k_{2y} = 0.467$$

$$f_{lex} := k_{2x} \cdot f_{lx} \qquad f_{lex} = 0.336\ ksi$$

$$f_{ley} := k_{2y} \cdot f_{ly} \qquad f_{ley} = 0.128\ ksi$$

$$f_{le} := \frac{f_{lex} \cdot b_{cx} + f_{ley} \cdot b_{cy}}{b_{cx} + b_{cy}} \qquad f_{le} = 0.255\ ksi$$

$$k_1 := 4.825 \cdot \left(\frac{f_{le}}{ksi}\right)^{-0.17} \qquad k_1 = 6.085$$

Maximum confined stress

$$f'_{cc} := f'_{co} + k_1 \cdot f_{le} \qquad f'_{cc} = 8.054\ ksi$$

More parameters required to obtain the confined stress-strain curve:

$$K := k_1 \cdot \frac{f_{le}}{f'_{co}} \qquad K = 0.239$$

Volumetric ratio

$$\rho := \frac{(n_y + n_x) \cdot A_{st.n4}}{s \cdot (b_{cx} + b_{cy})} \qquad \rho = 0.005$$

$$\varepsilon_1 := \varepsilon_{01} \cdot (1 + 5 \cdot K) \qquad \varepsilon_1 = 0.00621$$

$$\varepsilon_{85} := 260 \cdot \rho \cdot \varepsilon_1 + \varepsilon_{085} \qquad \varepsilon_{85} = 0.0119$$

Strain at which is reached the residual stress

$$\varepsilon_{c.res} := \frac{0.8\ (\varepsilon_{85} - \varepsilon_1)}{0.15} + \varepsilon_1 \qquad \varepsilon_{c.res} = 0.0367$$

Residual Stress

$$f_{res} := 0.2 \cdot f'_{cc} \qquad f_{res} = 1.611\ ksi$$

Stress-strain relation for confined concrete

$$f_{cc.SR.4}(\varepsilon_c) := \begin{cases} \text{if } 0 \le \varepsilon_c \le \varepsilon_1 \\ \quad f'_{cc} \cdot \left(\frac{2 \cdot \varepsilon_c}{\varepsilon_1} - \left(\frac{\varepsilon_c}{\varepsilon_1}\right)^2\right)^{\frac{1}{1+2 \cdot K}} \\ \text{else if } \varepsilon_1 < \varepsilon_c \le \varepsilon_{c.res} \\ \quad f'_{cc} \cdot \left(1 - 0.15 \cdot \frac{\varepsilon_c - \varepsilon_1}{\varepsilon_{85} - \varepsilon_1}\right) \\ \text{else} \\ \quad f_{res} \end{cases}$$

Plots

# of points $i := 1 .. 100$

Concrete strain values $\varepsilon_{c_i} := 0.002 \cdot (i - 1)$

Unconfined concrete strength $f_{c.unc_i} := f_{c.SR.1}\left(\varepsilon_{c_i}\right)$

Confined concrete strength (stories 1, 2 & 3) $f_{c.conf1_i} := f_{cc.SR.1}\left(\varepsilon_{c_i}\right)$

Confined concrete strength (stories 4, 5 & 6) $f_{c.conf2_i} := f_{cc.SR.2}\left(\varepsilon_{c_i}\right)$

Confined concrete strength (stories 7 & 8) $f_{c.conf3_i} := f_{cc.SR.3}\left(\varepsilon_{c_i}\right)$

Confined concrete strength (stories 9 & 10) $f_{c.conf4_i} := f_{cc.SR.4}\left(\varepsilon_{c_i}\right)$

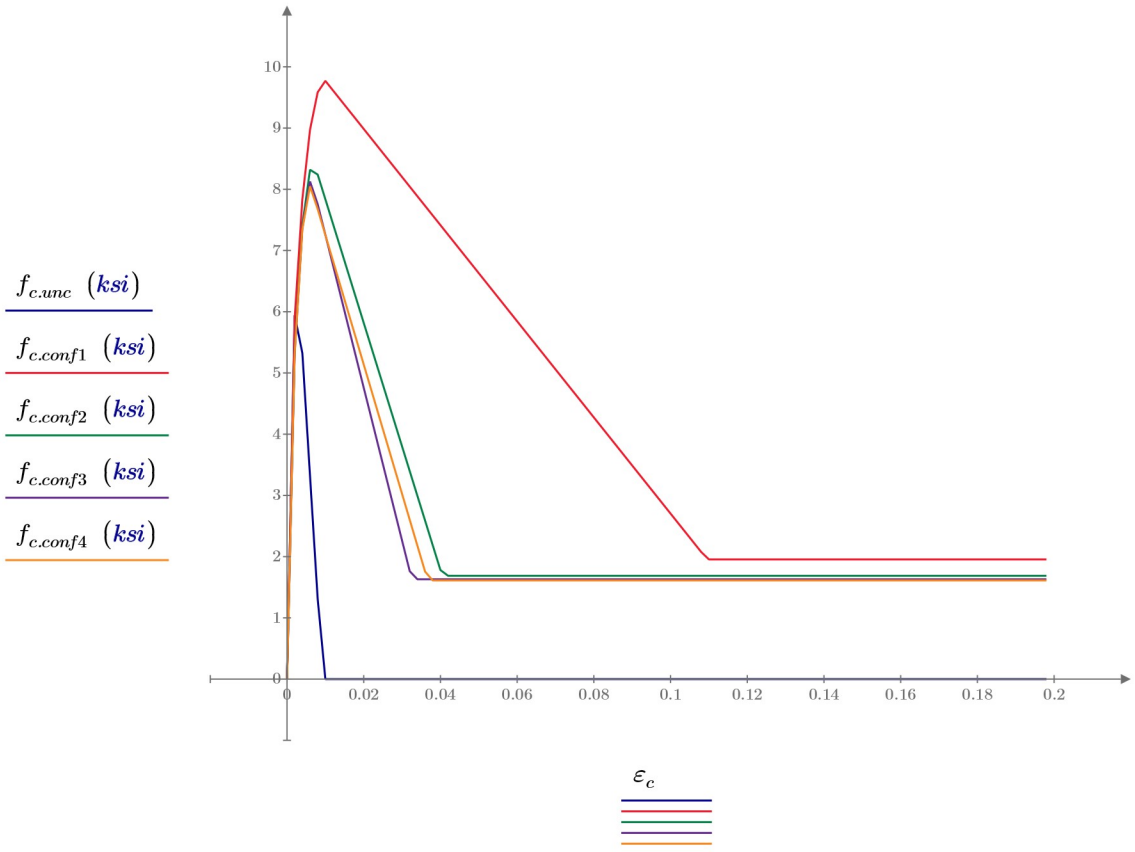

C.5 Sectional Analysis with Expected Material Properties and Δ_{roof} Capacity

Expected Material Properties

Unconfined Concrete

Max. compressive stress $f'_{c.unc} := 6.5\ ksi$

Strain at max. comp. stress $\varepsilon_{c.unc} := 0.003$

$\varepsilon_{085} := 0.0038$

Strain at which the descending branch touches the X axis $\varepsilon_{cf.unc} := \frac{(\varepsilon_{085} - \varepsilon_{c.unc})}{0.15} + \varepsilon_{c.unc}$

$$f_{c.unc}(\varepsilon_c) := \begin{cases} \text{if } 0 \le \varepsilon_c \le \varepsilon_{c.unc} \\ \quad f'_{c.unc} \cdot \left(\frac{2 \cdot \varepsilon_c}{\varepsilon_{c.unc}} - \left(\frac{\varepsilon_c}{\varepsilon_{c.unc}}\right)^2\right) \\ \text{else if } \varepsilon_{c.unc} < \varepsilon_c \le \varepsilon_{cf.unc} \\ \quad f'_{c.unc} \cdot \left(1 - 0.15 \cdot \frac{\varepsilon_c - \varepsilon_{c.unc}}{\varepsilon_{085} - \varepsilon_{c.unc}}\right) \\ \text{else} \\ \quad 0 \end{cases}$$

Confined Concrete

Length of BE $l_{be} := 69.0\ in$

Concrete peak stress $f'_c := 9.84\ ksi$

Strain at Concrete Peak Stress $\varepsilon_{cu} := 0.0101$

Rresidual stress $f_{res} := 0.2 \cdot f'_c$

Strain at residual stress $\varepsilon_{c.res} := 0.1335$

Other parameters (S&R model) $K := 0.51$

$\varepsilon_{c85} := 0.033$

$$f_c(\varepsilon_c) := \begin{cases} \text{if } 0 \le \varepsilon_c \le \varepsilon_{cu} \\ \quad f'_c \cdot \left(\frac{2 \cdot \varepsilon_c}{\varepsilon_{cu}} - \left(\frac{\varepsilon_c}{\varepsilon_{cu}}\right)^2\right)^{\frac{1}{1+2 \cdot K}} \\ \text{else if } \varepsilon_{cu} < \varepsilon_c \le \varepsilon_{c.res} \\ \quad f'_c \cdot \left(1 - 0.15 \cdot \frac{\varepsilon_c - \varepsilon_{cu}}{\varepsilon_{c85} - \varepsilon_{cu}}\right) \\ \text{else if } \varepsilon_{c.res} \le \varepsilon_c \\ \quad f_{res} \\ \text{else} \\ \quad 0 \end{cases}$$

Steel

Steel yielding stress $f_y := 70\ ksi$

Elastic modulus of steel $E_s := 29000\ ksi$

Yielding Strain $\varepsilon_y := \frac{f_y}{E_s} = 0.00241$

Post-yielding slope $E_{sh} := 0.01 \cdot E_s = 290.00\ ksi$

$\varepsilon_{sh} := \varepsilon_y$

$$f_s(\varepsilon_s) := \begin{cases} \text{if } 0 \le |\varepsilon_s| \le \varepsilon_y \\ \quad E_s \cdot \varepsilon_s \\ \text{else if } \varepsilon_y < |\varepsilon_s| \le \varepsilon_{sh} \\ \quad \text{sign}(\varepsilon_s) \cdot f_y \\ \text{else if } \varepsilon_{sh} < |\varepsilon_s| \le 0.3 \\ \quad \text{sign}(\varepsilon_s) \cdot (f_y + (|\varepsilon_s| - \varepsilon_{sh}) \cdot E_{sh}) \\ \text{else if } 0.3 < |\varepsilon_s| \le 0.80 \\ \quad \text{sign}(\varepsilon_s) \cdot (f_y + (0.8 - \varepsilon_{sh}) \cdot E_{sh}) \\ \text{else} \\ \quad 0 \end{cases}$$

LRFD Reduction Factor

$$\phi(\varepsilon_t) := \begin{cases} \text{if } |\varepsilon_t| \le \varepsilon_y \\ \quad 0.65 \\ \text{else if } |\varepsilon_t| \ge 0.005 \\ \quad 0.9 \\ \text{else} \\ \quad 0.65 + \frac{0.9 - 0.65}{0.005 - \varepsilon_y} \cdot (|\varepsilon_t| - \varepsilon_y) \end{cases}$$

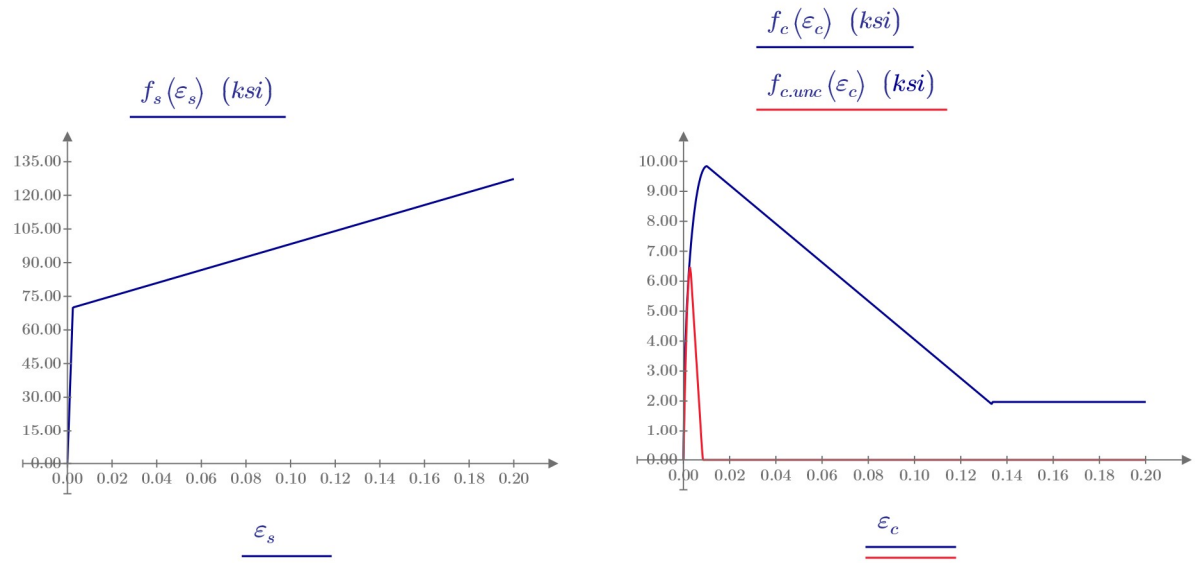

P-M Diagram & Critical Demand

Wall length	$l_w := 30\ ft$ $\quad (h := l_w)$
Web width	$b := 30\ in$
Flange thickness	$t_{fl} := 0\ ft = 0.00\ in$
Flange total width	$b_{fl} := 0\ ft$

Moment demand: $M_u := 87139\ kip \cdot ft$

Axial demands: $P_{min} := 2426\ kip$

$P_{avg} := 4098\ kip$

$P_{max} := 6159\ kip$

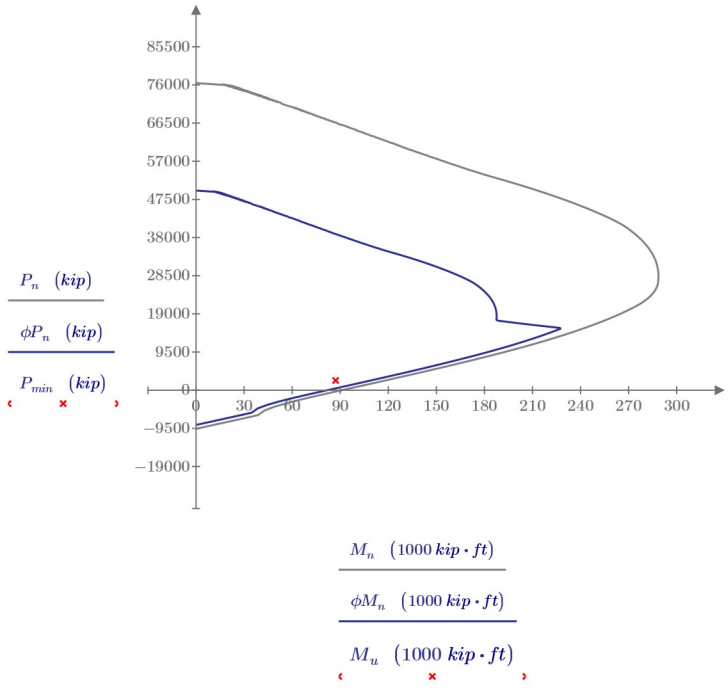

Web Ver.: #4 @ 5.3

#4 rebar	$A_{\#4} = 0.20\ in^2$
Spacing	$s_{wv} := 5.3\ in$
Reinf. ratio	$\rho_{wv} := \dfrac{2 \cdot A_{\#4}}{s_{wv} \cdot b} = 0.25\%$

Boundary Element: 36 #9

#9 rebar - area	$A_{\#9} = 1.00\ in^2$
Length of BE	$l_{be} = 69.00\ in$
Width of BE	$b = 30.00\ in$
Reinf. ratio	$\rho_{be} := \dfrac{36 \cdot A_{\#9}}{(l_{be} + 3\ in) \cdot b} = 1.67\%$

$\rho_{sb} := \dfrac{36 \cdot A_{\#9}}{A_{cv}} = 0.33\%$

Maximum Probable Moment

Sectional analysis with expected material properties and P_{max}, which comes from (1.2+0.2SDS)DL + 0.5LL

Story 1: Neutral axis depth $c := 58.52\ in$ (Iterate until obtain $P_{max} = 6159\ kip$)

P-M Capacity

$$P_{np} := \sum_l F_{cp_l} + \sum_i F_{sp_i} \qquad P_{np} = 6159\ kip$$

$$M_{pr} := \sum_l F_{cp_l} \cdot \left(h - y_{cp_l}\right) + \sum_i F_{sp_i} \cdot \left(h - d_i\right) - P_{np} \cdot \frac{h}{2} \qquad M_{pr} = 158805\ kip \cdot ft$$

Moment and Curvature at Yielding

Sectional analysis using expected material properties and expected axial load (DL + 0.25LL Condition)

$E_c := 57000 \cdot \sqrt{f'_c \cdot psi} = 5654.22\ ksi$

Story 1: Neutral axis depth $y := 66.217\ in$ (Iterate until obtain $P_{avg} = 4098\ kip$)

P-M Capacity

$$P_{np} := \sum_l F_{cp_l} + \sum_i F_{sp_i} \qquad P_{np} = 4098\ kip$$

$$M_{np} := \sum_l F_{cp_l} \cdot \left(h - y_{cp_l}\right) + \sum_i F_{sp_i} \cdot \left(h - d_i\right) - P_{np} \cdot \frac{h}{2} \qquad M_{np} = 110346\ kip \cdot ft$$

$$\phi_y := \frac{\varepsilon_y}{d_{N_i} - y} \qquad \phi_y = \left(9.961 \cdot 10^{-5}\right) \frac{1}{ft}$$

Expected Capacity

Sectional analysis using expected material properties and expected axial load (DL + 0.25LL Condition)

Story 1: Neutral axis depth $c := 47.84\ in$ (Iterate until obtain $P_{avg} = 4098\ kip$)

P-M Capacity

$$P_{np} := \sum_l F_{cp_l} + \sum_i F_{sp_i} \qquad P_{np} = 4098\ kip$$

$$M_{np} := \sum_l F_{cp_l} \cdot \left(h - y_{cp_l}\right) + \sum_i F_{sp_i} \cdot \left(h - d_i\right) - P_{np} \cdot \frac{h}{2} \qquad M_{np} = 136669\ kip \cdot ft$$

Design shear force with amplification factors

Maximum probable moment
(expected material properties and highest axial load) $M_{pr} = 158805\ kip \cdot ft$

Critical section at the bottom $h_{wcs} := 158\ ft$

Wall length $l_w := 30\ ft$

Shear demand $V_u := 1158\ kip$

Overstrength factor when $\frac{h_{wcs}}{l_w} = 5.27 > 1.5$: $\Omega_v := \max\left(\frac{M_{pr}}{M_u}, 1.5\right) = 1.82$

w_s when $\frac{h_{wcs}}{l_w} = 5.27 > 2.0$ and $n_s := \max\left(12, 0.007 \cdot \frac{h_{wcs}}{in}\right) = 13.27 > 6$: $\omega_v := min\left(1.3 + \frac{n_s}{30}, 1.8\right)$

$\omega_v = 1.74$

Therefore, accodring to ACI 318-19, 18.10.3.1:

$V_e := min\left(\Omega_v \cdot \omega_v \cdot V_u, 3\ V_u\right) = 3474\ kip$ $\left(\Omega_v \cdot \omega_v = 3.18\right)$

Predicted Drift Capacity

Wall length $l_w = 30.00\ ft$

Width of wall cross section $b = 30.00\ in$

Web cross-sectional area $A_{cv} := l_w \cdot b = 10800\ in^2$

Neutral axis depth at expected demand $c_e := 47.84\ in$

Maximum expected shear demand $V_e = 3474\ kip$

Nominal shear stress $v_{max} := \frac{V_e}{A_{cv}} = 321.67\ psi$

λ_b parameter $\lambda_b := \frac{l_w \cdot c_e}{b^2} = 19.14$

α parameter for combination of a single perimeter hoop with supplemental crossties $\alpha := 45$

Expected unconfined concrete strength $f'_{c.unc} = 6.50\ ksi$

Height of the wall $h_w := 158\ ft$

Roof drift capacity $\frac{\delta_c}{h_w} = 3.85 - \frac{\lambda_b}{\alpha} - \frac{v_{max}}{8 \cdot \sqrt{f'_{c.unc} \cdot psi}} = 2.93\ \%$

Deformation capcity $\delta_c := 0.029 \cdot h_w = 55\ in$

C.6 Selection of MCE Level Ground Motions

The methodology described by Baker and Lee (2018) was implemented. The scripts developed by the authors are available in Baker's GitHub repository (link here). The period used as the input T_{cond} in **Table A.1** corresponds to the fundamental period obtained with the OpenSees model. The spectral acceleration used as target when computing the conditional spectrum, $S_a(T_{cond})$ in **Table A.1**, was obtained by interpolating T_{cond} in the Uniform Hazard Response Spectrum of the site (shown in **Figure 10.3**).

***Table C.1**: Input values used in "Main_select_motions.m" script by Baker and Lee (2018)*

Parameter	Value
Tcond	1.20
Tmin	0.01
Tmax	5
SaTcond	0.57
rup.M_bar	6.92
rup..Rjb	8.4
rup.eps_bar	1.31
rup.Vs30	760
rup.z1	999
rup.region	1
rup.Fault_Type	1
rup.Rrup	4.60
rup.Rx	4.60
rup.W	11
rup.Ztor	0
rup.Zbot	11
rup.dip	90
allowedRecs.Vs30	[560 1130]
allowedRecs.Mag	[6.2 8.2]
allowRecs.D	[0 50]

***Table C.2**: Selected ground motions for the 12-Story Archetype MCE level analysis*

Tag	RSN*	Earthquake Name	Year	Horizontal Acc. Filename Utilized	Scale Factor
EQ 1201	1013	"Northridge-01"	1994	RSN1013_NORTHR_LDM334.AT2	1.3
EQ 1202	1078	"Northridge-01"	1994	RSN1078_NORTHR_SSU090.AT2	3.06
EQ 1203	1108	"Kobe_ Japan"	1995	RSN1108_KOBE_KBU000.AT2	0.62
EQ 1204	1202	"Chi-Chi_ Taiwan"	1999	RSN1202_CHICHI_CHY035-E.AT2	1.02
EQ 1205	1206	"Chi-Chi_ Taiwan"	1999	RSN1206_CHICHI_CHY042-E.AT2	2.57
EQ 1206	1234	"Chi-Chi_ Taiwan"	1999	RSN1234_CHICHI_CHY086-E.AT2	2.4
EQ 1207	1270	"Chi-Chi_ Taiwan"	1999	RSN1270_CHICHI_HWA020-E.AT2	4.19
EQ 1208	1279	"Chi-Chi_ Taiwan"	1999	RSN1279_CHICHI_HWA030-N.AT2	3.1
EQ 1209	143	"Tabas_ Iran"	1978	RSN143_TABAS_TAB-L1.AT2	0.69
EQ 1210	1492	"Chi-Chi_ Taiwan"	1999	RSN1492_CHICHI_TCU052-N.AT2	0.48
EQ 1211	1507	"Chi-Chi_ Taiwan"	1999	RSN1507_CHICHI_TCU071-N.AT2	1
EQ 1212	1510	"Chi-Chi_ Taiwan"	1999	RSN1510_CHICHI_TCU075-N.AT2	2.29
EQ 1213	1511	"Chi-Chi_ Taiwan"	1999	RSN1511_CHICHI_TCU076-N.AT2	0.91
EQ 1214	1551	"Chi-Chi_ Taiwan"	1999	RSN1551_CHICHI_TCU138-N.AT2	1.2
EQ 1215	1787	"Hector Mine"	1999	RSN1787_HECTOR_HEC000.AT2	1.33
EQ 1216	285	"Irpinia_ Italy-01"	1980	RSN285_ITALY_A-BAG000.AT2	1.94
EQ 1217	3274	"Chi-Chi_ Taiwan-06"	1999	RSN3274_CHICHI.06_CHY035E.AT2	1.3
EQ 1218	3548	"Loma Prieta"	1989	RSN3548_LOMAP_LEX000.AT2	0.66
EQ 1219	356	"Coalinga-01"	1983	RSN356_COALINGA.H_H-SC2090.AT2	4.63
EQ 1220	369	"Coalinga-01"	1983	RSN369_COALINGA.H_H-SCN315.AT2	1.55
EQ 1221	3744	"Cape Mendocino"	1992	RSN3744_CAPEMEND_BNH270.AT2	1.56
EQ 1222	3943	"Tottori_ Japan"	2000	RSN3943_TOTTORI_SMN015NS.AT2	2.74
EQ 1223	4213	"Niigata_ Japan"	2004	RSN4213_NIIGATA_NIG023EW.AT2	2.84
EQ 1224	4229	"Niigata_ Japan"	2004	RSN4229_NIIGATA_NIGH12EW.AT2	2.79
EQ 1225	4481	"L'Aquila_ Italy"	2009	RSN4481_L-AQUILA_FA030XTE.AT2	1.71
EQ 1226	4483	"L'Aquila_ Italy"	2009	RSN4483_L-AQUILA_AM043YLN.AT2	1.54
EQ 1227	4841	"Chuetsu-oki_ Japan"	2007	RSN4841_CHUETSU_65004NS.AT2	3.39
EQ 1228	4844	"Chuetsu-oki_ Japan"	2007	RSN4844_CHUETSU_65007NS.AT2	3.41
EQ 1229	4850	"Chuetsu-oki_ Japan"	2007	RSN4850_CHUETSU_65013NS.AT2	1.15
EQ 1230	4864	"Chuetsu-oki_ Japan"	2007	RSN4864_CHUETSU_65037NS.AT2	1.45
EQ 1231	4865	"Chuetsu-oki_ Japan"	2007	RSN4865_CHUETSU_65038EW.AT2	1.1
EQ 1232	4869	"Chuetsu-oki_ Japan"	2007	RSN4869_CHUETSU_65042EW.AT2	3.47
EQ 1233	4873	"Chuetsu-oki_ Japan"	2007	RSN4873_CHUETSU_65056NS.AT2	2.52
EQ 1234	5618	"Iwate_ Japan"	2008	RSN5618_IWATE_IWT010EW.AT2	2.48
EQ 1235	5681	"Iwate_ Japan"	2008	RSN5681_IWATE_MYGH06EW.AT2	3.23
EQ 1236	5775	"Iwate_ Japan"	2008	RSN5775_IWATE_54009EW.AT2	3.95
EQ 1237	5806	"Iwate_ Japan"	2008	RSN5806_IWATE_55461NS.AT2	1.98
EQ 1238	5807	"Iwate_ Japan"	2008	RSN5807_IWATE_55462NS.AT2	3.45
EQ 1239	6891	"Darfield_ New Zealand"	2010	RSN6891_DARFIELD_CSHSN76W.AT2	3.78
EQ 1240	751	"Loma Prieta"	1989	RSN751_LOMAP_CLR180.AT2	4.48
EQ 1241	755	"Loma Prieta"	1989	RSN755_LOMAP_CYC195.AT2	3.11
EQ 1242	779	"Loma Prieta"	1989	RSN779_LOMAP_LGP000.AT2	0.57
EQ 1243	801	"Loma Prieta"	1989	RSN801_LOMAP_SJTE315.AT2	2.86
EQ 1244	809	"Loma Prieta"	1989	RSN809_LOMAP_UC2090.AT2	2.55
EQ 1245	8164	"Duzce_ Turkey"	1999	RSN8164_DUZCE_487-NS.AT2	2.5
*Record Sequential Number of the PEER NGA-West2 database					

C.7 OpenSees Analysis Results

C.7.1 Model with Expected Material Properties and Expected Axial Load

This model uses the expected material properties defined by the application of the Saatcioglu and Razvi (1992) model. The applied gravity load comes from the load combination D+0.25L.

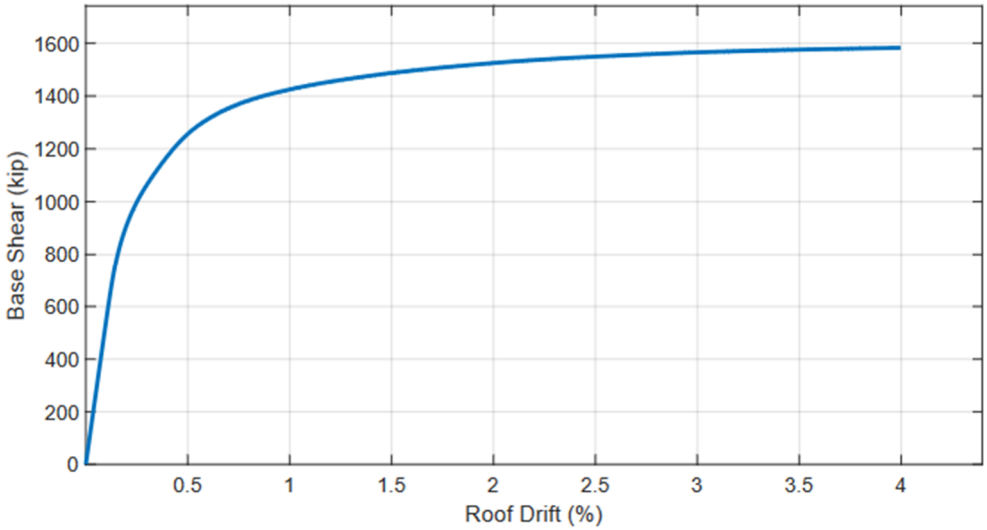

***Figure C.1**: Base shear versus roof drift – Monotonic Pushover with P_{avg} and w/o modification to expected material properties (12-Story Archetype)*

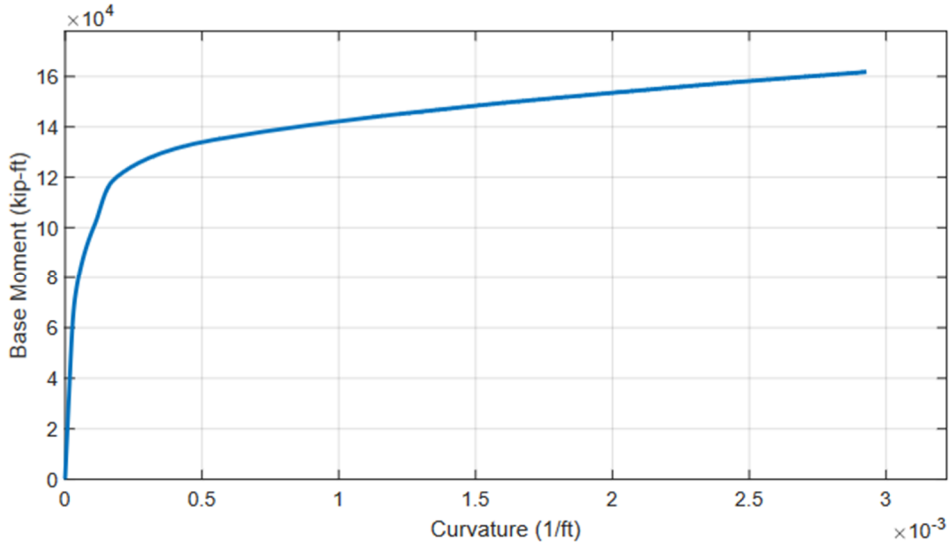

***Figure C.2**: Base moment versus curvature – Monotonic Pushover with P_{avg} and w/o modification to expected material properties (12-Story Archetype)*

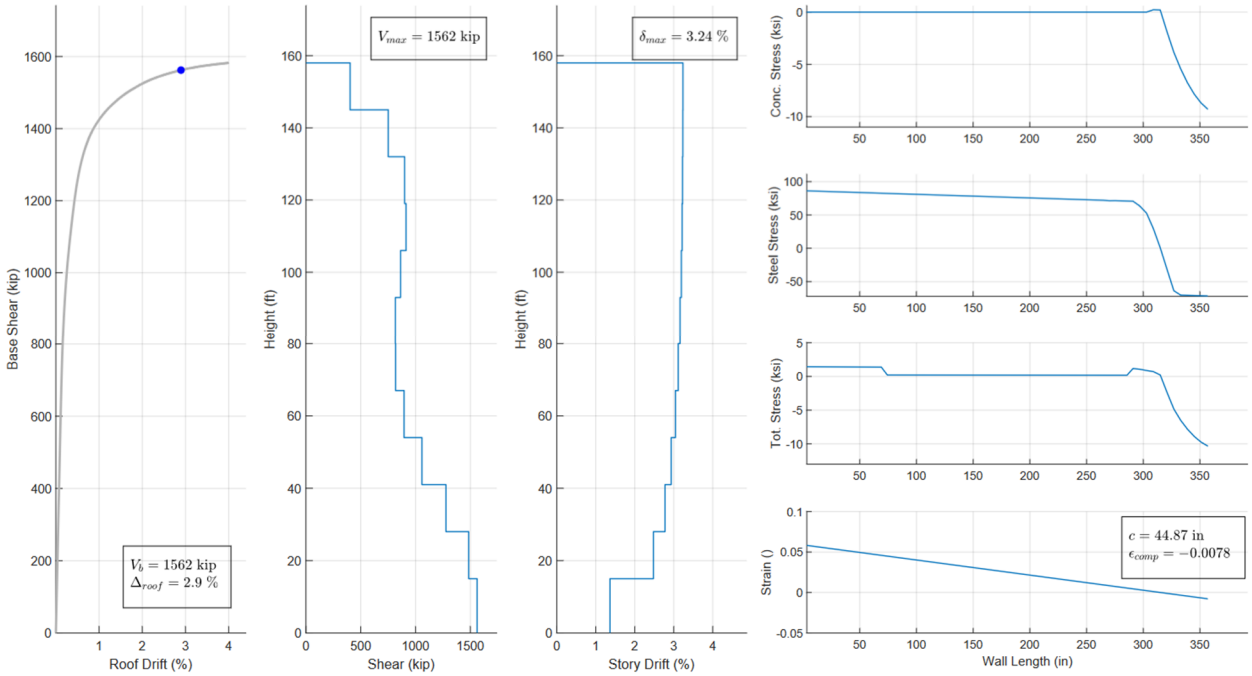

***Figure C.3**: Monotonic pushover results at predicted roof drift capacity (12-Story Archetype)*

C.7.2 Model with Modified Expected Material Properties and Expected Axial Load

C.7.2.1 Monotonic Pushover Results

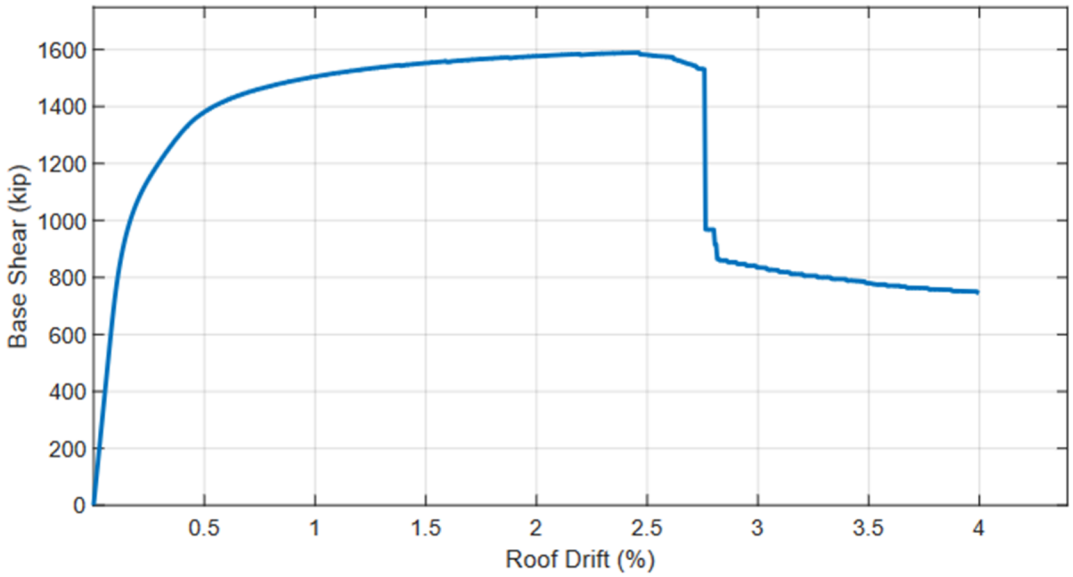

***Figure C.4**: Base shear versus roof drift – Monotonic Pushover with P_{avg} and modified expected material properties (12-Story Archetype)*

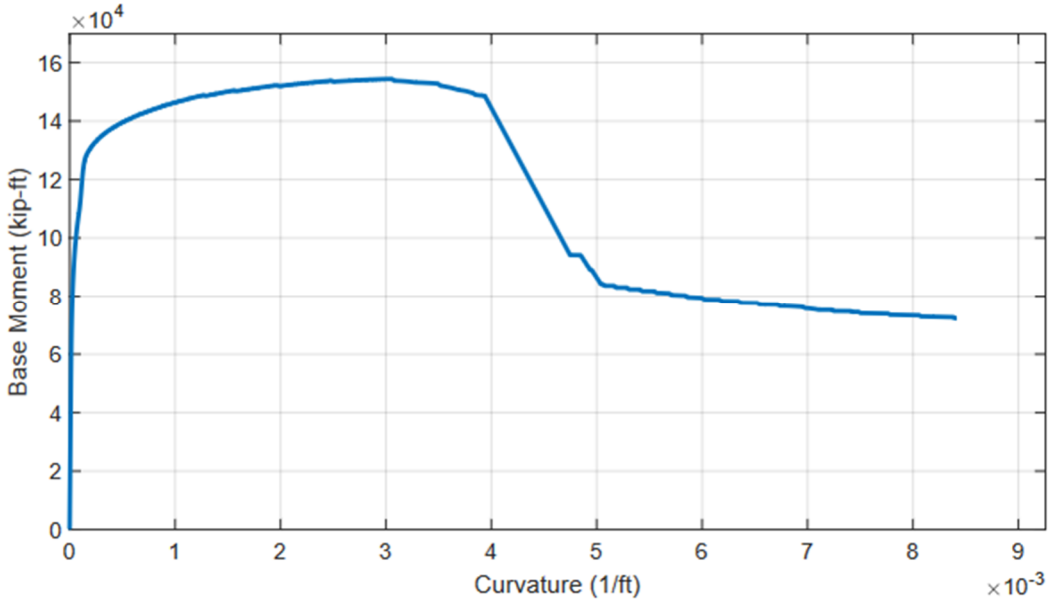

***Figure C.5**: Base moment versus curvature – Monotonic Pushover with P_{avg} and modified expected material properties (12-Story Archetype)*

C.7.2.2 Cyclic Pushover Results

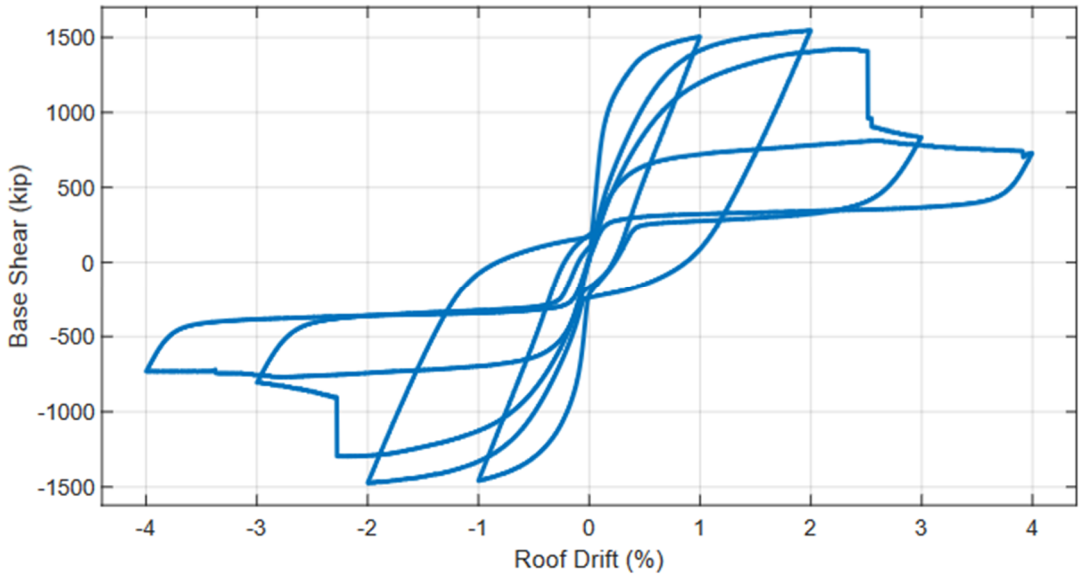

***Figure C.6**: Base shear versus roof drift – Cyclic Pushover with P_{avg} and modified expected material properties (12-Story Archetype)*

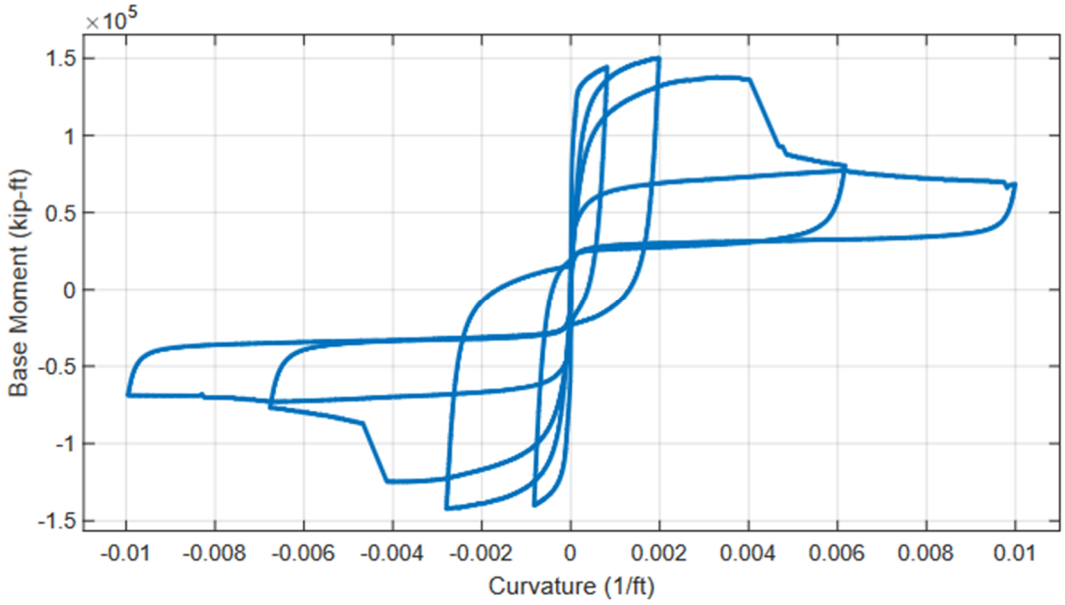

***Figure C.7**: Base moment versus Curvature – Cyclic Pushover with P_{avg} and modified expected material properties (12-Story Archetype)*

C.7.2.3 Dynamic Analysis Results – LC: (1.2+0.2SDS)D+0.25L

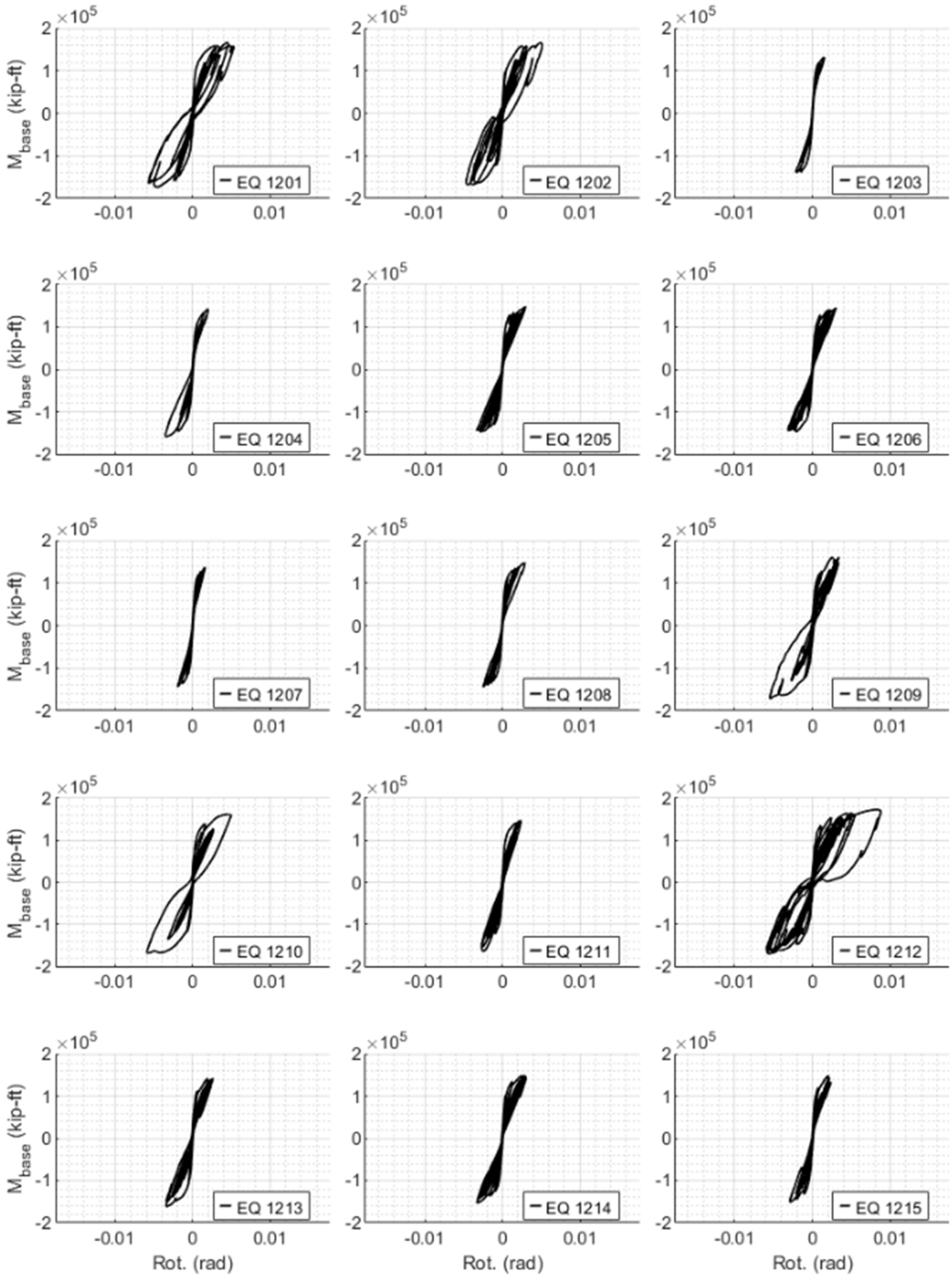

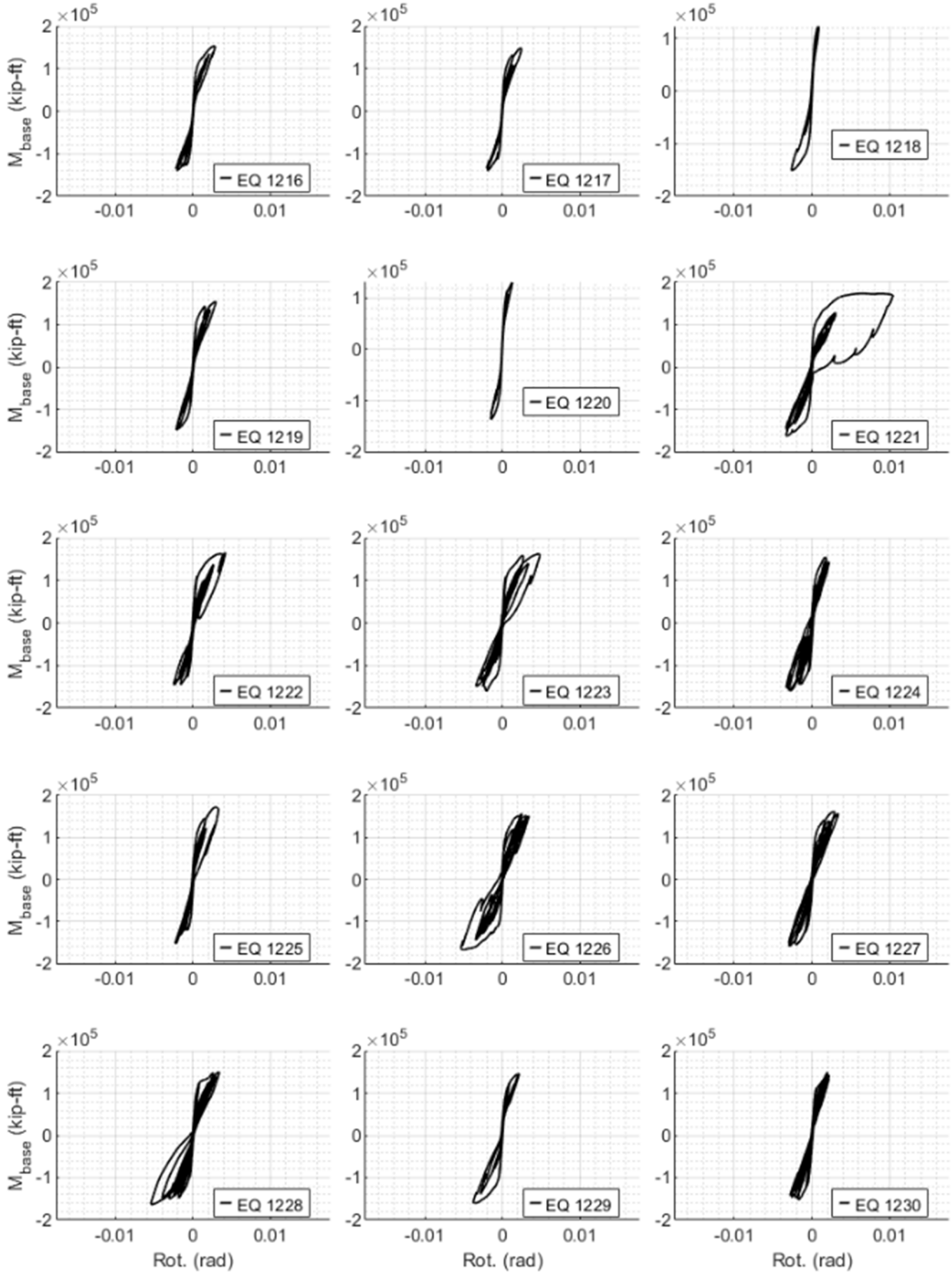
EQ 1216
EQ 1217
EQ 1218
EQ 1219
EQ 1220
EQ 1221
EQ 1222
EQ 1223
EQ 1224
EQ 1225
EQ 1226
EQ 1227
EQ 1228
EQ 1229
EQ 1230
M_base (kip-ft)
Rot. (rad)
×10^5

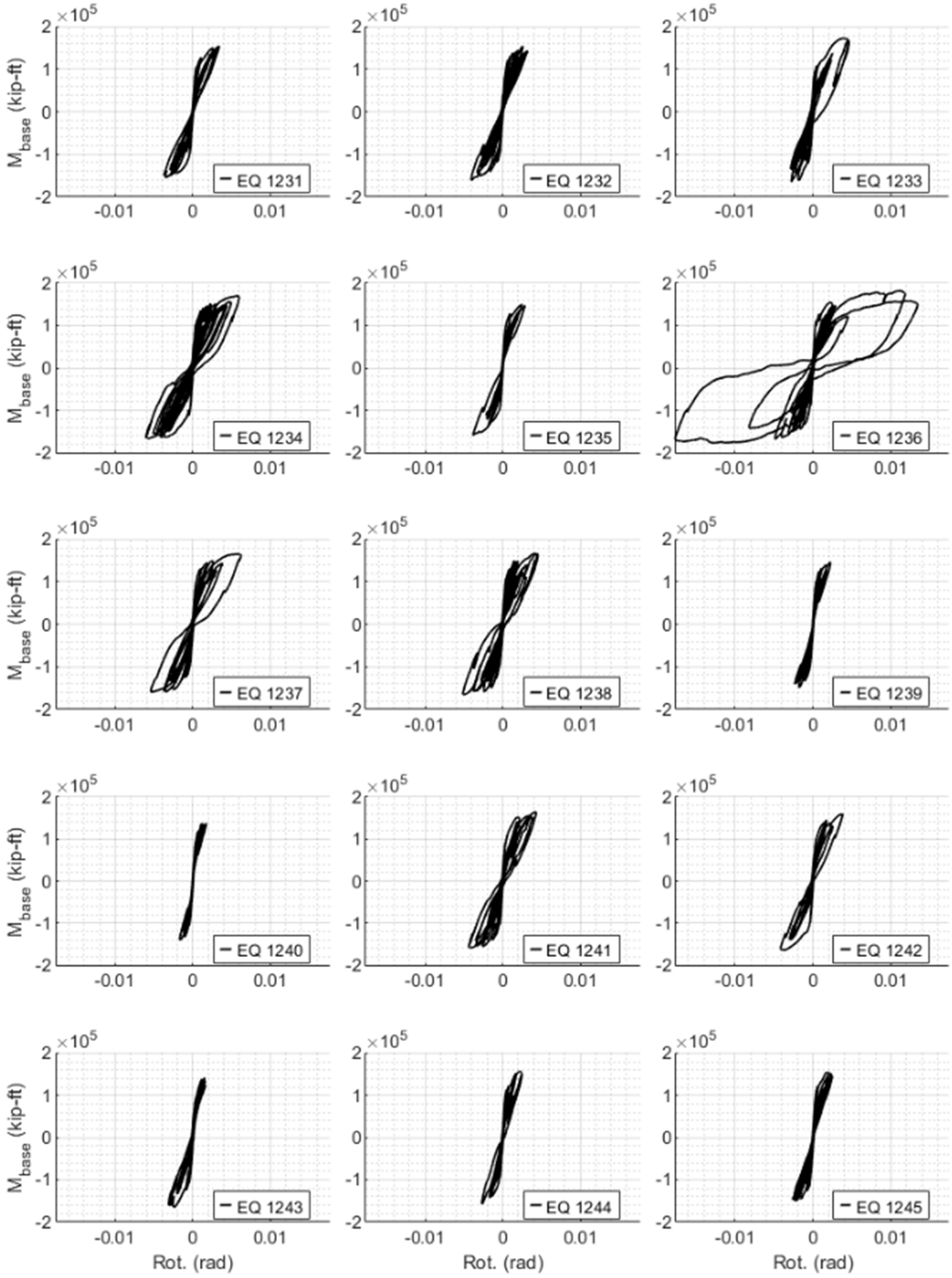
×10^5
2
1
0
-1
-2
M_base (kip-ft)
-0.01
0
0.01
Rot. (rad)
EQ 1231
EQ 1232
EQ 1233
EQ 1234
EQ 1235
EQ 1236
EQ 1237
EQ 1238
EQ 1239
EQ 1240
EQ 1241
EQ 1242
EQ 1243
EQ 1244
EQ 1245

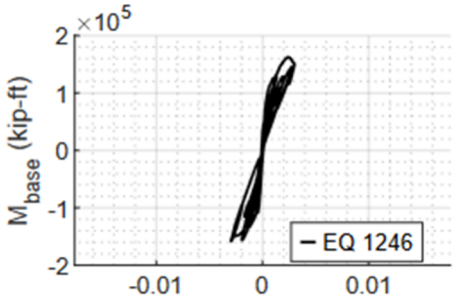
×10^5
2
1
0
-1
-2
M_base (kip-ft)
-0.01
0
0.01
EQ 1246

References

Abdullah, S A, and J W Wallace. 2020. "UCLA Database for Reinforced Concrete Structural Walls: UCLA-RCWalls." *Earthquake Spectra* 23.

Abdullah, S A, and J W Wallace. 2021. "New Nonlinear Modeling Parameters and Acceptance Criteria for RC Structural Walls." In *Proceedings of the 2021 Los Angeles Tall Buildings Structural Design Council Conference*. Los Angeles, California, USA: LATBSDC.

Abdullah, Saman Ali. 2019. "Reinforced Concrete Structural Walls: Test Database and Modeling Parameters." PhD thesis, Ann Arbor, United States: University of California; Los Angeles. ProQuest Dissertations Publishing.

ACI Committee 318. 2020. *Building Code Requirements for Structural Concrete and Commentary ACI 318-19 & ACI 318R-19)*. American Concrete Institute; American Concrete Institute.

Alzubi, Jafar, Anand Nayyar, and Akshi Kumar. 2018. "Machine Learning from Theory to Algorithms: An Overview." *J. Phys. Conf. Ser.* 1142 (1): 012012.

Amazon Web Services. 2019. *Amazon Machine Learning Developer Guide*. Amazon; Wiley.

ASCE/SEI 43, American Society of Civil Engineers. 2005. *Seismic Design Criteria for Structure, Systems and Components in Nuclear Facilities*. ASCE Standards.

Baek, Jang-Woon, Sung-Hyun Kim, Hong-Gun Park, and Byung-Soo Lee. 2020. "Shear-Friction Strength of Low-Rise Walls with 600 MPa Reinforcing Bars." *ACI Struct. J.* 117 (1).

Barda, F, J Hanson, and W Corley. 1977. "Shear Strength of Low-Rise Walls with Boundary Elements: Reinforced Concrete Structures in Seismic Zones, Publication SP-53-8." In. American Concrete Institute; American Concrete Institute.

Barrett, James P. 1974. "The Coefficient of Determination—Some Limitations." *Am. Stat.* 28 (1): 19–20.

Breiman, Leo. 2001. "Random Forests." *Mach. Learn.* 45 (1): 5–32.

Burkardt, John. 2014. "The Truncated Normal Distribution." *Department of Scientific Computing Website, Florida State University* 1: 35.

Bzdok, Danilo, Naomi Altman, and Martin Krzywinski. 2018. "Statistics Versus Machine Learning." *Nat. Methods* 15 (4): 233–34.

Cardenas, Alex E, and Donald D Magura. 1972. "Strength of High-Rise Shear Walls-Rectangular Cross Section." *Spec. Publ. Am. Philos. Soc.* 36: 119–50.

Carrillo, Julian, and Sergio M Alcocer. 2013. "Shear Strength of Reinforced Concrete Walls for Seismic Design of Low-Rise Housing." *ACI Struct. J.* 110 (3).

Chen, X L, J P Fu, J L Yao, and J F Gan. 2018. "Prediction of Shear Strength for Squat RC Walls Using a Hybrid ANN–PSO Model." *Eng. Comput.* 34 (2): 367–83.

Dey, Ayon. 2016. "Machine Learning Algorithms: A Review." *International Jounral of Computer Science and Information Technologies (IJCSIT)* 7 (3): 1174–79.

EC8, Code, Price. 2005. "Eurocode 8: Design of Structures for Earthquake Resistance-Part 1: General Rules, Seismic Actions and Rules for Buildings." *Brussels: European Committee for Standardization*.

Emmert-Streib, Frank, and Matthias Dehmer. 2019. "Evaluation of Regression Models: Model Assessment, Model Selection and Generalization Error." *Machine Learning and Knowledge Extraction* 1 (1): 521–51.

Gonfalonieri, Alexandre. 2019. "5 Ways to Deal with the Lack of Data in Machine Learning." *KDnuggets*. KDnuggets. https://www.kdnuggets.com/2019/06/5-ways-lack-data-machine-learning.html.

Google ML Education. n.d. "The Size and Quality of a Data Set | Machine Learning | Google Developers." Accessed August 30, 2022. https://developers.google.com/machine-learning/data-prep/construct/collect/data-size-quality.

Gulec, C, and A S Whittaker. 2011. "Empirical Equations for Peak Shear Strength of Low Aspect Ratio Reinforced Concret Walls." *ACI Struct. J.* 108 (1): 80–89.

Hoerl, Arthur E, and Robert W Kennard. 1970. "Ridge Regression: Biased Estimation for Nonorthogonal Problems." *Technometrics* 12 (1): 55–67.

Höge, Marvin, Thomas Wöhling, and Wolfgang Nowak. 2018. "A Primer for Model Selection: The Decisive Role of Model Complexity." *Water Resour. Res.* 54 (3): 1688–1715.

Kabeyasawa, T, T Ohkubo, and Y Nakamura. 1996. "Tests and Analysis of Hybrid Wall Systems." In *Proceedings, 11th World Conference on Earthquake Engineering, Acapulco, Mexico*. iitk.ac.in.

Kassem, Wael. 2015. "Shear Strength of Squat Walls: A Strut-and-Tie Model and Closed-Form Design Formula." *Eng. Struct.* 84 (February): 430–38.

Keshtegar, Behrooz, Moncef L Nehdi, Nguyen-Thoi Trung, and Reza Kolahchi. 2021. "Predicting Load Capacity of Shear Walls Using SVR–RSM Model." *Appl. Soft Comput.* 112 (November): 107739.

Kim, Ju-Hyung, and Hong-Gun Park. 2020. "Shear and Shear-Friction Strengths of Squat Walls with Flanges." *ACI Struct. J.*

Looi, D T W, and R K L Su. 2017. "Predictive Seismic Shear Capacity Model of Rectangular Squat RC Shear Walls in Flexural and Shear Zones." In *16th World Conference on Earthquake Engineering, Santiago, January*, 9–13. wcee.nicee.org.

Moradi, Mohammad Javad, and Mohammad Amin Hariri-Ardebili. 2019. "Developing a Library of Shear Walls Database and the Neural Network Based Predictive Meta-Model." *NATO Adv. Sci. Inst. Ser. E Appl. Sci.* 9 (12): 2562.

Morgan, Nelson, and Hervé Bourlard. 1989. "Generalization and Parameter Estimation in Feedforward Nets: Some Experiments." *Adv. Neural Inf. Process. Syst.* 2.

Murtaugh, Paul A. 2014. "In Defense of p-Values." *Ecology* 95 (3): 611–17.

NZS 3101, P 3101 Concrete Design Committe. 2006. *NZS 3101 Concrete Structures Standard, Part 1 & Part 2 (NZS 3101.1:2006 & NZS 3101.2:2006)*. Standards Council.

Sánchez-Alejandre, Alfredo, and Sergio M Alcocer. 2010. "Shear Strength of Squat Reinforced Concrete Walls Subjected to Earthquake Loading—Trends and Models." *Eng. Struct.* 32 (8): 2466–76.

Segal, Mark, and Yuanyuan Xiao. 2011. "Multivariate Random Forests." *Wiley Interdiscip. Rev. Data Min. Knowl. Discov.* 1 (1): 80–87.

Segura, Christopher L, and John W Wallace. 2018. "Seismic Performance Limitations and Detailing of Slender Reinforced Concrete Walls." *ACI Struct. J.* 115 (3).

Shear, Joint ASCE-ACI Task Committee 426 on, Diagonal Tension of the Committee on Masonry, and Reinforced Concrete of the Structural Division. 1973. "The Shear Strength of Reinforced Concrete Members." *Journal of the Structural Division* 99 (6): 1091–1187.

Tanaka, J S. 1987. "'How Big Is Big Enough?': Sample Size and Goodness of Fit in Structural Equation Models with Latent Variables." *Child Dev.* 58 (1): 134–46.

Tibshirani, Robert. 1996. "Regression Shrinkage and Selection via the Lasso." *J. R. Stat. Soc.* 58 (1): 267–88.

Wood, Sharon L. 1990. "Shear Strength of Low-Rise Reinforced Concrete Walls." *ACI Struct. J.* 87 (1): 99–107.

Zhang, C, and Y Ma. 2012. *Ensemble Machine Learning: Methods and Applications*. Edited by Cha Zhang and Yunqian Ma. Springer, Boston, MA.

Zou, Hui, and Trevor Hastie. 2005. "Regularization and Variable Selection via the Elastic Net." *J. R. Stat. Soc. Series B Stat. Methodol.* 67 (2): 301–20.